NASA Tech Briefs

National
Aeronautics and
Space
Administration

NASA engineers originally developed electronics for multiple pressure sensors to aid them in wind-tunnel research, as illustrated by this interference photograph of a Space Shuttle model under test. Now, the same technology is being used in a line of commercial products distributed by a Virginia company for monitoring pressures in industrial processes. *[See the bottom of page A1.]*

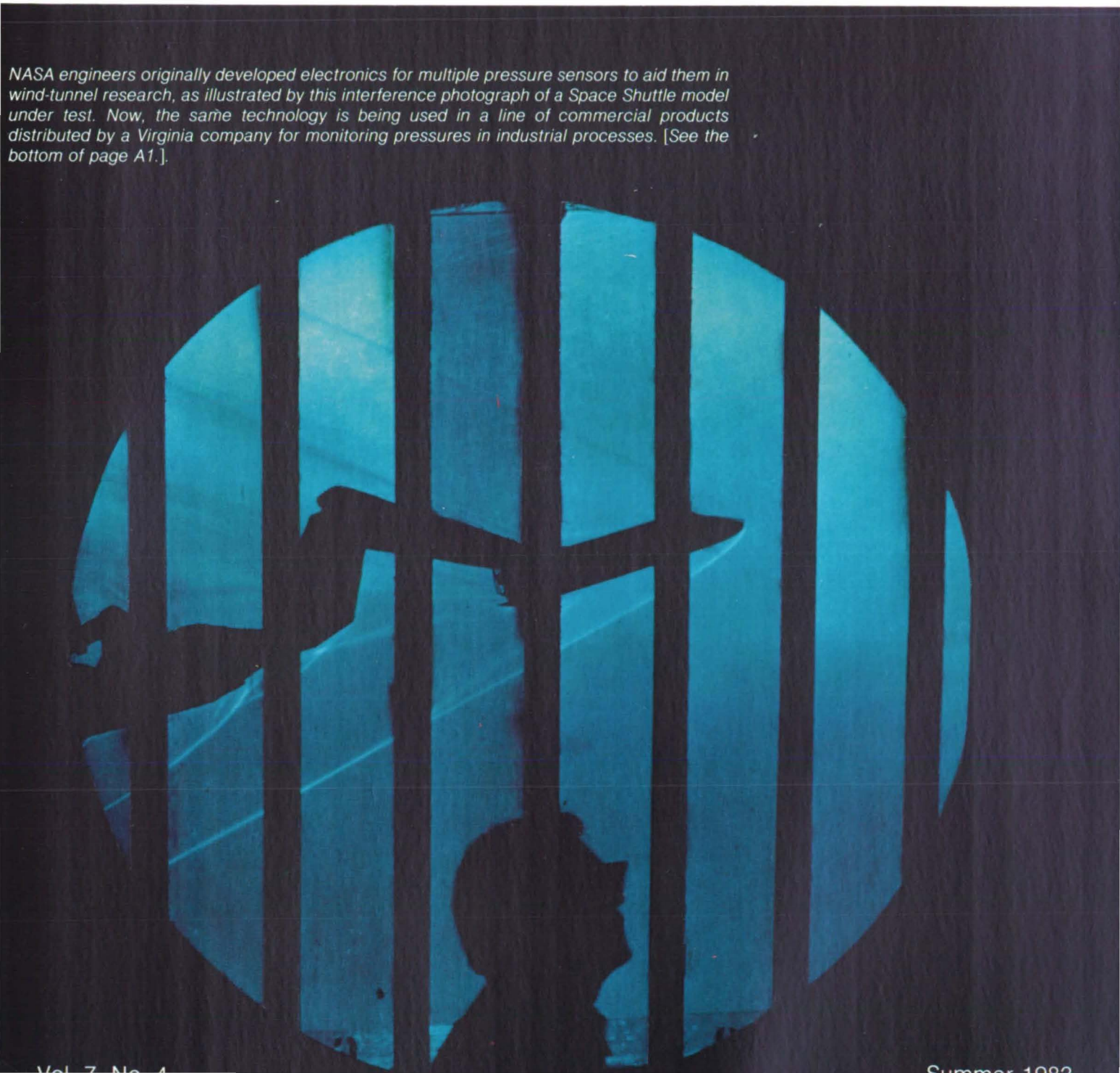

Vol. 7, No. 4 Summer 1983

About the NASA Technology Utilization Program

The National Aeronautics and Space Act of 1958, which established NASA and the United States civilian space program, requires that "The Administration shall provide for the widest practicable and appropriate dissemination of information concerning its activities and the results thereof."

To help carry out this objective, NASA's Technology Utilization (TU) Program was established in 1962. Now, as an element of NASA's Technology Utilization and Industry Affairs Division, this program offers a variety of valuable services to help transfer aerospace technology to nonaerospace applications, thus assuring American taxpayers maximum return on their investment in space research; thousands of spinoffs of NASA research have already occurred in virtually every area of our economy.

The TU program has worked for engineers, scientists, technicians, and businessmen; and it can work for you.

NASA Tech Briefs

Tech Briefs is published quarterly and is free to engineers in U.S. industry and to other domestic technology transfer agents. It is both a current-awareness medium and a problem-solving tool. Potential products . . . industrial processes . .. basic and applied research . . . shop and lab techniques . . . computer software . . . new sources of technical data . . . concepts . . . can be found here. The short section on New Product Ideas highlights a few of the potential new products contained in this issue. The remainder of the volume is organized by technical category to help you quickly review new developments in your areas of interest. Finally, a subject index makes each issue a convenient reference file.

Further Information on Innovations

Although some new technology announcements are complete in themselves, most are backed up by Technical Support Packages (TSP's). TSP's are available without charge and may be ordered by simply completing a TSP Request Card found at the back of this volume. Further information on some innovations is available for a nominal fee from other sources, as indicated. In addition, Technology Utilization Officers at NASA Field Centers will often be able to lend necessary guidance and assistance.

Patent Licenses

Patents have been issued to NASA on some of the inventions described, and patent applications have been submitted on others. Each announcement indicates patent status and availability of patent licenses if applicable.

Other Technology Utilization Services

To assist engineers, industrial researchers, business executives, Government officials, and other potential users in applying space technology to their problems, NASA sponsors Industrial Applications Centers. Their services are described on page A7. In addition, an extensive library of computer programs is available through COSMIC, the Technology Utilization Program's outlet for NASA-developed software.

Applications Program

NASA conducts applications engineering projects to help solve public-sector problems in such areas as safety, health, transportation, and environmental protection. Two applications teams, staffed by professionals from a variety of disciplines, assist in this effort by working with Federal agencies and health organizations to identify critical problems amenable to solution by the application of existing NASA technology.

Reader Feedback

We hope you find the information in *NASA Tech Briefs* useful. A reader-feedback card has been included because we want your comments and suggestions on how we can further help you apply NASA innovations and technology to your needs. Please use it; or if you need more space, write to the Manager, Technology Transfer Division, P.O. Box 8757, Baltimore/ Washington International Airport, Maryland 21240.

NASA Tech Briefs

National Aeronautics and Space Administration

SUMMER 1983
Volume 7, Number 4

COVERS: The photographs on the front and back covers illustrate developments by NASA and its contractors that have resulted in commercial and nonaerospace spinoffs. You can use the TSP Request Card at the back of this issue to learn more about the Electronically-Scanned Pressure Sensors [Circle 83] and the Tubular Energy Absorbers [Circle 84].

About This NASA Publication

NASA Tech Briefs, a quarterly publication, is distributed free to qualified U.S. citizens to encourage commercial application of U.S. space technology. For information on publications and services available through the NASA Technology Utilization Program, write to the Manager, Technology Transfer Division, P.O. Box 8757, Baltimore/Washington International Airport, Maryland 21240.

"The Administrator of National Aeronautics and Space Administration has determined that the publication of this periodical is necessary in the transaction of the public business required by law of this Agency. Use of funds for printing this periodical has been approved by the Director of the Office of Management and Budget."

Change of Address

If you wish to have NASA Tech Briefs forwarded to your new address, use the Subscription Card enclosed at the back of this volume of NASA Tech Briefs. Be sure to check the appropriate box indicating change of address, and also fill in your identification number (T number) in the space indicated.

Communications Concerning Editorial Matter

For editorial comments or general communications about NASA Tech Briefs, you may use the Feedback card in the back of NASA Tech Briefs, or write to: The Publications Manager, Technology Utilization Office (LGT-1), NASA Headquarters, Washington, DC 20546. Technical questions concerning specific articles should be directed to the Technology Utilization Officer of the sponsoring NASA Center (addresses listed on page A4).

Acknowledgements

NASA Tech Briefs is published quarterly by the National Aeronautics and Space Administration, Technology Transfer Division, Washington, DC: Administrator: **James M. Beggs;** Director, Technology Utilization and Industry Affairs Division: **Ronald J. Philips;** Publications Manager: **Leonard A. Ault.** Prepared for the National Aeronautics and Space Administration by **Logical Technical Services Corp.:** Editor-in-Chief: **Jay Kirschenbaum;** Art Director: **Ernest Gillespie;** Managing Editor: **Jerome Rosen;** Chief Copy Editor: **Oden Browne;** Staff Editors: **Donald Blattner, Larry Grunberger, Jordan Randjelovich, Ted Selinsky, George Watson;** Graphics: **Luis Martinez, Janet McCrie, Huburn Profitt;** Editorial & Production: **Richard Johnson, Stephanie Godino, Leslie Iwaskow, Frank Ponce, Elizabeth Texeira, Vincent Susinno, Ernestine Walker.**

NASA TU SERVICES

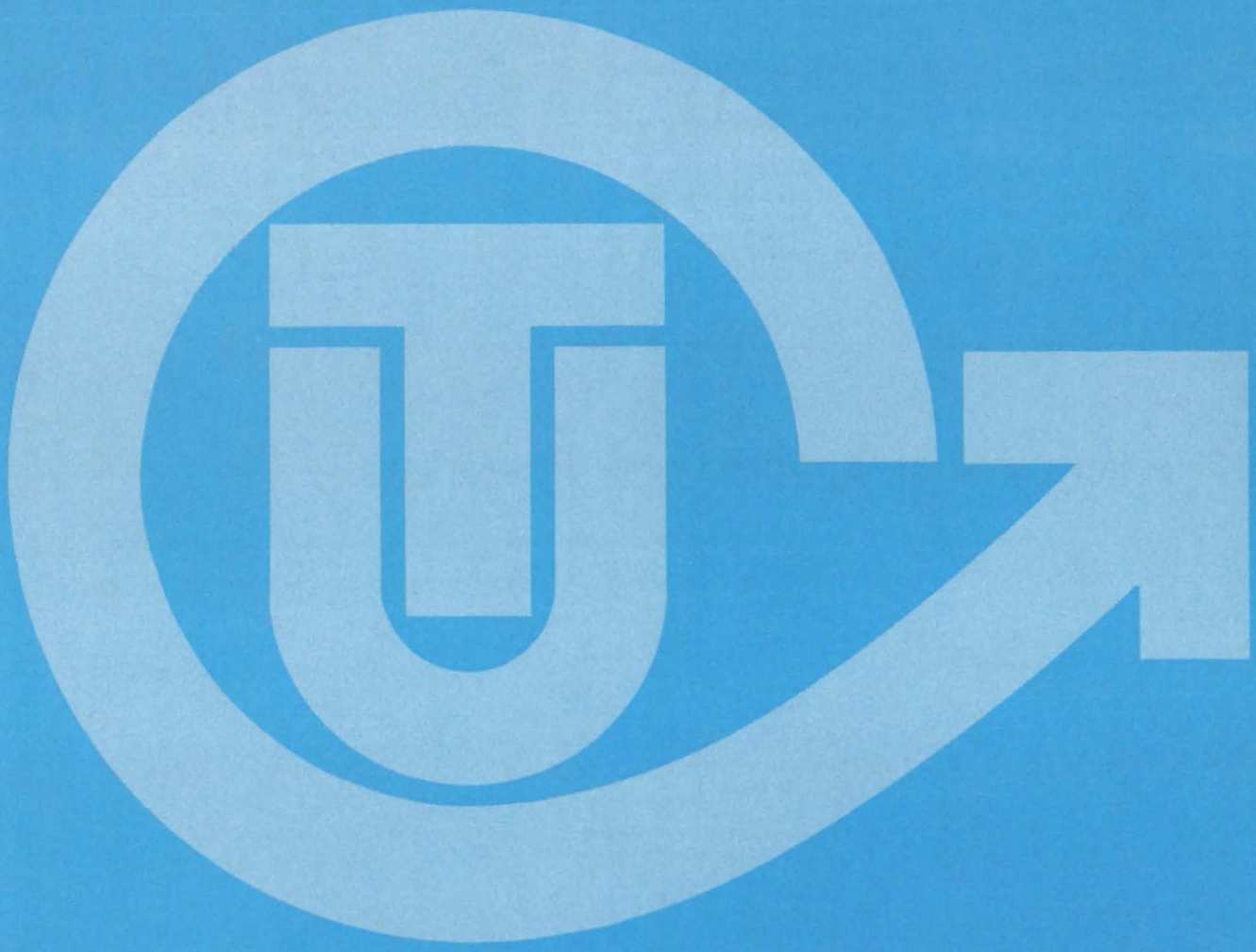

NASA TECHNOLOGY UTILIZATION NETWORK

★ TECHNOLOGY UTILIZATION OFFICERS

Stanley A. Miller
Ames Research Center
Code 240-10
Moffett Field, CA 94035
(415) 965-6471

Stanley A. Miller
Hugh L. Dryden Flight Research Center
Code 240-10
Moffett Field, CA 94035
(415) 965-6471

Donald S. Friedman
Goddard Space Flight Center
Code 702.1
Greenbelt, MD 20771
(301) 344-6242

William Chmylak
Lyndon B. Johnson Space Center
Code AL-32
Houston, TX 77058
(713) 483-3809

U. Reed Barnett
John F. Kennedy Space Center
Code PT-SPD
Kennedy Space Center, FL 32899
(305) 867-3017

John Samos
Langley Research Center
Mail Stop 139A
Hampton, VA 23665
(804) 865-3281

Harrison Allen, Jr.
Lewis Research Center
Mail Code 7-3
21000 Brookpark Road
Cleveland, OH 44135
(216) 433-4000, Ext. 6422

Ismail Akbay
George C. Marshall Space Flight Center
Code AT01
Marshall Space Flight Center, AL 35812
(205) 453-2224

Leonard A. Ault
NASA Headquarters
Code ETD-6
Washington, DC 20546
(202) 453-8424

Aubrey Smith
NASA Resident Office-JPL
4800 Oak Grove Drive
Pasadena, CA 91103
(213) 354-4849

Gilmore H. Trafford
Wallops Flight Center
Code OD
Wallops Island, VA 23337
(804) 824-3411, Ext. 201

● INDUSTRIAL APPLICATIONS CENTERS

Aerospace Research Applications Center
1201 East 38th Street
Indianapolis, IN 46205
John M. Ulrich, director
(317) 264-4644

Computer Software Management and Information Center (COSMIC)
Suite 112, Barrow Hall
University of Georgia
Athens, GA 30602
John A. Gibson, director
(404) 542-3265

Kerr Industrial Applications Center
Southeastern Oklahoma State University
Durant, OK 74701
James Harmon, director
(405) 924-0121, Ext. 413

NASA Industrial Applications Center
701 LIS Building
University of Pittsburgh
Pittsburgh, PA 15260
Paul A. McWilliams, executive director
(412) 624-5211

New England Research Applications Center
Mansfield Professional Park
Storrs, CT 06268
Daniel Wilde, director
(203) 486-4533

North Carolina Science and Technology Research Center
Post Office Box 12235
Research Triangle Park, NC 27709
James E. Vann, director
(919) 549-0671

Technology Applications Center
University of New Mexico
Albuquerque, NM 87131
Stanley Morain, director
(505) 277-3622

NASA Industrial Applications Center
University of Southern California
Denny Research Building
University Park
Los Angeles, CA 90007
Robert Mixer, acting director
(213) 743-6132

■ STATE TECHNOLOGY APPLICATIONS CENTERS

NASA/University of Florida
State Technology Applications Center
500 Weil Hall
University of Florida
Gainesville, FL 32611
J. Ronald Thornton, director

Gainesville:	(904) 392-6760
Boca Raton:	(305) 395-5100, Ext. 2292
Fort Lauderdale:	(305) 776-6645
Jacksonville:	(904) 646-2478
Orlando:	(305) 275-2706
Pensacola:	(904) 476-9500, Ext. 426
Tampa:	(813) 974-2499

NASA/University of Kentucky
State Technology Applications Program
109 Kinkead Hall
University of Kentucky
Lexington, KY 40508
William R. Strong, manager
(606) 258-4632

◆ PATENT COUNSELS

Robert F. Kempf
Asst. Gen. Counsel for patent matters
NASA Headquarters
Code GP-4
400 Maryland Avenue, SW.
Washington, DC 20546
(202) 755-3954

Darrell G. Brekke
Ames Research Center
Mail Code: 200-11A
Moffett Field, CA 94035
(415) 965-5104

Darrell G. Brekke
Hugh L. Dryden Flight Research Center
Mail Code: 201-11A
Moffett Field, CA 94035
(415) 965-5104

John O. Tresansky
Goddard Space Flight Center
Mail Code: 204
Greenbelt, MD 20771
(301) 344-7351

Marvin F. Matthews
Lyndon B. Johnson Space Center
Mail Code: AL-3
Houston, TX 77058
(713) 483-4871

James O. Harrell
John F. Kennedy Space Center
Mail Code: SA-PAT
Kennedy Space Center, FL 32899
(305) 867-2544

Howard J. Osborn
Langley Research Center
Mail Code: 279
Hampton, VA 23665
(804) 827-3725

Norman T. Musial
Lewis Research Center
Mail Code: 500-311
21000 Brookpark Road
Cleveland, OH 44135
(216) 433-4000, Ext. 346

Leon D. Wofford, Jr.
George C. Marshall Space Flight Center
Mail Code: CC01
Marshall Space Flight Center, AL 35812
(205) 453-0020

Paul F. McCaul
NASA Resident Office-JPL
Mail Code: 180-601
4800 Oak Grove Drive
Pasadena, CA 91103
(213) 354-2700

▲ APPLICATION TEAMS

Doris Rouse, director
Research Triangle Institute
Post Office Box 12194
Research Triangle Park, NC 27709
(919) 541-6980

James P. Wilhelm, director
SRI International
333 Ravenswood Avenue
Menlo Park, CA 94026
(415) 326-6200, Ext. 3520

TECHNOLOGY UTILIZATION OFFICERS

Technology transfer experts can help you apply the innovations in NASA Tech Briefs.

The Technology Utilization Officer at each NASA Field Center is an applications engineer who can help you make use of new technology developed at his center. He brings you NASA Tech Briefs and other special publications, sponsors conferences, and arranges for expert assistance in solving technical problems.

Technical assistance, in the form of further information about NASA innovations and technology, is one of the services available from the TUO. Together with NASA scientists and engineers, he can often help you find and implement NASA technology to meet your specific needs.

Technical Support Packages (TSP's) are prepared by the center TUO's. They provide further technical details for articles in NASA Tech Briefs. This additional material can help you evaluate and use NASA technology. You may receive most TSP's free of charge by using the TSP Request Card found at the back of this issue.

Technical questions about articles *in NASA Tech Briefs are answered in the TSP's. When no TSP is available, or you have further questions, contact the Technology Utilization Officer at the center that sponsored the research* [*see page A4*].

NASA INVENTIONS AVAILABLE FOR LICENSING

Over 3,500 NASA inventions are available for licensing in the United States — both exclusive and nonexclusive.

NASA grants patent licenses, both exclusive and nonexclusive, for the commercial use of U.S. and foreign patents and patent applications owned by NASA. All licenses require royalties and are granted by express written agreements in accordance with the NASA Patent-Licensing Regulations.

Additional information about NASA inventions may be found in the *"NASA Patent Abstract Bibliography"* (PAB), containing abstracts of all NASA inventions, which can be purchased from the National Technical Information Service, Springfield, VA 22161. The PAB is updated semiannually.

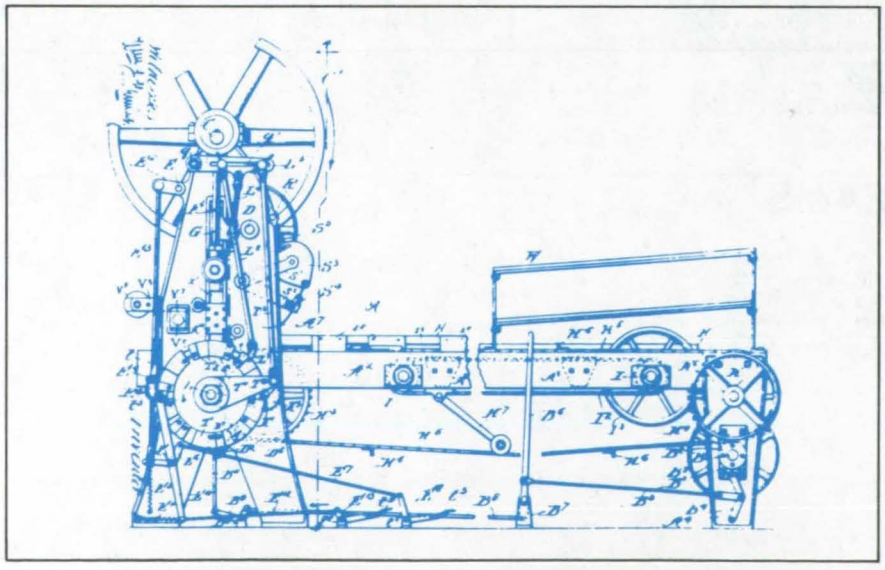

Patent licenses for inventions *described in NASA Tech Briefs are frequently available. Many of the inventions reported in NASA Tech Briefs are patented or are under consideration for a patent at the time they are published. The current patent status is described at the end of the article; if no patent action is contemplated by NASA, there is no statement about patents. If you want to know more about the patent program or are interested in licensing a particular invention, contact the Patent Counsel at the NASA Field Center that sponsored the research* [*see page A5*]. *Be sure to refer to the NASA reference number at the end of the Tech Brief.*

APPLICATION TEAMS

Technology-matching and problem-solving assistance to public-sector organizations

Application engineering projects are conducted by NASA to help solve public-sector problems in such areas as safety, health, transportation, and environmental protection. Some application teams specialize in biomedical disciplines; others, in engineering and scientific problems. Staffed by professionals from various disciplines, these teams work with other Federal agencies and health organizations to identify critical problems amenable to solution by the application of existing NASA technology.

Public-sector organization *representatives can learn more about application teams by contacting a nearby NASA Field Center Technology Utilization Office* [see page A4].

INDUSTRIAL APPLICATIONS CENTERS

Computerized access to over 10 million documents worldwide

Computerized information retrieval from one of the world's largest banks of technical data is available from NASA's network of Industrial Applications Centers (IAC's). The IAC's give you access to 1,800,000 technical reports in the NASA data base and to more than 10 times that many reports and articles found in nearly 200 other computerized data bases.

The major sources include:

- *750,000 NASA Technical Reports*
- *Selected Water Resources Abstracts*
- *NASA Scientific and Technical Aerospace Reports*
- *Air Pollution Technical Information Center*
- *NASA International Aerospace Abstracts*
- *Chem Abstracts Condensates*
- *Engineering Index*
- *Energy Research Abstracts*
- *NASA Tech Briefs*
- *Government Reports*
- *Announcements*

and many other specialized files on food technology, textile technology, metallurgy, medicine, business, economics, social sciences, and physical science.

The IAC services range from tailored literature searches through expert technical assistance:

- *Retrospective Searches:* Published or unpublished literature is screened, and documents are identified according to your interest profile. IAC engineers tailor results to your specific needs and furnish abstracts considered the most pertinent. Complete reports are available upon request.
- *Current-Awareness Searches:* IAC engineers will help design a program to suit your needs. You will receive selected monthly or quarterly abstracts on new developments in your area of interest.
- *Technical Assistance:* IAC engineers will help you evaluate the results of your literature searches. They can help find answers to your technical problems and put you in touch with scientists and engineers at appropriate NASA Field Centers.

Prospective clients *can obtain more information about these services by contacting the nearest IAC* [see page A4]. *User fees are charged for IAC information services.*

STATE TECHNOLOGY APPLICATIONS CENTERS

Technical information services for industry and state and local government agencies.

Government and private industry in Florida and Kentucky can utilize the services of NASA's State Technology Applications Centers (STAC's). The STAC's differ from the Industrial Applications Centers described on page A7, primarily in that they are integrated into existing state technical assistance programs and serve only the host state, whereas the IAC's serve multistate regions.

Many data bases, including the NASA base and several commercial bases, are available for automatic data retrieval through the STAC's. Other services such as document retrieval and special searches are also provided. (Like the IAC's, the STAC's normally charge a fee for their services.)

To obtain information *about the services offered, write or call the STAC in your state* [*see page A4*].

COSMIC®

An economical source of computer programs developed by NASA and other government agencies

A vast software library is maintained by COSMIC — the Computer Software Management and Information Center. COSMIC gives you access to approximately 1,600 computer programs developed for NASA and the Department of Defense and selected programs for other government agencies. Programs and documentation are available at reasonable cost.

Available programs range from management (PERT scheduling) to information science (retrieval systems) and computer operations (hardware and software). Hundreds of engineering programs perform such tasks as structural analysis, electronic circuit design, chemical analysis, and the design of fluid systems. Others determine building energy requirements and optimize mineral exploration.

COSMIC services go beyond the collection and storage of software packages. Programs are checked for completeness; special announcements and an indexed software catalog are prepared; and programs are reproduced for distribution. Customers are helped to identify their software needs; and COSMIC follows up to determine the successes and problems and to provide updates and error corrections. In some cases, NASA engineers can offer guidance to users in installing or running a program.

Information about programs *described in NASA Tech Briefs articles can be obtained by completing the COSMIC Request Card at the back of this issue. Just circle the letters that correspond to the programs in which you are interested.*

NEW PRODUCT IDEAS

NEW PRODUCT IDEAS are just a few of the many innovations described in this issue of NASA Tech Briefs and having promising commercial applications. Each is discussed further on the referenced page in the appropriate section in this issue. If you are interested in developing a product from these or other NASA innovations, you can receive further technical information by requesting the TSP referenced at the end of the full-length article or by writing the Technology Utilization Office of the sponsoring NASA center (see page A4). NASA's patent-licensing program to encourage commercial development is described on page A6.

Acoustic Emissions Reveal Combustion Conditions

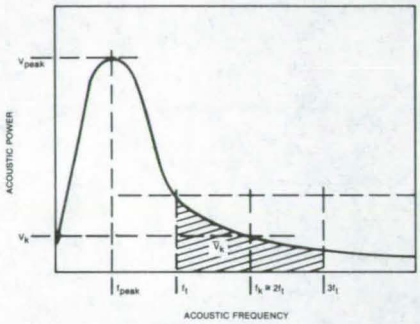

The acoustic emissions from turbulent gas flames may be useful for the diagnosis of combustion processes and for fuel/air mixture control. An experimental study of turbulent combustion in several burners, including a natural-gas boiler furnace, has identified acoustic spectra and characteristic audiofrequencies at which the amplitudes are sensitive to air/fuel ratios. The spectra were analyzed to determine distinct frequency domains where acoustic power correlates with combustion efficiency. The correlations can be used for control of the operation of gas-fired furnaces.
(See page 389.)

Self-Modulated Laser Rangefinder

A self-modulated laser transmitter/receiver measures distances and displacements of distant objects, such as vibrating buildings. The new laser ranging system exploits the presence of laser signals differing in frequency by the longitudinal-mode separation frequency. The instrument determines the target distance by measuring the phase difference between the detected modulation of the reference and return signals. For many applications, such as stability measurements of structures on construction sites, only a measure of the change in target distance is needed.
(See page 391.)

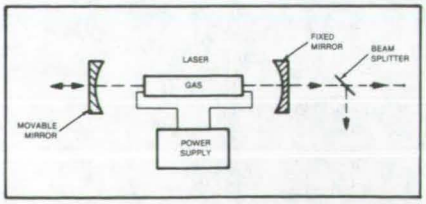

Cryogenic Vacuum Pump

A three-stage cryogenic vacuum pump has high pumping capacity for all gases including helium, requires only a 2-watt refrigerator to cool its two coldest stages, and is small enough for general laboratory use. The first stage, cooled by

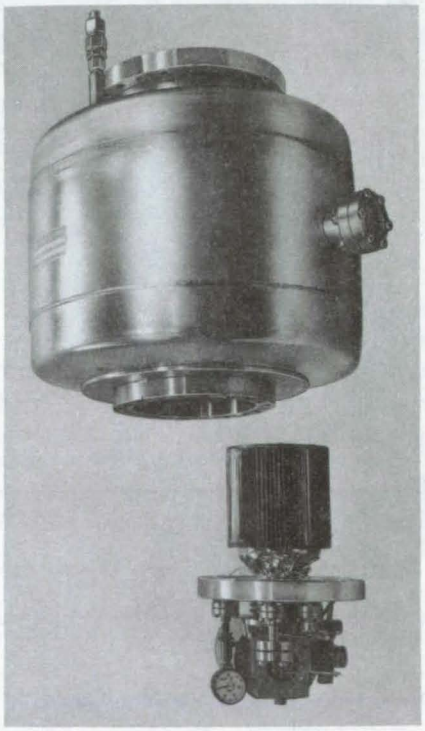

liquid nitrogen, removes water and CO_2 from input gas. The second stage, cooled to 38 K by the refrigerator, removes noble gases except helium and some of the lighter gases not trapped by the first stage. The third stage, cooled by the refrigerator, traps all remaining gases. All three stages are mounted inside the liquid-nitrogen Dewar that cools the first stage.
(See page 442.)

Flowthrough Bacteria-Detection System

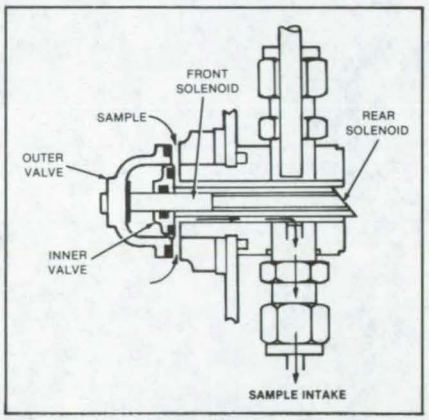

A microbe detection system collects a water sample on-line, adds a growth medium, incubates it, estimates the number of fecal coliform bacteria in the sample, and then sterilizes the broth in preparation for a new cycle. The bacteria count is estimated without the need for a skilled operator. More than one growth medium and incubation temperature can be incorporated in a cycle, making it possible to detect different groups of bacteria. The flowthrough system is effective in controlling the viable organisms, and steam at 15 psig sterilizes the system without altering the microbial flora.
(See page 413.)

Electronic Force Gage for Welders

A strain-gage system designed for the calibration and maintenance of resistance welding equipment produces an in-process oscilloscope trace showing the profile of the welding force. The unit provides a dynamic picture of the welding

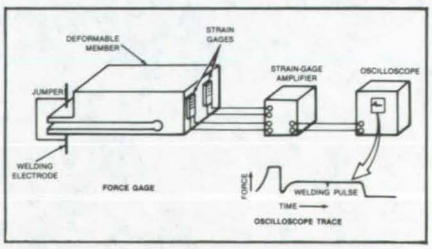

pressure and the current pulse. The strain gages detect the motion of a deformable member. Output signals from the gages are fed into an oscilloscope to produce a trace of the welding force. A photograph of the oscilloscope trace taken during troubleshooting is compared to a "standard" trace to locate faults, such as mistimed current pulses.
(See page 422.)

Electronic Dilatometer

A nonclamping electronic micrometer measures the minute dimensional changes caused by moisture absorption

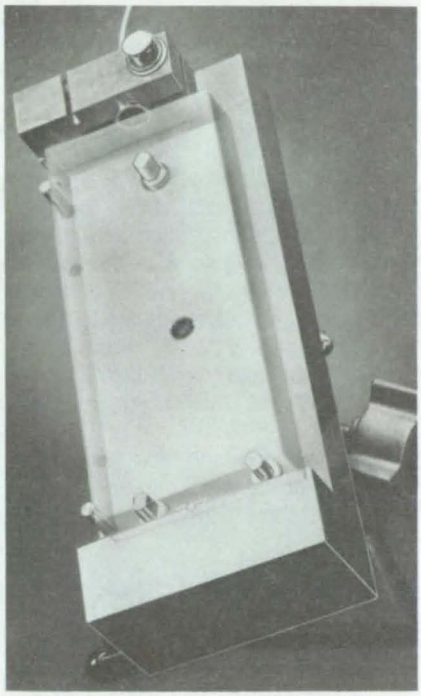

in graphite/epoxy composites. It uses an eddy-current sensor to detect changes in the length of a sample. The system could also be used to measure thermal expansion. Since the sample is not clamped, the precision and resolution are not affected by clamping forces. The instrument has a strain resolution of 0.1 microinch/inch.
(See page 419.)

Coaxial Redundant Drives

Originally developed for positioning an 800-lb X-ray telescope, an electromechanical drive provides high torque and redundancy in a compact package. The drive consists of two transmissions and brushless dc motors arranged in tandem in a single assembly. If the main drive should fail, the standby drive takes over and produces torque along the same

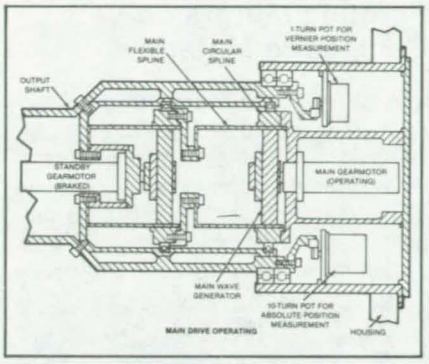

axis as that of the main drive. Potential uses include power units in robots for internal pipeline inspection, manipulators in deep submersible probes, or other applications in which redundancy could protect against costly failures.
(See page 441.)

Improved O_2/H_2 Gas-Mixture Sensor

A monitor for O_2/H_2 gas-mixture concentrations consists of a Pt-catalyzed temperature sensor mounted just downstream from an uncatalyzed sensor. Suitable for use in regenerative fuel cells, life-support systems, and other

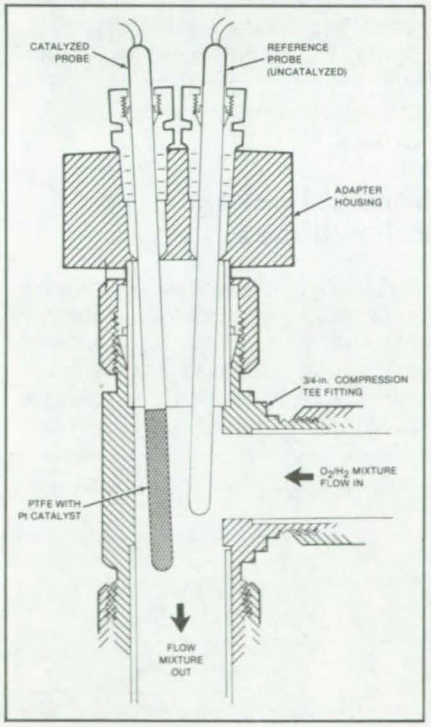

closed systems, the new unit is compact, corrosion-resistant under normal operating conditions, and assembled using standard tube fittings. It is intended primarily as an alarm sensor, initiating safe system shutdown in the event of high gas-mixture concentrations. However, temperature-difference reading may be recorded and compared to calibration curves as a means of measuring concentrations.
(See page 405.)

High-Power Switching Transistors

New large-area high-voltage switching transistors can handle 400-A peak currents and up to 1,200 V. The heart of the new transistors is a 33-mm-diameter, npn silicon wafer. Three significant innovations improve fabrication: a base-contact system for decreasing base resistance and equalizing the base/emit-

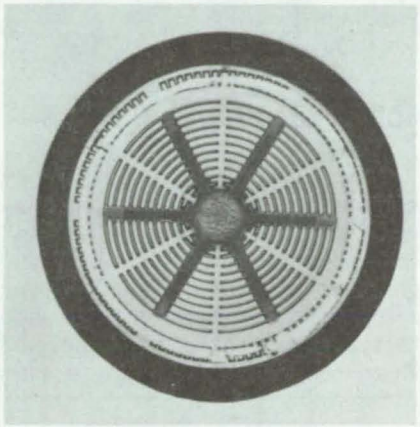

ter voltage at high currents; and emitter-contact preform that increases the silicon area available for current conduction; and an increase in the amount of interdigitation of emitter and base, permitting a gain-versus-collector-current performance that more closely approximates the ideal case. These innovations will make it possible to scale up to larger wafers, with power-handling capabilities of several hundred kVA. The new transistors could be used in 50-kW and larger power-system converters and power controllers. Additional uses would be the replacement of thyristors in high-frequency inverters, 100-kW vlf transmitters, 50-kHz RF induction heaters, and power supplies.
(See page 371.)

Normal-Incidence Soft-X-Ray Mirror

An interference mirror reflects carbon K X-rays of $\lambda = 4.48$-nm wavelength at normal incidence. The mirror consists of 76 layers of tungsten, each 0.765 nm thick, interspersed with layers of carbon, each 1.510 nm thick, all deposited on a <111> silicon wafer 0.38 mm thick and 76.2 mm in diameter. For carbon K

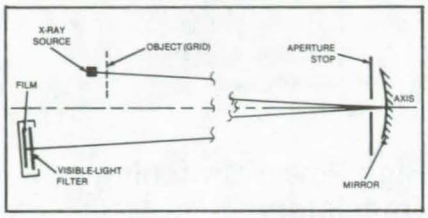

radiation at normal incidence, the multilayered structure is predicted to have a reflectivity of about 6 percent. Normal-incidence mirrors have potential applications in X-ray research and technology, where they offer advantages over grazing-incidence optics. Because their geometrical aberrations are smaller, these mirrors allow a larger field of view.
(See page 394.)

Holder for Fragile Parts

Originally designed to hold glass ampoules in a furnace, a gripping fixture has hundreds of springfingers, each of which applies a minute force. The total force approximates hydrostatic pressure, resulting in a well-distributed load that maintains a firm grip without high-stress concentrations. Because the

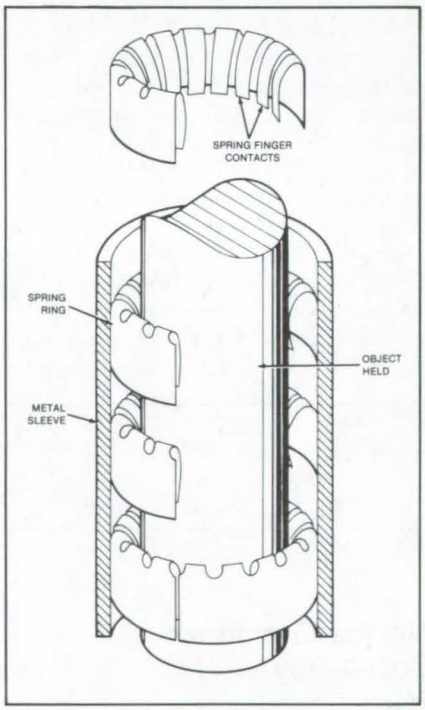

loading forces are distributed over the surface of the object and the spring contacts are flexible, the fixture could be used to hold irregularly-shaped fragile objects. It could, for example, be installed on the gripping end of a robot manipulator.
(See page 453.)

Forming Mirrors on Composite Materials

A strong, lightweight mirror is fabricated by applying a metallic reflective layer on a substrate coated with polyester resin. It is produced by depositing a coating of polyester resin on a carbon/carbon or graphite/epoxy composite structure that has been previously

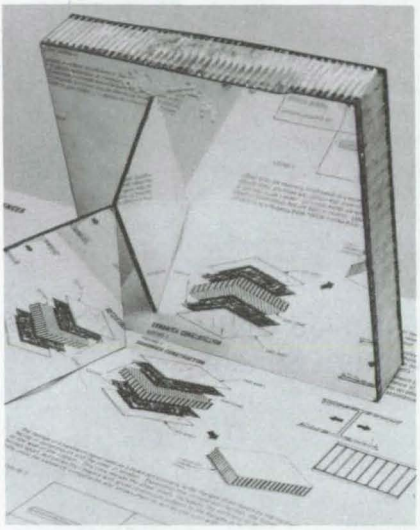

roughened with sandpaper and cleaned with isopropyl alcohol. The smooth surface of the polyester resin is obtained by covering the freshly applied resin with a piece of smooth glass that has been coated with a release agent.
(See page 458.)

Solvent-Resistant Polysulfones

New polysulfones of various molecular weights terminated with trimethylsilylethynyl, ethynyl, and phenylethynyl groups have increased solvent resistance. They are prepared in a technique in which upon the application of heat,

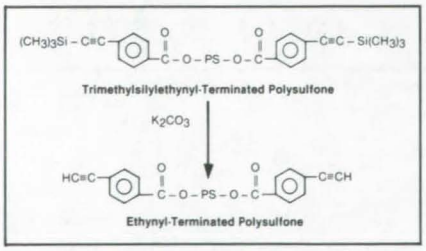

with or without a catalyst, these end groups react to provide cross-linking and chain extensions. The polysulfones are soluble in such solvents as cyclohexanone, chloroform, and N,N-dimethylacetamide. These solutions can be used conveniently for the prepartion of films, coatings, membranes, prepreg, and adhesive tapes. Depending upon the end group density, these materials are processed as adhesives or laminating resins under conditions similar to those of conventional polysulfones. The cured materials are thermoformable and relatively tough.
(See page 401.)

Spool-Valve Pressure-Difference Regulator

A pair of valves maintains a constant pressure difference between two gas streams. Consisting of two connected

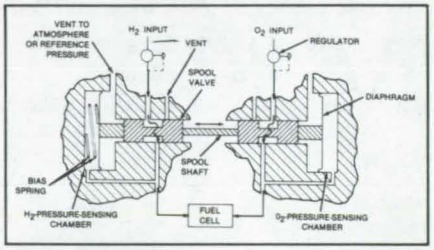

spools that slide in multiport cylinders, the unit was originally developed to regulate the relative pressures of hydrogen and oxygen gases flowing to a fuel cell. The valves allow the gases to be supplied in the quantities required by the electric load while maintaining the proper proportions of the reactants. The simple spool valves, which replace custom-made regulator valves, can be used for gases other than hydrogen and oxygen.
(See page 443.)

Measuring Surface-Shear Stress in Wind Tunnels

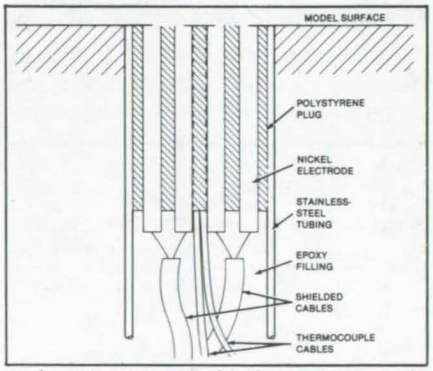

A compact skin-friction gage monitors the mean and fluctuating surface-shear stress beneath the three-dimensional boundary layer of flow in a wind tunnel. The gage measures the heat flux from heated wires embedded in the surface of the wind-tunnel model. The magnitude and direction of the skin friction are deduced from signals from a pair of hot-wire anemometers that maintain the wires at constant temperatures.
(See page 430.)

Electronic Components and Circuits

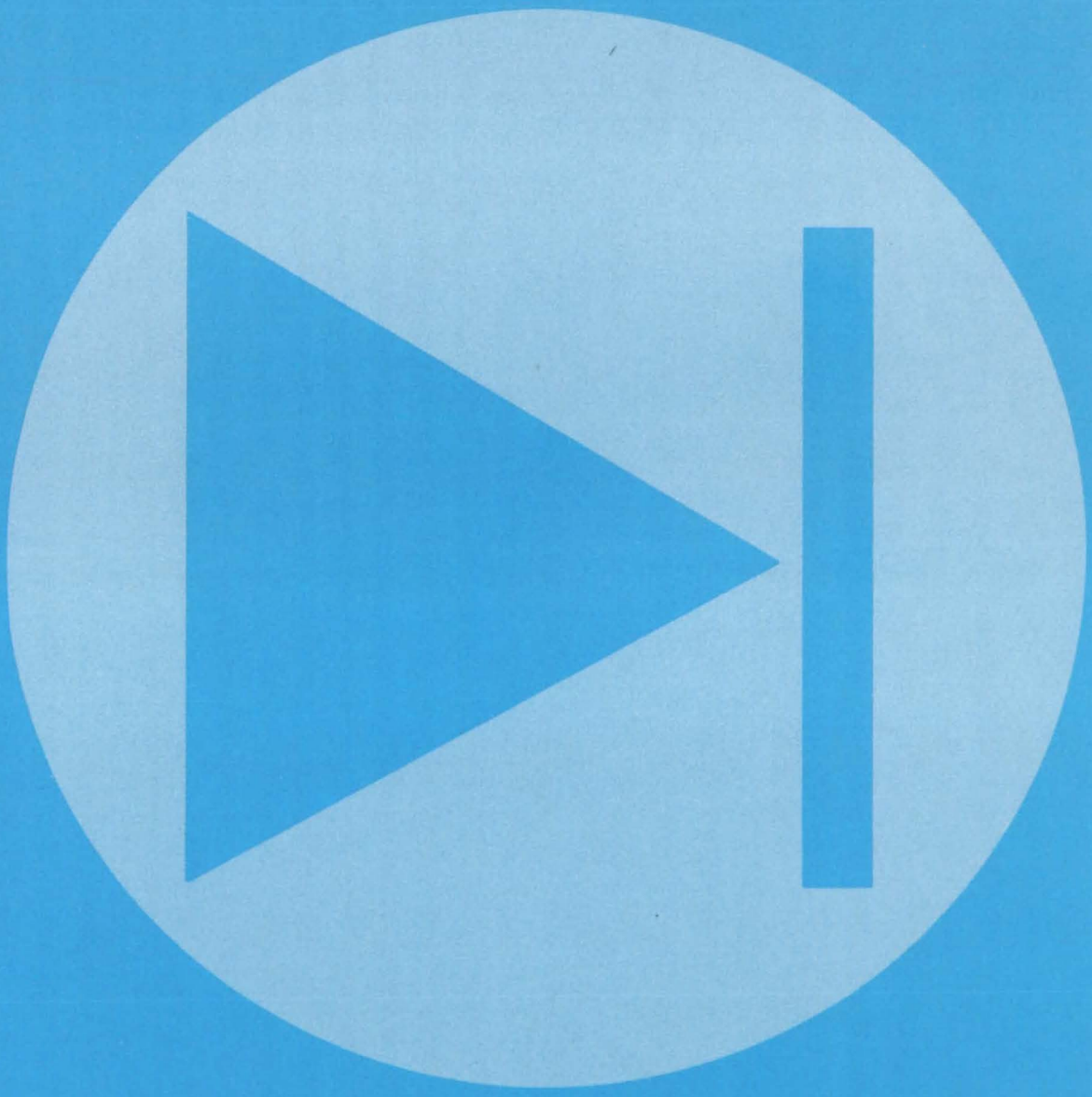

Hardware, Techniques, and Processes

Books and Reports

Digital Single-Phase Power-Factor Controller

Digital circuit has faster response to load changes.

Marshall Space Flight Center, Alabama

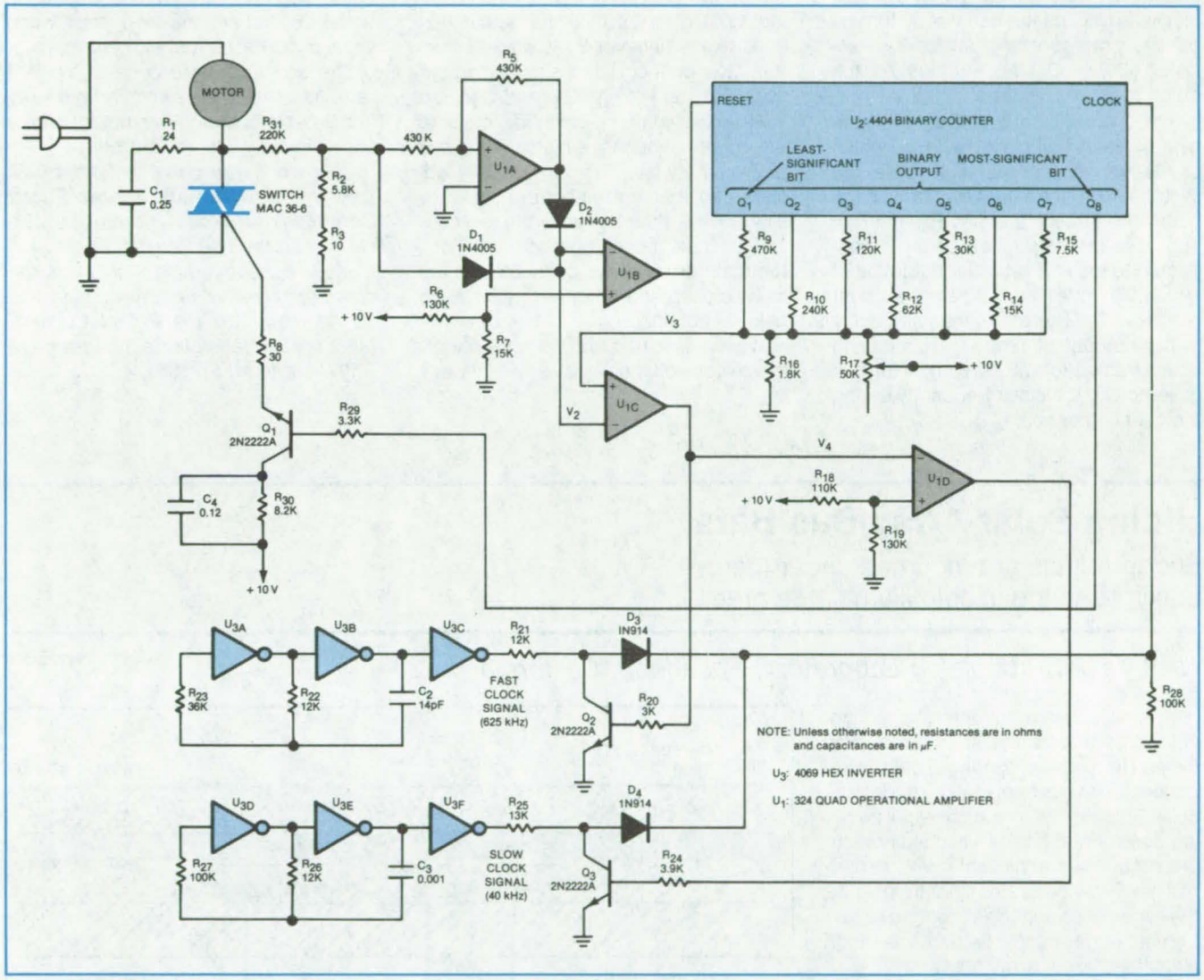

This **Digital Power-Factor Controller** senses changing motor-load torques by sampling the open-circuit voltage across the gate-controlled silicon switch. The circuit responds more rapidly to changing loads than do analog power-factor controllers because there is no low-pass filter in the feedback loop.

Although it is basically an analog circuit, the power-factor controller operates with better response characteristics if digital components are inserted in the feedback portion of the circuit. The changes eliminate several analog elements including an 8-hertz low-pass filter, making the circuit more responsive to sudden load changes — such as those encountered during the application of a clutch. Component aging and environmental changes also pose less of a problem with the new design.

As in other power-factor controllers, the motor current is varied by changing the turn-on time of a gate-controlled silicon switch in series with the motor and input powerline. The feedback is based on the absolute magnitude of the voltage across the switch during the "off" portion of the cycle: This voltage increases with increasing motor load. Since the open-circuit voltage across the switch is sampled at 120 Hz (every half cycle), the digital feedback circuit responds in less than 10 milliseconds to motor-load changes.

The digital feedback circuit includes a binary "up" counter (see figure), the counting rate of which is controlled by the open-circuit switch voltage. As motor torque increases, the counting rate increases, causing the switch to fire earlier in the cycle and conduct additional line current to the motor.

(continued on next page)

U_{1A} and associated components form an absolute-value circuit, into which the scaled switch voltage is fed. U_{3A} through U_{3C} and U_{3D} through U_{3F} constitute two square-wave oscillator circuits that generate clock signals for U_2, a 4404 8-bit up counter. Clock signals 1 and 2 have frequencies of 625 Hz and 40 Hz, respectively. Either of these clocks is fed into the counter by turning off the corresponding switching transistor (Q_2 or Q_3) and turning on the other one.

The counter is reset to 0 at the beginning of each half-cycle by U_{1B}, which drives the reset input high while the switch is on (and the switch voltage below the threshold set by R_6 and R_7). The base of firing transistor Q_1 is connected to the highest-order output bit of U_2, which goes high when the count reaches 128. Therefore, the firing delay is the amount of time U_2 requires to count from 0 to 128, which, in turn, is governed by the clock frequency during the counting period.

The seven lower order bits of U_2 are connected to a digital-to-analog converter network composed of resistors R_9 through R_{16}. R_{17} allows an adjustable dc bias to be applied to the output (V_3) of this converter, which is fed into the noninverting input of comparator U_{1C}. The absolute value of the switch voltage (V_2) is fed into the inverting input of U_{1C}; thus, its output (V_4) goes high whenever V_3 is greater than V_2. V_4 is connected to a switching circuit consisting of Q_2, Q_3, and U_{1D} (an inverter), which feeds the slow clock to the counter when V_4 is high and the fast clock otherwise. R_{17} is generally adjusted so that V_3 is about equal to or slightly less than V_2 while the motor is idling. Thus, under no-load conditions the counter is always connected to the slow clock, and the maximum firing delay is obtained.

If a higher load is applied to the motor, the switch voltage (V_2) rises and initially exceeds V_3, causing the fast clock to be switched in. As the numerical count rapidly increases, V_3 soon exceeds V_2, switching the counter back to the slow clock until 128 is reached and the trigger pulse is fired. Because the average clock rate during the period is higher, the switch is fired earlier than in the idle case, supplying the motor with additional current. At full load, the switch voltage increases further, causing most of the counting to be done at the fast rate. As a result, the switch is fired early in the cycle, allowing the motor to draw approximately full-load current.

This work was done by Richard W. Dabney of **Marshall Space Flight Center.** *For further information, Circle 1 on the TSP Request Card.*

Inquiries concerning rights for the commercial use of this invention should be addressed to the Patent Counsel, Marshall Space Flight Center [see page A5]. Refer to MFS-25861.

Hiding Solar-Array Bus Bars

End terminals are mounted under the cells, maximizing the usable illuminated area.

NASA's Jet Propulsion Laboratory, Pasadena, California

A new scheme for interconnecting cells in commercial solar panels allows the end terminals of a string of cells to be connected to bus bars that run under the cells. This results in a higher cell-packing density and higher silicon-utilization area than was achievable with earlier designs. Previously, the final tabbing at the edges of solar panels required larger frames, larger support structures, and, ultimately, larger array areas.

A portion of a solar panel of the new type is shown in the figure. The negative contact tab is wrapped around the top side of the last cell in a string of cells and connected to a specially-designed circuit board mounted underneath the cell. The board electrically insulates the wraparound tab from the edge and back side of the cell. The positive contact tab runs from the underside of the cell directly to a similar circuit board.

This work was done by William F. Hufnagel of Solarex Corp. for **NASA's Jet Propulsion Laboratory.** *For further information, Circle 2 on the TSP Request Card.*
NPO-15755

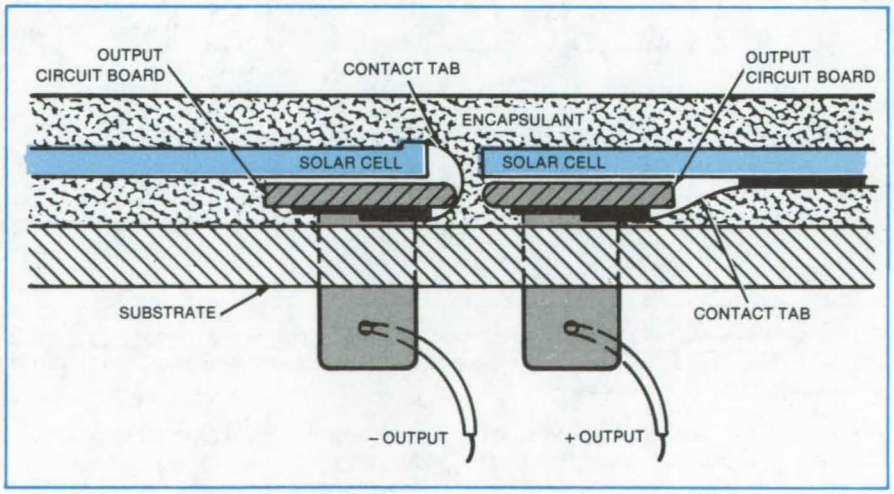

In the Reconfigured Solar Panel the bus bars are placed under the cells, thus reducing the portion of the module area not occupied by active silicon. The underside of the last cell in a string of cells serves as the contact for the positive bus. The negative tab of the last cell in a string is wrapped around from the top of the cell. Tabs are connected to output boards mounted under the cells.

High-Power Switching Transistor

Improved switching transistors handle 400-A peak currents and up to 1,200 V.

Lewis Research Center, Cleveland, Ohio

Large-area high-voltage transistors (D7ST) have been developed for use in advanced power-switching applications. For years the transistor has been the basic building block of low-power electronics while the thyristor has been the workhorse of the electrical power industry. Several years ago, however, a new power-switching transistor, model D60T, was developed and made commercially available [see "High-Speed, High-Power, Switching Transistor, (LEW-13021) on page 320 of *NASA Tech Briefs,* Vol. 3, No. 3] and has opened the door to high-power applications where transistors have previously been impractical. Since the development of the D60T, new high-power versions (D7ST) have been developed for space power applications. Using large-diameter silicon wafers with twice the effective area as the D60T, they form the basis for the D7 family of power-switching transistors.

The new D7ST transistor, shown in Figure 1, is rated on the basis of sustaining voltages of 400 to 600 volts and features a gain/current product of 1,000 to 1,700 amperes. It can handle collector currents of 250 amperes continuously and 400 amperes peak. The high power-handling capability combined with perhaps the largest forward- and reverse-bias safe operating areas of any transistor on the market give extremely rugged, versatile performance in high-energy circuits. In spite of their large size, however, their fast switching speeds (with rise and fall times of about 0.75 microsecond), low saturation voltage (about 1 volt at rated current), and low per-cycle switching losses allow reductions in the size and weight of associated circuit components and promote more efficient use of energy.

The second D7-size transistor with a doubled voltage rating has also been developed for use by NASA in solid-state remote power controllers and is finding applications in industrial 460-Vac motor controllers. This transistor has a collector/emitter sustaining voltage of 1,000 to 1,200 volts and a gain/current product of 250 to 500 amperes. The fast switching speed, the high power dissipation, the large forward- and reverse-bias safe operating areas, and other versatile performance advantages of the D7ST design remain intact in the high-voltage version. In addition, the high-voltage D7 uses the same packages as shown in Figure 1 and the same wafer configuration as the D7ST.

Figure 1. New **High-Power Switching Transistors** come in two package configurations.

The heart of the new D7 transistor family is a 33-mm-diameter, npn silicon wafer that is fabricated using processes and techniques developed for the D60T. The D7 wafer is shown on the top left of Figure 2. Rather than simply scaling up the D60T mask dimensions, three significant innovations and modifications were made to improve the overall performance of the new transistors. These innovations are:

1. An improved base-contact system for decreasing base resistance and equalizing the base/emitter voltage at high currents. The new base insert is shown on the top right of Figure 2.

(continued on next page)

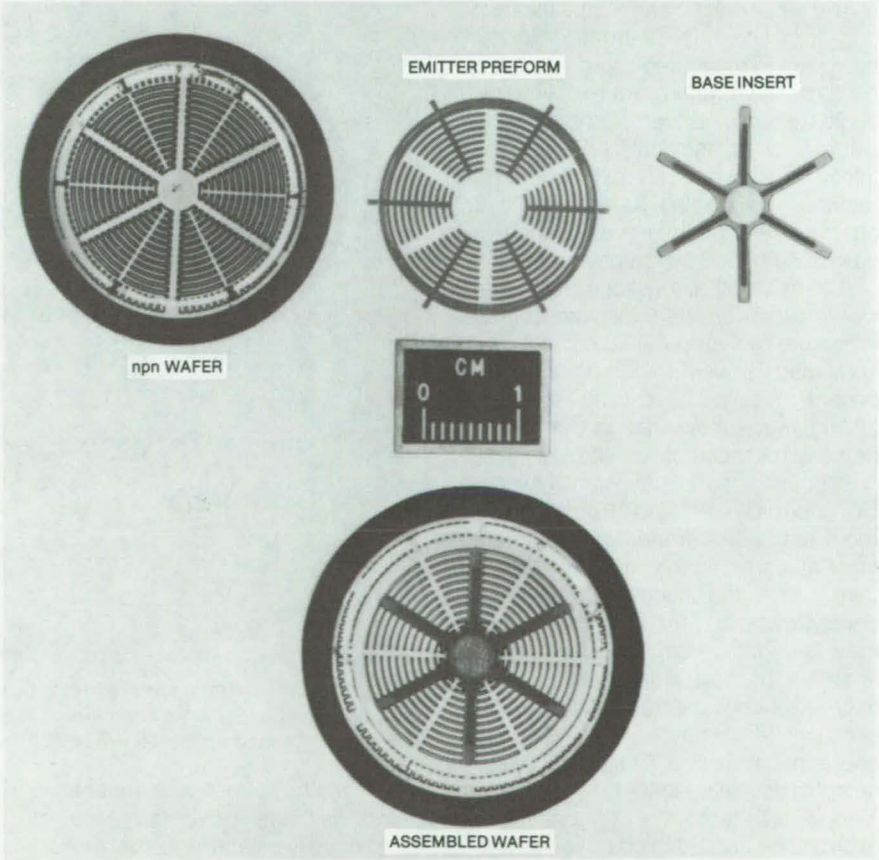

Figure 2. The **Improved Transistor Package** includes the npn wafer, emitter preform, and base-contact insert.

2. An improved emitter-contact preform that increases the silicon area available for current conduction, thereby increasing the power-handling capability. Figure 2 shows the emitter preform at top center.
3. An increase in the amount of interdigitation of emitter and base, permitting a gain-versus-collector-current performance that more closely approximates the ideal case. This increase is made possible by the new base insert and emitter-contact preforms described above. The assembled D7ST wafer is shown at the bottom of Figure 2. The high-voltage D7 transistor does not require the base insert.

In addition to their importance to the D7 transistor family, the three major innovations have some far-reaching consequences. They make it possible to scale up larger wafer sizes (to 50, 75, and perhaps even 100-mm diameters) with power-handling capabilities of several hundred kVa. They also benefit NASA and consumers by: (a) making possible 50-kilowatt and larger power-system converters and power controllers without paralleling transistors; (b) moving into important applications in aircraft power distribution and control; and (c) making high-power, fast-switching transistors available in quantity at reasonable cost.

Some of today's applications for the D7 transistors are: 25- to 50-kilowatt high-frequency dc/dc inverters, VSCF converters, and motor controllers for electric vehicles. Some additional uses are: replacement for thyristors in high-frequency inverters, 100-kW vlf transmitters, 50-kHz RF induction heaters, and power supplies for consumer and industrial applications.

This work was done by P. L. Hower, Y. C. Kao, and D. C. Carnahan of Westinghouse Electric Corp. for **Lewis Research Center.** *Further information may be found in:*

NASA CR-165372 [N81-28353/NSP], "High Current, Fast-Switching Transistor Development" [available only in microfiche for $4.50], and

NASA CR-165547 [N82-18506/ NSP], "High Voltage Power-Transistor Development" [$10 (paper copy)].

Copies of these reports may be purchased [prepayment required] from the National Technical Information Service, Springfield, Virginia 22161.

LEW-13728

Measuring Tension in Transistor Suspensions

Vibration analysis is nondestructive and noninvasive.

NASA's Jet Propulsion Laboratory, Pasadena, California

The tension in tiny filaments that support transistors for thermally isolated operation is measured using laboratory equipment. Vibrations are excited by an audio-frequency driver, observed under a stroboscope, and analyzed by conventional vibration analysis techniques. The method should also be applicable to other filament mounts that are too delicate to be tested by tension probes.

A transistor that must operate in thermal isolation is often suspended in its enclosure by filaments that minimize the conduction of heat to or from the component (Figure 1). Quality-assurance testing must show that the tension is properly balanced on all filaments.

Although a manufacturer may assemble thermally isolated transistors at room temperature and bond each filament at a specific tension, the adhesive that bonds the supporting filaments cures slowly, and the final tension may therefore vary from one filament to another. Tension differences are exacerbated when the transistor is used at very low temperatures. (For example, one application is a 62-channel photodetector operating at 77 K.)

In a vibration test (Figure 2), a microscope is used to observe the transistor in its enclosure while it is illuminated by a strobe lamp. The enclosure is mounted on a plate attached to a driver. As the driver vibrates, the standing-wave pattern is examined for evidence of unbalanced tension. Loose filaments vibrate with unusual standing waves. Correctly balanced units show harmonic motion and a main resonant frequency.

A transistor with correctly balanced filaments is subjected to further testing.

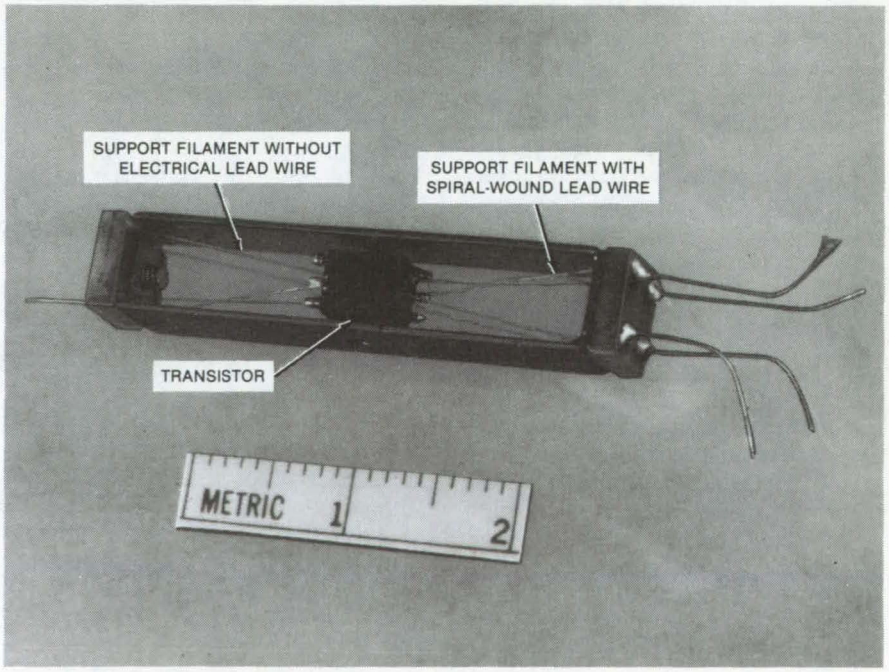

Figure 1. **A Transistor Is Isolated** from the heat (or cold) of its surroundings by filament suspension. The filaments are made of polyester and are (0.005 in.) 0.127 mm in diameter. The transistor lead wires are wrapped around certain of the filaments.

The frequency of vibration is adjusted until the motion appears frozen under the strobe light, thus permitting closer examination.

In one series of tests, filament-mounted transistors typically had resonant frequencies between 420 and 680 hertz. For individual transistors, the characteristic frequency was reproducible within hertz.

The tension on the filament can be calculated by standard equations that relate the resonant frequency, the mass, the driver power, and the physical constants of the filament. The criteria for rejection are established from test data on transistors that have failed after similar testing.

This work was done by William P. Hubbard of Caltech for **NASA's Jet Propulsion Laboratory.** *For further information Circle 3 on the TSP Request Card.*
NPO-15677

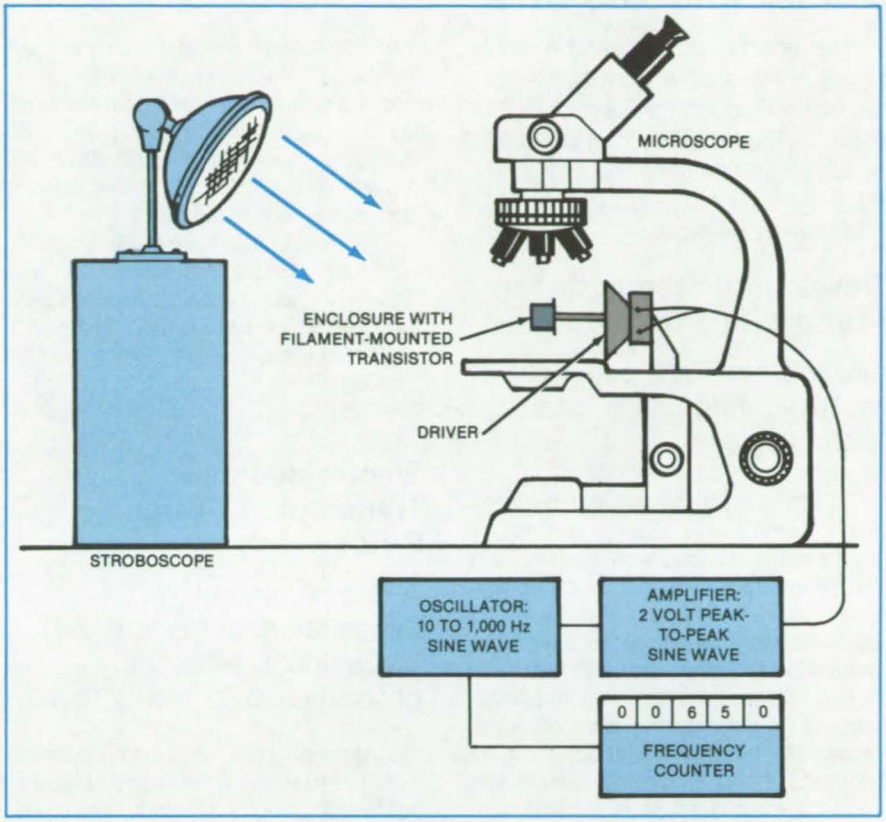

Figure 2. **A Strobe Lamp Reveals** unusual vibration patterns in the filament suspension.

Detecting Solar-Cell Failures

Circuit identifies a malfunctioning photovoltaic array.

NASA's Jet Propulsion Laboratory, Pasadena, California

The logic circuit shown in the figure detects the failure of one solar cell out of a large array of cells in a residential photovoltaic installation. The circuit indicates that there is a failure somewhere in the array, not which cell has failed.

The circuit monitors the normal operation of a photovoltaic array by comparing the voltage supplied to a load by the array to that supplied by a reference photocell. If any one of the cells fails, a comparator energizes a light-emitting diode.

To identify the defective cell, the homeowner photographs the array using infrared film in a 35-mm camera. A shorted cell appears on the film as a bright spot on a comparatively dark background.

This work was done by Timothy J. Maloney of AIA Research Corporation for **NASA's Jet Propulsion Laboratory.** *For further information, Circle 4 on the TSP Request Card.*
NPO-15741

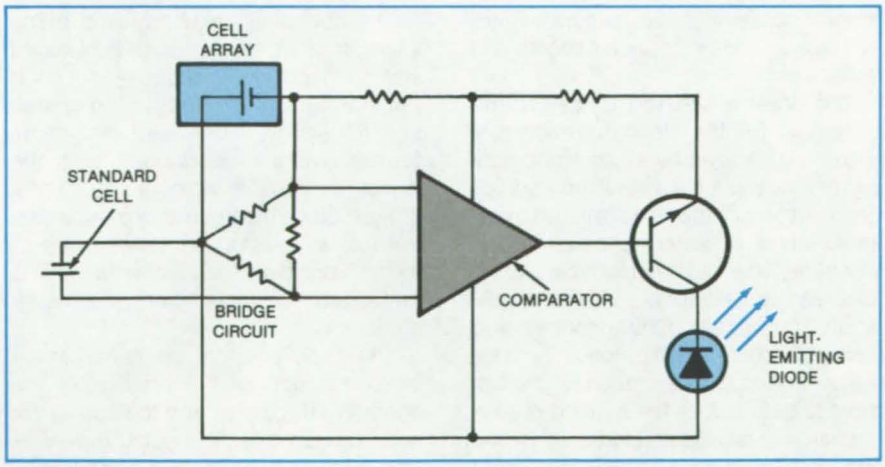

This **Cell-Failure Detection Circuit** compares the output of a photovoltaic array to that of a control cell. If any of the modules fails, it activates the light-emitting diode. If desired, the circuit could also sound an alarm.

Books and Reports

These reports, studies, and handbooks are available from NASA as Technical Support Packages (TSP's) when a Request Card number is cited; otherwise they are available from the National Technical Information Service.

Developing Standards for Photovoltaic Devices

Ground rules are outlined for evaluating photovoltaic technology.

Guidelines for developing performance criteria and test standards for photovoltaic devices and systems are described in a NASA/DOE report. Differences in terminology, testing methods, reporting conditions, and expectations of performance and reliability have begun to hinder the research and development of photovoltaic technology. In response to these difficulties, the methods and criteria suggested in this report are intended to facilitate standardization for the benefit of designers, distributors, builders, and users of photovoltaic devices and systems.

To achieve significance as renewable energy sources, photovoltaic systems must be able to replace nonrenewable electrical-energy sources. Standard criteria, test methods, and documentation relating to photovoltaic system performance will accelerate commercialization. Performance criteria and test standards will assist in the establishment of a technical basis for procurement and evaluation programs for systems, subsystems, components and materials.

The interim performance-criteria document for the standardization program is organized by system and subsystem (for example, by cell or module). Each section of the document addresses a number of performance attributes: electrical, thermal, mechanical, structural, safety, reliability, durability, installation, operation, maintenance, and building and site. Each criterion includes the user need or expectation for the element and describes the method of test.

Examples of issues addressed by the interim performance-criteria document include the following: terminology — definitions for such terms as "array," "panel," and "module"; cell-contact metalization integrity — the mechanical strength of connections under stress; and module thermal characterization — the effect of temperature on cell performance. The compilation of criteria and test methods is a technical resource for the photovoltaic industry that will evolve to meet changing needs. It will provide a basis for the generation of consensus-type standards.

This work was done by Alan R. Hoffman, Ronald G. Ross, Jr., and Steven H. Gasner of Caltech for **NASA's Jet Propulsion Laboratory.** *To obtain a copy of the report, Circle 5 on the TSP Request Card.*
NPO-15734

Electronic-Power-Transformer Design Guide

A compilation of information on design procedures, electrical properties, and fabrication

A design guide has been written to assist in the design and construction of lightweight, high-efficiency, and high-reliability space-type electronic power transformers. The design guide provides information on design procedures; magnetic and insulating-material electrical properties; and impregnating, encapsulating, and processing techniques.

The specific transformers investigated had output ratings of 1.1 kV at 2,620 VA and 10 kV and 15 kV at 500 VA. Both encapsulated and nonencapsulated coil constructions were investigated. Operating frequencies up to 40 kHz were used in the designs.

The operating frequency is of prime importance in the design of lightweight and high-efficiency space-type power transformers. In general, as the operating frequency increases, the transformer weight decreases; but the losses, particularly the core loss, can increase. Since the frequency plays a central role in the tradeoff between transformer weight and efficiency, its effect is investigated in some detail in this design guide.

The output power of a transformer is a linear function of the product of the operating frequency and the core magnetic flux density. The output power is also a linear function of the product of the core window area and cross-sectional area. The transformer weight is dependent on the dimensions of the core window area and cross-sectional area. Thus, for a specified output power, the transformer weight can be decreased by an increase in the frequency/flux density product.

The operating flux density of ferromagnetic core materials is limited to their saturation flux density. In general then, an increase in the frequency/flux density product requires an increase in the operating frequency.

While the transformer power output is a linear function of the frequency/flux density product, the specific core loss is a nonlinear function of this product. Thus, and improper choice of frequency and flux density can lead to higher core losses and hence lower transformer efficiency. By taking experimental specific core loss data and plotting them as a function of the frequency/flux density product with frequency as the parameter, a family of curves is generated from which the effect of the frequency/flux density product on the specific core loss is determinable. The plotting of specific core loss curves in this manner clearly illustrates that for a given frequency/flux density product, the specific core loss decreases as frequency increases. Therefore, the proper choice of frequency can lead to reductions in both transformer weight and loss.

The transformer design sequence is as follows:

1. Selection of Core Material;
2. Preliminary Calculation of Core Dimensions;
3. Selection of Insulating Materials, Including Magnet Wire Insulation, Coil Forms, and Layer and Interwinding Insulation;
4. Coil Design:
   - Calculation of Wire Size and Number of Turns and Layers,
   - Establishment of Margins, and
   - Establishment of Thickness of Layer and Interwinding Insulation;
5. Calculation of Copper Losses, Core Losses, and Efficiency;
6. Calculation of Temperature Rise; and
7. Optimization of Design With Change in Core Selection or Coil Design as May Be Necessary To Meet Specifications.

This work was done by G. E. Schwarze of **Lewis Research Center** *and J. C. Lagadinos and J. F. Ahearn of MagCap Engineering, Inc. Further information may be found in NASA CR-134992 [N78-29353/NSP] "Design of Space-Type Electronic Power Transformers" [$17.50]. A copy may be purchased [prepayment required] from the National Technical Information Service, Springfield, Virginia 22161.*
LEW-13208

Electronic Systems

Hardware, Techniques, and Processes

Microcomputer Multiplexes Alphanumeric Labels on CRT's

External, low-power alphanumeric label generator eliminates costly video circuitry.

Lyndon B. Johnson Space Center, Houston, Texas

A cathode-ray-tube (CRT) control system generates and multiplexes alphanumeric characters with continuously-varying analog waveforms. Designed to display simultaneous electrocardiogram waveforms with vital sign digital displays, the system generates vertical, horizontal, and intensity control signals to the CRT and adapts to most CRT equipment.

The display of each alphanumeric character is formatted in a 5-by-7 dot matrix and generated by a ramp-raster technique. Although similar CRT displays are based on this technique, the application of an independent, low-power microprocessor with simple user programing and peripheral control circuits to a CRT display control system is unique. Advantages of this control system include low power consumption, insensitivity to power-supply variations, wide adaptability, and relatively simple circuits and programing.

All software and display data are stored in system memory: This includes the electrocardiogram (ECG) waveform data, patient status data, and a complete set of alphanumeric character data. The stored program in the microprocessor EPROM (erasable programable read-only memory) controls the entire CRT system operation. ECG data constantly flowing through the ECG memory are multiplexed with the alphanumeric character information (see figure), which resides in the microprocessor EPROM. The software consists of an initialization routine, the main program, a display update subroutine, and a display interrupt service routine.

A CRT horizontal sweep control signal is generated by the ECG memory control each time the analog ECG signal input is sampled (at 240 samples/s). In addition, the ECG memory control initiates sequential CRT display control by its INTERRUPT signal: The INTERRUPT signal instructs the multiplexer to select an analog or alphanumeric display. A ramp signal is selected along with an intensity signal for an alphanumeric display.

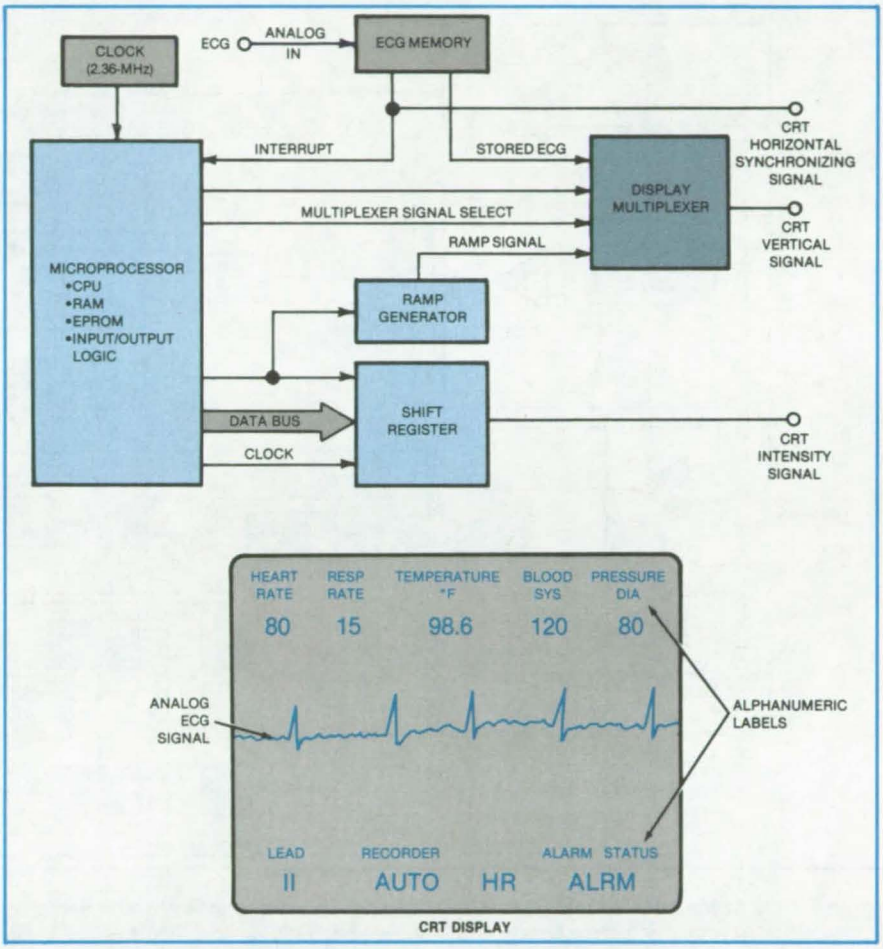

This **Microprocessor-Based System** for multiplexing alphanumeric and analog data stores both program and data. It uses inexpensive circuits, consumes minimal current, is programable by the user, and adapts to many CRT monitors. The system generates 5-by-7 dot-matrix characters. A representative CRT display is illustrated below.

When an analog data selection is made, data flow directly from the ECG memory into the multiplexer.

A vertical-deflection-control signal is derived from the dual multiplexer under microprocessor control. The multiplexer selects either the analog data or a ramp signal, which, in combination with a switched intensity signal, generates a dot-matrix character on the CRT.

Although the CRT control system described displays 2 rows of 20 characters, the configuration can be modified by appropriate user reprograming. Thus, changes in monitor operation or display format can be implemented by a software change.

Overall system speed is adequate for medical monitoring purposes. High-speed applications may require substantial design changes.

This work was done by Tommy Cooper of Narco Scientific for **Johnson Space Center.** *For further information, Circle 6 on the TSP Request Card.*
MSC-20079

NRZ Data Asymmetry Corrector and Convolutional Encoder

Circuit compensates for timing, amplitude, and symmetry perturbations.

Lyndon B. Johnson Space Center, Houston, Texas

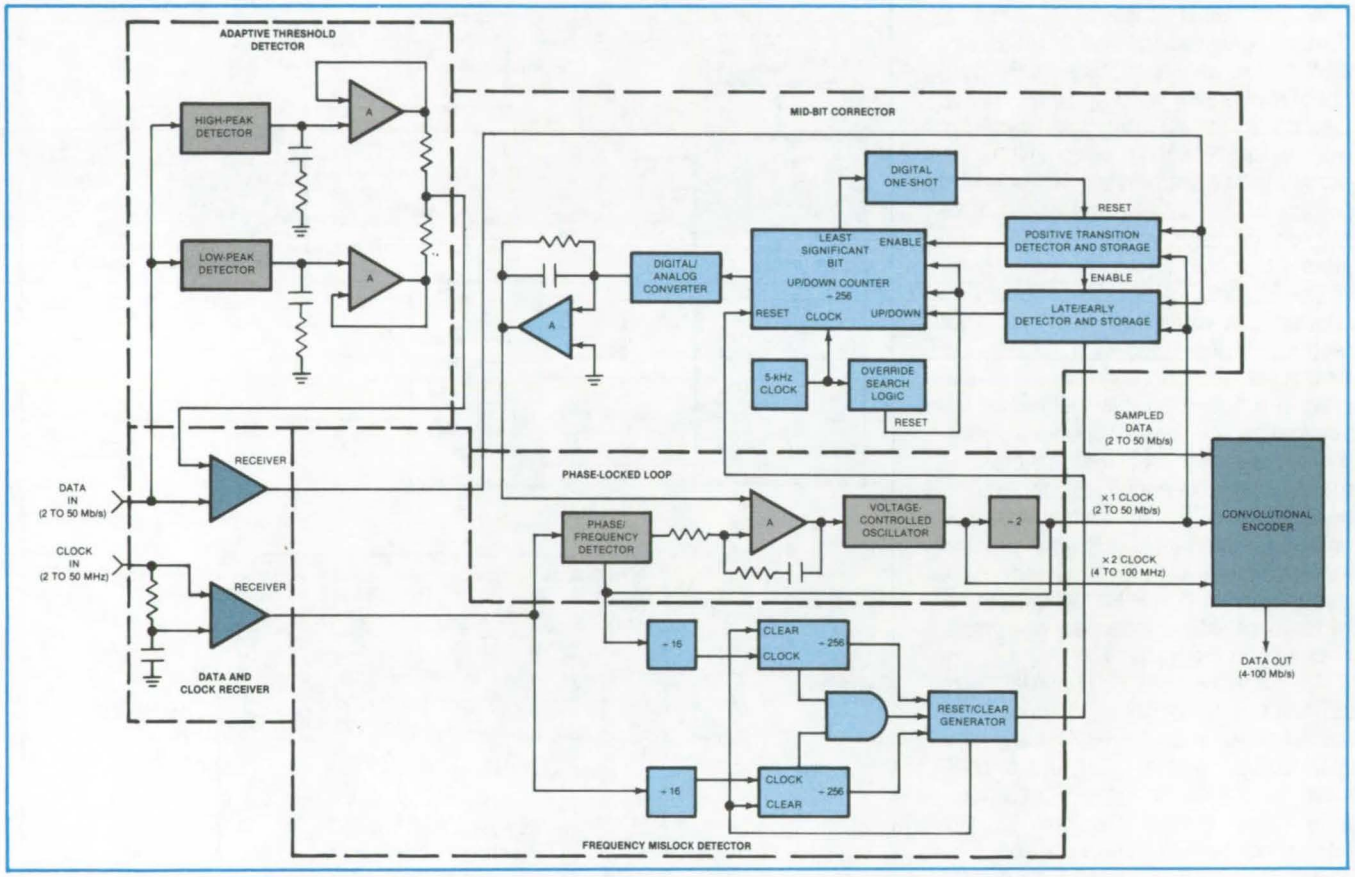

Figure 1. **Data Asymmetry Corrector and Convolutional Encoder** regenerate data and clock signals in spite of signal variations, such as data or clock asymmetry, phase errors, and amplitude variations, and then encode the data for transmission.

A system using an asymmetry corrector circuit with a convolutional encoder receives NRZ-L-M-S data (nonreturn-to-zero data in level, mark, or space convention) and clock signals at rates of 2 to 50 megabits per second; compensates for signal variations, such as data and clock asymmetry, phase errors, and amplitude variation; and convolutionally encodes the data for transmission at 4 to 100 Mb/s. The system was extensively tested using data and clock signals simulating "worst-case" timing.

The asymmetry corrector circuitry, which processes the input data and clock signals, comprises five major parts (see figure):

1. Data and Clock Receivers,
2. Adaptive Threshold Detector,
3. Phase-Locked Loop (PLL),
4. Mid-Bit Corrector, and
5. Frequency Mislock Detector.

The regenerated data stream and clock signal and a ×2 clock signal (4 to 100 Mb/s) generated by the PLL drive the convolutional encoder. The PLL is continuously phase-positioned relative to the data to counteract the effects of input signal variations.

The adaptive threshold detector generates a dc reference voltage centered between the two input logic levels. This reference is used by the data receiver to minimize input asymmetry. The mid-bit corrector adjusts the phase of the regenerated clock until the rising edges of clock and data coincide. The signal is then sampled at mid-bit to minimize bit-reading errors.

A dc feedback voltage generated in the mid-bit corrector is summed with the phase/frequency detector output by the PLL integrator, which in turn drives the voltage-controlled oscillator (VCO) producing the two clock signals. The feedback voltage depends on the results of a clock/data phase comparison made by the late/early detector. Depending on the result of the comparison, a modulo-256 up/down counter is incremented, which in turn drives a digital-to-analog converter to produce the final feedback voltage. Additional circuitry prevents the up/down counter from being incremented too rapidly under certain conditions.

The mid-bit corrector includes an override search function to ensure the detection (during acquisition time) of data patterns consisting of only narrow pulses of one bit period or less. During normal operation, positive data transitions occur at least once every 2 milliseconds, in which case the override search logic is continuously inhibited.

A frequency mislock detector monitors false frequency-lock conditions of the PLL. Such a condition can occur when a phase offset between input and output frequencies is being commanded by the dc control voltage from the mid-bit corrector, concurrent with a step change in input frequency or an on/off cycling of the circuit power.

The regenerated data are encoded by the convolutional encoder using the algorithm diagramed in Figure 2. The sampled data are clocked into the 31-bit serial shift register by the ×1 clock. Six taps from this register are fed to two modulo-2 adders. Each of the adders has one unique and four common inputs. (The unique input to adder G_2 is inverted to obtain the inversion shown in the output line.) The output from each adder is fed to the input of a 5-bit shift register and is clocked in by the ×1 clock. The registers are loaded for five ticks of the ×1 clock, and then the contents of both registers are transferred in parallel to the 10-bit output shift register and then clocked out serially by the ×2 clock.

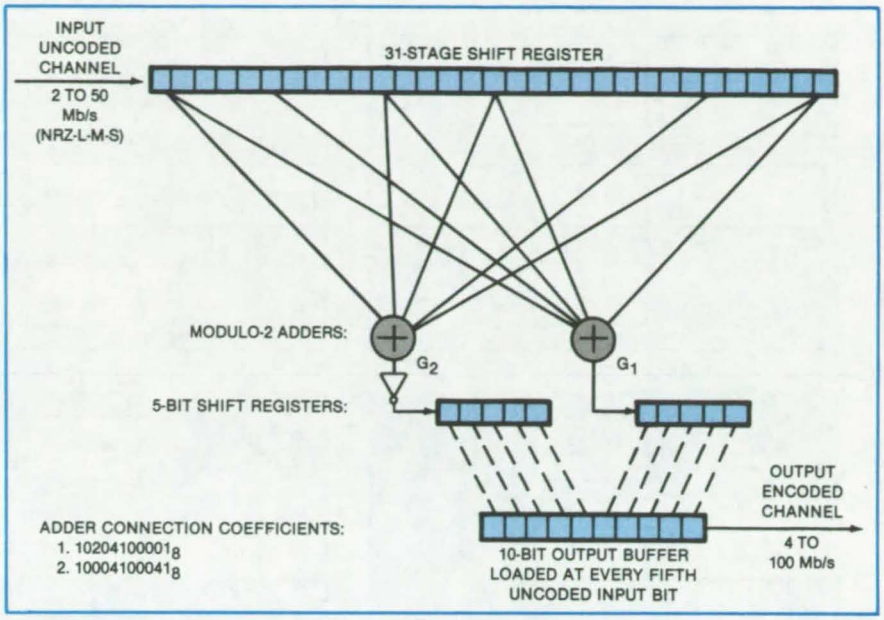

Figure 2. The **Convolutional Encoder** processes the corrected data by using the algorithm shown.

This work was done by Harold J. Pfiffner of Hughes Aircraft Co. for **Johnson Space Center.** *For further information, Circle 7 on the TSP Request Card.*

Inquiries concerning rights for the commercial use of this invention should be addressed to the Patent Counsel, Johnson Space Center [see page A5]. Refer to MSC-20187.

Linking "Smart" Modules by a Single Channel

System architecture brings order to a potentially chaotic situation.

NASA's Jet Propulsion Laboratory, Pasadena, California

A new configuration allows many "smart" modules (each containing memory and a microprocessor) to be linked by a common data channel. The architecture allows each module to carry on its own operations at its own data rate within a block of time, while communications between modules occur in strict synchronism.

Because smart modules process their own data to a limited extent, they reduce the quantity of data that must pass between modules. In spacecraft, for example, the modules (usually sensors and instruments) reduce the traffic load on the telemetry and uplink/downlink systems. However, the autonomous nature of the modules can create chaos if they must use a common data channel, such as a radio link or data bus, and must communicate with each other. Because communication delays between Earth and spacecraft stations are long, order must be maintained automatically, but the exchange of data must not be unduly slowed down. Long pauses between data packets must be avoided.

The new system employs two data and command buses for redundancy (see figure). Bus 1 is controlled by its own high-level module. A memory in the high-level module contains tables that determine the routing and priority of data packets. A bus controller sends the address header of each packet out on the bus (the header describes the source and receiver modules for that packet). Immediately thereafter, the bus controller extracts data packets from the source bus adapter and places them on the bus for the recipient adapter. Incoming data are stored for buffering and are unloaded during the next available time interval.

The bus operates on a time-shared basis. There are designated time intervals for uplink commands, for data transfers between modules, and so forth. There is no possibility of data collisions; only one data packet is permitted on the bus at any given moment.

Bus 2 is controlled similarly by its own high-level module. Thus, loss of a high-level module does not leave the system totally disabled.

Between the two buses are bulk-memory modules, which extend the storage capacity of the smart modules as necessary. Certain bulk-memory adapters are connected to both buses, thereby allowing bus-to-bus communication. A data packet can be unloaded from one bus during a timeslot and transferred to the other bus during the next timeslot.

(continued on next page)

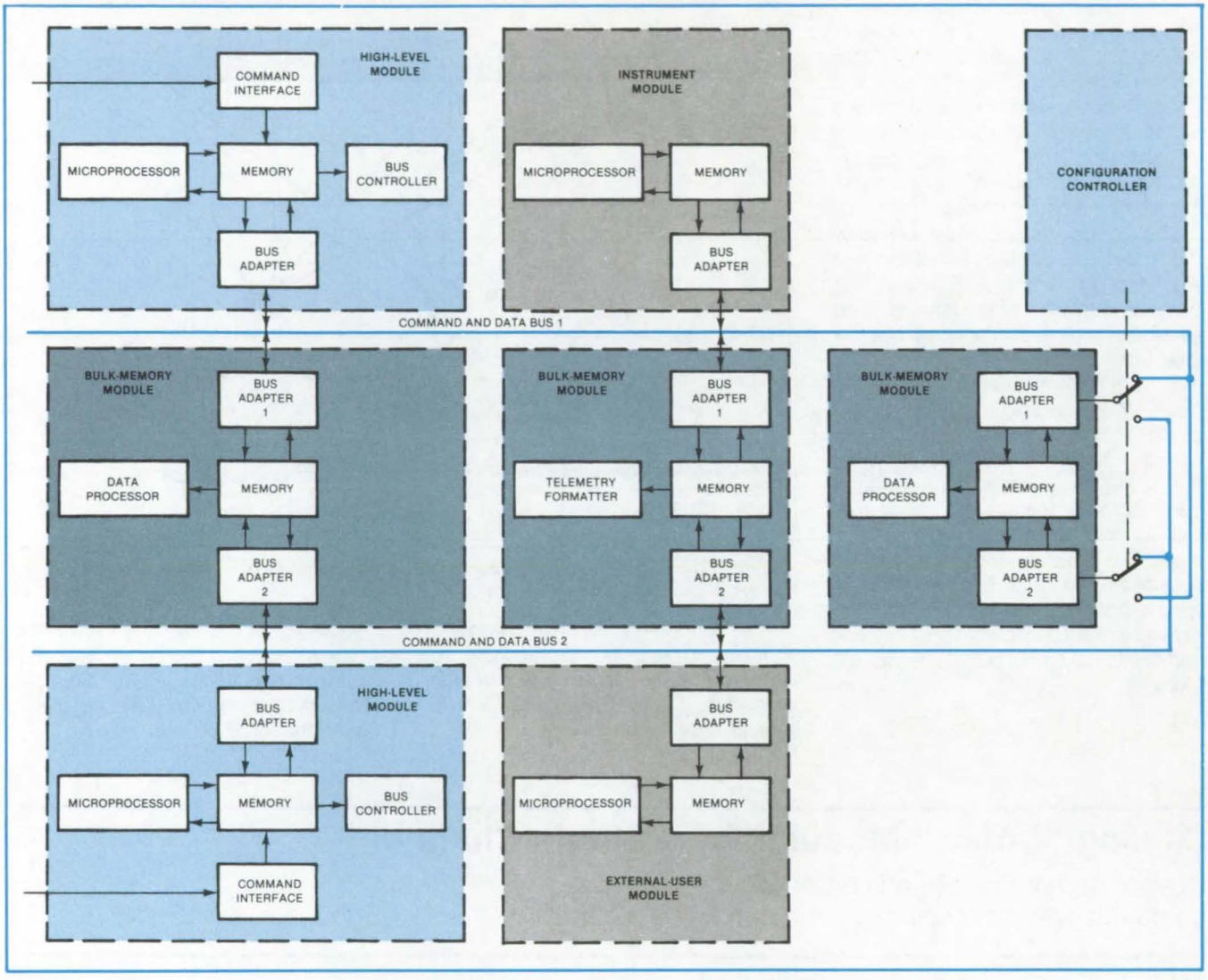

Bus Adapters Are a Key element in distributed multiport memory, offering synchronized and coordinated communication over a common link. The boxes to the right of the high-level modules represent sensors, instruments, and the like, each having its own memory and data-processing capability. They, like the high-level modules, are connected to the buses by bus adapters, which provide buffering and isolation.

Some of the modules (e.g., the high-level and bulk-memory modules) also have time-shared memory access for their different internal functions. Each function has a different memory port with access scheduled according to the maximum demands of the specific function. In the high-level module, the microprocessor port is given every other memory-access opportunity, while the command interface, bus controller, and bus adapter ports are each given access once each 10 opportunities. This brings order to the internal functions of a module and allows internal interactions to be scheduled at a high level in the same manner the bus schedules the external interactions. Since the memory becomes the central focus of a module, the modules and buses together comprise a distributed multiport memory system.

The entire system is synchronized at 15 pulses per second by a real-time interrupt (RTI) pulse. Between RTI pulses, internal data transfers are made while the various off-bus data processes take place. In most cases, the interval between RTI pulses is long enough to ensure that processing has finished and that the modules are ready to exchange data. However, in some cases, such as in formatting certain telemetry signals, computations cannot be finished within one or even several RTI pulse intervals. In such cases, processing continues until it is finished, and the module waits, idling until the next RTI pulse makes a data packet available. Careful choice of an RTI interval can minimize idling.

This work was done by Wayne H. Kohl of Caltech for **NASA's Jet Propulsion Laboratory.** *For further information, Circle 8 on the TSP Request Card.*

This invention is owned by NASA, and a patent application has been filed. Inquiries concerning nonexclusive or exclusive license for its commercial development should be addressed to the Patent Counsel, NASA Resident Office-JPL Center [see page A5]. *Refer to NPO-15342.*

Radar for Mapping Sea Ice

X-band system would have 100-m^2 resolution.

NASA's Jet Propulsion Laboratory, Pasadena, California

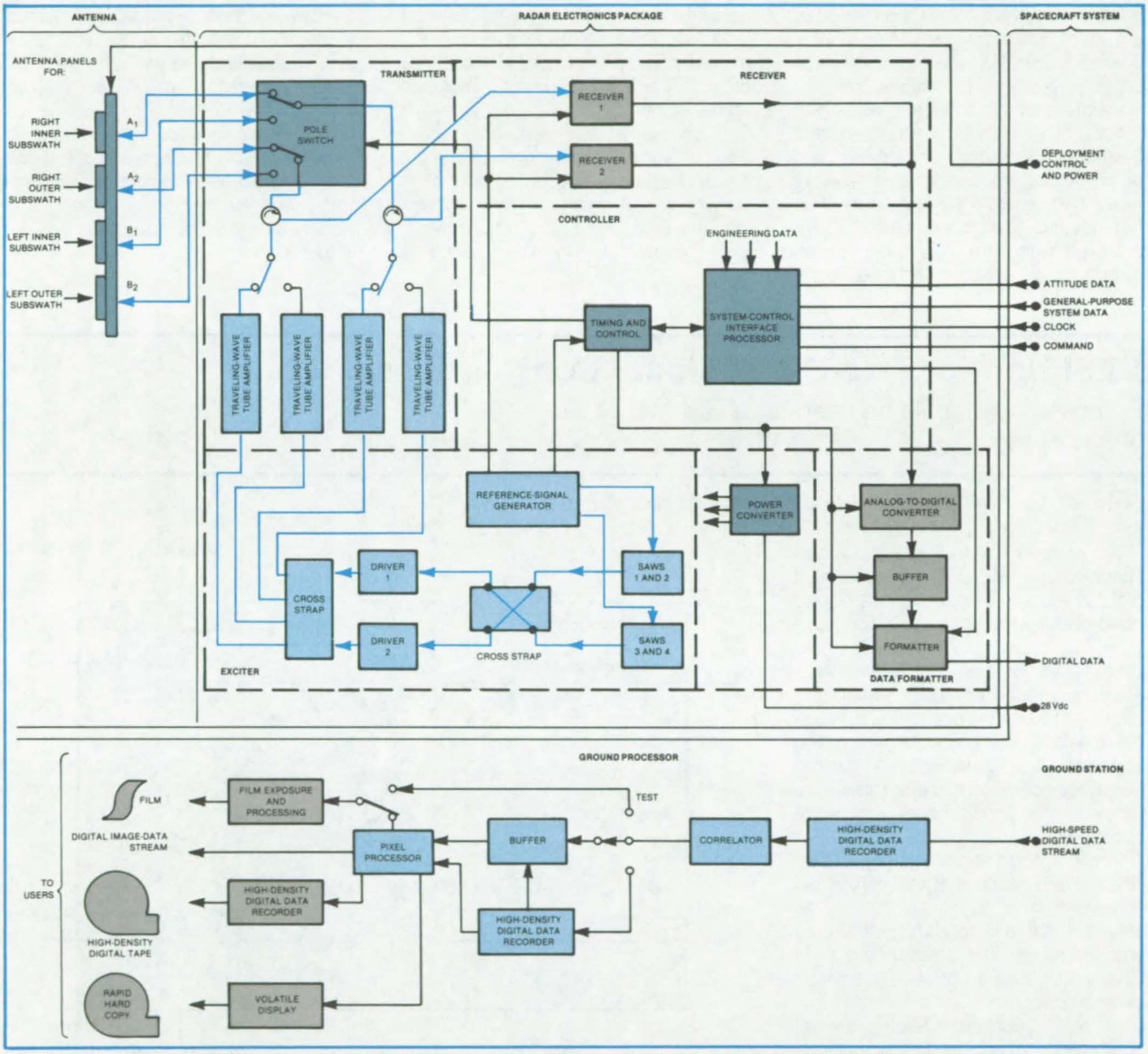

The **Wide-Swath Imaging Radar** is of the synthetic-aperture type. It transmits signals to a ground station for subsequent processing into imagery. Subsystems on the spacecraft are shown at the top. The ground-based analysis system is shown below.

A concept for a spaceborne synthetic-aperature radar (SAR) meets the functional requirements for continuously mapping sea ice in the north and south polar regions. The design is an outgrowth of existing SAR's operated from aircraft and spacecraft and should interest those involved in the design and use of such radar systems.

The radar would operate in the X-band (9.6 GHz) from a satellite in a 700-km near-polar orbit. It would provide high-quality imagery over a continuous-swath 360-km width with 100- by 100-m picture elements (pixels) and a 23-dB dynamic range. An alternate high-resolution mode would provide 25- by 25-m pixels over a selectable 90-km portion of the swath. The 360-km swath width would allow complete polar coverage above 60° latitude every 2 days.

A block diagram of the proposed system is shown in the figure. The dual left- and right-looking antenna and the radar sensor are flown on the satellite. An onboard high-density tape recorder

(continued on next page)

and a data channel using a communications satellite would link the spacecraft with the analysis equipment on the ground. A digital correlator and a pixel processor, both located on the ground, would prepare film images and data tapes in the formats required by users.

The system operates as follows: Upon command from the controller, a frequency-modulated pulse is generated by a surface-acoustic-wave (SAW) device. There are four SAW lines, each of which provides a signal for one of the four possible subswath and resolution modes. The signal is amplified and frequency-translated to X-band and amplified by a pulsed traveling-wave tube. Two amplifiers are pulsed alternatively to illuminate two 180-km subswaths in turn. The pole switch allows the selection of either antenna pair on the two sides of the spacecraft to image the desired polar region. The radiated power is approximately 2.5 kW peak (70 W average).

In the receiver, the return echo is amplified and down-converted with spectrum inversion to the SAW line intermediate frequency and range-compressed by an SAW line. The signals are then translated in frequency to range-offset video, digitized, stored in a buffer, formatted, and tape-recorded at 19.8 Mbps or 26.7 Mbps in the low- or high-resolution mode, respectively.

Subsequently the data are played back at high rate to the ground station. There the data are recorded on a high-density digital recorder for playback into the data correlator, which generates the raw imagery. The raw image data are recorded on tapes for transfer to the pixel processor.

The pixel processor combines output from two separate subswaths to produce the full 360-km range lines, performs resampling in range to convert from slant range to ground range and to obtain 100-m pixels, and provides radiometric correction. As they are produced, the data are recorded on tape and film at a rate of 270 kilobytes per second. Each byte corresponds to the reflectivity (at 3-cm wavelength) of a 100-m^2 region on the sea.

This work was done by Frank T. Barath and Rolando L. Jordan of Caltech for **NASA's Jet Propulsion Laboratory.** *For further information, Circle 9 on the TSP Request Card.*
NPO-15350

VLSI Unit for Two-Dimensional Convolutions

Proposed chip could be used for a variety of functions.

NASA's Jet Propulsion Laboratory, Pasadena, California

A proposed very-large-scale integrated-circuit (VLSI) chip would be a building block in a computer to perform rapid two-dimensional cyclic convolutions. Calculations of this type are essential to image-processing synthetic-aperture radar and digital-signal processing. The new system would implement a fast polynomial transform and eliminate the complicated matrix-transpose operation that must otherwise be performed in fast-Fourier-transform techniques.

The increased speed and circuit density and decreased cost that very-large-scale integration offers can be realized only if suitable algorithmic structures can be found. The structures should have a high degree of parallelism and geometric regularity.

In the proposed system, a fast polynomial transform technique has been extended into a tree computational structure composed of two units: a fast polynomial transform (FPT) unit and a Chinese remainder theorem (CRT) computation unit. A universal VLSI chip architecture enables the same type of chip to be used for both the FPT and CRT units. The chips could also be cascaded to form a long serial memory.

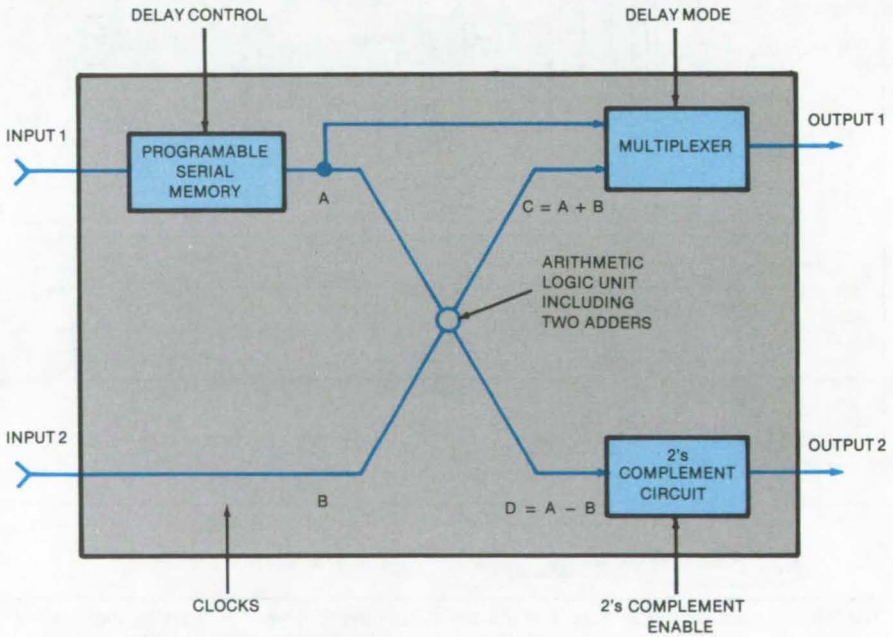

A **Universal Logic Structure** allows the same VLSI chip to be used for a variety of computational functions required for two-dimensional convolutions.

The proposed VLSI chip (see figure) can be operated in four distinct modes. In the delay mode, the chip behaves like a programable delay line. The amount of delay is controlled externally. For example, random-access memories can provide delay-control signals through their address control. In the delay mode, the output of the chip is taken from the on-chip serial memory and fed to the next chip.

In the FPT mode, the chip is operated as an FPT "butterfly" unit. In the CRT mode, the chip acts as part of a CRT computation circuit. Two chips are required for each CRT unit. In the polynomial modulo mode, the chip acts as a modulo-P circuit (where P is a parameter related to the dimensionality of the matrix).

This work was done by Kuang Y. Liu of Caltech for **NASA's Jet Propulsion Laboratory.** *For further information, Circle 10 on the TSP Request Card.*
NPO-15224

Circuitry for Angle Measurements

An angle resolver is pulsed and read under microprocessor control.

Marshall Space Flight Center, Alabama

An electronics package for a shaft-angle measurement system features a resolver, a high-speed data-acquisition system, and a microprocessor. It is suited for such applications as rate tables, robots, antenna direction controllers, and machine tools.

The microprocessor triggers the pulse generator (see figure), causing it to energize the resolver. The microprocessor then quickly reads the resolver sine and cosine windings with the aid of the data-acquisition system. The sine winding is read first, then the cosine winding; then the sine winding is read a second time. Both sine values are used in the calculations to eliminate the effect of a slope in the winding-output voltages. The microprocessor calculates the ratio of sine to cosine to obtain the tangent, then calculates the arc tangent to obtain the principal value of the angle. From the polarities of the sine and cosine voltages, the quadrant is determined, and the complete value of the angle is then known.

Each pulse-generator output pulse has two rising slopes. The first (higher) slope is adjusted to prevent the resolver from ringing. The second (lower) slope is selected so that the sine and cosine outputs are as nearly constant as possible while they are being read.

The pulse technique can be used with a three-phase synchro transformer as well as with the two-phase resolver described above. It is necessary only to change the output phase angle from 120° to 90°. A resistor network is used to provide the requisite phase shift. The pulse technique can also be applied to multispeed resolvers. Coarse and fine windings are pulsed together. From the fine sine and fine cosine and the coarse sine and coarse cosine, the fine and coarse angles are calculated. The true angle is calculated from the fine and coarse values, from the resolver speed, and from the part of the resolver cycle the device is in at the time of measurement.

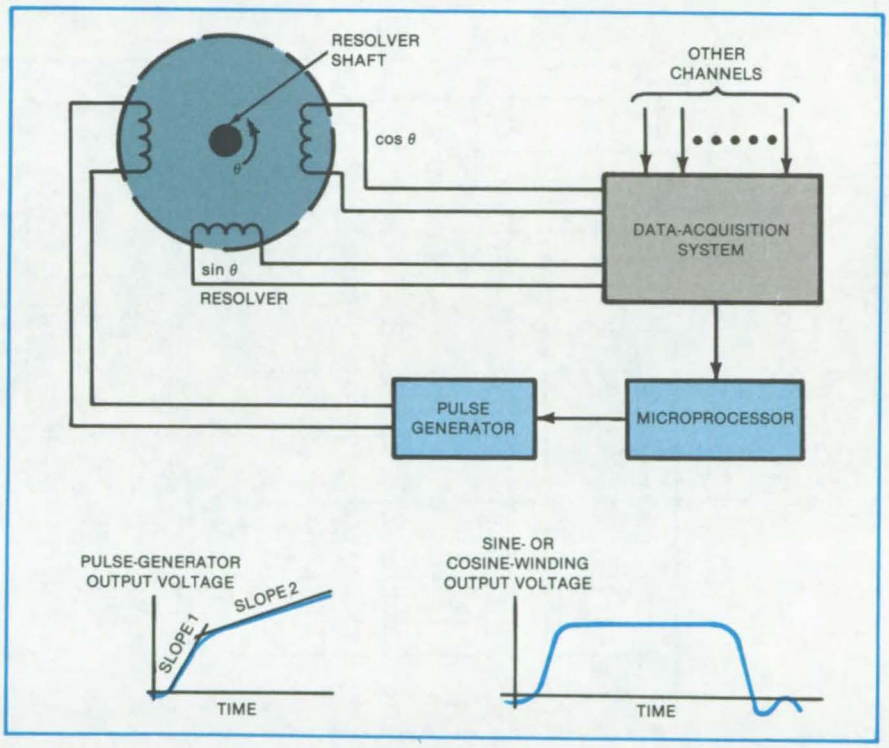

Under Microprocessor Control, the pulse generator excites the resolver windings with a dual-slope pulse as shown in the inset. The data-acquisition system sequentially reads the sine and cosine windings. From the readings, the microprocessor determines the angle θ through which the resolver shaft has turned from the reference (zero) angle. The microprocessor and data-acquisition equipment can be used in a system of many resolvers.

This work was done by James R. Currie and Ralph R. Kissel of **Marshall Space Flight Center.** *For further information, Circle 11 on the TSP Request Card.*

Inquiries concerning rights for the commercial use of this invention should be addressed to the Patent Counsel, Marshall Space Flight Center [see page A5]. Refer to MFS-25825

Measuring Power Flow in Electric Vehicles

Instrument accommodates switching transients and common-mode voltages.

NASA's Jet Propulsion Laboratory, Pasadena, California

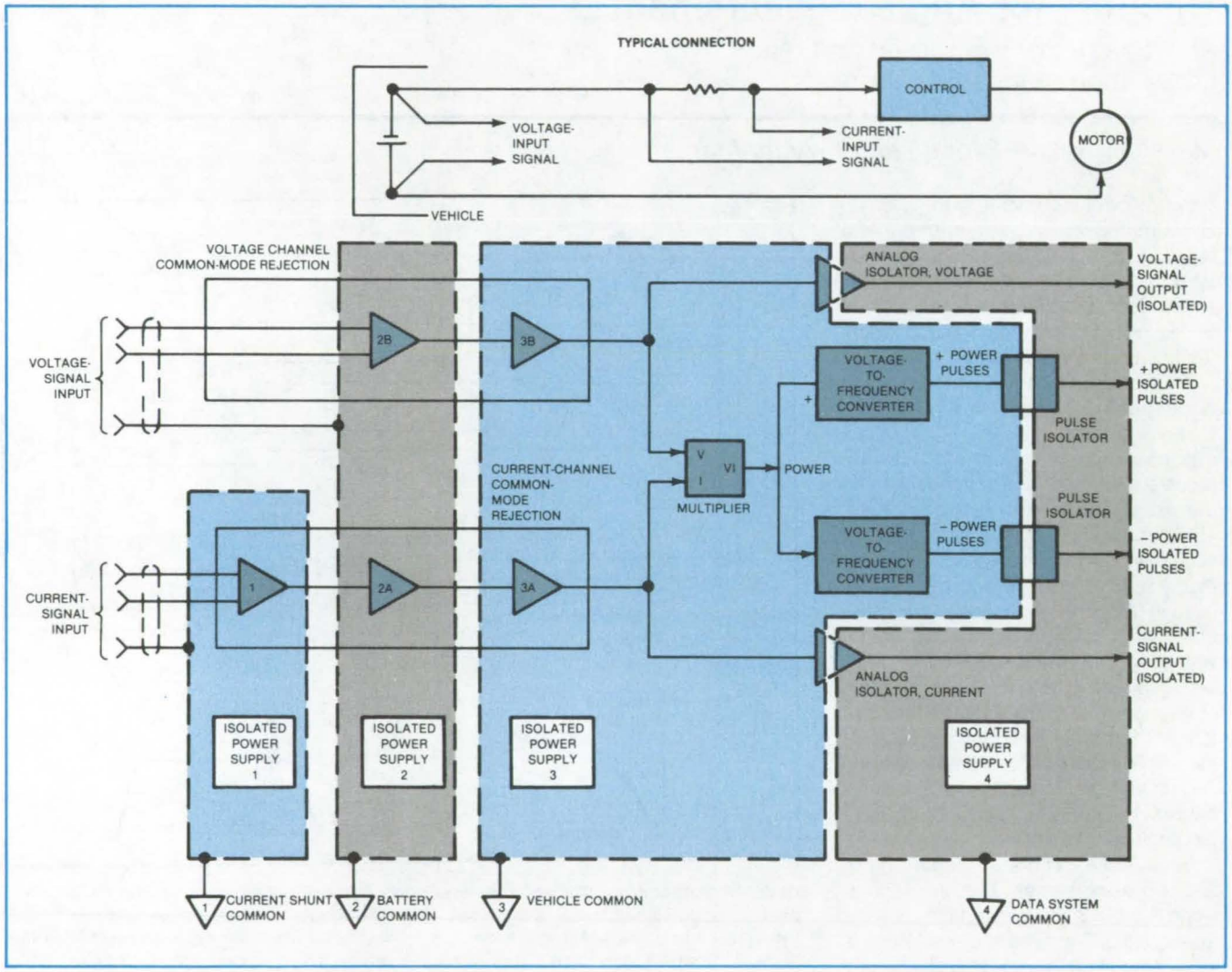

The **Power-Measuring Instrument** includes six data channels, of which one for measuring battery voltage and total system current is shown here.

The power to and from the battery of an electric vehicle is recorded by a new instrument. The instrument accommodates the fast rise and fall times of the waveforms characteristic of modern, efficient power controllers.

The new power meter multiplies analog signals proportional to voltage and current and converts the resulting signal to a frequency. Included are isolated power supplies, which are necessary for common-mode rejection.

The analog signals proportional to voltage and current are fed to a signal-conditioning circuit (see figure). The current signal enters the conditioner at a nominal 0.25 volts full-scale and is amplified up to 10 volts full-scale, while the voltage signal is reduced from a nominal full scale of 160 volts to 10 volts. The common-mode voltage of both the current and voltage signals is removed by the conditioner, while the frequency response is maintained at approximately dc to 50 kHz.

The two signals are sent to the analog multiplier. The multiplier is a commercial circuit assembly selected for its transient response characterized by symmetrical rise and fall times of about 2 μs.

This feature permits symmetric measurement of charging and discharging power. The multiplier output signal is thus proportional to the instantaneous electric power, regardless of the direction of power flow.

The instantaneous power signal is sent to a voltage-to-frequency converter, which converts the multiplier output signal to a frequency proportional to instantaneous power. Like the analog multiplier, the voltage-to-frequency converter is a commercial circuit.

The signal from the converter passes through isolation circuitry so that external components cannot introduce ground loops. The frequency signal is also sent to mechanical counters that integrate the signal to provide a watt-hour display of energy transmitted. Two mechanical counters are provided: one for charging and one for discharging. The frequency signal is also sent to an external digital data system, which provides integrals at 0.1-second intervals.

This work was done by Daniel C. Griffin, Jr., and Gordon A. Wiker of Caltech for **NASA's Jet Propulsion Laboratory.** *For further information, Circle 12 on the TSP Request Card.*
NPO-15514

Portable Data Logger for Photovoltaic Panels

Instrument measures rapidly changing knee of V-I curve with extra care.

NASA's Jet Propulsion Laboratory, Pasadena, California

A new battery-powered instrument measures the performance of photovoltaic panels and stores the data for later analysis. The data logger (Figure 1) is light and compact and can easily be carried to remote field locations.

The data logger measures the output-voltage-vs.-load-current characteristic of solar-cell panels. It is very accurate around the knee of the V-I curve, where voltage changes rapidly with current. Previous instruments set the load current and measured the resulting output voltage. They therefore produced large increments of voltage for the increments of current in the knee, and the curve was thus approximate in that region.

To improve accuracy, the new logger divides the load curve into two sections (Figure 2). The first section extends from the open-circuit voltage to about halfway into the knee. The second section begins at that point and extends to the lowest voltage reading possible (maximum current).

In the first section, the logger microcomputer increases the load current in 256 evenly spaced steps, and the logger records the solar-panel output voltage at each step. This method of data taking is continued until the unit (fraction of full scale) change in voltage is equal to or greater than the unit change in current. At that point, the microcomputer changes to the second-section mode of data acquisition. The solar panel is then loaded to produce a given output voltage, and the corresponding current is measured for about 240 evenly-spaced voltage steps.

(continued on next page)

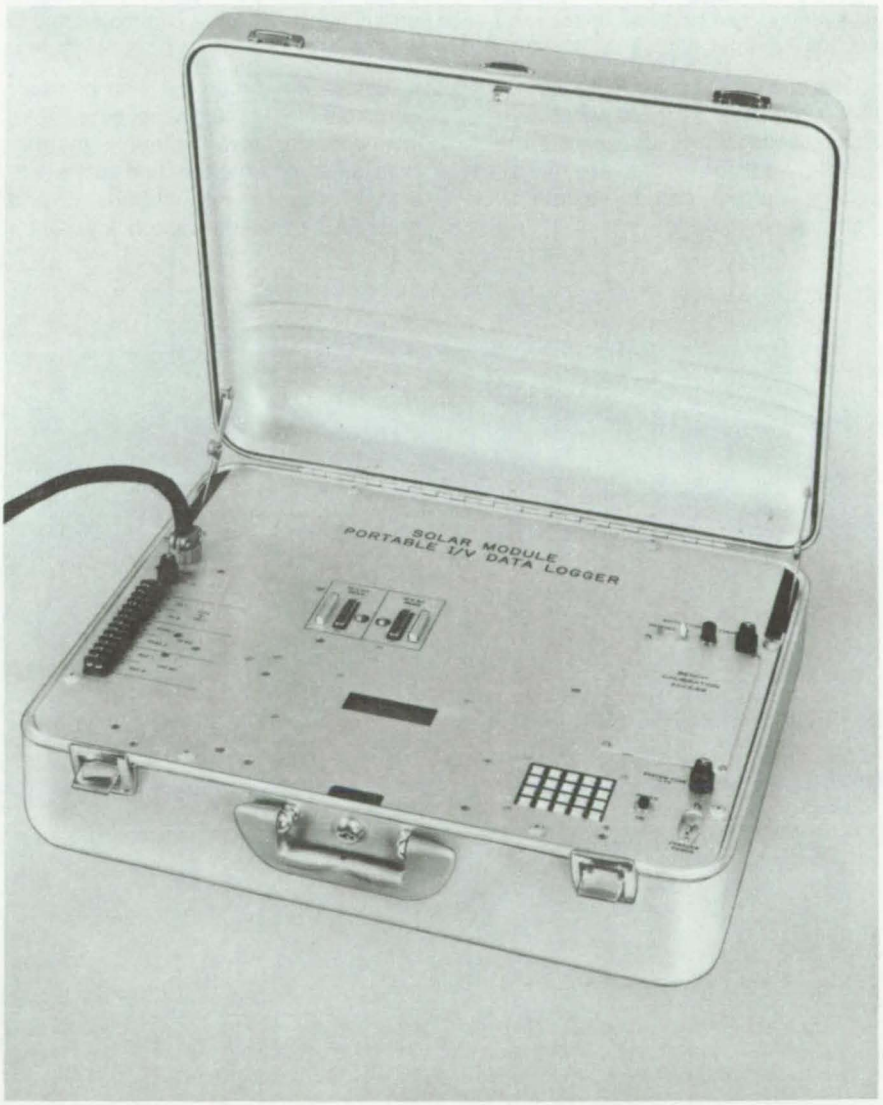

Figure 1. This **Portable Data Logger** runs on its own batteries. It includes a microcomputer, which controls voltage- and current-measurement increments, and a solid-state memory, which stores data until they can be transferred to an EPROM module.

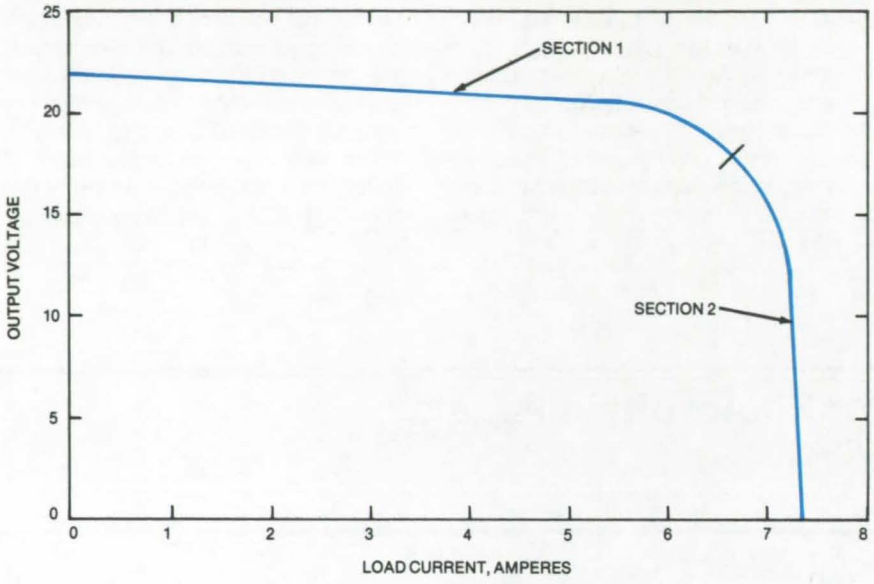

Figure 2. For **Accurate Measurement of a Characteristic-Curve Knee,** the data logger measures in two sections. In section 1, load current is the controlled parameter; and in section 2, output voltage is the controlled parameter.

The current at zero voltage cannot be measured because there will always be a small voltage drop across the current-sensing resistor. However, the zero-voltage current can be extrapolated from the curve trend.

To use the data logger, an operator connects it to a solar panel by a cable. The operator also connects thermocouples, pyranometers, and reference-signal cells to the instrument and presses the power-on button. After automatically testing its memory, the instrument automatically calibrates its input and load-control channels.

The logger initially measures the maximum current and maximum voltage of the panel to determine the ranges over which it will measure. It then takes voltage readings as it varies the load current (section 1 of the curve) and current measurements as it varies the voltage (section 2). The logger processes the measurements, correcting them according to the channel calibrations, and stores them in its memory.

The data are compressed by discarding points that can be interpolated to within 0.5 percent of full scale. On command from the operator, the logger transfers its stored data to an EPROM (Erasable Programable Read-Only Memory) module, and it becomes ready for more data collection.

This work was done by Steven W. Cole of Caltech for **NASA's Jet Propulsion Laboratory.** *For further information, Circle 13 on the TSP Request Card.*
NPO-15158

Physical Sciences

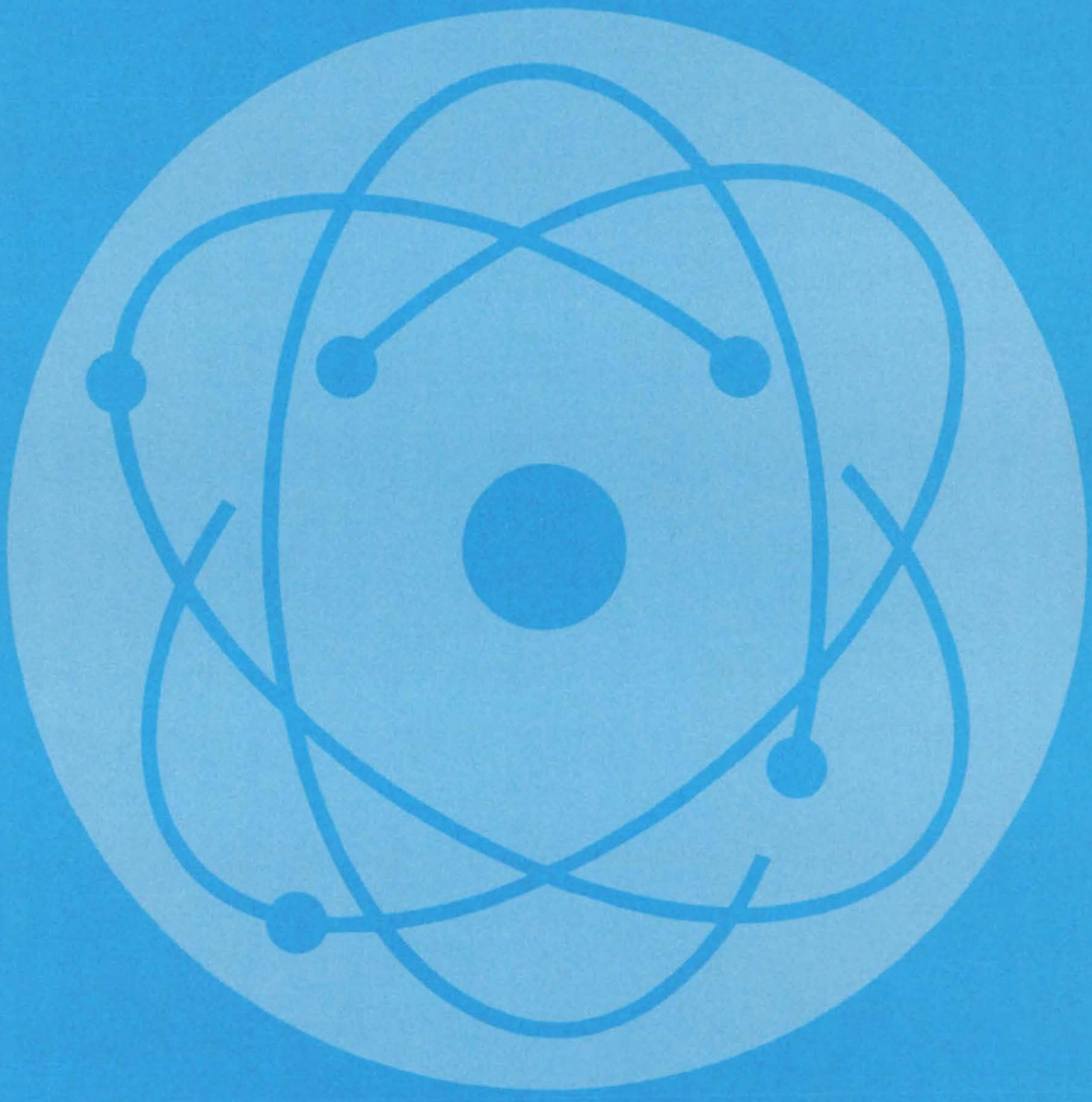

Hardware, Techniques, and Processes

Books and Reports

Acoustic Emissions Reveal Combustion Conditions

Turbulent-flame acoustic emissions change with air/fuel ratio variations.

NASA's Jet Propulsion Laboratory, Pasadena, California

The acoustic emissions from turbulent gas flames may be useful both for the diagnosis of combustion processes and for fuel/air control. An experimental study has identified a turbulent-flame acoustic spectrum and characteristic audiofrequencies at which the amplitudes are sensitive to air/fuel ratios. The exact quantitative relationships among acoustic spectra, combustion efficiency, and fuel/air ratios will have to come from further studies. Nevertheless, it already appears that acoustic emissions might be sensed and processed to detect inefficient operation; and a control system would respond by adjusting the fuel/air mixture for greater efficiency.

The experimental study was concerned with three frequency domains corresponding to the three scales of classical turbulence: the Integral scale, the Taylor microscale, and the Kolmogorov dissipation scale. Among these, the Kolmogorov dissipation scale corresponds to the low-power, high-frequency emission largely independent of burner geometry and flow rates. Thus, the Kolmogorov scale is, perhaps, a rough approximation for the yet-undefined combustion scales of interest (based on heat release, chemical reaction, and other physical/chemical parameters).

Acoustic emission spectra were obtained from a small-diameter laboratory burner, two commercial burners, and a large burner in the firebox of a boiler. The changes in burner size and firing rate represent changes in Reynolds number, and changes in air/fuel ratio represent departures from stoichiometric proportions. The combustion efficiency was measured independently through gas analyses. The acoustic spectra were analyzed for the identification of distinct frequency domains where acoustic power readily correlates with combustion efficiency.

Principal results are shown in the figure. The upper curve shows the acoustic spectrum obtained from the various burners and is typical for nonpremixed combustion of gaseous fuels. This general spectrum shape persists

(continued on next page)

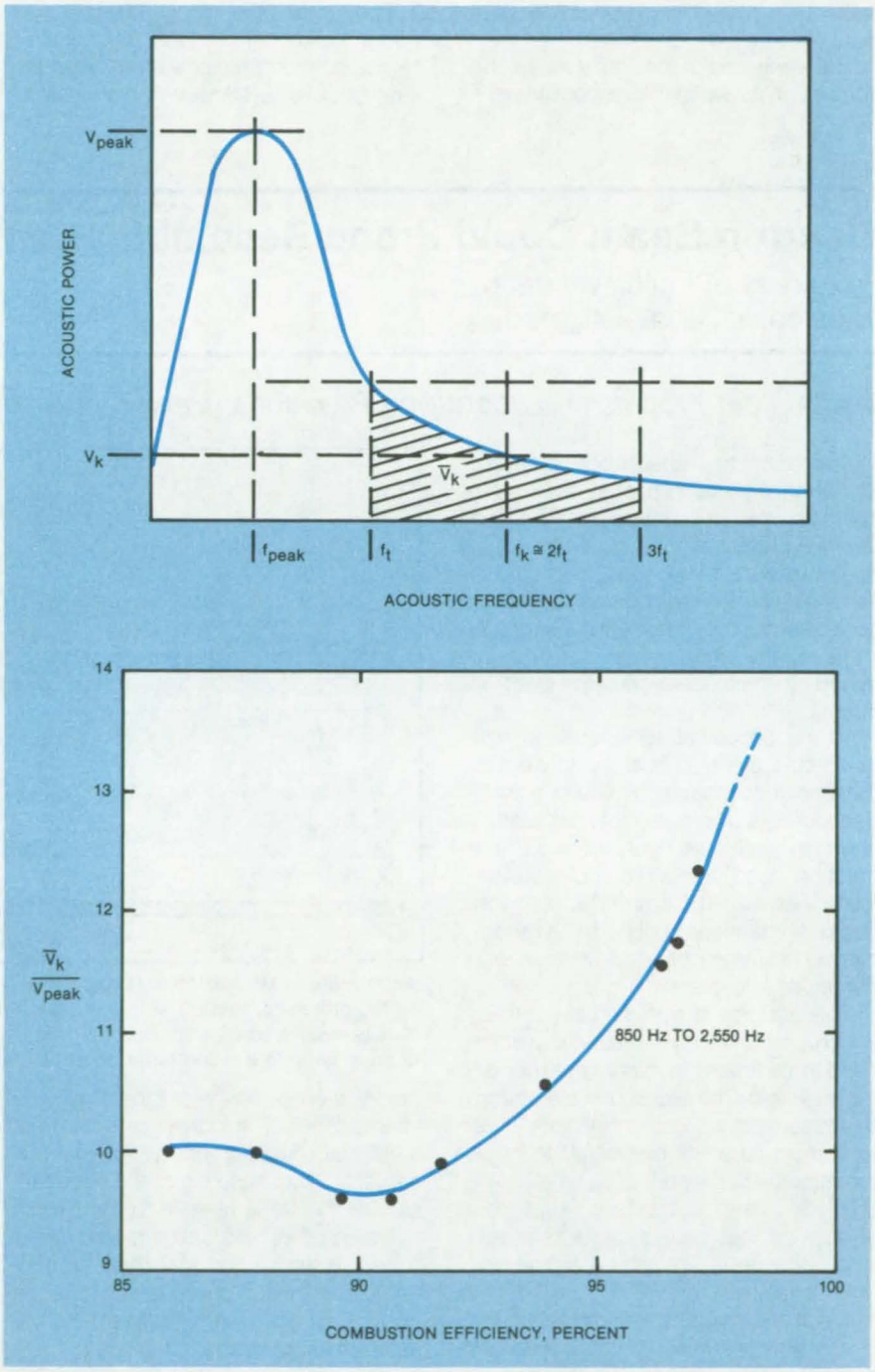

The **Acoustic Spectra of Turbulent Flames** have the general shape shown in the upper curve: This shape persists over wide ranges of physical and chemical properties of the fuel and air flows. The lower curve shows the dependence of the ratio of acoustic amplitudes ($\overline{V}_k/V_{peak}$) upon combustion efficiency of a furnace at Caltech.

over large variations of Reynolds number (8,200 to 82,000), burner geometry, fuel, firing rate, and air/fuel ratio.

In these spectra, f_{peak}, the loudest acoustic frequency, could be readily estimated as the ratio of mean velocity to maximum flame width. The transition frequency, f_t, was found to be nearly one-half of the Kolmogorov frequency estimate, f_k, over the range of Reynolds numbers studied.

The lower part of the figure shows the correlation between the responsiveness parameter, $\overline{V}_k/V_{peak}$ and the combustion efficiency. This curve is derived from acoustic spectra of natural-gas combustion in a boiler furnace at Caltech. The monotonal rise of $\overline{V}_k/V_{peak}$ as combustion efficiency approaches 100 percent is characteristic of combustion at high Reynolds numbers (82,000 for the correlation shown).

The identification of such frequencies and the discovery of their relationships to combustion phenomena may be the key to advanced acoustic diagnosis of combustor performance. Further studies are planned to help refine the correlations between acoustic output and combustion efficiency. These can then be utilized for diagnosis and control of the operation of gas-fired furnaces.

This work was done by Kumar N. R. Ramohalli and Panchalam K. Seshan of Caltech for **NASA's Jet Propulsion Laboratory.** *For further information, Circle 14 on the TSP Request Card.*
NPO-15699

Electron Beam Could Probe Recombination Centers

Properties of multilevel deep traps could be investigated.

NASA's Jet Propulsion Laboratory, Pasadena, California

According to a theoretical analysis, an electron-beam probe technique could be used to estimate electron/hole capture cross sections in semiconductors with wide band gaps. Such cross sections can be determined in heavily doped samples by measuring the phase shifts of the short-circuit currents induced by amplitude-modulated electron beams.

In the proposed technique, a well-collimated electron beam with sinusoidal amplitude modulation strikes a semiconductor surface and penetrates a short distance (see figure). The surface must be clean, with a recombination velocity less than 100 cm/s. The semiconductor is intentionally doped with recombination centers more heavily than with donors or accepters.

The distance, d, between the surface and the depletion layer must equal or exceed three times the minority-carrier diffusion length. The radius of the electron-beam/semiconductor interaction volume must be small compared to twice the minority-carrier diffusion length. The electron-beam current is kept low enough so that it produces a relatively small change in the total electron and hole densities.

Electron/hole pairs are created in the interaction volume. Minority carriers thus generated diffuse to the space-charge region, are accelerated across the region, and are collected by the ohmic contacts. This constitutes the measured short-circuit current.

The applicable equations of statistical mechanics, electrostatics, and diffusion theory were employed to analyze the interactions of minority carriers with multilevel deep traps (recombination centers). The phase lag of the occupancies of the traps relative to the overall diffusion of excess carriers was determined. It was found that this lag influences the overall phase shift of the minority carriers with respect to the electron-beam modulation.

Numerical examples were calculated for a gold doping of 5×10^{14} cm^{-3} in n-type silicon with a donor concentration of 10^{13} cm^{-3}. The phase shift of the short-circuit current was predicted to range from about $-7.5°$ to $+3°$, with values depending on carrier lifetimes and the excitation frequency. (A typical frequency would be 200 kHz.)

In general, once the phase shift is measured as a function of frequency, the results can be used to calculate the electron and hole capture rates and the energy level of the active deep trap. Since recombination centers strongly affect semiconductor performance, the technique should have great practical value in the industry.

This work was done by Oldwig VonRoos of Caltech for **NASA's Jet Propulsion Laboratory.** *For further information, Circle 15 on the TSP Request Card.*
NPO-15285

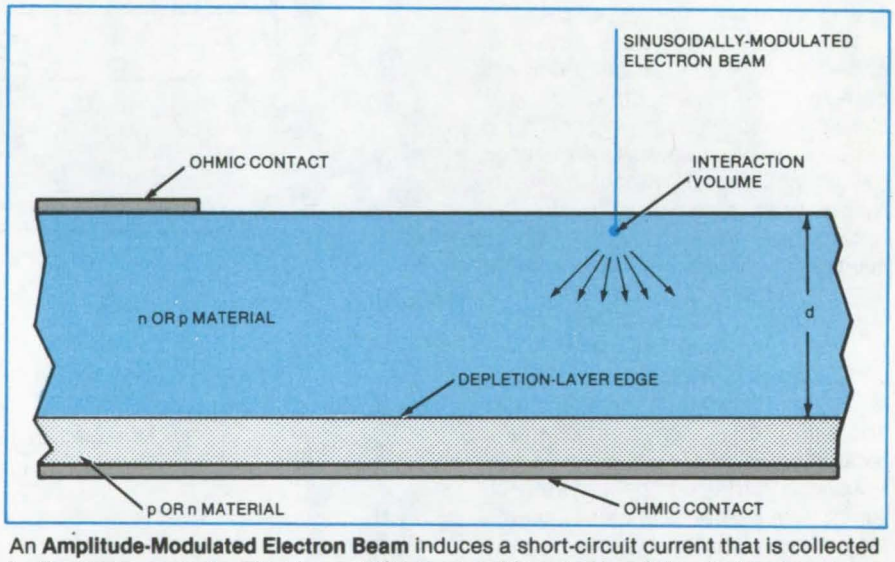

An **Amplitude-Modulated Electron Beam** induces a short-circuit current that is collected by the ohmic contacts. The phase shift between this current and the electron-beam current is measured as a function of frequency. The results of the measurements can be used to ascertain recombination rates and energy levels.

Self-Modulated Laser Rangefinder

Longitudinal resonance modes are exploited.

Goddard Space Flight Center, Greenbelt, Maryland

A laser transmitter/receiver measures distances as well as displacements of distant objects (such as vibrating buildings). Unlike previous laser rangefinders, the new instrument does not modulate its laser beam with an electro-optic or acoustic/optic device. Instead, modulation produced spontaneously by the laser itself is exploited.

A typical gas laser has several longitudinal resonances, which are present in different optical frequencies at the laser output. The difference frequency, f_m, between two successive longitudinal modes equals the reciprocal of the time required for a signal to make one round trip within the laser cavity. When the optical beam is incident on a square-law detector, the superposition of the separate longitudinal modes results in a detector output that is modulated by the frequency f_m. The new rangefinding system determines the target distance by measuring the phase shift between this detected modulation in the transmitted and received beams.

The laser includes an excited gas medium in a resonant cavity between one fixed and one movable mirror (see figure). The longitudinal-mode separation frequency, f_m, is controlled by the mirror separation, and hence by the setting of the movable mirror.

A small fraction of the laser output energy (the reference beam) is reflected from a beam splitter and detected by a square-law photodetector. The detector output is fed through a filter that passes only modulation around the longitudinal-mode separation frequency. The filtered signal is sent to a phasemeter. Since the exact separation frequency is unknown, the filtered signal is also sent to a frequency counter.

About 99 percent of the laser output is sent through collimating lenses over the path to a reflector on the target. The weak return signal from the reflector is collected by the receiving telescope and is optically filtered to reject stray light. This signal is also detected and band-pass-filtered around the longitudinal-mode separation frequency, f_m. The filtered return signal is sent to the phasemeter, which measures the phase difference between the detected modulation on the reference and return signals. The target distance is a function of both the phase difference and the distance between laser mirrors.

For many applications, such as stability measurements of structures or

(continued on next page)

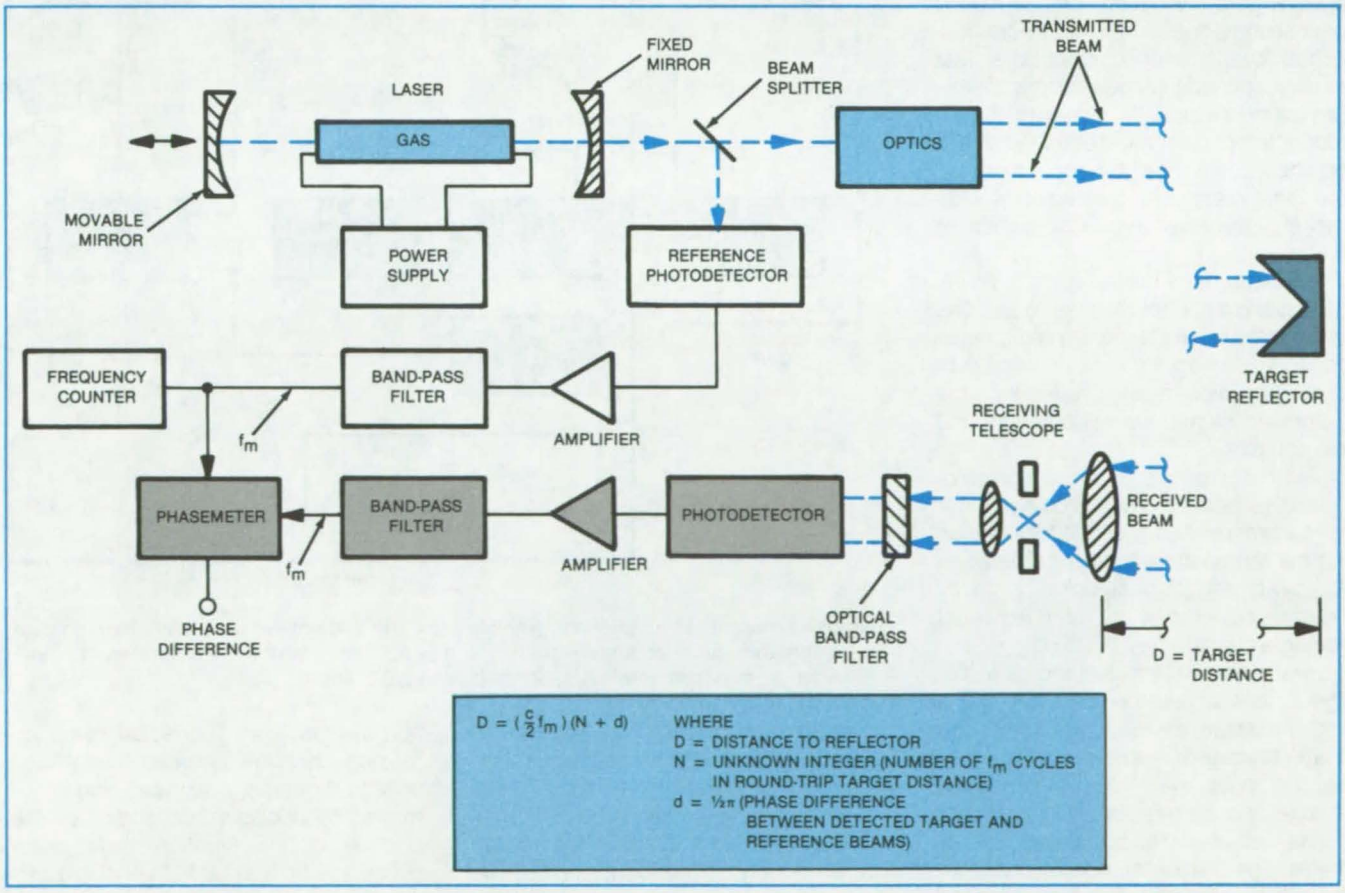

The **Self-Modulated-Laser Ranging System** exploits the presence of signals differing in frequency by the longitudinal-mode separation frequency, f_m. The two square-law photodetectors have outputs modulated by f_m, and the phase difference between these two outputs is related to the target distance.

construction sites, only a measure of the change in target distance is needed. Here, only the measurement of phase difference and an estimate of f_m are required, and a movable laser mirror and a frequency counter are not needed. Inexpensive helium/neon lasers with sealed end mirrors can be used as light sources.

For applications requiring a knowledge of the absolute distance, the multiple-2π ambiguity in phase difference must be resolved. This requires at least two phase measurements at different values of f_m, and the movable mirror and frequency counter are therefore necessary. A range computer must control the position of the movable mirror and monitor the phase and frequency to calculate range. These are simple tasks for a small microprocessor.

This work was done by James B. Abshire of **Goddard Space Flight Center.** *For further information, Circle 16 on the TSP Request Card.*

This invention is owned by NASA, and a patent application has been filed. Inquiries concerning nonexclusive or exclusive license for its commercial development should be addressed to the Patent Counsel, Goddard Space Flight Center [see page A5]. Refer to GSC-12761.

Pyrheliometer With Improved Accuracy

Instrument maintains components at constant temperature and allows tenfold improvement in instrumental accuracy.

NASA's Jet Propulsion Laboratory, Pasadena, California

An improved pyrheliometer is expected to measure solar irradiance with high accuracy. With a maximum error of only 0.01 percent, the instrument would be 10 times more accurate than previous versions.

The improvement in accuracy results from using circuit components having low temperature coefficients, mounting critical components in temperature-controlled ovens and using circuits that cancel connecting-cable errors. These provisions essentially eliminate the effect of temperature and other variations on accuracy. This is important because the instrument is subjected to a wide range of temperatures in its exposures to the Sun.

The instrument comprises a radiometer unit and a control unit (see figure). The radiometer converts the incoming radiation into a voltage. The control unit contains signal-processing circuitry, the calibration circuit, the panel meter, and the controls.

The radiometer consists of a thermocouple sensor in a cavity, a cavity heater for calibration, and a circuit for measuring the temperature difference between the cavity and its heat sink. The cavity heater is powered by the same regulated power supply used by the control unit.

Heater current is measured as a voltage across a resistor in an oven. The heater voltage is measured across the heater terminals. A precise analog multiplier computes the product of the heater voltage and current, and the multiplier output is displayed as power on the panel meter. The use of the analog multiplier and simple controls facilitates setting the gain so that the instrument gives direct readings in millivolts. This speeds up data collection and calibration. This also indirectly contributes to accuracy by limiting the time available for a change in insolation during a measurement.

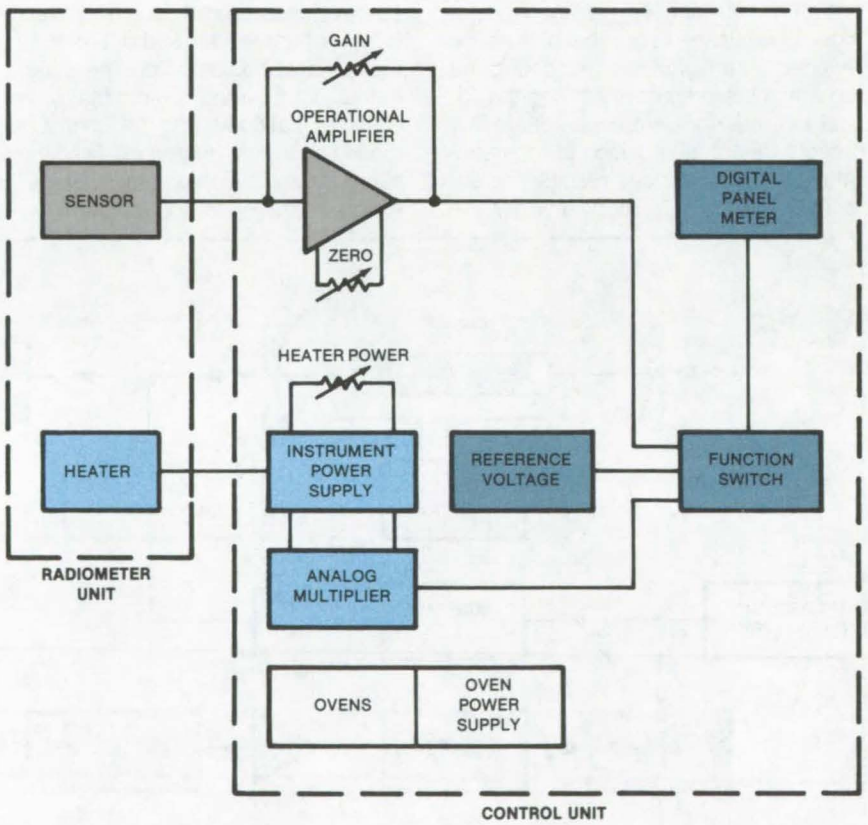

Two Units make up the improved pyrheliometer. The radiometer absorbs radiant energy and generates an electrical signal. The control unit, which incorporates the improvements, provides amplifiers, controls, and calibration circuits.

The control unit includes the heater power supply, signal-conditioning circuitry, and voltage reference. The control panel contains potentiometers for controlling system zero, heater power, and system gain. The digital meter on the panel displays meter zero, reference voltage, heater power, scale factor, or measured insolation, depending on the position of the function switch. The ovens are held at 60° C — above any temperature that might be expected in the field — and thus furnish a constant-temperature environment.

An adjustable-gain operational amplifier boosts the thermopile signal so that the panel meter, when calibrated, can display it directly in milliwatts. The amplifier and its trimming resistors are in the oven.

A precise voltage reference for the calibration of the digital panel meter is in an oven: This is because the digital panel meter is slightly sensitive to temperature. With the reference voltage, the meter can be calibrated from time to time. The voltage reference is set to a value close to the full-scale meter reading. The reference is calibrated to an accuracy higher than that of the panel meter by a reference traceable to the National Bureau of Standards.

This work was done by Roger S. Estey and Michael F. Hanna of Caltech for **NASA's Jet Propulsion Laboratory.** *For further information, Circle 17 on the TSP Request Card.*
NPO-15398

Estimating Waveguide-Feed Directivity and Spacing

Approximate curves simplify initial steps of antenna design.

NASA's Jet Propulsion Laboratory, Pasadena, California

The preliminary design of a multiple-beam reflector antenna is made faster and easier by approximate formulas for the radiation patterns of standard feed elements. The formulas and the graphs plotted from them give rapid estimates of the relationship between directivity and element spacing for a given feed-element arrangement.

For most types of standard feed elements (waveguides), the amplitude of a linearly-polarized radiation field emerging from the open end can be approximated at a distance r much greater than the aperture size and in the forward hemisphere by:

$$E(r,\theta,\phi) = \frac{e^{-jkr}}{4\pi r}\left[\hat{\theta}(\cos\theta)^{q_1}\cos\phi - \hat{\phi}(\cos\theta)^{q_2}\sin\phi\right]$$

where E = electric field,
r = the radial coordinate,
θ = polar angle,
ϕ = azimuthal angle,
q_1 = directivity exponent for the E-plane,
q_2 = directivity exponent for the H-plane,
$j = \sqrt{-1}$,
$k = 2\pi/\lambda$, and
λ = wavelength.

The ratio of amplitude squared in the forward direction ($\theta = 0$) to amplitude squared and averaged over all directions is called the directivity and is given by:

$$D = \frac{2(2q_1 + 1)(2q_2 + 1)}{(q_1 + q_2 + 1)}$$

In those cases with equal E- and H-plane patterns, the two exponents have the same value, q, and $D = 2(2q + 1)$.

(continued on next page)

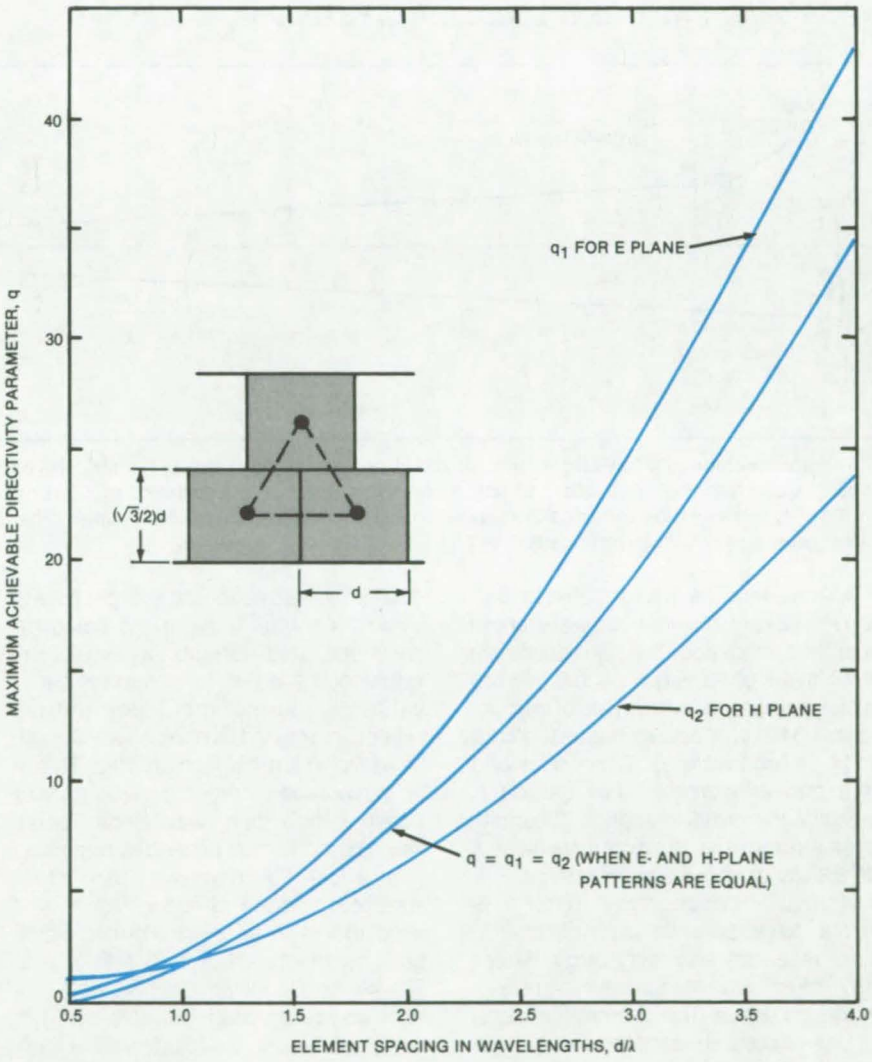

Maximum Achievable Directivity Exponents are plotted as functions of the element spacing in wavelengths for an equilateral triangular array of rectangular waveguides. The directivities and exponents have also been calculated for circular waveguides, pyramidal horns, and other standard feeds.

For feed elements that are not perfectly matched, that are coupled, or that otherwise interact with other feed or antenna elements, the exact field equations are very complex and q is difficult to determine. In some cases — for example, cigar antennas — one can use an empirical formula for the upper bound of q. The directivities and therefore the maximum realizable values of q have been calculated as a function of element spacing for a number of standard feed-element geometries (for example, see figure). Using the curve applicable to the contemplated geometry, the designer can quickly estimate the element spacing necessary to achieve the required directivity or the directivity achievable with a given element spacing.

This work was done by Yahya Rahmat-Samii, Paul W. Cramer, Kenneth E. Woo, and S. W. Lee of Caltech for **NASA's Jet Propulsion Laboratory.** *For further information, Circle 18 on the TSP Request Card.*
NPO-15603

Normal-Incidence Soft-X-Ray Mirror

A multilayered interference structure has about 6 percent reflectivity.

NASA's Jet Propulsion Laboratory, Pasadena, California

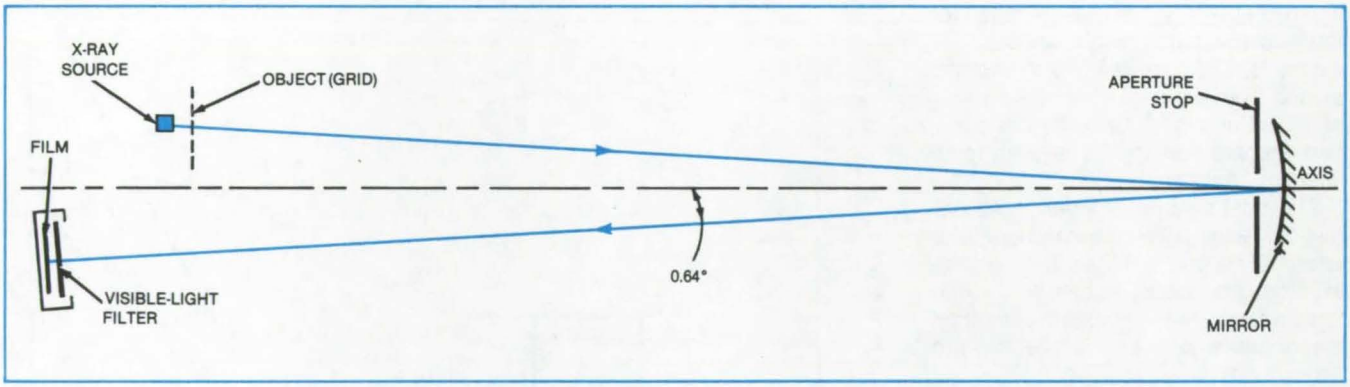

The **Normal-Incidence X-Ray Mirror,** bent into a spherical surface of radius 1.1 mm, was used to image an electroformed-nickel grid onto a photographic film that is sensitive to soft X-rays. The grid, set at a distance of 1,067 mm from the mirror, was illuminated by a simple Coolidge-type X-ray tube with a carbon-coated anode operated from a 1.5-kV supply. The film was set at a distance of 1,186 mm from the mirror, with a resultant magnification of 1.11.

An interference mirror reflects carbon K X-rays of $\lambda = 4.48$-nm wavelength at normal incidence. The mirror consists of 76 layers of tungsten, each 0.765 nm thick, interspersed with layers of carbon, each 1.510 nm thick, all deposited on a <111> silicon wafer 0.38 mm thick and 76.2 mm in diameter. For carbon K radiation at normal incidence, the multilayer structure is predicted to have a reflectivity of about 6 percent.

Normal-incidence X-ray mirror elements have potential applications in X-ray research and technology, where they offer advantages over grazing-incidence optics. The geometrical aberrations of normal-incidence mirrors are smaller, thereby allowing a larger field of view. In contrast to a grazing-incidence telescope that reflects X-rays of all wavelengths down to a certain cutoff value, a normal-incidence mirror reflects mainly in the narrow wavelength band for which it is constructed: This is an advantage where it is necessary to observe only one wavelength band, since no additional filtering is required.

In a test, the mirror was bent into a spherical surface of radius 1.1 m and used to image an electroformed-nickel grid onto film sensitive to soft X-rays. The filmholder included a filter of 2-μm-thick polycarbonate foil coated with 120 nm of aluminum to exclude visible light.

The apparatus, shown in the figure, was alined and focused using visible light to illuminate the grid. To reduce aberrations, the mirror aperture was stopped down to 7.6 mm. The film was exposed for 1 hour with an X-ray source current of 2.5 mA at 1.5 kV. The grid was discernible in the image, corresponding to a resolution of about 5 lines/mm, or about 40 arc-seconds angular resolution.

This work was done by James H. Underwood of Caltech and Troy W. Barbee, Jr. of Stanford for **NASA's Jet Propulsion Laboratory.** *For further information, Circle 19 on the TSP Request Card.*
NPO-15828

Multispectral Dual-Aperture Schmidt Objective

Off-axis focal planes make room for beam splitters.

Goddard Space Flight Center, Greenbelt, Maryland

A telescope with 2 off-axis catadioptric Schmidt objectives produces up to 12 outputs, each representing a different wavelength interval. The separate images have precise registration, so that they can be used for multispectral resource mapping or remote sensing.

As shown in Figure 1, two off-axis mirror segments are joined at a common plane. The mirrors are oriented so that the two optical axes are parallel to the common plane and to each other and are separated from the common plane by a distance about equal to the aperture size. The two mirrors may have the same or different focal lengths: If precise duplication is required, both might be cut from the same parent spherical mirror.

Each mirror is concentric with the point on its axis that intersects the aperture plane. The refractive correctors (which compensate for optical aberrations) are placed at the apertures. To reduce aberrations further, the beam splitter for each objective is placed as close as possible to its focal surface and is constructed with optically-concentric entrance and exit surfaces.

The off-axis arrangement assures the large aperture necessary to achieve good resolution: The focal surfaces are located outside the path of the central incident light rays, so that the beam splitters can occupy large spaces near the focal surfaces without interfering with the incoming light.

Each beam splitter consists of nine cemented prisms, with thin dielectric coatings as dichroic elements between them. Each dichroic element reflects most of the light of wavelengths shorter than its designated wavelength, while passing most of the light with longer wavelengths. As shown in Figure 2, the succession of reflections from the various dichroic elements divides the incoming light into six wavelength bands, A through F, in the order of increasing wavelengths.

The two beam splitters need not be identical. For example, one might

(continued on next page)

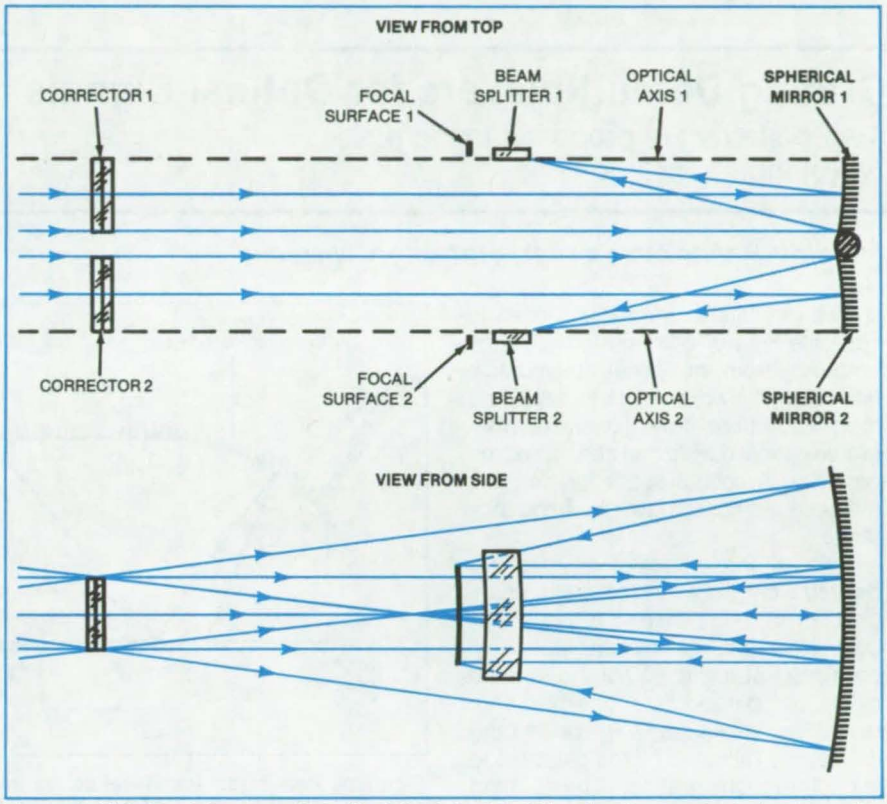

Figure 1. This **Dual-Aperture Catadioptric Schmidt Objective System** includes two off-axis primary spherical reflectors, each concentric with a refractive corrector at its aperture. The off-axis design assures the large aperture required for adequate spatial resolution.

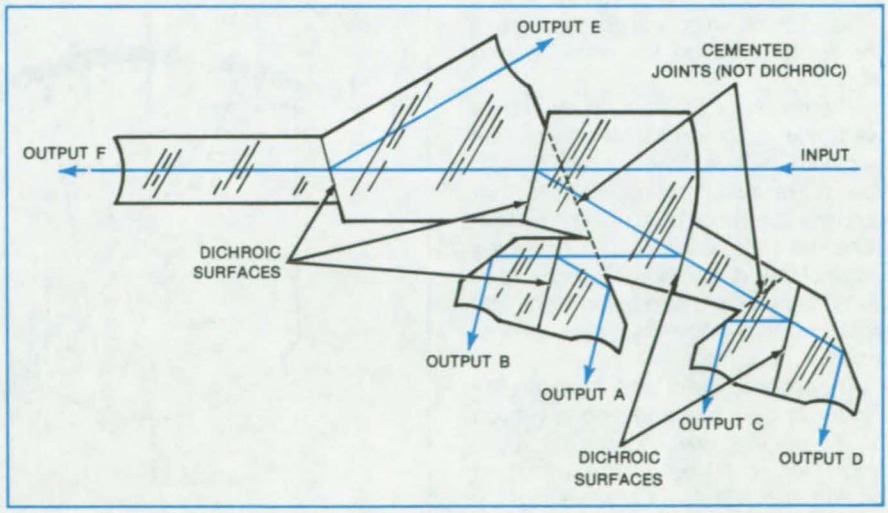

Figure 2. **Beam Splitter 2** is shown here magnified from the top view in Figure 1. In an assembly of nine cemented prisms, buried dichroic surfaces reflect selectively according to wavelength to produce six output beams, each in a different wavelength band. The input surface is convex, and the output surfaces are concave, all being optically concentric with the mirror surface.

operate in the visible spectrum; the other, in the infrared. An output beam can be used to form an image of the scene in its wavelength band or can be focused upon an array of detectors.

The system has good stray-light rejection. It provides images with good spectral and spatial resolution. The useful spectral range of this system is wider than that of other systems because each half can be separately corrected for color and spherical aberrations.

This work was done by Peter O. Minott of **Goddard Space Flight Center.** *For further information, Circle 20 on the TSP Request Card.*

This invention is owned by NASA, and a patent application has been filed. Inquiries concerning nonexclusive or exclusive license for its commercial development should be addressed to the Patent Counsel, Goddard Space Flight Center [see page A5]. Refer to GSC-12756.

Grating Demultiplexers for Optical Signals

Two systems are proposed to increase wavelength resolution.

Langley Research Center, Hampton, Virginia

Two demultiplexers are proposed to separate light of different wavelengths emerging from an optical communication fiber. The objective is to develop a high-resolution, low-crosstalk, integrated optical device that can exploit the potential of optical fibers for carrying many signals spanning a wide frequency range.

Both of the proposed devices are derived from the Rowland grating concept. In the first case, the input fiber containing the multiplexed signals is positioned at the focal point of a tilted cylindrical parabola or paraboloid of revolution (see Figure 1). The beam from the fiber is reflected by the parabola to the diffraction grating. The grating deflects the beam, breaking it into several planar waves, each having a distinct wavelength and deflection angle. A second parabola focuses the planar waves at discrete spots around its focal point. An optical fiber at each of the spots picks up the demultiplexed signals.

The double-parabola structure has a wedge-shaped cross section. This geometry aids in directing rays toward the diffraction grating and further reduces aberration by eliminating reflections from the sidewall. The half apex angle of the wedge should be equal to or larger than the arc sine of the numerical aperture of the fiber to insure against side-wall reflections.

The second type of demultiplexer (see Figure 2) is an integrated-optic version of the original Rowland grating. Light from the input fiber strikes a curved grating that reflects each wavelength in a different direction. The grating cur-

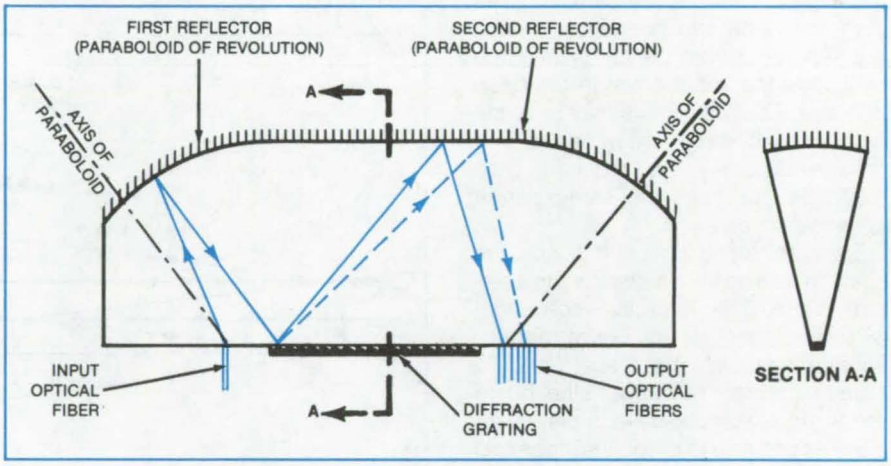

Figure 1. **Two Paraboloidal Reflectors and a Grating** separate light into component colors. The first paraboloid forms the input light into nearly planar waves. These waves are reflected from the planar grating at various angles that depend on wavelength. The second paraboloid focuses the separate wavelengths to separate lines.

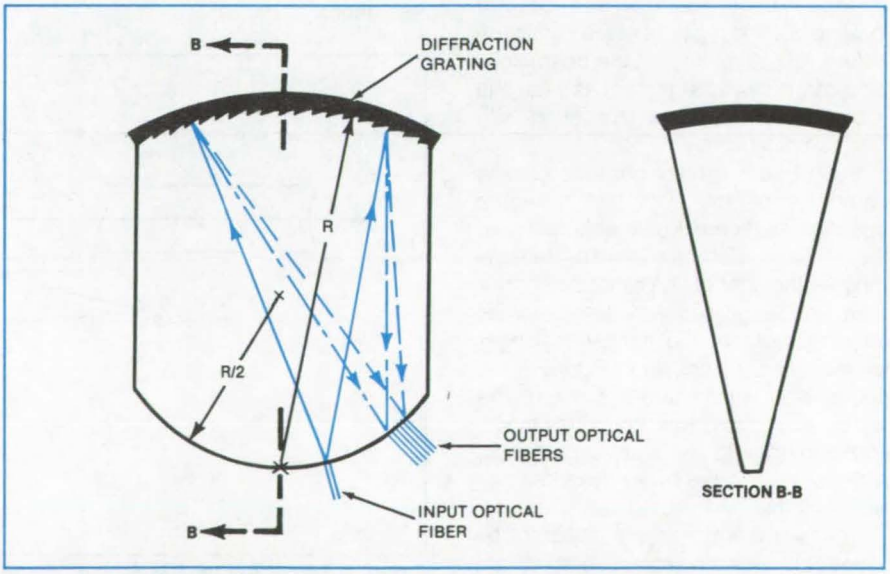

Figure 2. A **Grating on a Spherical (or Cylindrical) Surface** separates the incident light into different directions according to wavelength. Because of the spherical or cylindrical shape, the different wavelengths are focused to different lines and channeled into the output optical fibers.

vature and the locations of the input and output fibers are chosen so that the separate wavelengths are focused onto the ends of the output fibers. As in the first type, a wedge-shaped cross section prevents unwanted sidewall reflections.

This work was done by Emanuel Marom and O. Glenn Ramer of Hughes Aircraft Co. for **Langley Research Center.** *For further information, Circle 21 on the TSP Request Card. LAR-12748 and LAR-12749*

Fuse Protects Parabolic-Dish Solar Collector

A sliding barrel and shutter protect against overheating.

NASA's Jet Propulsion Laboratory, Pasadena, California

A sliding cylindrical barrel and a shutter have been proposed to protect the faceplate and receiver of a parabolic-dish solar collector. In case of tracker failure or the loss of fluid circulation, the system is initiated by the burning of a fuse wire (see figure). A hydraulic actuator could also raise and lower the barrel and the shutter under the control of the operator.

The sliding barrel surrounds the receiver and is concentric with it. The barrel can slide parallel to the receiver axis, up or down, within specified limits. When the barrel slides down, the brackets (which are attached to the shutter flaps) are moved away from the studs, thus permitting springs in the hinges to close the flaps, which are made of heat-resisting material. The barrel and shutter flaps then shield the receiver from concentrated Sunlight. Since the barrel diameter is significantly greater than that of the receiver and since the shutter flaps are not in the focal plane, these components will not receive the highest level of the concentrated solar flux.

In case of a failure of the tracker system, the image of the Sun moves across the faceplate, heating it excessively. When the faceplate gets hot, the shielded fuse wire stretched across the faceplate will also heat up. If the solar image dwells sufficiently long on the faceplate to cause overheating, the fuse wire melts, and the barrel, slides down because of its own weight, causing the shutters to close.

If the receiver faceplate is not exposed to high flux but the fluid circulation is interrupted, the receiver tubes will overheat. If the temperature of the receiver-tube wall exceeds that of the fuse wire, the fuse wire will melt, causing the cylindrical barrel to drop. Thus, the system provides a protection both for the faceplate during tracking failures and for the receiver tubes during fluid-flow interruption.

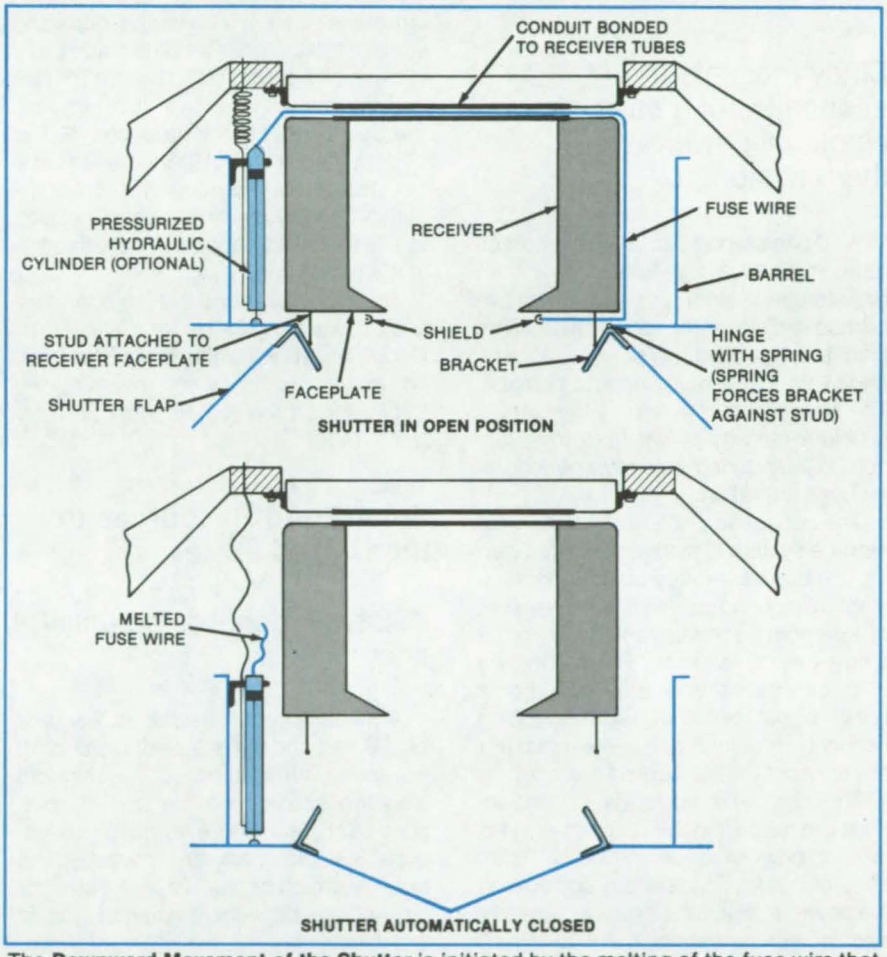

The Downward Movement of the Shutter is initiated by the melting of the fuse wire that suspends it. The shutter can also be lowered or raised under the operator's control by depressurizing or pressurizing the hydraulic cylinder.

In an alternative version of the proposed system, the hydraulic cylinder would be rapidly depressurized in case of overheating. In this system, the fuse wire is replaced by a tube that is sealed at one end and connected to the pressure reservoir at the other end. The tube melts if the receiver-tube wall or faceplate becomes overheated, thus causing a leak that depressurizes the cylinder.

This work was done by M. Kudret Selcuk of Caltech for **NASA's Jet Propulsion Laboratory.** *For further information, Circle 22 on the TSP Request Card.*

This invention is owned by NASA, and a patent application has been filed. Inquiries concerning nonexclusive or exclusive license for its commercial development should be addressed to the Patent Counsel, NASA Resident Office-JPL [see page A5]. Refer to NPO-15662.

Books and Reports

These reports, studies, and handbooks are available from NASA as Technical Support Packages (TSP's) when a Request Card number is cited; otherwise they are available from the National Technical Information Service.

Cost Effectiveness of Hybrid Solar Powerplants

Study presents the economics of a solar electrical powerplant with thermal storage.

A 10-page report discusses the cost effectiveness of a high-temperature thermal-storage system for a representative parabolic-dish solar powerplant. The plant supplies electrical power in accordance with a seasonally-varying demand. The solar power received by the plant is supplemented by power from fossil-fuel combustion during extended periods of reduced insolation.

The economic viability of the thermal-storage system is assessed by comparing the bus-bar energy cost of the solar plant using storage with the energy cost of a competing powerplant that does not utilize thermal storage. The competing plant can be either a solar hybrid or a conventional fossil-fuel plant, depending upon which plant has the lower bus-bar energy cost for a specified fuel cost.

The cost and performance projections are made for a 5-MW plant in mass production at an assumed rate of 10,000 units per year. The system considered employs a high-temperature receiver and power-conversion unit with an assumed conversion efficiency of 42 percent.

The cost of electricity generated by the solar powerplant is calculated, using the cost of mass-producible subsystems (parabolic dishes, receivers, and power-conversion units) now being designed for this type of solar plant. The tradeoff between fuel and thermal storage is derived in terms of storage effectiveness, the cost of storage devices, and the cost of fuel. Thermal-storage requirements, such as storage capacity, storage effectiveness, and storage cost, are established based on the cost of fuel and the overall objective of minimizing the cost of electricity produced by the system. As the cost of fuel increases at a rate faster than general inflation, thermal-storage systems in the range of $40 to $70/kWh could become cost-effective in the near future.

This work was done by Liang-Chi Wen and Howard L. Steele of Caltech for **NASA's Jet Propulsion Laboratory.** *To obtain a copy of the report, Circle 23 on the TSP Request Card.*
NPO-15735

Solar-Pond Resources in the United States

A survey identifies potential sites.

A 33-page report describes a survey of U.S. salt and brine deposits, providing essential information for developers who are considering the use of solar ponds for heat and electricity production. Suitable sites are classified as areas in which ponds of about 1 km^2, or larger, can be accommodated and in which salt, clay, and water are available. The primary criterion is the availability of salt or heavy brines, and the secondary criteria include water, land, and clay availability.

Potential sites are listed by states in which they are located. By a partly subjective assignment, they are further divided into primary and secondary sites. Those regions or singular sites that did not meet the criteria to be placed in primary or secondary categories but still exhibited potential are listed under the category for other potential sites. Most of the states can support various numbers of ponds, but not all states have large-enough local sources of salt or brine.

Fourteen states are assigned as primary states, and 10 are assigned as secondary. The primary states, with the exception of Delaware, lie in the Sun Belt of the country. Here, favorable weather makes year-round operation likely. In the secondary category, operation of the facility may be limited to less than year-round. When the primary and secondary category states are combined with the other states that may be able to support a pond, a total of 38 states exhibit the possibility of supporting power-generation ponds of varying size.

The report includes a table of potential sites for the placement of solar ponds by state and by site categories; brief summaries of the relevant geological features of each state; and maps showing the locations of salt deposits. A bibliography directs the reader to more-detailed regional geological information.

This work was done by Michael G. Hurick of Caltech for **NASA's Jet Propulsion Laboratory.** *To obtain a copy of the report, Circle 24 on the TSP Request Card.*
NPO-15681

Materials

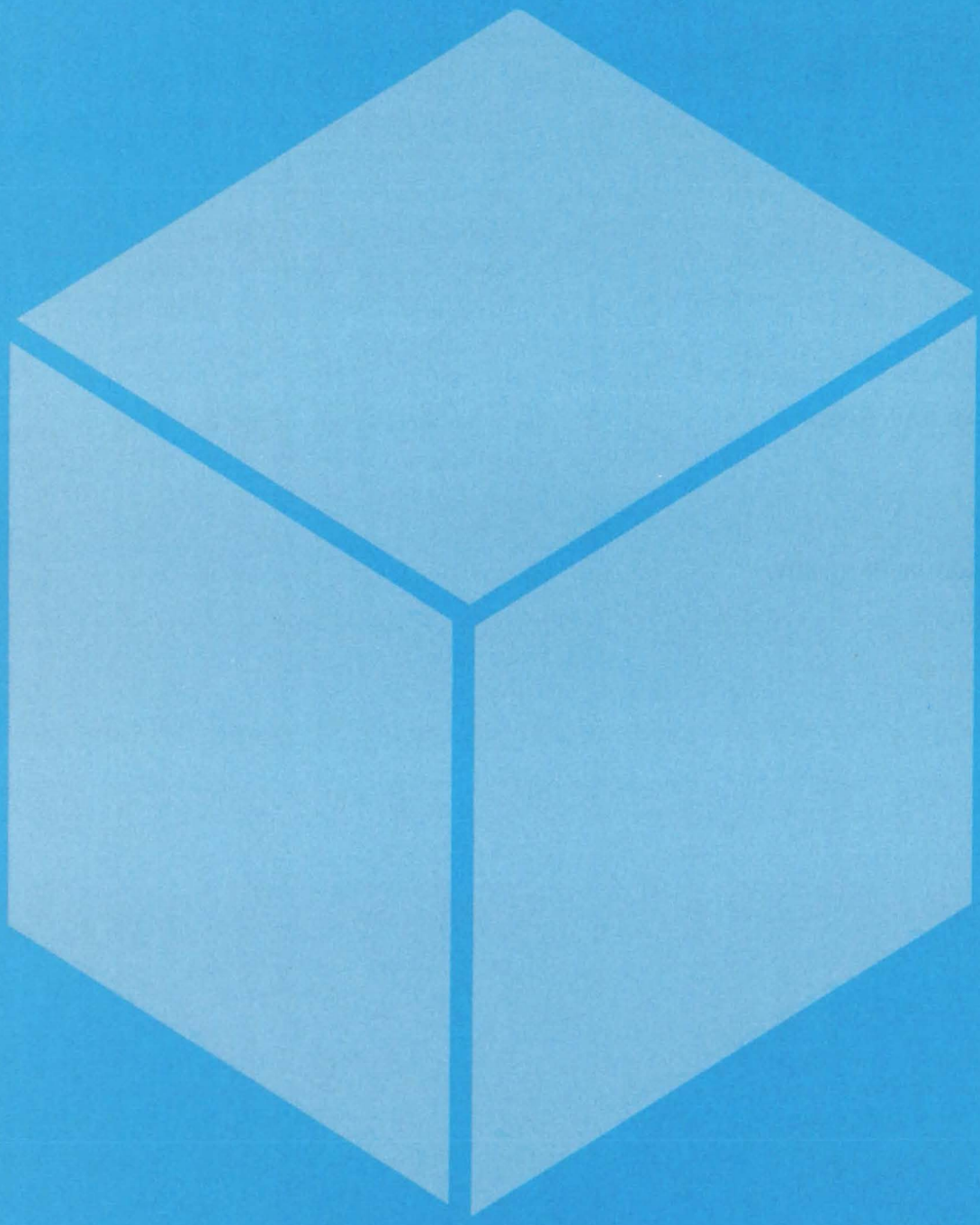

Solvent-Resistant Polysulfones

Polysulfones terminated with trimethylsilylethynyl, ethynyl, and phenylethynyl groups have increased solvent resistance.

Langley Research Center, Hampton, Virginia

Polysulfones are widely-used commercially available thermoplastics. They are generally amorphous and creep under load at elevated temperatures. A more severe shortcoming is their sensitivity to solvents, especially when stressed.

Because of the solvent-sensitivity problem, conventional polysulfones cannot be used in such applications as adhesives or composite matrices on commercial airplanes. Composites on aircraft are exposed to such solvents as hydraulic and deicing fluids, fuel, and paint strippers. Composites from polysulfones, especially under load, exhibit pronounced crazing and cracking upon exposure to solvents, with the loss of mechanical properties.

Various routes have been employed in an attempt to overcome the two major shortcomings of polysulfones — creep at elevated temperature and solvent sensitivity. Generally, the methods result in more difficult processability, brittleness, and poor or no thermoformability.

In a new technique, polysulfones of various molecular weights terminated with trimethylsilylethynyl, ethynyl, and phenylethynyl groups are prepared. Upon the application of heat, with or without a catalyst, these end groups react to provide cross-linking and chain extension. As a result, the use temperature of the polymer is increased, and, more importantly, the solvent resistance is greatly improved relative to conventional polysulfones. Depending upon the molecular weight of the polysulfone segment and, accordingly, the trimethylsilylethynyl, ethynyl, or phenylethynyl group density, these improvements are achieved without severely compromising the attractive features of thermoplastic polysulfones, such as toughness and thermoformability.

The materials are synthesized in two ways. Hydroxy-terminated polysulfones of various molecular weights are reacted with bromobenzoyl chloride, and the bromo group is subsequently converted to the trimethylsilylethynyl group as depicted in the reaction scheme. The trimethylsilyl group is readily cleaved with a weak base to afford the ethynyl group. Alternately, the hydroxy-terminated polysulfones are reacted with ethynyl or phenylethynyl benzoyl chloride to yield the desired polysulfones terminated with ethynyl or phenylethynyl groups directly as shown.

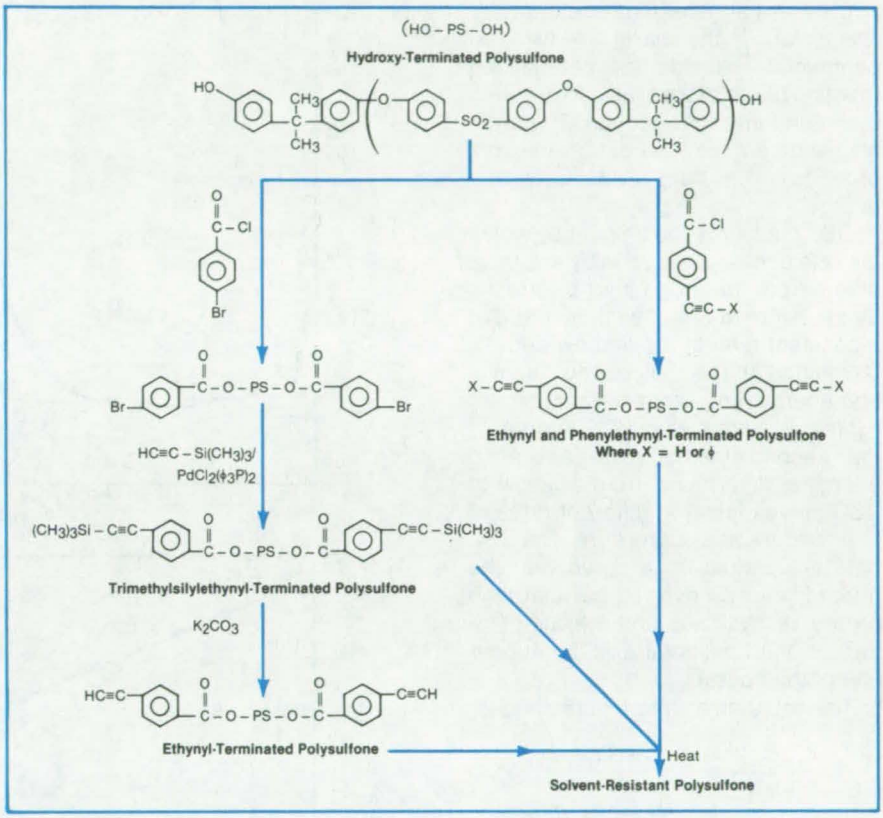

This **Representative Reaction Scheme** produces a solvent-resistant polysulfone.

The cross-linked density is controlled by controlling the molecular weight of the polysulfones and the amount of trimethylsilylethynyl, ethynyl, and phenylethynyl groups. High cross-linked density provides better solvent resistance, less thermoformability, higher processing conditions, and lower toughness (impact resistance). The reaction parameters can be readily controlled to provide tailormade materials for specific applications.

Polysulfones terminated with trimethylsilylethynyl, ethynyl, or phenylethynyl groups are soluble in such solvents as cyclohexanone, chloroform, and N,N-dimethylacetamide. These solutions can be used conveniently for the preparation of films, coatings, membranes, prepreg, and adhesive tapes. After curing the trimethylsilylethynyl-, ethynyl-, or phenylethynyl-terminated polysulfones, the resultant materials are more solvent-resistant and exhibit higher use temperatures than conventional polysulfones.

Depending upon the end group density, these materials are processed as adhesives or laminating resins under conditions similar to those of conventional polysulfones. The cured materials are thermoformable and relatively tough.

This work was done by Paul M. Hergenrother of **Langley Research Center.** *For further information, Circle 25 on the TSP Request Card.*

This invention is owned by NASA, and a patent application has been filed. Inquiries concerning nonexclusive or exclusive license for its commercial development should be addressed to the Patent Counsel, Langley Research Center [see page A5]. Refer to LAR-12931.

Measuring Epoxy-Curing Kinetics

Key reaction parameters are estimated from a single run.

NASA's Jet Propulsion Laboratory, Pasadena, California

Differential scanning calorimetry (DSC) forms the basis of two experimental methods for determining reaction parameters of an epoxy curing by a condensation reaction. The techniques determine the heat of reaction, order of reaction, and activation energy.

DSC measures the amount by which the rate of heat absorption by a sample differs from that of an inert reference, as the temperature of each is raised at a constant rate. In the first experimental method, the heat of reaction, activation energy, and order of reaction are estimated from a single DSC curve. In the second method, the activation energy is determined from a family of DSC curves taken at different rates of temperature rise during cure. The DSC data are plotted on a curve with the heat of reaction evolved per unit time on the vertical axis and the temperature on the horizontal axis (see upper half of the figure).

The equation for the first method is

$$\frac{ST^2}{h} = \frac{E}{R} - \frac{nT^2h}{A_r}$$

where S and h represent, respectively, the slope and height of the DSC curve at absolute temperature T, E = the activation energy, R = the ideal-gas constant, n = the reaction order, and A_r = the area remaining under the portion of the DSC curve lying to the right of temperature T. If the DSC data are replotted with (ST^2/h) on the vertical axis and (T^2h/A_r) on the horizontal axis, the result should be a straight line (see lower half of the figure). The vertical-axis intercept of this line gives the activation energy, while the slope gives the reaction order.

The second method is based on the relationship between the temperature-scan rate, ϕ, and the peak temperature, T_p, at which the reaction rate is a maximum.

$$\frac{d(\ln \phi)}{d(1/Tp)} = -\frac{E}{R} - 2\,T_p$$

$$\approx -\frac{E}{R} \text{ if } \frac{E}{R} >> T_p,$$

When the values of $\ln\phi$ and $1/T_p$ are plotted from different runs at various scan rates, ϕ, the result should be a straight line with a slope proportional to the activation energy.

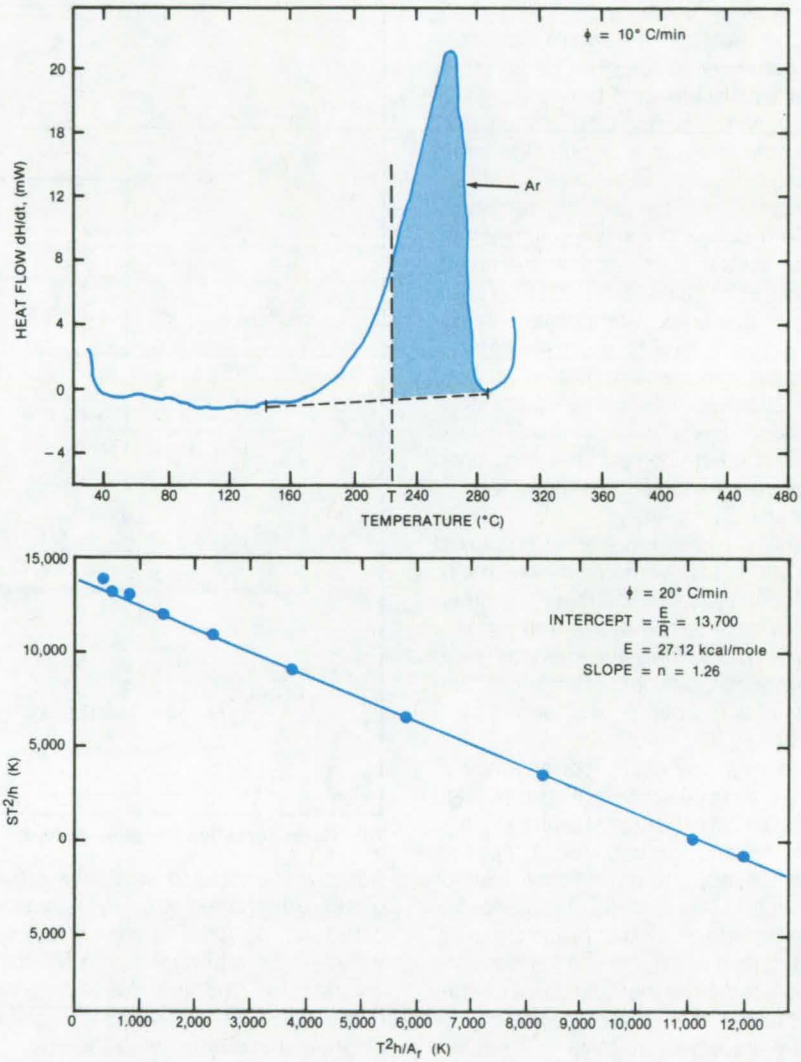

A Single DSC Curve (above) is used to construct a linearized plot (below) from which kinetic reaction parameters can be obtained: The vertical-axis intercept is proportional to the activation energy, while the slope equals the reaction order.

DSC runs were conducted on a commercial epoxy resin. The reaction order estimated by the first method varied between 1 and 2, depending on the temperature-scanning rate; that is, n is about 2.0 at slow scan rates but is reduced to about 1.0 at higher scan rates. The activation energy was calculated to be 25.6 kcal/mole by the first method and 24.7 kcal/mole by the second method.

The two DSC methods show promise for the rapid screening and estimation of the cure kinetic parameters of epoxy resins. Further studies are necessary to determine the applicability of these methods to other addition-curing systems.

This work was done by Muzaffer Cizmecioglu of Caltech for **NASA's Jet Propulsion Laboratory.** *For further information, Circle 26 on the TSP Request Card.*

NPO-15710

Supercritical-Multiple-Solvent Extraction From Coal

Large and small molecules dissolve different constituents.

NASA's Jet Propulsion Laboratory, Pasadena, California

Multicomponent fluids at or near supercritical temperatures and pressures may be more effective in extracting hydrogen-rich material from coal than are single compounds. According to experiments, mixtures of solvents enable supercritical extraction at temperatures below 400° C: This is desirable because some coal components rapidly polymerize above 400° C.

Supercritical extraction is based on the increased solubility of certain solids in compressed fluids. Using the apparatus shown schematically in the figure, samples of an Illinois No. 6 bituminous coal were immersed at various temperatures and pressures in several different solvents (methanol, toluene, acetone, and others). The weight loss of the coal was measured to determine the degree of extraction, and processed coal samples were examined with a scanning electron microscope to determine changes in the pore structure.

The extraction yield proved to be strongly dependent on temperature, roughly doubling from 320° to 380° C. The increase is believed to be due to the thermal depolymerization of coal components that occurs in that temperature range. The measured extraction was found to increase in pressure in a manner that correlates well with theoretical expressions based on the virial coefficients of the molecules involved.

The multicomponent extraction proposal arose, in part, from coal-structure changes that were observed to occur during extraction. In a multicomponent extraction fluid, the smaller molecules would first enter the pores that are too small for the larger molecules. The dissolution of material by the smaller molecules would enlarge the pores, thus allowing the larger molecules to enter. Since the larger solvent molecules dissolve some coal components that are insoluble by the smaller molecules and vice versa, the overall extraction would be enhanced.

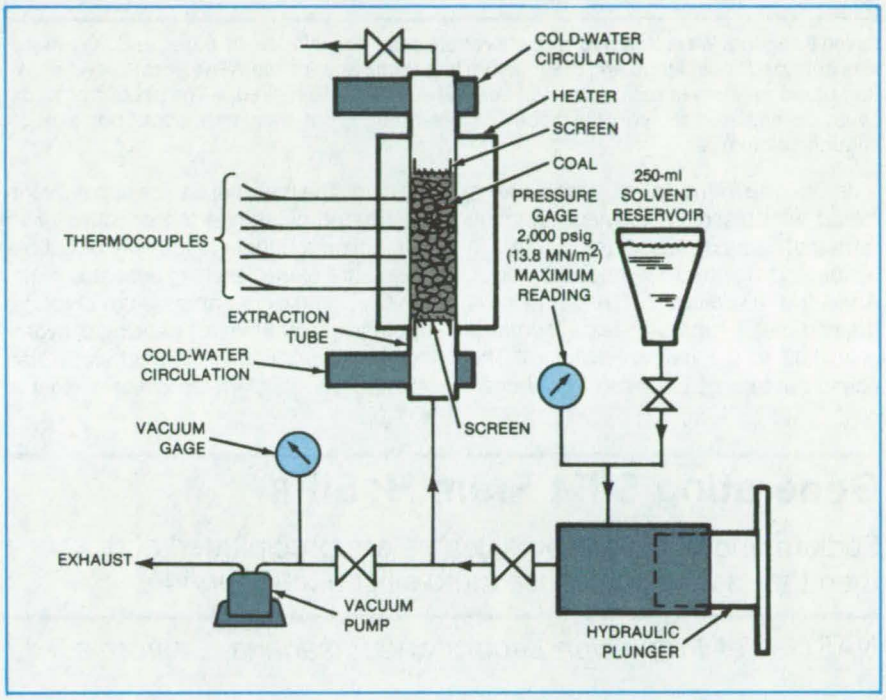

This **Experimental Apparatus** was used to test the supercritical extraction of hydrogen-rich compounds from coal in various organic solvents. In decreasing order of importance, the relevant process parameters were found to be temperature, solvent type, pressure, and residence time.

This work was done by W. Corcoran, W. Fong, P. Pichaichanarong, P. Chan, and D. Lawson of Caltech for **NASA's Jet Propulsion Labratory.** *For further information, Circle 27 on the TSP Request Card.*
NPO-15767

Calcium-Free Asbestos for Fuel Cells

An organic-acid salt removes unwanted calcium without weakening the asbestos.

Lyndon B. Johnson Space Center, Houston, Texas

A new treatment removes calcium, but not magnesium, from the asbestos matrix in fuel cells. For long life, the matrix should be calcium-free. However, fuel-cell-grade asbestos contains substantial amounts of calcium as calcium carbonate — between 2.5 and 7.5 percent. Attempts to extract the calcium with acids have been successful, but acids also extract magnesium from the asbestos fibers and weaken them (the chrysotile asbestos in fuel cells is composed of $3MgO{\cdot}2Si_2O_2{\cdot}2H_2O$). Alkalies do not attack the asbestos, but neither do they remove calcium.

(continued on next page)

Reagent	Percent Ca Removed	Percent Asbestos Removed
Saturated CO_2, 16 Hours	98.2	7.3
Saturated CO_2, 40 Hours	98.0	7.1
1.0M Ammonium Chloride	98.0	2.1
1.0M Potassium Hydroxide	0.0	0.0
0.01M EDTA	98.6	2.9
Acetic Acid, pH Adjusted 6 to 7	98.0	2.0
Hydrochloric Acid, pH Adjusted 6 to 7	96.8	1.4
Citric Acid, pH Adjusted 6 to 7	88.7	1.2

Seven Reagents Were Reacted with chrysotile asbestos in distilled water, and the filtrate was analyzed for calcium and magnesium by atomic absorption. (The filtrate concentration of magnesium is expressed as "Percent Asbestos Removed.") The pH of the acids could be adjusted to limit the asbestos dissolution, but then they could not extract enough calcium.

In the new treatment, asbestos is mixed with disodium ethylene diamine tetraacetic acid (disodium EDTA) in water and agitated for about 2 hours. After the disodium EDTA solution is drained away, the asbestos contains only 0.02 to 0.1 percent calcium. The fiber structure of the asbestos is unaffected. The material can be subsequently treated by standard procedures with no adverse effects on density or bubble pressure of the resulting asbestos mats.

Carbon dioxide, ammonium chloride, potassium hydroxide, acetic acid, hydrochloric acid, and citric acid were also tested as calcium-removing reagents (see table). Disodium EDTA was the most effective, while acetic acid and ammonium chloride were almost as effective in their ability to remove calcium without dissolving excessive asbestos. Because chloride residue from the ammonium chloride could interfere with fuel-cell operation, disodium EDTA is the preferred reagent. It is possible that chelates other than disodium EDTA may be equally or more effective.

This work was done by Barry A. Snitzer of United Technologies Corp. for **Johnson Space Center.** *For further information, Circle 28 on the TSP Request Card.*

Inquiries concerning rights for the commercial use of this invention should be addressed to the Patent Counsel, Johnson Space Center [see page A5]. *Refer to MSC-20207.*

Generating SiF_4 From H_2SiF_6

Sodium and barium fluorosilicates are precipitated and then thermally decomposed into silicon tetrafluoride.

NASA's Jet Propulsion Laboratory, Pasadena, California

A new process generates silicon tetrafluoride (SiF_4) gas from hexafluorosilicic acid (H_2SiF_6), a waste byproduct of the phosphate-fertilizer industry. The method of generating SiF_4, a source of silicon for the manufacture of solar cells, involves the precipitation and decomposition of an insoluble salt of the acid.

Aqueous solutions of sodium and barium salts (NaCl, NaF, NaOH, Na_2CO_3, $BaCl_2$, and BaF_2) added to a 23 percent aqueous solution of H_2SiF_6 quickly precipitate fluorosilicates, Na_2SiF_6 and $BaSiF_6$. For NaCl, NaF, and Na_2CO_3, the reactant ratio that yields the maximum precipitation of fluorosilicates is about 1:1. For NaOH, the reaction ratio is 3:1. The optimum reactant ratio for $BaCl_2$ is 1:1; and for BaF_2, it is 1.5:1. At the optimum reactant ratio, the yields of fluorosilicates are 90 percent or better.

The filtered and dried fluorosilicates are thermally decomposed into SiF_4 gas at temperatures ranging from 350° to 600° C. The Na_2SiF_6 is 90 percent decomposed after 30 minutes at 550° C and after 15 minutes at 600° C. The $BaSiF_6$ is more than 90 percent decomposed after 30 minutes at 450° C and after about 10 minutes at 500° C. The

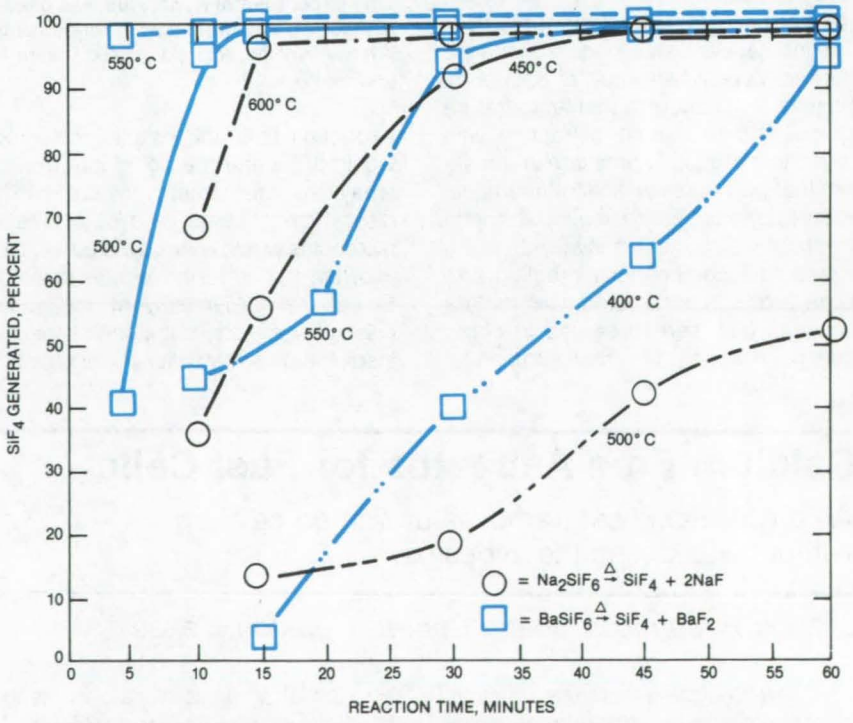

Barium Fluorosilicate Thermally Decomposes at lower temperatures and in shorter times, to give the same percentage yield of silicon tetrafluoride gas, than does sodium fluorosilicate. The salt byproducts of the decompositions can be recycled to precipitate fluorosilicates from hexafluorosilicic acid, the primary reactant.

figure shows the percent of SiF_4 recovered as a function of time for different temperatures.

The $BaSiF_6$ precursor has several advantages over Na_2SiF_6: $BaSiF_6$ is less soluble than Na_2SiF_6 by a factor of about 30, which should result in a more efficient recovery of SiF_4 from a solution of H_2SiF_6. If BaF_2 is used to precipitate the $BaSiF_6$, there would be no coprecipitation. Also, the thermal decomposition of $BaSiF_6$ to give SiF_4 occurs at a lower temperature than that for Na_2SiF_6.

This work was done by Keith C. Hansen and Carl L. Yaws of Lamar University for **NASA's Jet Propulsion Laboratory.** *For further information, Circle 29 on the TSP Request Card.*
NPO-15721

Improved O_2/H_2 Gas-Mixture Sensor

Monitor of mixture concentration uses a catalyzed and an uncatalyzed temperature probe.

Lyndon B. Johnson Space Center, Houston, Texas

A monitor for O_2/H_2 gas-mixture concentrations consists of a Pt-catalyzed temperature sensor mounted just downstream from an uncatalyzed sensor. Suitable for use in regenerative fuel cells, life-support systems, and other closed systems, the new unit is compact, corrosion-resistant under normal operating conditions, and assembled using standard tube fittings.

The exothermic chemical reaction between hydrogen and oxygen on the catalyst heats the catalyzed probe (see figure). The uncatalyzed temperature probe serves as a reference-temperature monitor. The temperatures sensed by the probes are manifested as resistance values, from which analog voltages are derived representative of the temperatures of the probes. The temperature-difference signal, derived from the amplified and processed probe signals, is calibrated for known O_2-in-H_2 or H_2-in-O_2 mixtures under process conditions.

Mounting both probes in the same flowthrough housing requires small probe diameters and a special adapter. A new catalyst support for a probe 0.125 in. (3 mm) in diameter has been conceived for this purpose. Layers of powdered Pt-catalyst, screen, and porous polytetrafluoroethylene (PTFE) are hot-pressed together. The PTFE is a hydrophobic binder to prevent a water film from masking the catalyst.

After cooling, the PTFE is peeled away from the screen with almost all of the catalyst bonded to the film in a pattern imparted by the screen. A strip as wide as the sensing length of the 1/8 in. temperature probe is wrapped (catalyst side in) once about a mandrel, cut, and seam-welded. The formed catalyzed tube is stretched over the end of the probe to complete the sensor.

(continued on next page)

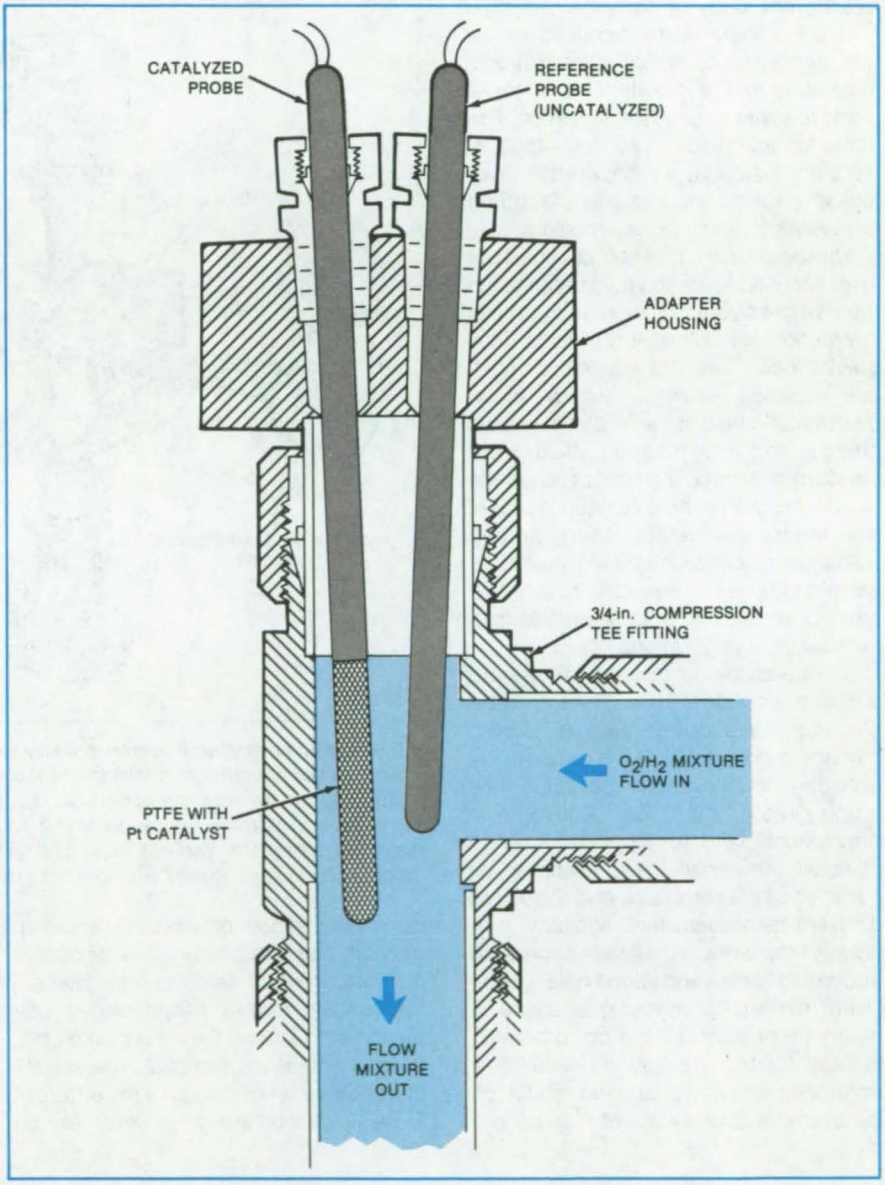

The improved **O_2/H_2 Gas-Mixture Sensor** includes a Pt-catalyzed temperature probe mounted in line with a similar but uncatalyzed temperature probe. The use of common temperature probes and standard, flareless, high-pressure tube fittings has resulted in a design conducive to installation in almost any system.

The new O_2/H_2 monitors are intended primarily as alarm sensors, initiating a safe system shutdown in the event of high gas-mixture concentrations. However, temperature-difference readings may be recorded and compared to calibration curves as a means of measuring concentrations.

[See the related article "Detecting Oxygen in Hydrogen or Hydrogen in Oxygen" (MSC-18380) on page 380 of *NASA Tech Briefs*, Vol. 4, No. 3.]

This work was done by Lawrence C. Moulthrop of General Electric Co. for **Johnson Space Center.** *For further information, Circle 30 on the TSP Request Card.*
MSC-20408

Classifying Particles by Acoustic Levitation

Separation technique is well suited to material processing.

NASA's Jet Propulsion Laboratory, Pasadena, California

Different kinds of particles in a mixture are separated by acoustic levitation, according to recent investigations. This adds to the growing list of tasks made feasible by acoustic levitation. The acoustic technique may find applications in fusion-target separation, biological separation, and manufacturing processes in liquid or gas media.

The equilibrium position of a particle in an acoustic-levitation field depends on the particle size and shape and upon its interaction with other force fields. In a gravitational field, the equilibrium position depends on mass density; in an electrostatic field, it depends on electric charge; and in a magnetic field it depends on magnetic moment or magnetic permeability. For the gravitational case, the theoretical relationships among mass density, size, acoustic pressure, wavelength, and equilibrium position have been experimentally verified in a number of configurations.

This behavior can be used to separate different particles in a dilute mixture placed in the acoustic field. (A "dilute" mixture is one in which the separations between the levitated particles are much greater than their sizes.) In a gravitational field, for example, a range of equilibrium positions is assumed by particles of the same size and shape but different mass densities. Similarly, particles of the same density are separated according to size and shape (see figure).

For material processing in space, a magnetic or electric field could be substituted for the gravitational field, or a controlled gravitational field could be generated artificially by rotation as in a centrifuge. In both gravitational and nongravitational processing, the acoustic-field parameters (amplitudes, phases, frequencies, and excitation modes) can be adjusted to vary the equilibrium positions or rotate the samples. The variety of possible combinations of the different force fields confers great versatility on the acoustic levitation/separation technique.

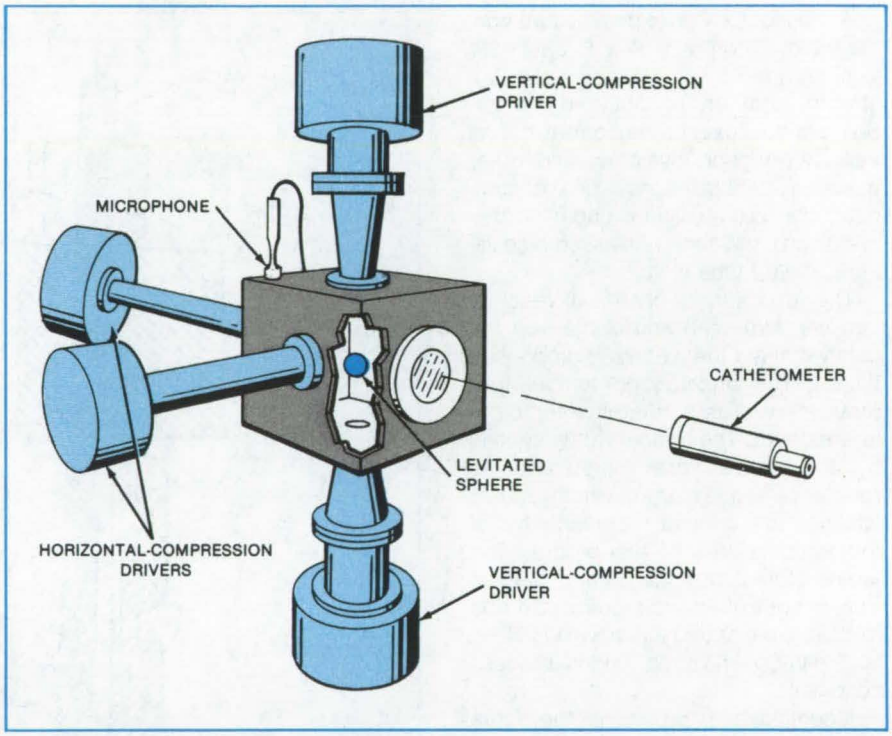

An **Acoustic Levitation Apparatus** with a rectangular-cross-section chamber was used to measure the equilibrium positions of low-density spheres in the gravitational field. Vertical acoustic forces were generated by two opposing compression drivers exciting the fundamental plane-wave mode at 1.2 kHz. Additional horizontal drivers centered the samples along the vertical axis. The variations in sample position with radius and acoustic pressure agreed with predictions.

This work was done by Martin B. Barmatz and James D. Stoneburner of Caltech for **NASA's Jet Propulsion Laboratory.** *For further information, Circle 31 on the TSP Request Card.*
NPO-15561

Predicting Sintered-Metal Resistivity From Porosity

An equation with one adjustable parameter fits the experimental data for nickel.

NASA's Jet Propulsion Laboratory, Pasadena, California

A formula with one adjustable parameter relates the electrical resistivity of a sintered metal plate to the porosity of the plate. A sintered plate is formed by heating compressed metal powder — without melting — until the particles adhere. Sintered nickel plates of high porosity are used as substrates for the electrodes in nickel/cadmium batteries.

The formula gives the ratio of the resistivity, ϱ, of the sintered material to the resistivity, ϱ_0, of the solid bulk metal:

$$\frac{\varrho}{\varrho_0} = 1 + \frac{A(1 - \phi)}{\phi - \phi_{min}}$$

where ϕ is the volume fraction of the conductive metal in the sintered material, ϕ_{min} is the minimum volume fraction to which the given metal powder can pack, and A is the adjustable parameter.

The value of ϕ_{min} is estimated as the ratio of the bulk density of the uncompressed metal powder to the bulk density of the solid metal. The value of the adjustable parameter depends on particle shape and type.

The formula is exact at the extremes of low and high packing density: Since the ϕ's are defined in terms of the volume fraction of metal, the quantities $1 - \phi$ and $1 - \phi_{min}$ represent the relative void volume or porosity and the maximum possible relative void volume or porosity, respectively. Hence, when ϕ approaches 1, the ratio of resistivities ϱ/ϱ_0 approaches 1, and the resistivity of the sinter approaches that of the bulk metal. On the other hand, when ϕ approaches ϕ_{min}; i.e., when the volume fraction of metal in the bed approaches the minimum value consistent with stable packing, the denominator of the right-hand term approaches zero, and the electrical resistivity of the sinter increases without limit.

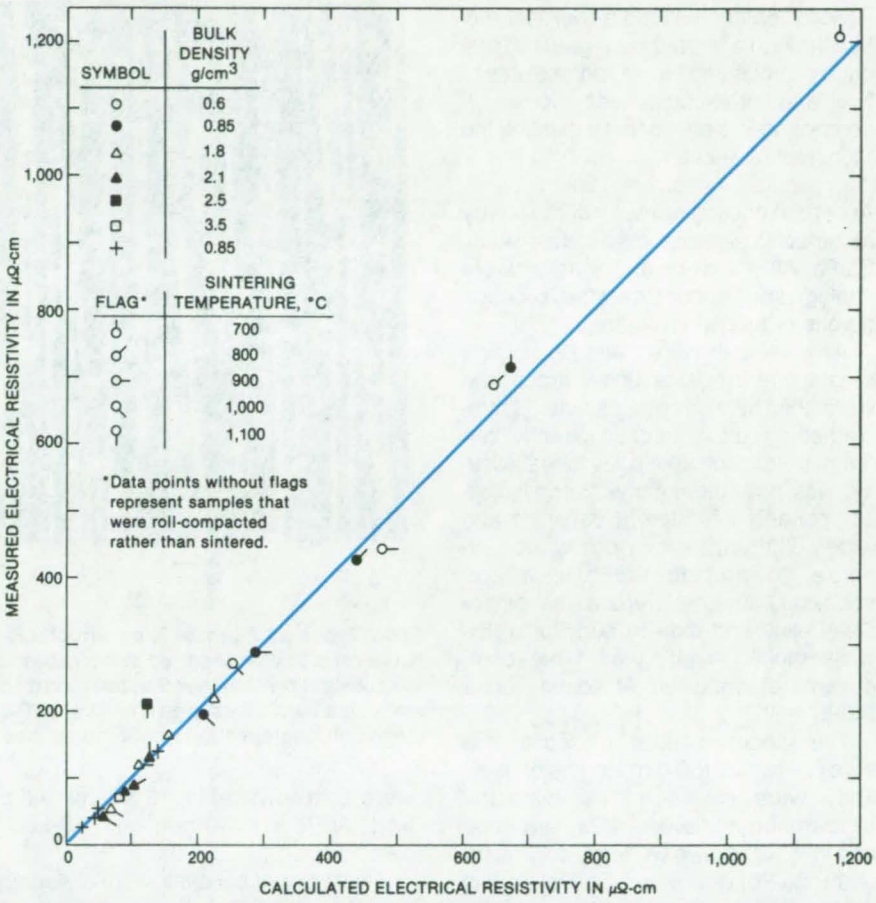

Resistivities of Sintered Nickel Samples calculated using the formula in the text agree well with measured values found in the literature. The value of the adjustable parameter was A = 4.

For a given powder, the value of A could be determined from measurements on one sintered sample of known volume fraction, ϕ. Then the formula could be used to predict what volume fraction to use to obtain a desired resistivity.

While the formula should be applicable to sinters of various metals, it has been tested for sinters made from nickel carbonyl powders. As shown in the figure, resistivities calculated with the formula are in excellent agreement with published experimental values. The sinters included cover a bulk density range of almost 6 to 1 and a resistivity range of 50 to 1. They were prepared at temperatures ranging from 700° to 1,100° C. Resistivity values were calculated for all of these samples using the value of A = 4.

This work was done by Robert F. Fedors of Caltech for **NASA's Jet Propulsion Laboratory.** *For further information, Circle 32 on the TSP Request Card.*

NPO-15587

Directional Solidification of Monotectic Alloys

Cooling at certain rates produces fibrous composite structures.

Marshall Space Flight Center, Alabama

Solidification induced by vertical motion through a temperature gradient produces fibrous and tubular composites of two- and three-component alloys with compositions close to that exhibiting the monotectic reaction

liquid 1 ⇌ solid + liquid 2.

At certain cooling rates, all of the binary monotectic systems investigated (Al/In, Cu/Pb, Al/Bi, Cd/Ga, and a transparent analog, succinnonitrile/water) produce fibrous or tubular structures.

Alloy samples were melted in alumina or graphite crucibles under argon and were then either chill-cast into 3-mm-diameter rods or sucked directly into 3-mm-bore alumina or silica tubes. Alloying was not automatic with immiscible components of different densities and widely-different melting points. For example, to prepare Cu/Pb/Al, it was necessary first to prepare the binary Cu/Al alloy and then to add Pb to this while molten. Melting all three components at once left Al floating on a Cu/Pb melt.

The specimen tubes, closed at one end, contained 150-mm lengths of alloy. They were driven into a platinum/rhodium furnace over a 1/2-hour period and then withdrawn vertically downward (Al/In, Cu/Pb) or upward (Cd/Ga, Pb/Ga) through a water-cooled cylinder at traction rates between 1 and 250 μm/s. (The direction of withdrawal was determined by the relative densities of the two liquid phases and the requirement that any excess of the lower-melting liquid 2 must collect at the start of the growth.) Temperature gradients at the monotectic temperatures were controlled by the furnace settings and the position of the water-cooled cylinder insert relative to that of the furnace. The gradients used were as follows: Al/In, 19 K/mm; Cu/Pb and Al/Bi, 15 K/mm; and Cd/Ga, 12.5 K/mm.

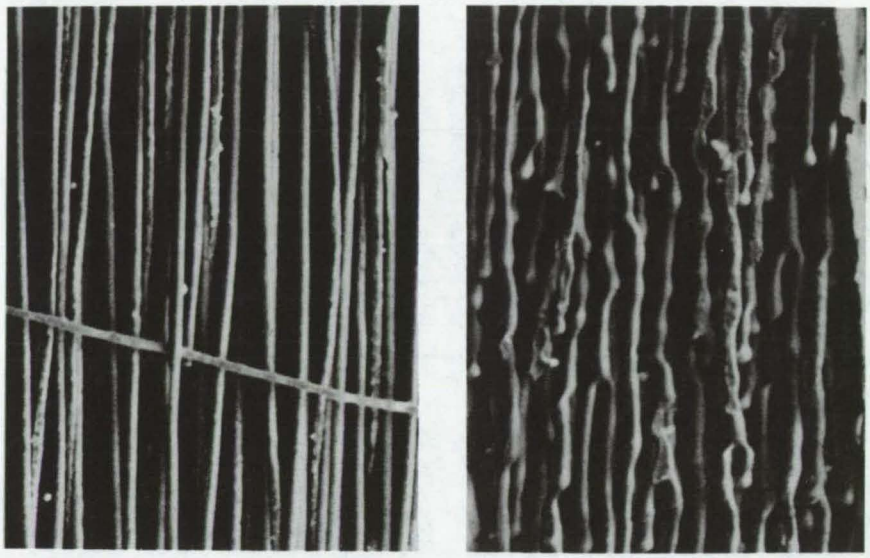

Two Types of Fibrous Alloy Structures were observed: (a) Closely packed fibers of uniform diameter occurred at low growth rates (indium fibers grown from an Al/In melt of 17.5 weight percent In at 2.5 μm/s) and (b) coarse, branched, irregular fibers at high growth rates (gallium fibers grown from a Cd/Ga melt of 15.4 weight percent Ga at 50 μm/s). In these photographs the nonfibrous phase has been etched away.

Two types of behavior were observed (see figure). (a) Closely packed tubes of nearly uniform diameter occurred only at slow growth rates, typically ⩽10 μm/s. (b) Coarser, branched, irregular tubes occur only above a certain growth rate, typically ⩾50 μm/s. Structure (a) was found to be characteristic of alloy systems with a high miscibility gap (about 300° C). Structure (b) occurred in systems in which the miscibility gap was small (about 15° to 30° C).

Directionally solidified samples of monotectic alloys can be selectively etched to remove the fibrous phase, leaving a metallic matrix permeated by parallel, closely packed holes. Sieves or filters of this type have been produced having hole diameters of about 10 μm, spacing of about 30 μm, and length:diameter ratios of 50:1.

This work was done by Angus Hellawell of Michigan Technological University for **Marshall Space Flight Center.** *For further information, Circle 33 on the TSP Request Card.*

Inquiries concerning rights for the commercial use of this invention should be addressed to the Patent Counsel, Marshall Space Flight Center [see page A5]. Refer to MFS-25767.

Books and Reports

These reports, studies, and handbooks are available from NASA as Technical Support Packages (TSP's) when a Request Card number is cited; otherwise they are available from the National Technical Information Service.

Stress-Corrosion Cracking of Certain Aluminum Alloys

The SC resistance of new high-strength alloys is tested.

A research report describes progress in a continuing investigation of stress-corrosion (SC) cracking of some aluminum alloys. The objective of the program was to compare the SC behavior of the newer, high-strength alloys (7475-T7351, 7050-T73651, and 7049-T7351) with that of the established SC-resistant alloy, 7075-T73.

Tests were conducted with both smooth and precracked specimens. The smooth specimens were 3.175-mm-diameter tensile rounds stressed in window-frame jigs. Four stress levels were used; 25, 35, 45, and 55 kpsi (172, 241, 310, and 379 MPa, respectively).

Double-cantilever-beam (DCB) specimens of various sizes were used for crack-growth tests. The DCB specimens were oriented so that cracking would occur in either the short-transverse plane or long-transverse and propagate in the rolling direction. (The directions refer to the axes of the rolled plates from which the specimens were machined.) The specimens had chevron notches and side grooves to control crack configuration. Most of the specimens were precracked by turning a pair of stainless steel bolts into machined notches at the ends.

After precracking and loading, the specimens were exposed to the weather at Daytona Beach, Florida. Crack-length measurements were taken at the ends of various intervals from 1 day up to 1 year. The average of the crack lengths measured at each edge was used in the calculation of stress intensities and crack-growth rates.

After exposures as long as 4 years, DCB specimens of 7475-T7351 reached threshold stress-intensity limits and appeared to be approaching crack arrest. Cracks in DCB specimens of the 7050 and 7049 materials continued to grow at stress intensities below 13 MPa$\sqrt{m}$ with only a slight indication of a downturn. Further studies will be required to determine the effect of self-loading from corrosion-product wedging.

This work was done by K. R. Hasse and R. C. Dorward of Kaiser Aluminum & Chemical Corporation for **Marshall Space Flight Center.** *To obtain a copy of the report, Circle 34 on the TSP Request Card.*
MFS-25773

Cracks in Glass Polymers Induced by Solvent Absorption

The combination of soluble particles and absorbed solvents cause polymer cracking.

A new failure mechanism in glassy polymers has been identified. It is cracking caused by the presence of particles that are insoluble in the polymer matrix but are soluble in a solvent. The experiments performed and equations that describe the cracking phenomenon are set forth in a concise report.

Cracks and cavities were observed in a rigid glassy epoxy where such water-soluble materials as sucrose, potassium acetate, cobaltous chloride, and calcium nitrate were present. Some of the cavities developed into cracks that grew until they were 5 to 10 times longer than the original particle. Calculation of the pressure on a cavity surface shows considerable loading; for example, potassium acetate in epoxy resin yields a calculated cavity pressure of about 19,000 psi (1.3×10^8 N/m^2). This pressure is sufficient to initiate cracks and to cause them to grow.

Cracking occurs for a number of solvents, including water, and is caused by a solvent diffusing to the vicinity of an particle, dissolving it, and forming a cavity. The primary requirement for cavity formation is that the soluble particles be insoluble in the polymer matrix but soluble in the solvent.

Generally, the more soluble the particle and the smaller the particle size, the faster it dissolves. The difference in chemical potential between the pure solvent and the solution, which shows up as an osmotic pressure tends to make the solution in the cavity more dilute and is the driving force for the growth of the cavity.

By removing soluble particles from a polymer before it is used in an environment containing the solvent, cracking and subsequent material failure can be avoided. A potential use of the mechanism would be in determining the strength of transparent polymers.

This work was done by Robert F. Fedors of Caltech for **NASA's Jet Propulsion Laboratory.** *To obtain a copy of the report, Circle 35 on the TSP Request Card.*
NPO-15072

Freeze/Thaw Properties of Cellular Glass

Without moisture, temperature cycles do no harm.

Cellular glass has been proposed as a substrate for glass reflectors in solar concentrators. Considerable concern among designers has been expressed regarding the environmental degradation of celular glass in field service, particularly in regard to its resistance to high-humidity freeze/thaw cycles. A set of experiments described in a new report indicates inherent material variability to be a greater deterrent to application of the material than freeze/thaw effects.

Two types of cellular glass blocks — bare blocks and blocks that had been coated with a highly-moisture-resistant coating — were cycled in an environmental test chamber. No degradation in physical or mechanical properties of either the coated or uncoated specimens was observed after 53 high-humidity freeze/thaw cycles. The study also revealed that the results from freeze/thaw experiments on cellular glass are highly sensitive to experimental design.

This work was done by Peter O. Frickland, Edward L. Cleland, and Takashi Hasegawa of Caltech for **NASA's Jet Propulsion Laboratory.** *To obtain a copy of the report, Circle 36 on the TSP Request Card.*
NPO-15854

Computer Programs

These programs may be obtained at very reasonable cost from COSMIC, a facility sponsored by NASA to make new programs available to the public. For information on program price, size, and availability, circle the reference letter on the COSMIC Request Card in this issue.

Random Life Curves for Common Engineering Materials

Program incorporates non-Rayleigh effects in evaluating structure life.

The RMS2 computer program converts constant-amplitude fatigue allowables to random-loading allowables, with the influence of peak distribution and mean stress considered. RMS2 has been used in the random-loading fatigue analyses of the Shuttle orbiter structure.

Random stress-life data are required in measuring the allowable life of a structure loaded in a random environment. Conventionally, it is assumed that the probability of peak stress distributions follows a Rayleigh curve, and the root-mean-square stress-life curve is derived from a constant stress-vs.-cycle curve based on this assumption.

However, peak distributions in a random process are rarely fully Rayleigh. In the case of non-Rayleigh distribution, mean stress affects peak counts considerably. The shape of the real peak distribution can be expressed in terms of an "irregularity factor." RMS2 incorporates this irregularity factor and the stored fatigue data of 30 common engineering materials to measure the stress life of materials in a random environment.

Goodman stress-vs.-cycle for 30 common engineering materials are built into the program. These data may be modified or new materials added as needed. Standard input to RMS2 consists of a material code, an upper limit of the root-mean-square stress to be used in the life curve, the mean stress value in consideration, the stress concentration factor, the ultimate strength (if known), and the peak distribution parameter. Output includes lists of root-mean-square stress, percentage of ultimate strength, and number of life cycles.

RMS2 is written in FORTRAN IV for batch execution and has been implemented on two machines: a CDC CYBER 170-series computer with a central-memory requirement of approximately 100K (octal) of 60-bit words and an IBM 370-series computer with a central-memory requirement of approximately 65K of 8-bit bytes. The RMS2 program was developed in 1980.

This program was written by Tianlai Hu of Rockwell International Corp. for **Johnson Space Center.** *For further information, Circle A on the COSMIC Request Card.*
MSC-20433

Life Sciences

Hardware, Techniques, and Processes

Flowthrough Bacteria-Detection System

An online system allows repetitive cycling of sample intake, bacteria counting, and sterilization.

Langley Research Center, Hampton, Virginia

A microbe detection system developed at Langley Research Center collects a water sample on-line, adds a growth medium, incubates it, estimates the number of fecal coliform bacteria in the sample, and then sterilizes the broth in preparation for a new cycle. The bacteria count is estimated without the need for a skilled operator. More than one growth medium and incubation temperature can be incorporated in a cycle, making it possible to detect different groups of bacteria.

A schematic of the system is shown in Figure 1. The major components are the intake valve, the incubator, and the media reservoir. Figure 2 is a detailed view of the intake valve.

The intake valve has two solenoids and two concentric valve stems. The valve operates in a sample intake mode and a system sterilization mode. In the intake mode, energizing the rear solenoid moves the entire front solenoid forward and opens the inner valve. Energizing the front solenoid opens the outer dome valve and permits sample inflow through the path shown at the left of Figure 2. In the sterilization mode, only the rear solenoid is energized, allowing the steam to flow around the inner valve and through the path shown at the right of Figure 2.

The operating sequence always begins with sterilization, followed by a purge, in which the incubator is flushed for 20 minutes to remove residual organisms from the previous test. Sample intake occurs in two steps: First, a measured sample fills the accumulator; and second, the intake valve is energized in the intake mode to pass the sample to the incubator. The growth medium is introduced through a separate flow line.

The quantity of bacteria is determined by incubating the sample until the bacteria count reaches a critical value, as determined by the voltage indication on the electrode-response recorder. The time it takes for this critical value to be reached is a measure of the initial bacteria count — the larger the initial count, the less time is required. The incubation temperature of 44.5° C is

(continued on next page)

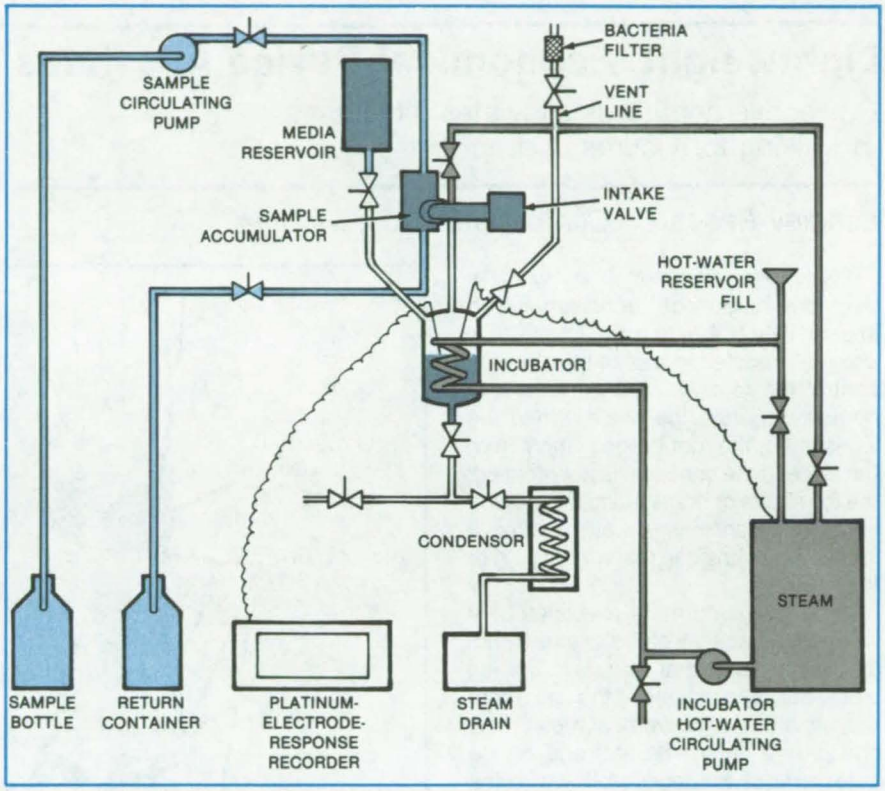

Figure 1. This **Flowthrough System** measures the bacteria count by using a sample/incubate/measure cycle. The steps in the cycle are on/off operations, so that the cycle can be automated easily.

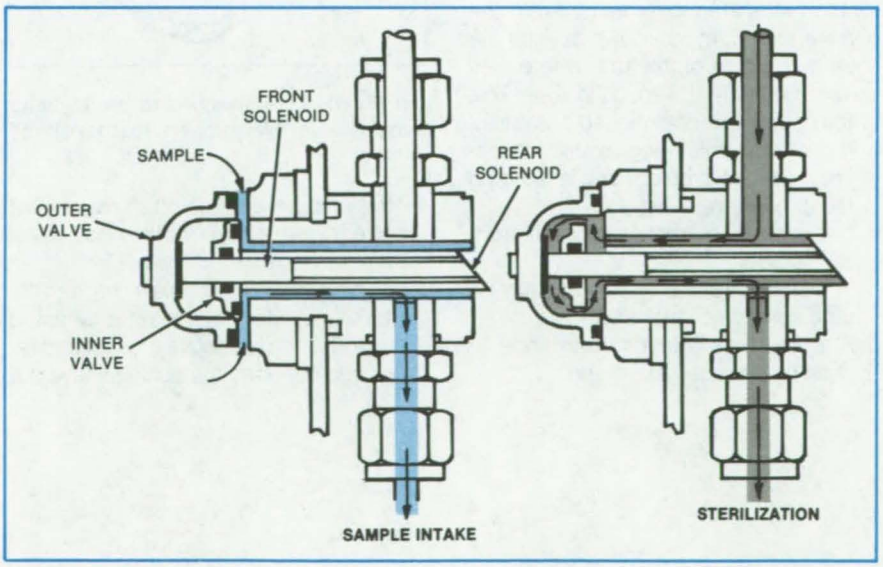

Figure 2. The **Intake Valve** has two operating modes: sample intake and sterilization. Samples containing *Escherichia coli* and *Bacillus subtilis* spores and a natural stream sample were used to test the system. A 15-minute sterilization was needed to kill all *E. coli* and to sterilize the stream sample. The spores require about 60 minutes.

maintained by circulating hot water through a glass coil. After a measurement, the sample is drained from the system, sterilized, and discarded.

The correlation of endpoint response time to the number of fecal coliforms per 100 ml of sample for the flowthrough system compares favorably with that for laboratory controls. Results indicate that the flowthrough system is effective in controlling the viable organisms and that steam at 15 psig (0.1 N/m2) sterilizes the system without altering the microbial flora.

This work was done by Judd R. Wilkins and David C. Grana of **Langley Research Center.** *For further information, Circle 37 on the TSP Request Card.*

Inquiries concerning rights for the commercial use of this invention should be addressed to the Patent Counsel, Langley Research Center [see page A5]. *Refer to LAR-12871.*

Lightweight, Economical Device Alleviates Drop Foot

Corrective apparatus alleviates difficulties in walking for victims of drop foot.

Langley Research Center, Hampton, Virginia

Many people suffer from what is termed a "drop-foot" condition, which impairs their ability to walk. This term is used to indicate the loss of the ability to control the foot with the muscles that normally operate the ankle. When the leg is lifted, the foot droops limply from the ankle. If the condition is not rectified, the toe scuffs or drags along the walking surface, which makes walking difficult for the victim and can result in tripping or falling.

Drop foot is normally alleviated by a "short leg brace," which includes a padded metal band that encircles the leg below the knee but above the calf. From this metal band two vertical metal rods, one on the inner side and one on the outer side of the leg, run down to the area of the ankle where each rod is bent into a coil torsion spring to provide the flexibility and resilience required to match the ankle movements. From the coil the rods continue down outside the shoe to the area of the arch where they are permanently affixed to the shoe. This brace has several objectionable features;

a. It is heavy, which aggravates the victim's walking problem and is tiring on the already-weak leg;
b. It is expensive, costing typically from $30 to $50;
c. It is limited to use with shoes having hard soles and low heels;
d. It is costly to transfer from shoe to shoe by a bracemaker; and

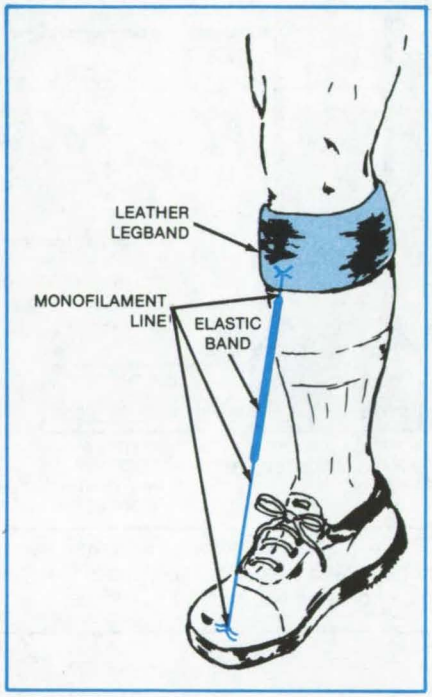

An **Elastic Line** attached to the legband provides flexible support to toe of the shoe.

e. It is unsightly, which often causes the already-sensitive victim additional embarrassment.

A new device consists of an adjustable, comfortable leather legband that girdles the leg above the calf and retains and supports the ankle joint with a flexible ligament connected to the toe of the shoe (see figure). The soft leather band approximately 3 inches (7.5 cm) wide is fitted to the leg below the knee and above the calf. An elastic band is attached to a monofilament loop at the legband, and another larger loop of monofilament line is attached to the lower end of the elastic band. The loop on the device is simply inserted through a small loop installed on the toe of the shoe.

This device provides the flexibility and support to alleviate the drop-foot condition. It is very inexpensive, costing less than $1 for the basic device and less than 1 cent for each shoe adapted for the device. It is lightweight, weighing less than an ounce (30 cm^3), can be transferred easily from shoe to shoe, and can be detached and attached at will.

The leather legband and the elastic band are visible, but the monofilament line is not readily visible, so the device is not as obvious or unsightly as the standard short leg brace. Also, the device can be used with flat (heelless) shoes, sneakers, crepe-soled shoes, canvas shoes, and many other types of shoes that are not usable with the short leg brace.

This work was done by Bert C. Deis of **Langley Research Center.** *No further documentation is available.*
LAR-12259.

Transducer Joint for Kidney-Stone Ultrasonics

Improved mounting allows joint to last long enough for effective treatment.

Goddard Space Flight Center, Greenbelt, Maryland

Ultrasonic therapy for kidney stones is improved by a new way of connecting a wire-probe ultrasonic waveguide to its transducer. The nonsurgical disintegration of kidney stones by ultrasonic energy had previously been hampered by the tendency of the wire probes to break. The new mounting method prevents breakage, so that the disintegration can be completed.

In ultrasonic therapy, a catheter is positioned by a cystoscope at the site of a kidney stone in the urinary tract, and a long wire probe — an ultrasonic waveguide — is passed through the catheter so that it contacts the stone. The opposite end of the waveguide is attached to an ultrasonic transducer, which sets the wire into longitudinal and transverse vibrations. The wire transmits the ultrasonic energy to the stone, causing it to fracture into small fragments that the patient can then pass spontaneously after the catheter is withdrawn.

In the past, stresses induced in the wire by the 20-kilohertz ultrasound have broken the wire at the point of connection to the ultrasonic transducer after about 15 seconds of operation. A considerably longer period — about 1 minute — is needed to ensure that the stone is adequately disintegrated. When the wire was inserted in the transducer bore, it was clamped by a setscrew. The setscrew crimped the wire, and the stresses thereby created were the primary cause of premature breakage when the wire was subjected to lateral vibration by the transducer. In addition, the undamped lateral motion of the vibrating wire at the point where it emerged from the transducer bore contributed to wire fatigue.

A new way of supporting the wire at and near the transducer reduces deformations and stresses. Two flat-ended setscrews now hold the wire in the transducer bore (Figure 1). A groove in the end of one setscrew serves as an anvil for the wire. When the other setscrew is tightened against the grooved one, it does not crimp the wire but merely presses it into the groove, and stress concentrations are thereby greatly reduced. The change in mass distribution due to the additional setscrew is small enough that it does not significantly unbalance the transducer or reduce its efficiency.

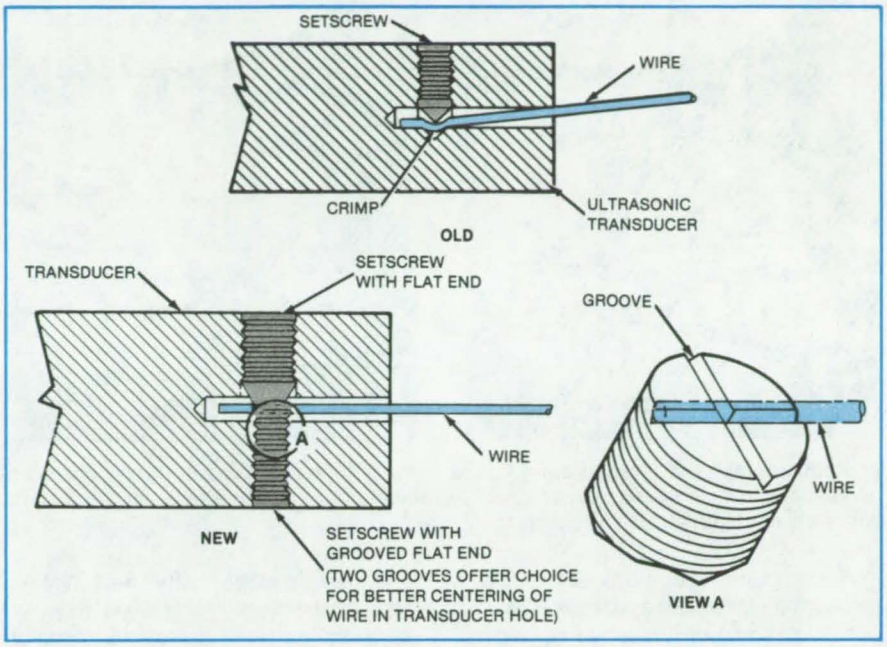

Figure 1. A **V-Shaped Groove** in a setscrew nests the probe wire without crimping or otherwise applying a damaging stress.

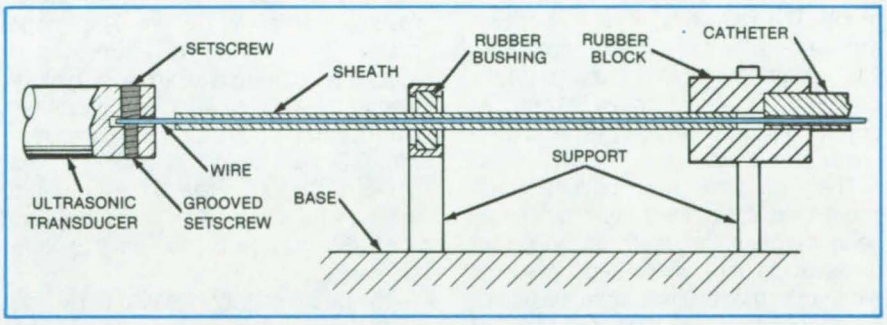

Figure 2. A **Sheath and Rubber Dampers** constrain the lateral vibration of the wire waveguide. The combination of V-shaped mounting groove, sheath, and rubber dampers increases the life expectancy of the wire 15 times or more.

Excessive lateral vibration of the wire is now prevented by a sheath extending 3 to 4 inches (7.6 to 10.2 cm) over the wire from the point of emergence from the transducer to a thick, soft rubber block (Figure 2). A rubber bushing supports the sheath midway along its length. Besides damping lateral wire vibration, the rubber block supports the catheter. Within the catheter, and especially at the stone, the wire has ample freedom to develop the random lateral vibrations necessary to shatter the stone.

This work was done by Earl D. Angulo of **Goddard Space Flight Center.** *For further information, Circle 38 on the TSP Request Card.*

This invention is owned by NASA, and a patent application has been filed. Inquiries concerning nonexclusive or exclusive license for its commercial development should be addressed to the Patent Counsel, Goddard Space Flight Center [see page A5]. Refer to GSC-12652.

Sharp-Focus Composite Microscope Imaging by Computer

Enhanced depth of focus
aids medical analysis.

NASA's Jet Propulsion Laboratory, Pasadena, California

Photomicrographs of Alveolar Lung Tissue show different portions in focus (left and middle), depending on the depth setting of the microscope in each instance. A composite photomicrograph of the same area (right) was made by the new system, which scanned the entire object depth in 1.0-μm increments.

A computer image-processing system synthesizes a sharply-focused composite picture from a series of photomicrographs of the same object taken at different depths. The computer rejects the blurred parts of each photomicrograph. The remaining in-focus portions are used to form a focused composite. The system has been used to study alveolar lung tissue (see figure) and has applications in medicine and the physical sciences.

The view through an optical microscope typically contains blurred portions because often the depth of the object exceeds the microscope depth of focus. A common practice is to scan the microscope manually over the entire range of depth and attempt to reconstruct the object mentally from the parts in focus in each plane or else to take photomicrographs at a series of depths, then manually cut and paste together the focused parts. The new computerized system performs, in effect, a faster, more precise version of the cut-and-paste technique.

The microscope in the new system has a 40 × objective and a dual-moving-mirror image-plane digitizer in place of an eyepiece. The microscope stage is controlled by stepping motors and is capable of scanning in depth increments as small as 0.5 μm. The image plane, 1 cm^2, is divided into a 1,024-by-1,024 square array of picture elements. With the 40 × magnification, each element corresponds to a square with 0.244-μm sides in a square object plane of 250-μm sides. At each depth setting, the image data are stored as 1 of 256 gray levels for each picture element.

The range of gray values in the image at each depth is normalized to a standard range of values by computer processing, so that identical features from one depth to the next will correspond in gray value. If the depth increment is small enough, sufficient duplication of feature data ensures that each point in the image field will be in focus in at least one image in the series.

The image from each depth setting is divided into regions having common generally-in-focus areas. An area is divided into a square grid of subregions, each of which is a square of 20-by-20 picture elements. Within each grid square, the computer calculates the average rate of change of the gray level from element to element. A higher rate of change denotes sharper edges, signifying sharper focus. The squares having the highest rates will yield the most sharply focused subimages, and these are selected by the computer for assembly into the final composite. A photographic film or paper is exposed with the composite image in the same manner as in converting from space-exploration images to photographs.

This work was done by Ray J. Wall of Caltech for **NASA's Jet Propulsion Laboratory.** *For further information, Circle 39 on the TSP Request Card.*
NPO-15207

Mechanics

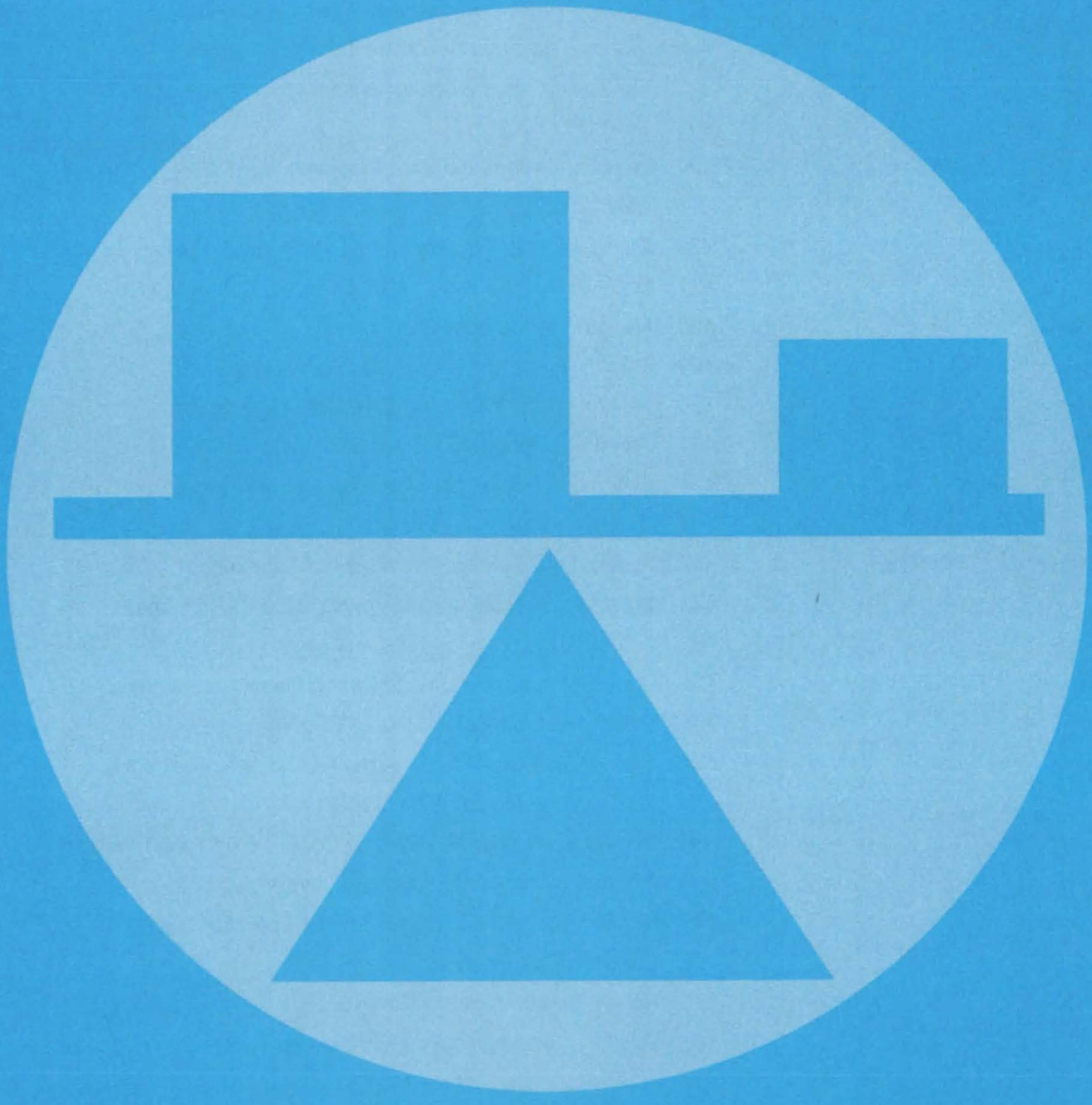

Hardware, Techniques, and Processes

Books and Reports

Computer Programs

Electronic Dilatometer

A nonclamping micrometer measures small strains.

Goddard Space Flight Center, Greenbelt, Maryland

An electronic dilatometer measures the minute dimensional changes caused by moisture absorption in graphite/epoxy composites. The instrument handles a sample 6 inches (15 cm) long and has a strain resolution of 0.1 microinch/inch (0.1 micron/meter).

The dilatometer is a relatively-inexpensive electronic micrometer that can accurately measure small changes in the length of a sample. Since the sample is not clamped, the precision and resolution are not affected by clamping forces.

The jig on which the sample rests during measurement (see figure) is machined from a solid metal block to eliminate bolted joints that might otherwise affect measurement accuracy. The metal is Invar alloy (or equivalent), which has a low and accurately-known thermal-expansion coefficient. Thus the system could also be used to measure thermal expansion.

A nonmagnetic metal (aluminum) target is attached to the sample so that a change in the length of the sample can be detected by an eddy-current sensor. A commercially available unit, the sensor gives an output voltage that changes with the distance to the target.

To determine the voltage/distance calibration of the instrument, a differential-micrometer translation stage was temporarily attached to the sample-holding jig and used to move an aluminum eddy-current target through known displacements. A digital voltmeter with 0.1 mV resolution was used for the display. The sensor circuits were adjusted to produce an output signal change of 1 mV per microinch/inch of target strain.

The dilatometer head was placed on a granite surface plate during measurements. To correct for instrument drift between measurement sessions, readings were also taken from quartz reference samples. An external computer was utilized for drift error correction of the data and for curve plotting.

Moisture absorption in the graphite/epoxy samples was determined by weighing the samples on an analytical semimicrobalance, which was also placed on the granite surface plate for stability. Weight readings were corrected for drift by reference to quartz weight standards.

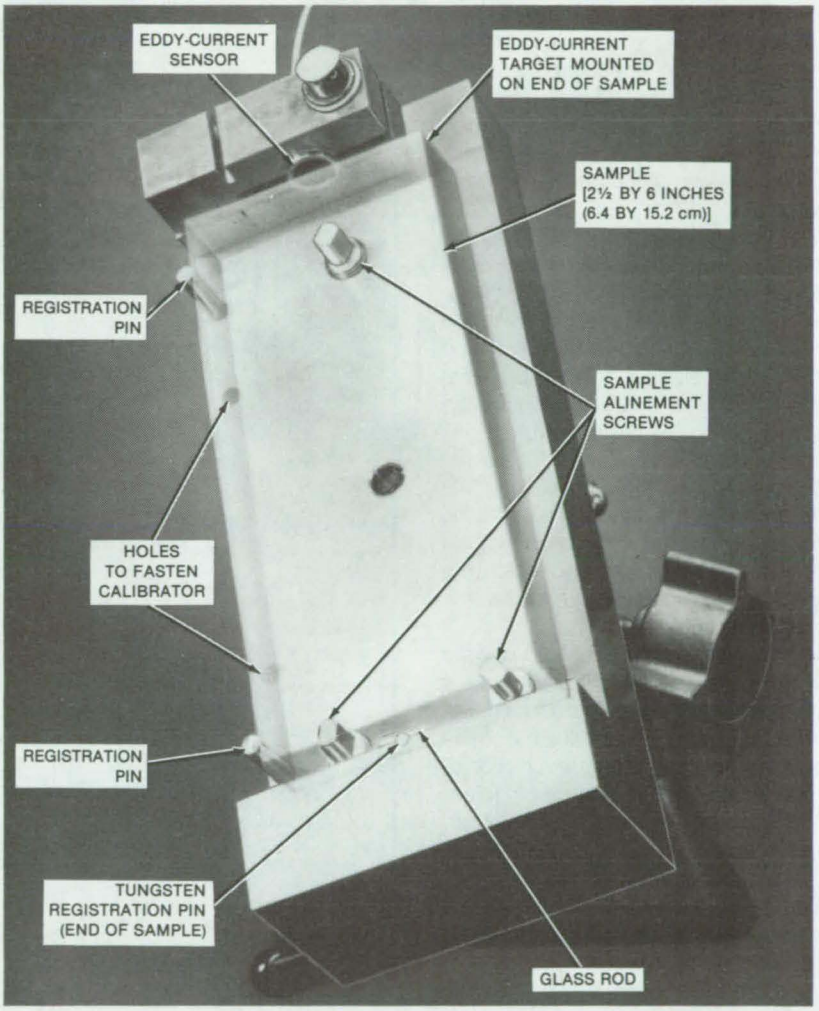

The **Dilatometer Head** is mounted at an angle so that gravity will hold the sample against the registration pins. This permits the samples to be repositioned accurately in the jig without clamps. (Clamps could easily cause strains larger than those being measured.) An eddy-current target is fastened to the upper end of each sample. A stable wear-resistant contact point is provided at the other end of the sample by a semicircular Vycor glass rod held by epoxy. During measurement the rod rests against a tungsten vertical registration pin at the lower end of the holding jig.

A correlation of the measurements of strain and moisture absorption as a function of time yields moisture-diffusion and moisture-expansion coefficients. With this information, it is possible to predict the humidity-induced dimensional changes in items constructed of the sample material.

This work was done by C. R. Stroope, G. S. Plews, and J. Ermlich of Hughes Aircraft Co. for **Goddard Space Flight Center.** *For further information, Circle 40 on the TSP Request Card.*

This invention is owned by NASA, and a patent application has been filed. Inquiries concerning nonexclusive or exclusive license for its commercial development should be addressed to the Patent Counsel, Goddard Space Flight Center [see page A5]. *Refer to GSC-12738.*

Torque Compensator for Mirror Mountings

Device nulls flexural distributions of pivotal torques.

Goddard Space Flight Center, Greenbelt, Maryland

A magnetic torque-compensating device nulls the angular acceleration of a scanning mirror by opposing the torque generated in the mirror pivots. With the magnetic compensator, the net torque on the mirror is nearly zero, resulting in a scanning angular velocity that is nearly constant.

The compensator assembly (see the figure) consists of two major components, each containing two magnets. The rotating magnet bar attaches to the back of the scanning mirror. The fixed magnet bar attaches to the bridge that supports the stationary portion of the mirror torquer (the flexing pivots). This magnet assembly is surrounded by the bridge, and adjustments to the magnets are made through access holes in the bridge. The two fixed magnets may be extended or retracted by adjusting the position of either or both ends of the fixed magnet bar.

As the movable bar rotates, the airgap between the fixed and movable magnets increases at one end and decreases at the other end. The resultant magnetic torque is typically a nonlinear function of the rotation angle. Since a nearly-linear torque variation with angle is needed to balance the flexing-pivot torque, the magnet positions are adjusted to straighten the torque curve, bringing it as close as possible to a straight line of the desired slope.

The hysteresis loops of the magnets should have little or no area; otherwise, the system will lose energy from the magnets pulling harder when going than when coming. To minimize the hysteresis-loop area, the magnets are made of samarium/cobalt alloy or of ferrite, and the magnet bars are made of a low-hysteresis alloy and are laminated.

Some experimentation is required to find the best magnet settings, and several different kinds of adjustments are possible. The torque curve is steepened by moving the moving-bar pivot closer to the fixed bar. The zero-torque angular position is changed by tilting the fixed magnet. The shape of the torque-versus-angle curve is changed by varying the distances between the two magnets on each bar (not necessarily by the same amounts). Fine adjustments can also be made by varying the positions of setscrews or other small magnetic objects in the fringing field of the magnets.

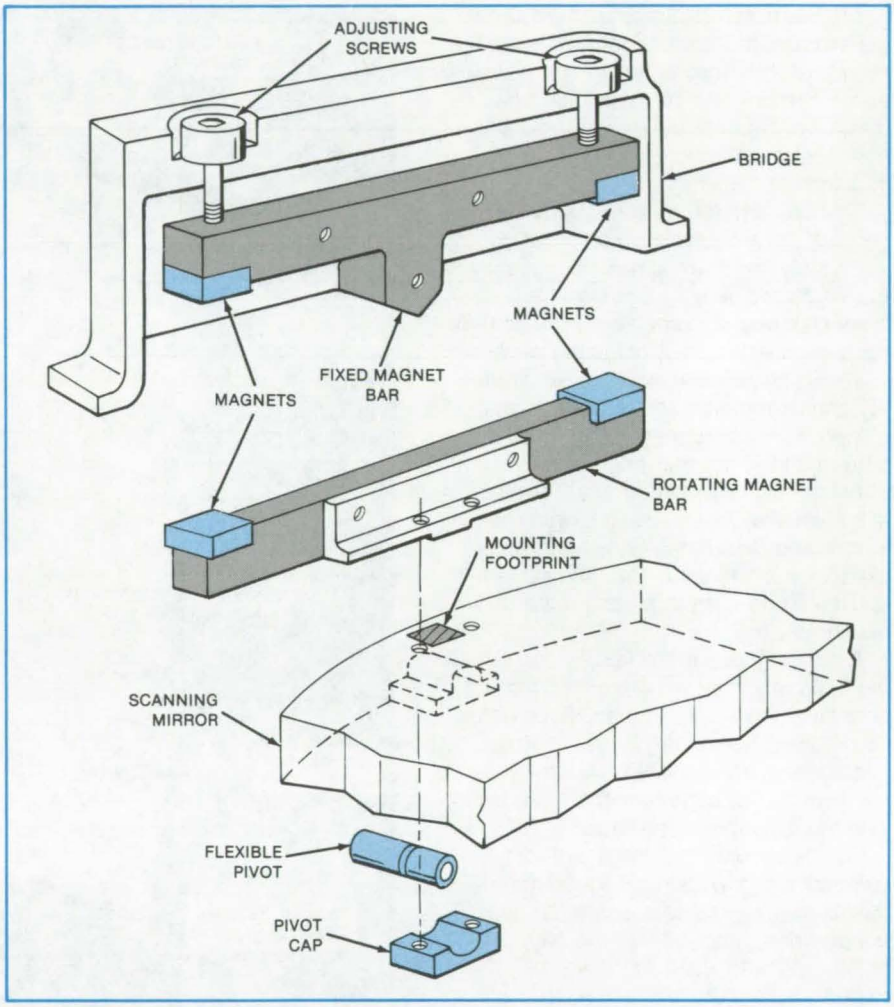

A **Magnetic Compensator** for flexing-pivot torque consists of opposing fixed and movable magnet bars. The magnetic torque varies nonlinearly as a function of the angle of tilt of the movable bar. The positions of the fixed magnets can be changed to improve the magnetic-torque linearity.

With only one fixed and one moving bar per pivot, the attractive force of the magnets loads the mirror, which may be a significant part of the total load on the mirror. The temptation to compensate for the load from the magnets with a larger suspension pivot spring will only result in a still greater load on the mirror. With two or more symmetrically-counterbalanced moving bars, the mirror load that results from the magnets attracting each other can be diminished. The bars are adjusted by moving them from side to side.

This work was done by S. D. Howe of Hughes Aircraft Co. for **Goddard Space Flight Center.** *For further information, Circle 41 on the TSP Request Card.*

This invention is owned by NASA, and a patent application has been filed. Inquiries concerning nonexclusive or exclusive license for its commercial development should be addressed to the Patent Counsel, Goddard Space Flight Center [see page A5]. Refer to GSC-12742.

Controlling Heat-Exchanger Outlet Temperature

Nearly constant temperature is maintained regardless of fluid flow.

Marshall Space Flight Center, Alabama

A bypass channel provides some temperature regulation for the output of a fixed-area heat exchanger. The arrangement was devised to maintain constant-temperature output under varying flow rates.

The heat-exchanger surfaces cannot be varied to alter the amount of heat transferred. However, a constant output temperature can be maintained if one stream of fluid is heated to nearly the maximum heat-exchanger temperature, then cooled by mixing it with an unheated stream at the outlet to achieve the desired intermediate temperature.

The heat-exchanger area is made sufficiently large to assure adequate heat transfer at the maximum flow rate. Unheated fluid is ducted around the exchanger in the bypass stream, and the two streams are combined at the outlet (see figure). The bypass flow is adjusted to obtain the desired output temperature.

This method is used for a heat exchanger on the Space Shuttle main engine. The demand for oxygen flow through the heat exchanger varies during a flight, depending on engine power level, trajectory, acceleration, and aerodynamic heating. The temperature of the oxygen must not vary even though the flow varies and for safety must remain below a maximum value to protect control-valve seals and the main tank structure.

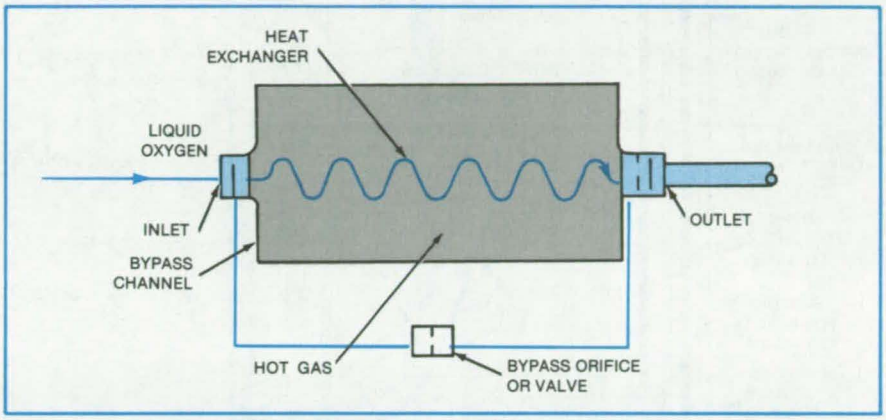

Mixing Heated and Unheated Fluids ensures a constant temperature at the outlet of a heat exchanger. The main-stream fluid (in this case oxygen) is heated, and the bypass fluid is unheated.

The bypass flow rate is in the range of 30 to 35 percent of or the total flow rate through the heat exchanger as the total flow of liquid oxygen varies from 1.1 to 2.2 lb/s (0.5 to 1 kg/s). The bypass principle can be used with fluids other than liquid oxygen — water, for example.

This work was done by C. M. Daniels of Rockwell International Corp. for **Marshall Space Flight Center.** *No further documentation is available.*
MFS-19667

Vibration-Isolation Bench for Testing in Vacuum

Precise optical systems can be tested without contamination.

Goddard Space Flight Center, Greenbelt, Maryland

A vibration-isolated test bench is made from low-outgassing materials so that it can be used in vacuum. It was developed for precise optical systems that must not pick up contamination from the outgassing of nearby objects. A scaled-down version might find wider application in electron optics or electron-beam lithography.

The bench top is a cast-iron table 90 in. (2.29 m) in diameter, with a mass of 6,630 lbm (3,000 kg). The table is supported by three vibration isolators. The bench is designed for a maximum load of 3,500 lb (15.6 kN, the weight of 1,590 kg).

Each vibration isolator (see figure) has an air spring to suppress vertical vibrations. The leveling valve controls the air pressure to maintain the steady-state level of the piston: The vertical position is sensed by the valve-activating lever. A fine screw adjustment sets the lever bias.

The pressure chamber that houses the air spring is supported at its base by three inner pendulum rods. These rods are supported at their upper ends by a supporting cylinder that is, in turn, supported by three outer pendulum rods. This double-pendulum support system is used because it provides the required low stiffness for horizontal vibrations while requiring less height than would be needed for a single-pendulum suspension. The tubes that run from the pressure chamber to the gas supply and exhaust lines are flexible to minimize horizontal-vibration coupling.

The air-spring components are all heremetically sealed within the pressure chamber to prevent leakage into the

(continued on next page)

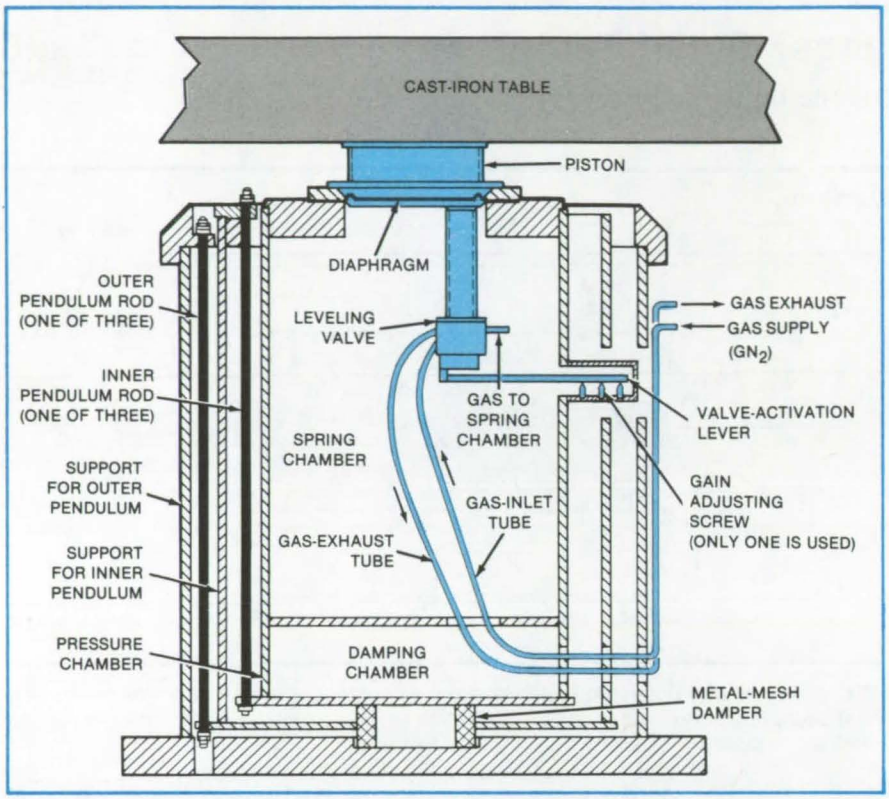

A **Vibration Isolator** is one of three such units that support a cast-iron table. The table is used to test optical systems in a vacuum. The isolator is made from commercially available components.

vacuum chamber: No control rods pass through walls, and the gas tubes are ducted through the pressure-chamber and outer vacuum-chamber walls. All materials and finishes are selected for low outgassing and compatibility with equipment sensitive to contamination in a vacuum: For example, the gas tubes are of stainless steel.

The vertical fundamental frequency is less than 0.7 Hz, while the horizontal fundamental frequency is 0.5 Hz. The system provides 85 percent or greater isolation for both vertical and horizontal vibrations of frequencies at and above 5 Hz. The gas-leakage rate is less than 4×10^{-2} atm-cm^3/s (4×10^{-3} Pa-m^3/s).

This work was done by J. C. Dankowski of Hughes Aircraft Co. for **Goddard Space Flight Center.** *No further documentation is available.*
GSC-12753

Electronic Force Gage for Welders

Welding force is monitored in process.

Marshall Space Flight Center, Alabama

A system designed for the calibration and maintenance of resistance welding equipment produces an oscilloscope trace showing the profile of the welding force. The apparatus, shown in Figure 1, was originally developed to check pneumatic equipment used to make stitch welds on the Space Shuttle main-engine controller.

The new strain-gage system provides a dynamic picture of the welding pressure and the current pulse. It also allows a permanent record of the variation of the force during the welding cycles.

The motion of the deformable member is sensed by the strain gages. Output signals from the strain gages are amplified and fed into an oscilloscope to produce a trace of the welding force. A reference trace is photographed for use

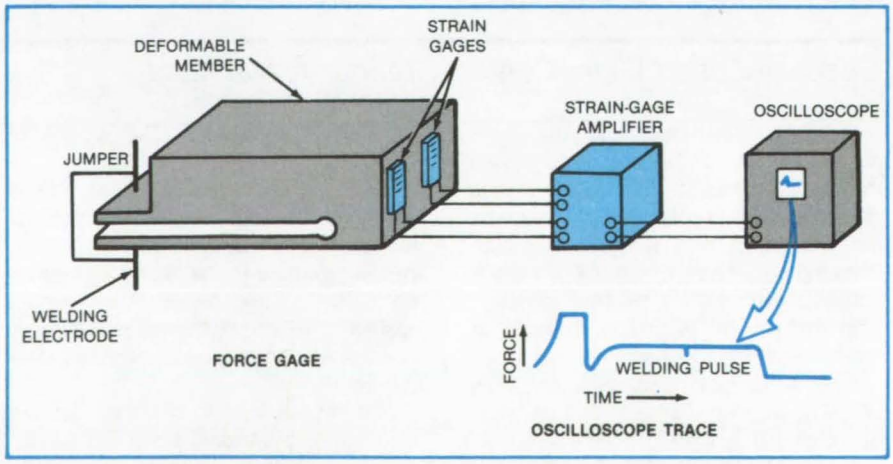

Figure 1. The **Electronic Force Gage** uses a strain gage on a deformable member. An oscilloscope trace of the welding force can be photographed and compared with a standard trace during the calibration and troubleshooting of resistance welding equipment.

as a standard during equipment troubleshooting and calibration as shown in Figure 2.

A photograph of the oscilloscope trace, taken during troubleshooting, is compared to the standard trace to locate the fault. After repair, a final photograph is taken and compared again to the standard. The system can be adapted to small-scale resistance welding in the electronics industry.

This work was done by J. W. Bradley and G. Gates of Honeywell Inc. for **Marshall Space Flight Center.** *No further documentation is available.*

Inquiries concerning rights for the commercial use of this invention should be addressed to the Patent Counsel, Marshall Space Flight Center [see page A5]. Refer to MFS-25798.

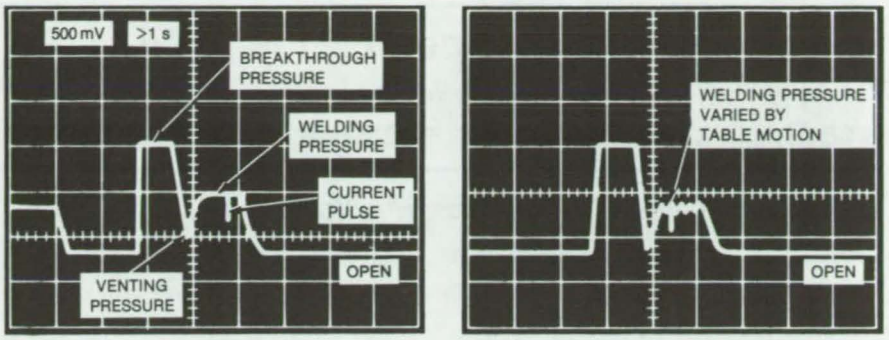

Figure 2. **Trace A** shows typical weld breakthrough, welding pressure, current pulse, and venting. In Trace B, taken during troubleshooting, the current pulse has moved to the left, indicating trouble in the timing circuits; and table motion has caused the weld pressure to vary. The traces shown here are representations of actual oscilloscope traces.

Swirl Diffuser

A gas diffuser, based on swirling flow, dissipates the incoming gas velocity in a relatively short distance.

Lyndon B. Johnson Space Center, Houston, Texas

By creating a swirling flow, a gas diffuser dissipates incoming gas velocity rapidly and quietly so that the gas enters a tank without disturbing the gas in it. Possible applications for the diffuser would be in fuel burners, in room inlets for heating and air-conditioning, and in carburetors for internal-combustion engines.

As shown in the figure, the swirl diffuser includes an inlet pipe, a pinwheel (swirl) nozzle, and a can. The pinwheel nozzle creates a flow that swirls along inside the length of the can and then spins out of the open end into the tank. Because the diffuser is an open pipe, the pressure drop within it is negligible. The pinwheel nozzle can be made of almost any material, depending upon its specific application; it has been fabricated from corrosion-resistant stainless steel and welded to the swirl-diffuser assembly.

In conventional diffusers, the incoming gas is brought through a perforated chamber, creating many small jets with velocities that decay fairly rapidly over a short distance. The swirl diffuser, however, rapidly dissipates velocity without the pressure drop associated with a chamber.

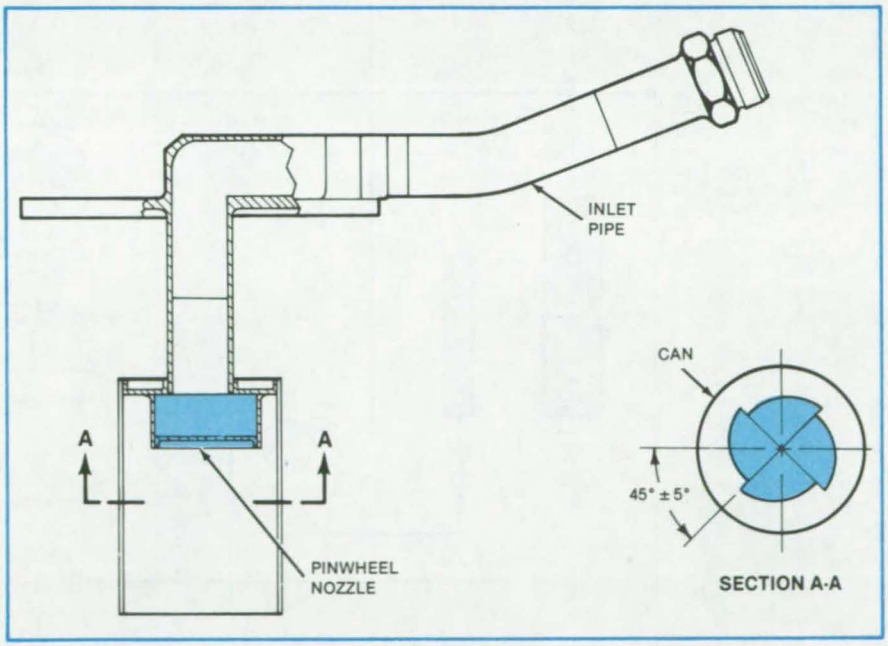

A **Pinwheel Nozzle** welded to the end of an inlet pipe creates a swirling flow. Because the diffuser is essentially an open pipe with a pinwheel nozzle, the pressure drop in the diffuser is almost the same as in an open pipe.

This work was done by Wayne E. Simon of Martin Marietta Corp. for **Johnson Space Center.** *For further information, Circle 43 on the TSP Request Card.*
MSC-18996

Leak Tester for Cryogenic Flowlines

A gas chromatograph measures leakage into cavity surrounding the joint under test.

Lyndon B. Johnson Space Center, Houston, Texas

A technique originally developed to monitor leakage in hydrogen flowlines could also measure the leakage of other cryogenic fluids or volatile liquids, including petroleum and natural gas. The new system surrounds the joint being tested with a sealed cavity. The presence of leakage gas in the cavity is monitored by a gas chromatograph.

In addition to the chromatograph (see figure), the leak tester includes pressure gages, flow valves, relief valves, regulating valves, and flowmeters to achieve the controlled gas flows required for the purge cavity and gas chromatograph. A purge gas (different from the leakage gas) is fed into the cavity from a storage cylinder. The gas chromatograph compares the composition of the purge gas with a calibrated mixture of the purge and effluent gases of known relative concentration. The concentration ratio is chosen to approximate that expected in the event of leakage.

To measure the leakage rate, the purge gas is introduced into the cavity

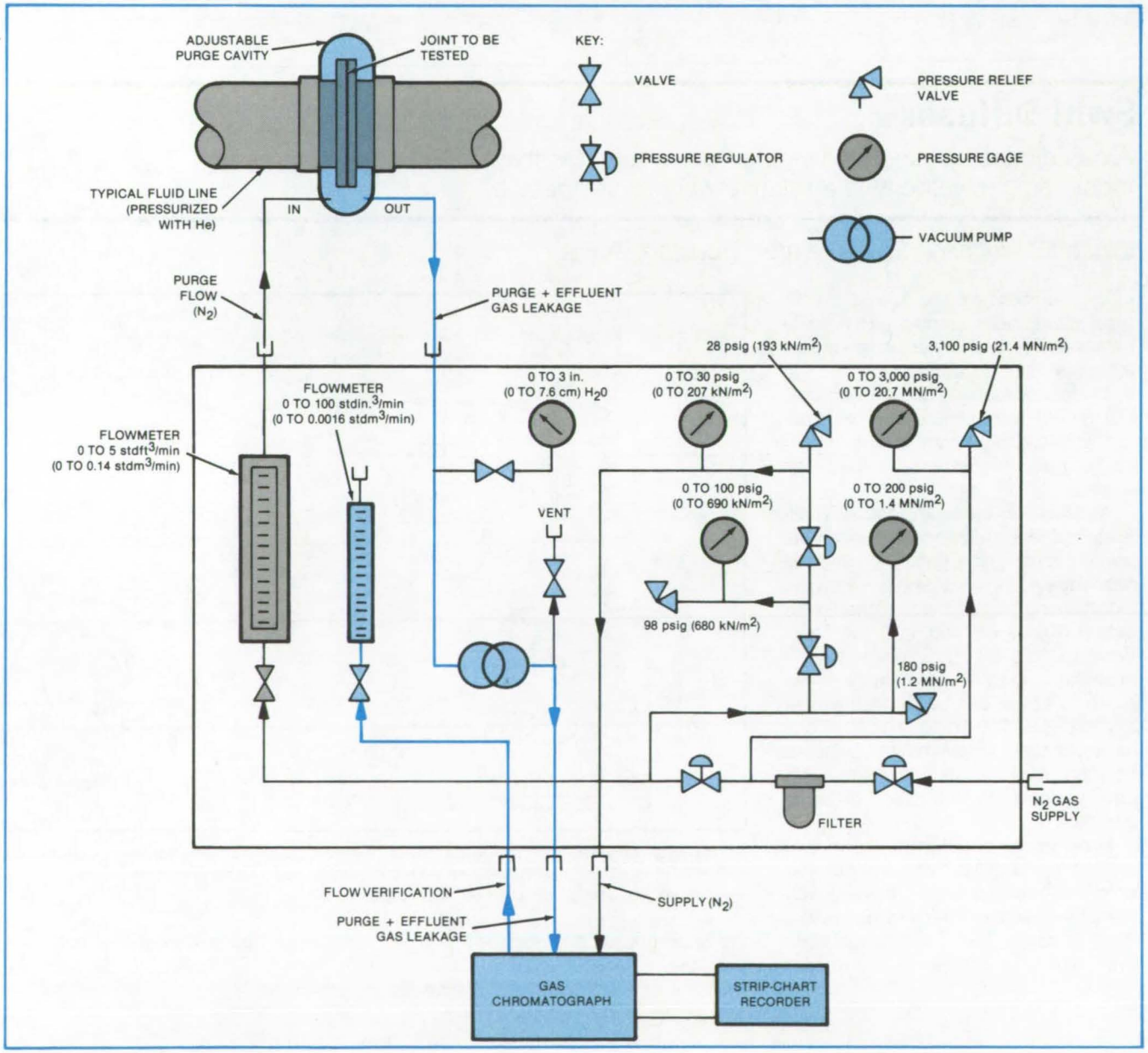

The **Quantitative Leak Tester** is connected to a sealed purge cavity that surrounds the joint to be tested. In the example shown, the leakage gas is helium, and the purge gas is nitrogen.

at a known flow rate. The gas chromatograph reads the leakage-gas concentration in the cavity and gives a readout directly in relative concentration by weight (typically, in parts per million). The leakage rate is found by multiplying the relative leakage-gas concentration by the mass-flow rate of the purge gas into the cavity.

The cavity need not meet any particularly stringent requirements. It operates at a pressure only slightly above atmospheric, and small leaks in the purge cavity have little effect on measurement accuracy.

This work was done by Garry D. Mortensen, J. Neil Olney, and John M. Mardesic of Rockwell International Corp. for **Johnson Space Center.** *For further information, Circle 44 on the TSP Request Card.*
MSC-20233

Calculating Static-Seal Leakage Correlation

Operational leakage rates of various working fluids are predicted from test data.

Goddard Space Flight Center, Greenbelt, Maryland

An expression that converts the leakage rates of fluids at various pressures and temperatures to rates at other pressures and temperatures has been modified by a multiplying factor to include the effects of changing leak-path area. The method was developed to use a leakage measured at engine test conditions to predict the leakage at engine operating conditions for a pressure-assisted silver-plated elastomeric seal.

Based on a modified expression for laminar flow between parallel plates, the method converts leakage through a fixed-area flow passage from one set of fluid conditions to another. The figure shows a plot of the multiplying factor. Although developed for Naflex (or equivalent) seals, the method could be adapted for other pressure-assisted seals.

Pressure-assisted elastomeric static seals, used throughout the Space Shuttle main engine, were installed in bolted-flange pressure-test fixtures simulating the hardware to be used in flight. Seal diameter tested was 2.7 in. (69 mm). Because leakage of the seal is so small [less than one-fourth standard cubic inch/minute (4 stdcm^3/min)], a groove was scratched across the seal tip to cause sufficient leakage to be measured and correlated among different test fluids. The test fixtures were pressurized with He and N_2 at both ambient and liquid-nitrogen [-320° F (-196° C)] temperatures. Leakage versus pressure was measured at values from 30 to 9,500 psig (207 kN/m^2 to 65.5 MN/m^2).

There was good agreement of the test data with an expression correlating leakage rates at different test conditions. However, the data indicated that the pressure-assisted seals did not

(continued on next page)

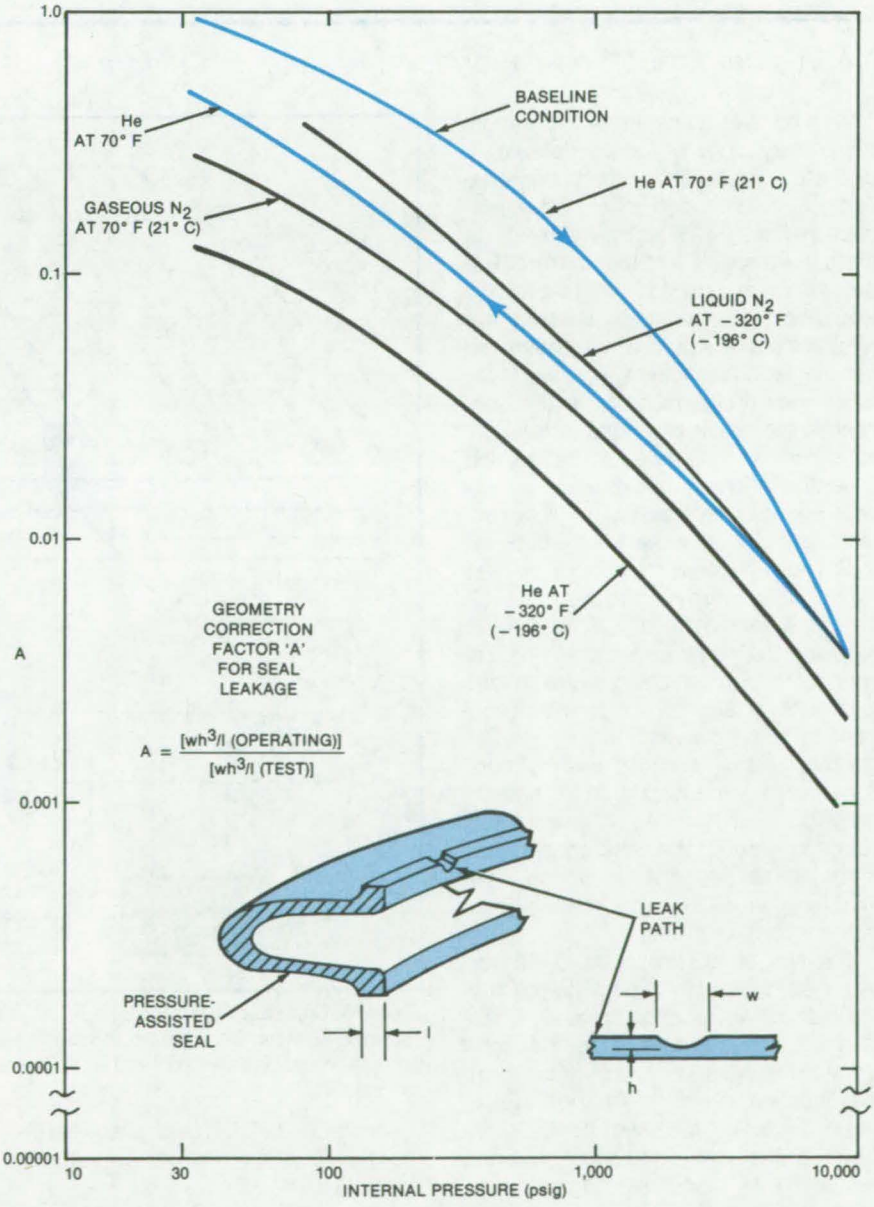

A Correction Factor improves the correlation of the measured engine static-seal leak rate under test conditions with the rate under operating conditions.

follow a constant-area prediction with increasing applied pressure. It was hypothesized that the soft silver plating of the seals was being forced into the asperities of the mating flange, as well as into the intentionally-scratched leak path, thus reducing the flow area.

A correction factor for the area change was calculated and applied to the correlation expression. The correction factor is a function of the geometry of the leak path shown in the figure. Although this particular correlation is unique to the particular elastomeric seals tested, the method could be applied to other pressure-assisted seals after test data is acquired in a similar manner.

This correlation method has many potential applications for extrapolating from test conditions to operating conditions. For example, this method was prepared for calculating gas leakage during the incident at the Three-Mile-Island nuclear reactor plants.

This work was done by C. M. Daniels and M. E. Burr of Rockwell International Corp. for **Marshall Space Flight Center.** *For further information, Circle 45 on the TSP Request Card.*
MFS-19674

Dielectric Scanning Locates Voids in Glass Foam

Capacitive probes may succeed where X-ray and ultrasonic equipment do not.

NASA's Jet Propulsion Laboratory, Pasadena, California

A proposed capacitive-probe technique may quickly locate defects in dielectric materials. When fully developed, it is intended to be used on production lines to detect large voids in glass-foam panels for solar mirrors: The detection of strength-limiting flaws would hold down costs by enabling the rejection of parts before subsequent expensive fabrication steps. The new technique may find application in the nondestructive testing of other dielectric objects for internal defects that exhibit dielectric inhomogeneities.

In one version (see Figure 1), a rectangular slab of material to be examined is placed between two electrode planes. In one plane, there is an array of parallel, evenly spaced [typically, 0.125 in. (3 mm) apart] conductors, each of which is connected by a switching matrix, either to ground or else to one terminal of a three-terminal capacitance bridge. In the other plane, a similar array of conductors lies perpendicular to the first array, and each conductor is switched either to ground or to the second terminal of the capacitance bridge. The third terminal of the capacitance bridge is connected to ground.

The two or four conductors (one or two, respectively, from each plane) that cross at a given location are selected to measure the effective dielectric constant of the small volume of material at that location, in terms of the capacitance between the two conductors. Each of the two conductors is connected to its respective capacitance-bridge terminal. The remaining unused conductors in both planes are grounded to control the fringing field and shield the measuring system from extraneous capacitive effects.

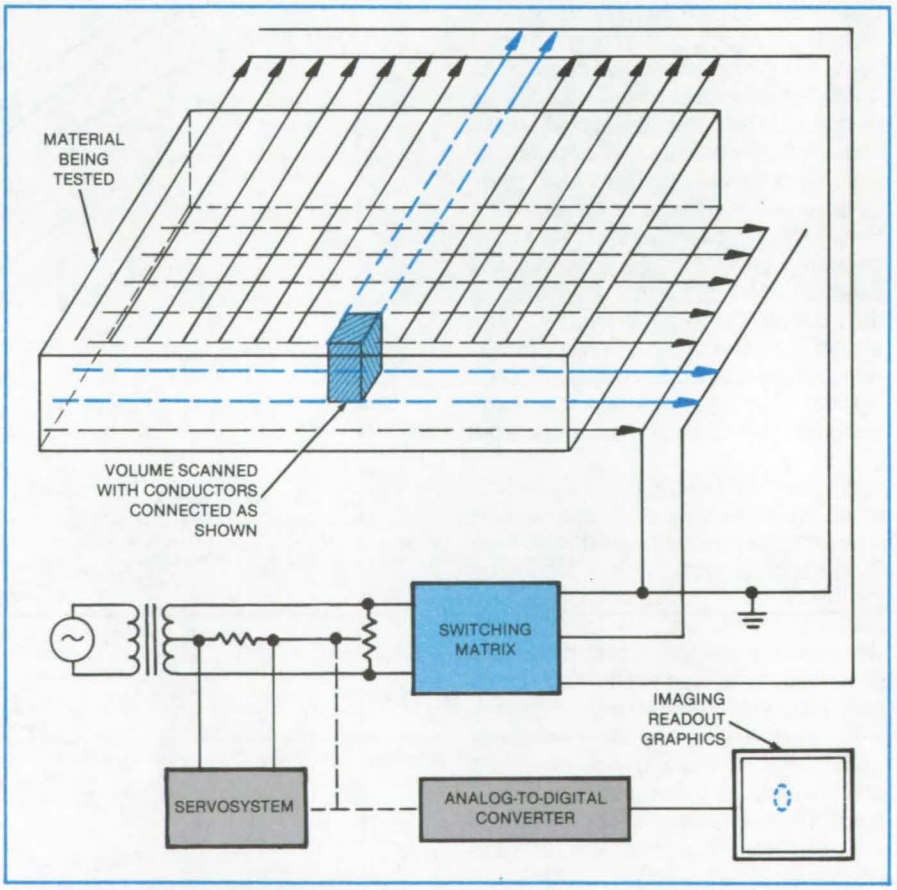

Figure 1. **Crossbar Switching** of pairs of conductors enables the detection of dielectric inhomogeneities in selected small volume elements of a slab of material. A large void in the sample would be detected as a low capacitance reading for the volume element containing the void.

Each conductor pair or double pair is switched in sequence to obtain a capacitance measurement for each volume element, until the entire sample volume has been scanned. Since a detectably large void in a volume element would result in a decrease in

measured capacitance, the results of the measurements could be processed electronically or manually to construct a two-dimensional void map. If a visible image is not necessary, the measurement results could be processed to extract a parameter representative of the expected maximum void size; and this parameter would serve as an accept/reject criterion. To obtain the speed required for production-line use, the switching, bridge balancing, and processing of results would all be done automatically.

In another version, the motion of the slab along an assembly line would provide one dimension of the two-dimensional scan. In each electrode plane, small electrodes facing the corresponding electrodes of the opposite plane would lie along a line perpendicular to the motion. A prototype of this system with one electrode pair has been tested (see Figure 2). A pair of measuring electrodes is held 1.375 in. (34.9 mm) apart in a yoke. With a measuring-electrode diameter of 0.27 in. (6.9 mm), the volume over which measurements are made is roughly a cylinder of 0.5 in. (13 mm) in diameter extending through the thickness of the sample.

Measurements of capacitance were taken from two foamed-glass panels, scanning each along a line at 0.5-in. (12.7-mm) intervals. Typical capacitances varied from 5 to 9 fF, the exact value depending on sample position and the local void distribution. These measurements were relatively coarse: It is expected that with improved accuracy in position and capacitance measurement, voids as small as 0.125 in. could be located, provided that the regular pores are an order of magnitude smaller.

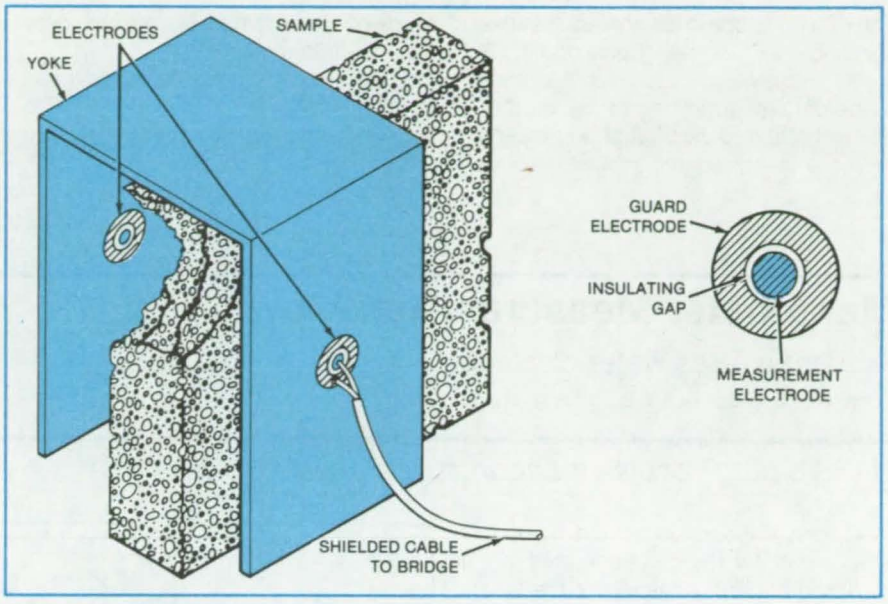

Figure 2. **A Small Core** of the sample is scanned by small electrodes in a yoke that moves them across the sample. Each measuring electrode is surrounded by a guard electrode that controls the fringing field, thus confining the measurement to a narrow volume element.

This work was done by Paul M. Gammell of Caltech for **NASA's Jet Propulsion Laboratory.** *For further information, Circle 46 on the TSP Request Card.*
NPO-15728

Eddy-Current Damage Test for Carbon Composites

A nondestructive test method detects cracks in materials of low conductivity.

Marshall Space Flight Center, Alabama

An eddy-current technique detects cracks in reinforced carbon/carbon composites of low electrical conductivity. Originally developed to assess damage to the Space Shuttle leading-edge panel — a carbon/carbon substrate — the method can be used in many other applications where materials of low conductivity are to be evaluated for damage.

The carbon/carbon substrate, coated with silicon carbide ranging in thickness from 0.020 to 0.040 in. (0.5 to 1 mm), had a conductivity of 0.03 to 0.05 IACS (International Annealed Copper Standard). The coating had a conductivity of less than 0.003 IACS and was relatively brittle. The total thickness of the test piece was approximately 0.50 in. (1.3 cm). Radiography could not be used since the density of the coating was greater than that of the substrate and would not permit imaging of the less dense substrate.

The test setup includes an eddy-current unit with a frequency of 2 to 20 MHz and a storage oscilloscope. The high frequency is required to assure that the depth of penetration is less than the substrate thickness, to prevent the thickness from influencing the readings.

Two reference test pieces are fabricated to adjust the settings of the test instruments. One is stepped by machining the coating and successive layers from the substrate. This furnishes a standard that assures that penetration is adequate and that the substrate thickness does not influence the results. The second reference piece contains slots of different depths, with the shallowest just penetrating the coating and the deepest penetrating through the entire sample.

With the optimized setup, there is no meter deflection when the probe is placed over undamaged material or over the slot that just penetrates the coating of the second reference specimen. Maximum deflection is obtained for the slot that penetrates the entire specimen thickness.

With the instrument thus adjusted to produce maximum deflection, the damaged area is scanned from every direc-

(continued on next page)

tion with the probe in full contact with the part under test. A meter deflection of 15 to 50 percent indicates probable substrate damage (cracking or ply separation or both). A deflection of 50 percent or more is considered indicative of a crack or other damage extending some distance into the substrate.

For the tested panels, damaged areas ranging in width from 0.5 to 1.5 in. (13 to 38 mm) were easily detected by the eddy-current scan. The eddy-current analysis was confirmed by visual inspection as the damaged area was sectioned and evaluated.

This work was done by Anthony B. Hamilton of Vought Corp. for **Johnson Space Center.** *No further documentation is available.*
MSC-20358

Manometer Measures Gas Flow

Apparatus uses water displacement to measure gas flow at low rates.

NASA's Jet Propulsion Laboratory, Pasadena, California

A simple apparatus uses a manometer to monitor the gas generated in a lead/acid battery. It measures the time required for the gas to displace a known volume of water.

The apparatus was constructed as part of an effort to determine the charging efficiency of a lead/acid cell. The gas generated during charging must be measured accurately since the energy required to generate the gas reduces the amount of energy left for charging.

At the beginning of overcharge, the rates are in the range of 1 to 10 ml/min, but quickly increase to more than 100 ml/min, and finish at about 1,000 ml/min. Because the flow rate and pressure are small, at the beginning of the cycle, standard gas flowmeters do not give accurate results.

At the start of measurements, valve B (see figure) is opened to allow some water to flow into the slanted measuring tube. The tube is not filled completely, but merely with enough water to produce a meniscus to the left of mark M_1. Valve B is then closed, and valve A is opened to permit the flow of gas from the battery into the measuring tube.

The entering gas forces the water to move along the tube toward the outlet. As the meniscus passes mark M_1, a timer is started. As the meniscus passes mark M_2, the timer is stopped. Thus the gas-flow rate may be determined by dividing the known volume between the two marks by the elapsed time.

In calibrating the volume between marks, the tube is allowed to fill completely, until water runs out of the outlet. Then gas is fed in until the meniscus reaches the first mark, M_1. A container is set under the outlet to catch the remaining water forced out by the gas

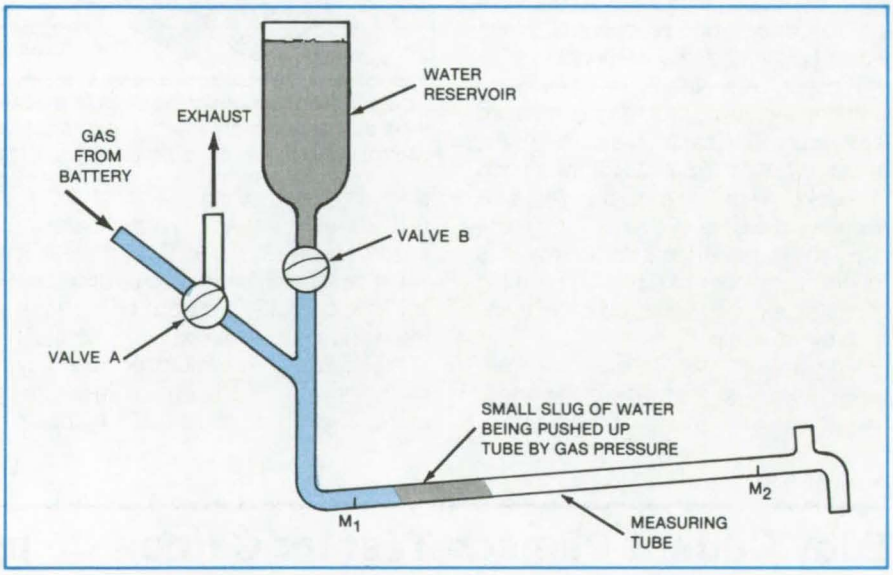

This **Gas-Flow Measuring Apparatus** determines the amount of gas generated in a lead/acid cell during charging, by measuring the time required for the gas to displace a measured volume of water between marks M_1 and M_2 in the slanted manometer. The optimum tube size is about 8-mm O.D. (6-mm I.D.). For larger tubes, the measuring gases may bubble past the water in the tube.

pressure as the meniscus is moved along to the second mark, M_2. The water in the container is weighed, thus establishing the volume between marks.

The slant of the measuring tube is set to the minimum angle that will permit the formation of a meniscus that closes the tube. In this way, the incoming gas works against a minimum pressure. For the same reason, a minimum amount of water is let into the tube by valve B, at the start of each measurement.

For greater accuracy, the water used during each run can be totally expelled into the weighing container, and the head pressure and resulting gas compression can be calculated for each run. Alternatively, valve A can be turned to exhaust the gas in the tube after each measurement, so that the same volume of water remains in the tube during every measurement. In that case, the water can be expelled and weighed and the results applied to all measurements in that group.

Accuracy at high flow rates is limited by the timing accuracy. With a stopwatch, there is a practical limit of about 1,000 ml/min. The accuracy increases without limit as the rate decreases.

This work was done by John J. Rowlette of Caltech for **NASA's Jet Propulsion Laboratory.** *For further information, Circle 47 on the TSP Request Card.*
NPO-15686

J-Channel Locks Potting to Compression Panel

Panel ends are supported to prevent edge failure during testing.

Langley Research Center, Hampton, Virginia

J-shaped channels embedded in potting compound prevent compression-panel end failures during high-temperature testing. Previous methods of potting the panel ends used glass-bead filler to prevent shrinkage and debonding of the compound from the panel. However, these methods were unsuccessful, as the potting compound cracks and debonds from the panel during cooldown.

To ensure uniform loading in a skin-stringer compression panel, the ends must be ground flat, parallel, and perpendicular to the skin. Each end is typically set in a mold. Potting compound is then poured around the panel and allowed to harden at room temperature. After grinding the ends, the potting is left on the panel to prevent the panel ends from crushing when a load is applied during testing.

For room-temperature testing, a panel is readily potted, ground flat, and tested without complications. However, for elevated-temperature testing, high-temperature potting compound must be used that is cured at a temperature near the panel test temperature. The potting compound has a different thermal expansion from the panel material; and as they cool down from the curing temperature, this difference in thermal expansion typically causes stresses to develop, resulting in the potting compound cracking and debonding from the panel.

The new technique (see figure) uses J-shaped channels, formed from the same material as the panel, that are spot-welded to the panel ends. The panels are then potted with the potting compound covering the J-channels. The potting compound adheres to the J-channels to form a mechanical lock on the panel. The panel ends can then be machined flat and parallel and the panel tested at elevated temperature without the potting material debonding from the panel.

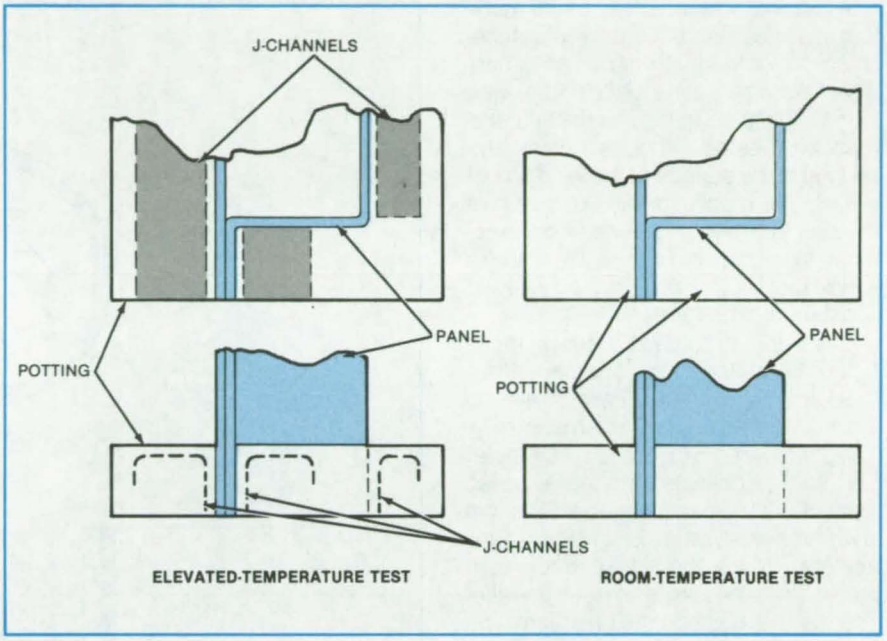

J-Channels Attached to the Panel Ends form a mechanical lock with the potting compound during elevated-temperature tests. They are not needed during room-temperature tests.

The advantage of this potting method over previous methods is that the J-channels give the potting materials something to adhere to. In the previous methods, however, the potting compound adhered to smooth surfaces, resulting in a bond easily broken by thermal expansion.

This work was done by Dick M. Royster and W. Albert Shearin, Jr., of **Langley Research Center.** *No further documentation is available.*

This invention is owned by NASA, and a patent application has been filed. Inquiries concerning nonexclusive or exclusive license for its commercial development should be addressed to the Patent Counsel, Langley Research Center [see page A5]. *Refer to LAR-12913.*

Multispectral Dual-Aperture Schmidt Objective

A telescope with 2 off-axis catadioptric Schmidt objectives produces up to 12 outputs, each representing a different wavelength interval. The separate images have precise registration, so that they can be used for multispectral resource mapping or remote sensing.

(See page 395.)

Electrolytic Sharpening of Diode-Contact Whiskers

An improved technique sharpens the point on tiny phosphor bronze wires commonly used to contact Schottky-barrier diodes. The process not only allows control of the cone angle and the diameter of the tip but also employs relatively-nontoxic sulfamic acid.

(See page 464.)

X-Ray Inspection of Transistors

A simple but effective technique speeds and helps to assure the regularity of X-ray inspection of matched pairs of potted transistors. The only extra equipment required is small blocks of plastic and a roll of adhesive tape.

(See page 466.)

Measuring Surface-Shear Stress in a Wind Tunnel

Two-wire skin-friction gage gives both magnitude and direction of mean and fluctuating stresses.

Ames Research Center, Moffett Field, California

A compact skin-friction gage monitors the mean and fluctuating surface-shear stress beneath the three-dimensional boundary layer of flow in a wind tunnel. The gage measures the heat flux from two heated orthogonal wires embedded in the surface of the wind-tunnel model. The magnitude and direction of the skin friction are deduced from electrical signals from a pair of hot-wire anemometers that maintain the wires at constant temperatures.

The skin-friction gage is shown in the figure. Four nickel rods are placed in a mold, and polystyrene is injected around them to form a 3.18-mm-diameter plug. Tungsten wires 5 microns in diameter are then spotwelded to the exposed ends of the rods and immersed in a thin layer of polystyrene dissolved in ethyl acetate. When the liquid hardens, it buries the wires in a smooth surface. The thermocouple at the upstream side of the plug monitors wall temperature.

In operation, the plug is placed in the wind tunnel, flush with the test surface. The gage has been calibrated in a two-dimensional turbulent boundary layer on a subsonic wind-tunnel wall, with a Preston tube and mean velocity measurements as a standard. It was used successfully in various turbulent flow fields, including a separating three-dimensional boundary layer over a cone at high angle of incidence.

This work was done by Fred Lemos of **Ames Research Center** *and Hiroshi Higuchi of Dynamics Technology, Inc. Further information may be found in NASA TM-78531 [N79-14330/NSP], "Bi-Directional, Buried-Wire Skin-Friction Gage" [$8.50]. A copy may be purchased [prepayment required] from the National Technical Information Service, Springfield, Virginia 22161.*

ARC-11384

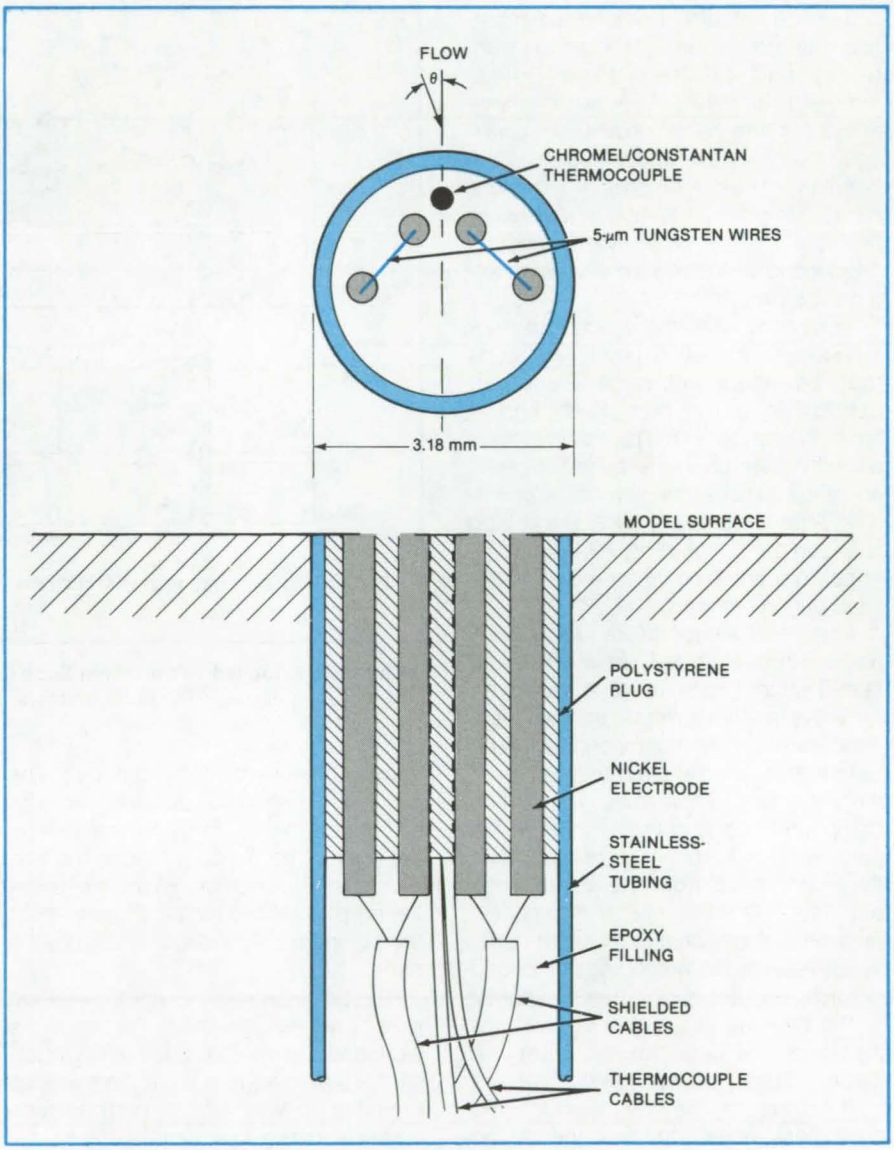

The **Heated Wires** that lie at the surface of the gage (which is flush with the surface of the wind-tunnel model) measure airflow by its cooling effect. The wires are perpendicular to each other to measure flow direction as well as magnitude.

Fracture Strength of Silicon Solar Cells

Tests during processing show the way to reduce breakage and increase yield.

NASA's Jet Propulsion Laboratory, Pasadena, California

A four-point twisting test has been developed as a standard test for determining the strength of silicon solar cells. The test is used to study cell cracking and changes in fracture strength at various process steps as a blank silicon wafer is converted to a finished photovoltaic cell. The test is helping to develop reliable information on the nature and source of flaws that cause cell fracture — information that will lead to improved processing methods and ultimately to higher production yields and lower costs.

In the twisting test, a 76-mm-diameter wafer of silicon is placed in a specially designed jig that is then placed in a standard compression-testing machine. The jig applies two dowel pins to the bottom of the wafer and two to the top of the wafer at 90° apart. As the machine places a compressive load on the jig, the bottom dowel pins apply an upward force to the wafer, and the upper pins place a downward force on it. The combination of forces tends to twist the wafer (see figure). The compressive load is increased until the wafer breaks, and the fracture strength is computed.

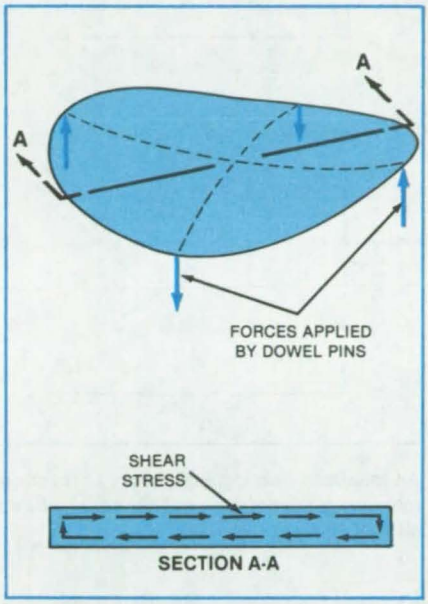

A Silicon Wafer Is Twisted by four equally-spaced dowel pins, two pushing up and two pushing down. A uniform shear stress is found along a line 45° from the axes of the two load pairs — along section A-A, for example.

The four-point twisting method was selected after a comparison with two other methods: cylindrical bending and biaxial flexure. The four-point twisting method was selected because it has a number of advantages: It stresses the entire specimen, including the edges and internal portions; it has a simple and symmetrical loading configuration; and it is easy to perform.

Measurements with the new test have shown that strength is decreased by exterior flaws (at the edge and on the surface of a wafer) created during wafer sawing or handling. On the average, chemically polished wafers are more than twice as strong as wafers in the as-cut state because the polishing removes all but large flaws. Application of an antireflection coating and a metal-contact pattern causes little change in strength.

This work was done by Chern P. Chen of Caltech for **NASA's Jet Propulsion Laboratory.** *For further information, Circle 48 on the TSP Request Card.*
NPO-15187

Estimating Design Loads in Coupled Vibrating Structures

Approximate spectral analysis is faster and less expensive than transient analysis.

NASA's Jet Propulsion Laboratory, Pasadena, California

A method of vibration analysis combines the separate modes of a spacecraft and its launcher to determine approximate conditions for resonance. The method would be useful for the analysis of any complex structure made up of substructures that are not coupled too closely; however, it is important to note that the method includes the effect of dynamic impedance between the launcher and the payload.

The new method is an alternative to transient analysis. Called the "generalized" shock spectra method, it is an extension of an earlier shock spectra method. The generalized method formalizes derivation and computation steps, explicitly stating the necessary assumptions, relaxing unessential ones, and introducing several significant improvements.

The forcing function corresponding to the modes of the launch vehicle loaded by a rigid mass at the spacecraft interface is modeled by an equivalent impulsive forcing function, represented by a delta function (see figure). The choice of an impulse emphasizes the view that the shape of the response as a function of time is of no consequence and that only the peak or bound of the response is of interest. Any forcing function that would reproduce a response with the same maximum or bound as the actual forcing function would be acceptable.

Expressions are derived for bounds on the displacement and load in each modal subspace consisting of one spacecraft mode coupled with one launch-vehicle mode. Next, a bound is constructed on the complete solution in the total space from the subspace bounds by summing absolute values or by taking root sum squares that are weighted to account for phasing.

(continued on next page)

The use of modal shock spectra, rather than interface degrees-of-freedom shock spectra, is significant because it automatically accounts for the matching of all interface physical degrees of freedom. Knowledge of the modal properties of the launch vehicle with or without a payload is required; however,such information is usually available.

This work was done by Marc R. Trubert, Moktar A. Salama, and Robert M. Bamford of Caltech for **NASA's Jet Propulsion Laboratory.** *Further information may be found in JPL Publication 79-2 [N79-20177/NSP], "A Generalized Modal Shock Spectra Method for Spacecraft Loads Analysis" [$11.50]. A copy may be purchased [prepayment required] from the National Technical Information Service, Springfield, Virginia 22161.*

NPO-14872

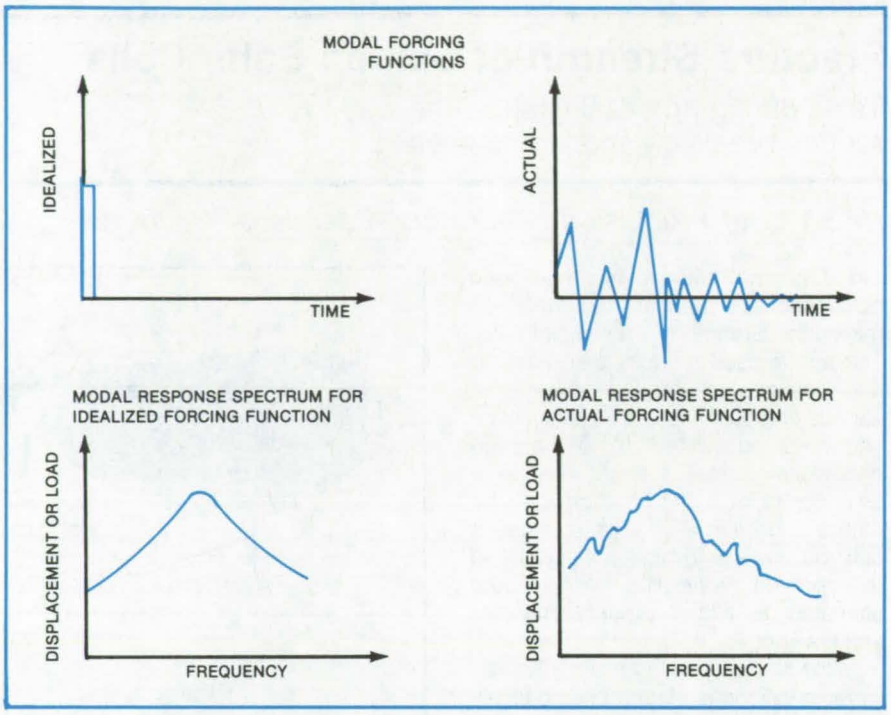

An Idealized Forcing Function can be used because it produces approximately the same maximum response as the actual function. Use of the idealized function greatly simplifies analysis.

Books and Reports

These reports, studies, and handbooks are available from NASA as Technical Support Packages (TSP's) when a Request Card number is cited; otherwise they are available from the National Technical Information Service.

Multivalued-Velocity-Field Model of Turbulence

The origin and propagation of vortexes are analyzed.

A recent report presents a multivalued-velocity model to be used in calculations of turbulence formation. Developed as part of a continuing study of turbulent fluid motion, the model is expected to evolve into a comprehensive mathematical tool to explain the origin and effects of turbulence. Interest should be widespread: A reliable turbulence model would have great theoretical and practical value in such fields as aerodynamics, meteorology, and combustion.

The report discusses an incompressible fluid with the velocity, $\vec{v}$, at each point represented as the sum of a mean component, $\vec{v}_C$, and a multivalued pulsating component, $\vec{v}_r(\xi)$, where ξ is three-dimensional multivaluedness parameter. The portion of the total mass density ϱ_C taking part in the motion $\vec{v}_r(\xi)$ is given by $\varrho(\xi)$, where

$$\varrho_C = \int_\xi \varrho(\xi) d\xi$$

The fluid is treated as having a constant scalar viscosity but not in the usual way. Instead, the effect of viscosity is incorporated into the equations of motion as a collision term describing the force between two fluid bodies having different velocities but superimposed at the same place. The multivalued-velocity field thus gives rise to an equivalent turbulent-friction force for which a turbulent-friction parameter can be evaluated from energy-dissipation considerations.

The model leads to characteristic wave equations for the propagation of turbulence near surfaces of discontinuity in the flow field. In contrast to Euler's equation, which predicts that discontinuities of vortexes propagate only by convection, the new model predicts that they can propagate at velocities different from that of the mean flow.

If a two-valued flow field is postulated, and interesting result is obtained by applying a simplified form of the equations of motion to the flow field about a streamlined body. For the rear stagnation point, the model predicts that any small random disturbance $\vec{v}_r$ will grow to a stable finite value that can be calculated from the $\vec{v}_C$ field, the turbulent-friction parameter, and the Reynolds number.

For free turbulent flow (as in free jets), the formation of turbulence is represented in the model as the propagation of initial discontinuities form the boundary into the flow, with a characteristic velocity that is the sum or difference of the components of $\vec{v}_C$ and $\vec{v}_r$ perpendicular to the boundaries. For a body placed in an initially-potential flow field,

the model predicts that velocity discontinuities tangential to the boundary will start propagating out of the surface to be subsequently occupied by the boundary, thus forming a physical boundary that starts at the nose point and sweeps downstream. Upstream of the boundary, the flow is potential, while downstream it is rotational. The flow is turbulent in both zones (even upstream), because the normal components of $\vec{v}_T$ are continuous across the boundary.

This work was done by Michael A. Zak of Caltech for **NASA's Jet Propulsion Laboratory.** *To obtain a copy of the report, Circle 49 on the TSP Request Card.*
NPO-15748

Methods for Estimating Payload/Vehicle Design Loads

Several methods are compared with respect to accuracy, design conservatism, and cost.

A report presents a survey of earlier reports on methods for estimating the dynamic loads on payload support members in the Space Shuttle. The objective of the survey is to reduce the time and expense of load calculation by selecting an approximate method that has sufficient accuracy for the problem at hand. Described in the report are methods for obtaining upper bounds to the dynamic loads on support members and for calculating actual transient time histories of loads. These methods are generally applicable to dynamic-load analysis in other aerospace and other vehicle/payload systems.

References are given to other reports that describe the individual methods in detail. The upper bounds methods are recommended for use with lower-mass relatively uncritical payloads: In such cases, the expense and complexity of designing for accurately predicted loads would not be justified by the relatively small weight savings over the more conservative designs that would result from using upper bounds. The more-expensive load-prediction methods are appropriate for large, expensive, or vulnerable payloads.

Two upper bounds methods are presented. The first, which is for preliminary design-load estimates, provides a "rule of thumb" for preliminary sizing of various support members. This method uses a semiempirical mass-versus-acceleration curve based on flight data from previous payloads and on an analysis of the space transport system. This method, which applies to payloads over 200 lb (90 kg), gives an upper bound for payload acceleration equal to a number divided by the square root of the weight of the payload. The value of the number varies somewhat among different launch vehicles. Using the upper bound acceleration estimated by this method for significant mass points in the payload, a complete set of support-member loads can be calculated.

A second, moderately-conservative, and more-accurate upper bound can be obtained by using the generalized shock spectra method to obtain the most adverse combination of vehicle and payload dynamic responses. Load estimates are obtained by combining the maximum responses for various combinations of launch-vehicle-and-payload normal modes of vibration and by allowing for the effects of impedance between the launch vehicle and the payload. Uncertainty in the knowledge of the normal-mode frequencies is allowed for by examining responses over a range of frequencies bracketing the nominal frequencies.

Two more-precise load-prediction methods are described: the rigid-body interface acceleration (RBIA) method and the recovered transient analysis (RTA) method. These simulate a time-response solution of payload behavior in one launch-vehicle/payload composite system from a known response solution from another such system under the same forcing function.

In the RBIA method, the organization responsible for the vehicle provides the payload organization with the vehicle/rigid-payload interface acceleration time histories of the events under consideration, the corresponding eigenvectors of the interface degrees of freedom, and the modal damping. The payload organization uses these data to calculate the elastic-payload responses and loads for other payloads for the same dynamic events without solving a new launch-vehicle/elastic-payload composite model for each payload. This eliminates a costly and time-consuming iterative interaction between the two organizations.

In the RTA method, the payload dynamic loads are obtained for one vehicle/payload combination either by direct measurement or by mathematical analysis. From this information, the analysis recovers the vehicle/payload interface accelerations for the unloaded launch vehicle and then modifies them to include the dynamic characteristics of the new payload. This method should provide the same results as a full-scale transient analysis for the case of low damping. Since damping is generally low in payload structural systems, accuracy is expected.

This work was done by Jay C. Chen, John A. Garba, Moktar A. Salama, and Marc R. Trubert of Caltech for **NASA's Jet Propulsion Laboratory.** *To obtain a copy of the report, Circle 50 on the TSP Request Card.*
NPO-15550

Computer Programs

These programs may be obtained at very reasonable cost from COSMIC, a facility sponsored by NASA to make new programs available to the public. For information on program price, size, and availability, circle the reference letter on the COSMIC Request Card in this issue.

Dissociated Airflow Effects During Plasma-Arc Testing

Program computes heating rates and surface-friction effects.

COLDARC predicts the heating rate and surface friction on a test article during plasma-arc testing. It uses a simplified frozen-flow model to represent the dissociated airflow and to predict the heat flux and surface friction, including the effects of retarded atomic recombination, from test facility data.

(continued on next page)

COLDARC was developed as part of an effort to predict the heating rate and surface-friction effects on the thermal-protection system of the Space Shuttle orbiter during reentry. It takes into account the effects of dissociated airflow over the specimen and the associated heat flux and surface temperatures. Normally, plasma-arc testing involves airflow over a test specimen having a relatively smooth surface. Since the orbiter thermal-protection system does not constitute a smooth mold line surface, COLDARC was needed to assess the impact of this surface roughness and the dissociated airflow.

COLDARC is written in FORTRAN IV for batch execution and has been implemented on a CDC CYBER 170-series computer with a central-memory requirement of approximately 40K (octal) of 60-bit words. COLDARC was developed in 1981.

This program was written by Bruce A. Miller and John A. Bertani of Rockwell International Corp. for **Johnson Space Center.** *For further information, Circle B on the COSMIC Request Card.*
MSC-20522

Solutions of Transonic Flow in Turbomachines

Accurate approximations are obtained using perturbation techniques.

Perturbation procedures and associated computational codes were developed for determining nonlinear flow solutions of transonic flows in turbomachines. The perturbation procedures determine highly accurate approximations to families of nonlinear solutions that are either continuous or discontinuous and that represent variations in some arbitrary parameter.

The procedures employ a unit perturbation, determined from two nonlinear solutions that differ from one another by a nominal change in some geometric flow parameter, to predict a family of related nonlinear solutions. Coordinate straining is used in determining the unit perturbation to account properly for the motion of discontinuities and maximums of high-gradient regions.

The perturbation calculations are based on full potential nonlinear solutions. These calculations cover a variety of flow and geometric parameter perturbations involving isolated airfoils and compressor cascades at both subsonic and transonic flow conditions. Particular emphasis is placed on supercritical transonic flows that exhibit large surface shock movements and on subsonic flows that display large pressure variations in the stagnation and peak suction-pressure regions. Perturbation results for single-parameter perturbations, characterized by both extreme solution interpolation using widely-separated base flow solutions and extreme solution extrapolation using closely-spaced base flow solutions, are obtained to determine the accuracy and range of validity.

Solution interpolation and extrapolation are both feasible. Results evaluating the polynomial and piecewise-continuous straining functions indicate that the piecewise-continuous functions are superior. The latter class of straining functions eliminates both the problem of unwanted straining of the domain of interest as well as the problem of spurious straining out of the domain. This procedure can successfully treat flows containing multiple shocks and high-gradient regions by simultaneously straining all of these characteristic points.

The computer program is configured to predict and plot an arbitrary flow variable (e.g., pressure coefficient) on the surface of a blade or airfoil and can account for the motion of: (a) one or more critical points (shock points), (b) a stagnation point, and (c) a maximum-suction-pressure point, or simultaneously for any combination of these. The program is written in FORTRAN IV for use on an IBM 3033 computer.

This program was written by S. Stahara, J. Elliott, and J. Spretter of Nielson Engineering & Research, Inc., for **Lewis Research Center.** *For further information, Circle C on the COSMIC Request Card.*
LEW-13896

Transonic, Axisymmetric Flow Over Nozzle Afterbodies With Supersonic Jet Exhausts

Predictions require less computation than the Navier-Stokes solutions.

The nozzle afterbody is one of the main drag-producing components of an aircraft propulsion system. Thus, considerable effort has been devoted to developing techniques for predicting the afterbody flow field and drag.

The RAXJET computer program predicts the transonic, axisymmetric flow over nozzle afterbodies with supersonic jet exhausts and includes the effects of boundary-layer displacement, separation, jet entrainment, and inviscid jet-plume blockage. RAXJET iteratively combines the South-Jameson relaxation procedure, the Reshotko-Tucker boundary-layer solution, the Presz separation model, the Dash-Pergament mixing model, and the Dash-Thorpe inviscid plume model into a single, comprehensive model. The approach requires considerably less computational time than the Navier-Stokes solutions and generally yields results of comparable accuracy.

In RAXJET, the viscous/inviscid interaction model is constructed by dividing the afterbody flow field into six separate computational regions:

1. The inviscid external flow solution is based on the relaxation procedure of South and Jameson for solving the exact nonlinear potential flow equation in nonconservative form.
2. The flow field in the inviscid jet exhaust is solved by explicit spatial marching of the conserative finite-difference form of the inviscid flow equations for a uniform composition gas mixture.
3. The properties in the attached boundary-layer region are solved by a modified version of the Reshotko-Tucker integral method for turbulent flows.
4. The analysis of the separated flow region uses integral control-volume methods for predicting the separation

location and calculating the discriminating streamline shape.

5. The jet wake portion of the separated region is determined by either a simple extrapolation model or an integral method that accounts for entrainment effects.
6. The displacement-thickness distribution arising from entrainment into the jet mixing layer is calculated by the overlaid mixing model.

The viscous and inviscid flow fields are iteratively solved until a final solution is obtained.

Input to RAXJET consists of body geometry data, free-stream conditions, main logic control parameters, and condition and control parameters for each of the six computational flow regions. Output includes detailed flow results and aerodynamic coefficients.

RAXJET is written in FORTRAN IV for batch execution and has been implemented on a CDC CYBER 170-series computer with a central-memory requirement of approximately 76K (octal) of 60-bit words. The RAXJET program was developed in 1982.

This program was written by Richard G. Wilmoth of **Langely Research Center.** *For further information, Circle D on the COSMIC Request Card.*
LAR-12957

Compressible Stability Analysis Code for Transition Prediction in Three-Dimensional Boundary Layers

"Black box" code for swept and tapered wings.

COSAL is a fast compressible stability analysis code for transition prediction in three-dimensional boundary layers. It is specifically designed to compute the compressible linear stability characteristics and integrate the amplification rates of boundary-layer disturbances on swept and tapered wings.

The stability properties of compressible laminar boundary layers are particularly relevant to the phenomenon of laminar/turbulent flow transition. Recently, interest in this problem has increased because of its importance in the application of laminar flow control technology.

The linear stability analysis of compressible boundary layers involves solution of an eigenvalue problem for an eigth-order system of differential equations. The basic equations for the linear stability analysis are derived using small disturbance theory. Assuming that the mean flow is locally parallel, one obtains a set of five ordinary differential equations: three second-order momentum equations, one second-order energy equation, and one first-order continuity equation.

COSAL employs a finite-difference method to solve these compressible stability equations in their original form. The code includes two eigenvalue search procedures. A global procedure is provided for use when no initial guess is available. A fast local eigenvalue search procedure is provided for use when a good initial guess is available.

Input to COSAL consists of boundary-layer profile data, control parameters, and stability problem description parameters. A companion program generates the required three-dimensional compressible boundary-layer profiles for swept and tapered wings.

Output from COSAL includes nondimensional wave numbers, nondimensional complex frequency, nondimensional group velocity components, disturbance frequency and orientation, and logarithmic exponent of the disturbance amplitude ratio, an indicator of local growth rate. Displacement thickness Reynolds number and edge mach number are also computed.

COSAL and its companion profile generator program are written in FORTRAN IV for batch execution and have been implemented on a CDC CYBER 170-series computer with a central-memory requirement of approximately 170K (octal) of 60-bit words. The COSAL program was developed in 1982.

This program was written by Mujeeb R. Malik of High Technology Corp. for **Langley Research Center.** *For further information, Circle E on the COSMIC Request Card.*
LAR-13042

Steady, Nonrotating, Blade-to-Blade Potential Transonic Cascade Flow Analysis Code

Program numerically solves an artificially time-dependent form of the actual full-potential equation.

An exact, full-potential-equation model and appropriate boundary conditions have been derived for the steady, irrotational, homoentropic, and homoenergetic flow of a compressible, inviscid fluid through a two-dimensional planar cascade. The CAS2D computer program numerically solves an artificially time-dependent form of the actual full-potential equation, providing a steady, nonrotating, blade-to-blade potential transonic cascade flow analysis code. Comparisons of results with test data and theoretical solutions indicate very good agreement.

In CAS2D, the governing equation is discretized by using type-dependent, rotated finite differencing and the finite-area technique. The flow field is discretized by providing a boundary-fitted, nonuniform computational mesh. This mesh is generated by using a sequence of conformal mapping, nonorthogonal coordinate stretching, and local, isoparametric, bilinear mapping functions.

The discretized form of the full-potential equation is solved iteratively by using successive-line over relaxation. Possible isentropic shocks are captured by the explicit addition of an artificial viscosity in a conservative form. In addition, a four-level, consecutive, mesh refinement feature makes CAS2D a reliable and fast algorithm for the analysis of transonic, two-dimensional cascade flows. The results from CAS2D are not directly applicable to three-dimensional, potential, rotating flows through a cascade of blades because CAS2D does not consider the effects of the Coriolis force that would be present in the three-dimensional case.

(continued on next page)

This program is written in FORTRAN IV for batch execution and has been implemented on an IBM 370-series computer with a central-memory requirement of approximately 200K of 8-bit bytes. CAS2D was developed in 1980.

This program was written by Djordje S. Dulikravich of **Lewis Research Center.** *For further information, Circle F on the COSMIC Request Card.*
LEW-13854

PANEL Code for Planar Cascades

Plane cascade flow is solved using improved surface-singularity methods.

Current external aerodynamic integral-equation techniques may be adapted for use in internal flow calculations. The inherent computational speed and flexibility of integral-equation solutions can make them very useful for design calculations. The present cascade method is a versatile design tool that will allow a designer to explore many preliminary blade designs in a short period of time. Although the method does not give exact solutions for compressible flows, example calculations do demonstrate that it is sufficiently accurate to provide a means of selecting blade designs for further analysis.

A general description of the PANEL code and information needed to run the code are given in "Panel Code for 2D Blade-to-Blade Solutions" by Eric R. McFarland of Lewis Research Center. An improved surface-singularity method is formulated in the PANEL code. The code calculates compressible, inviscid, irrotational flow through a plane cascade of arbitrary blade shapes. The improved singularity method is described in "Solution of Plane Cascade Flow Using Improved Surface Singularity Methods" by McFarland in NASA TM-81589, a copy of which is included in the above document describing the PANEL code.

The PANEL code provides a rapid stable calculation of plane cascade flows. A typical design calculation using 60 panel elements to describe the blade shape requires less than 4 seconds CPU time on the IBM 3033 computer at Lewis Research Center. Additional solutions for variations in flow conditions require less than 1 second CPU time after the initial calculation has been made.

Arbitrary cascade body shapes and configurations can be analyzed using the PANEL code. However, the analysis is limited to flow conditions in the subsonic and shock-free transonic ranges. The calculation does become less accurate as compressibility effects become more significant. It is nearly exact for incompressible flows. This version of the PANEL code requires approximately 120,000 words of computer storage. It is written for double-precision calculations and is dimensioned to use a maximum of 98 panel elements to describe the blade.

This program was written by Eric R. McFarland of **Lewis Research Center.** *For further information, Circle G on the COSMIC Request Card.*
LEW-13862

Design of Multistage Axial-Flow Compressors

Computer program develops blading geometry and performance parameters.

A program has been developed for computing the aerodynamic design of a multistage axial-flow compressor and, if desired, the associated blading geometry input for internal flow analysis. The aerodynamic solution gives velocity diagrams on selected streamlines of revolution at the blade row edges. Blading is defined from stacked blade elements associated with the selected streamlines. The blade element inlet and outlet angles are established through empirical incidence and deviation angle adjustments to the relative flow angles of the velocity diagrams. The blade element centerline is composed of two segments tangentially joined at a transition point. The local blade angle variation of each segment can be specified with a fourth-degree polynomial function of path distance. Blade element thickness also can be specified with fourth-degree polynomial functions of path distance from the maximum thickness point.

Steady axisymmetric flow is assumed; so the aerodynamic problem can be reduced to solving the two-dimensional flow field in the meridional plane. Because the developed equations of motion are only applicable for calculation stations outside the blade rows, stations at the blade edges but not inside the blade rows are used. The streamline curvature method is used for the iterative aerodynamic solution. If a blade design is desired, the blade elements are defined and stacked within the aerodynamic solution. Thus the design velocity diagrams can be located at the blade edges.

The program input includes the annulus profile, the overall compressor mass flow, the pressure ratio, and the rotative speed. A number of parameters are input to specify and control the blade row aerodynamics and geometry. There are numerous options for controlling the way information is input and for specifying the amount of output. The output from the aerodynamic solution has an overall blade row and compressor performance summary followed by blade element parameters for the individual blade rows.

If desired, blade coordinates in the streamwise direction for internal flow analysis codes and/or coordinates on plane sections through blades for fabrication drawings can be printed and punched. This program is written in FORTRAN IV for use on a UNIVAC 1110 or an IBM 360-67 computer.

This program was written by James E. Crouse of **Lewis Research Center** *and William T. Gorrell of the U.S. Army Aviation Research and Development Command. For further information, Circle H on the COSMIC Request Card.*
LEW-13505

Extended Vortex Lattice Method

Aerodynamic characteristics are determined for up to four complex planforms.

The Extended NASA-Langley Vortex Lattice Method computer program, VLM, estimates the subsonic aerodynamic characteristics of up to four

complex planforms. These complex planforms include wings with variable-sweep outer panels, wings with several changes in dihedral angle across the span, wings with twist and camber, wings with winglets, and a wing (or wings) in conjunction with a tail and/or a canard.

The aerodynamic characteristics that are determined by VLM are lift; drag; pitching moment; leading-edge thrust, leading-edge suction, and their distributions; side-edge suction; distributions of several span-loading coefficients; distribution of lifting-pressure coefficient; damping-in-pitch parameter; damping-in-roll parameter; and lift coefficient due to pitch rate. The user can also obtain vortex-flow aerodynamics on cambered planforms, flow-field properties off the configuration in attached flow, and planform longitudinal load distributions.

VLM employs a vortex lattice method that is an extension of the finite step lifting-line method. This method assumes steady, irrotational, inviscid, incompressible, attached flow. The effects of compressibility are represented by application of the Prandtl-Glauert similarity rule to modify the planform geometry. Potential flow theory in the form of the Biot-Savart law is used to represent disturbances created in the flow field by the lift distribution of the planform.

Each planform is divided into panels. VLM is capable of handling up to 4 planforms with up to 400 panels. For computational purposes each panel is replaced by a horseshoe vortex. The horseshoe-vortex representation of each planform is used to determine the appropriate circulation values consistent with the no-flow boundary conditions. Then, the Kutta-Joukowski theorem is applied to each spanwise vortex filament to determine the forces on the panel. These forces are used to obtain the overall forces and moments.

VLM is written in FORTRAN IV for batch execution and has been implemented on a CDC CYBER 170-series computer with a central-memory requirement of approximately 130K (octal) of 60-bit words. VLM was first developed in 1971 and was last updated (Mark IV Version) in 1982.

This program was written by John E. Lamar of **Langley Research Center** *and Henry E. Herbert of Computer Sciences Corp. For further information, Circle J on the COSMIC Request Card.*
LAR-13039

Subcritical Wing Design Code

Program uses higher-order far-field drag minimization.

The computer program WDES WDEM is a preliminary aerodynamic design tool for one or two interacting, subsonic lifting surfaces. The program offers the user a subcritical wing design code employing a higher-order far-field drag-minimization technique. Linearized aerodynamic theory is used, in the form of a vortex lattice representation of the wings in the near field, along with a piecewise linearly-varying vortex sheet, higher-order panel method, model of the undistorted wake.

The far-field wake model assumes that the strength of the wake vortex sheet varies piecewise linearly in the spanwise direction. This model allows for the development of analytical expressions for lift coefficient, induced-drag coefficient, pitching-moment coefficient, and bending-moment coefficient. From these relationships a direct optimizaton scheme is used to determine the optimum wake vorticity distribution for minimum induced drag, subject to constraints on lift and pitching or bending moment. Integration spanwise yields the bound circulation, which is interpolated in the near-field vortex lattice to obtain the design camber surface(s). Use of a higher-order panel method in the farfield leads to significant improvements in accuracy over use of a discrete vortex filament wake model for wings with dihedral.

This program is written in FORTRAN IV for batch execution and has been implemented on a CDC CYBER 170-series computer with a central-memory requirement of approximately 130K (octal) of 60-bit words. WDES WDEM was documented in 1981.

This program was written by John M. Kuhlman and Jin-Yea Shu of Old Dominion University Research Foundation for **Langley Research Center.** *For further information, Circle K on the COSMIC Request Card.*
LAR-12959

Interactive Graphics Analysis for Aircraft Design

Aircraft geometry is displayed on an interactive terminal.

The QUICK Interactive Graphics Analysis program, QUIAGA, displays aircraft QUICK-geometry data to aid in the detection and analysis of errors. The QUICK-geometry program generates a completely-analytical aircraft geometry description for use by finite-difference flow codes and is included in the COSMIC package "A Code for Calculating the Steady Super/Hypersonic Inviscid Flow Around Real Configurations" (LAR-11891), reported on in *NASA Tech Briefs,* Vol. 2, No. 1 (Spring 1977), on page 124.

QUIAGA incorporates selected QUICK-geometry subroutines to allow examination of the analytic definition of a configuration by generating cross-section plots and body-line plots on a graphics terminal. Available options include multiple cross-section views, hidden-line removal, the display of control point locations, and the comparison of cross sections with reference data. Use of these options for the detection and analysis of errors in the QUICK-geometry definition can be of great assistance in speedily arriving at a correct analytical geometry description.

QUIAGA is designed for interactive use on a Tektronix 4014 computer display terminal connected to a host computer supporting the PLOT10 graphics library. The program uses the QUICK-geometry data preprocessed into the intermediate form that is required by the flow codes.

The QUIAGA user may interactively request various cross-section and body-line plots to inspect visually the configuration defined by the QUICK-geometry data. The user may also interactively request plots with control point locations and/or reference cross-section data (if they are available) to analyze any errors detected. After corrections have been made and the data again batch-processed on the QUICK-geometry program, the QUIAGA user can again interactively check if the desired configuration has been achieved.

(continued on next page)

QUIAGA is written in FORTRAN IV for interactive execution and has been implemented on a CDC CYBER 170-series computer with a central-memory requirement of approximately 75K (octal) of 60-bit words. QUIAGA was developed in 1981.

This program was written by James C. Townsend of **Langley Research Center.** *For further information, Circle L on the COSMIC Request Card.*
LAR-12951

Off-Design Turbine Modeling

Off-design efficiency and flow function are obtained from design-point input data.

A turbine modeling technique rapidly obtains off-design performance from design-point input. This technique is applicable to large axial-flow turbines that may or may not incorporate variable geometry in the first-stage stator. A user-specified option permits the calculation of design-point cooling-flow levels and the corresponding change in turbine efficiency.

The NASA Lewis Research Center employs a general computer program (NNEP) for calculating the thermodynamic performance of jet propulsion engines. To calculate off-design engine performance, the user must input component maps. These maps define the characteristics of the various components over their full range of operating conditions. For advanced propulsion systems, these characteristics are not generally known. Furthermore, the typical user of the program is not sufficiently knowledgeable and may not be able to afford the time to do an extensive design analysis of the component in question. Instead the user usually scales an available map.

Computer program PART is an improved method of representing the turbine component when performing calculations of off-design performance for advanced air-breathing engines. This method is compatible in both form and format with the cycle program NNEP. The program uses turbine design-point data as input to generate off-design values of turbine flow-function and total-to-total efficiency over a range of pressure ratios and speeds specified by the user.

The basic output from the program consists of two tables. These tables show the turbine efficiency and turbine flow-function variations for each of the first-stage nozzle area ratios, pressure ratios, and percent corrected speeds specified in the input. The input values of area ratio are converted to first-stage nozzle angles before being printed out.

After the input has been read and processed, the program carries out a simple pitch line analysis starting with the last stage of the turbine. The analysis starts at the exit of the turbine stage (to avoid iteration) and calculates the bucket and nozzle flow characteristics using the analytically based correlations developed during the study. Successive stages are then calculated until the first stage is reached. The first-stage characteristics are then generated, and the stages are stacked for each value of the first-stage turbine nozzle area specified. If the turbine is cooled, then calculations are made to determine the cooling-flow requirement and the cooled-turbine efficiency. Finally, the output is processed to obtain a turbine map representation.

PART is written in FORTRAN IV and is accessible from an IBM 360/67 time-sharing system terminal.

This work was done by G. L. Converse of General Electric Co. for **Lewis Research Center.** *For further information, Circle M on the TSP Request Card.*
LEW-13674

Axial Compressor Design and Analysis

Program yields blade configurations and aerodynamic flow fields.

A computer program for multistage axial compressor design and analysis consists of three sections — two blade design sections and an aerodynamic section. The program is structured such that any one section may be used alone, or the aerodynamic section may be used in conjunction with either or both of the blading sections.

The Analytic Meanline Section offers four alternative meanlines for blade design. Output from the Analytic Meanline Section is compatible with the NASTRAN stress analysis program and may be used as partial input to the Aerodynamic Section. With this input, the Aerodynamic Section will give the flow characteristics for the blading.

The Arbitrary Meanline Section takes relative flow angles, either entered directly or as output from the Aerodynamic Section, and produces a blade section for each defined streamsurface. The streamsurface sections are then stacked to produce the blade.

The Aerodynamic Section utilizes the streamline curvature approach to solve for the compressor flow field (streamlines). A flow-field grid is established by the intersection of streamlines with specified axial stations. These axial stations provide "work" and "loss" inputs to the Aerodynamic Section and are inserted at strategic locations within the flow field (such as leading and trailing edges of blades). The axisymmetric compressible-flow equations, written in terms of radial, circumferential, and meridional components and containing streamline curvature and slope terms, are solved given an initial guess for the streamline pattern. The program iterates, each time improving the streamline pattern, until the specified tolerance is achieved. Aerodynamic Section output consists of velocity triangle components, flow angle, streamline curvature, and thermodynamic information as a function of radius. Output pressure force data are in a format compatible with the NASTRAN stress analysis program.

Modifications have been made to the Aerodynamic Section of the computer program to allow direct input of measured radial pressure and temperature profiles obtained from engine or cascade data. The modifications do not change the program input format. The program is written in FORTRAN IV language for use on a UNIVAC 1100 computer.

This work was written by Jeffrey G. Williams of **Lewis Research Center** *and Robert M. Hearsey of the University of Dayton. For further information, Circle N on the COSMIC Request Card.*
LEW-13488

Machinery

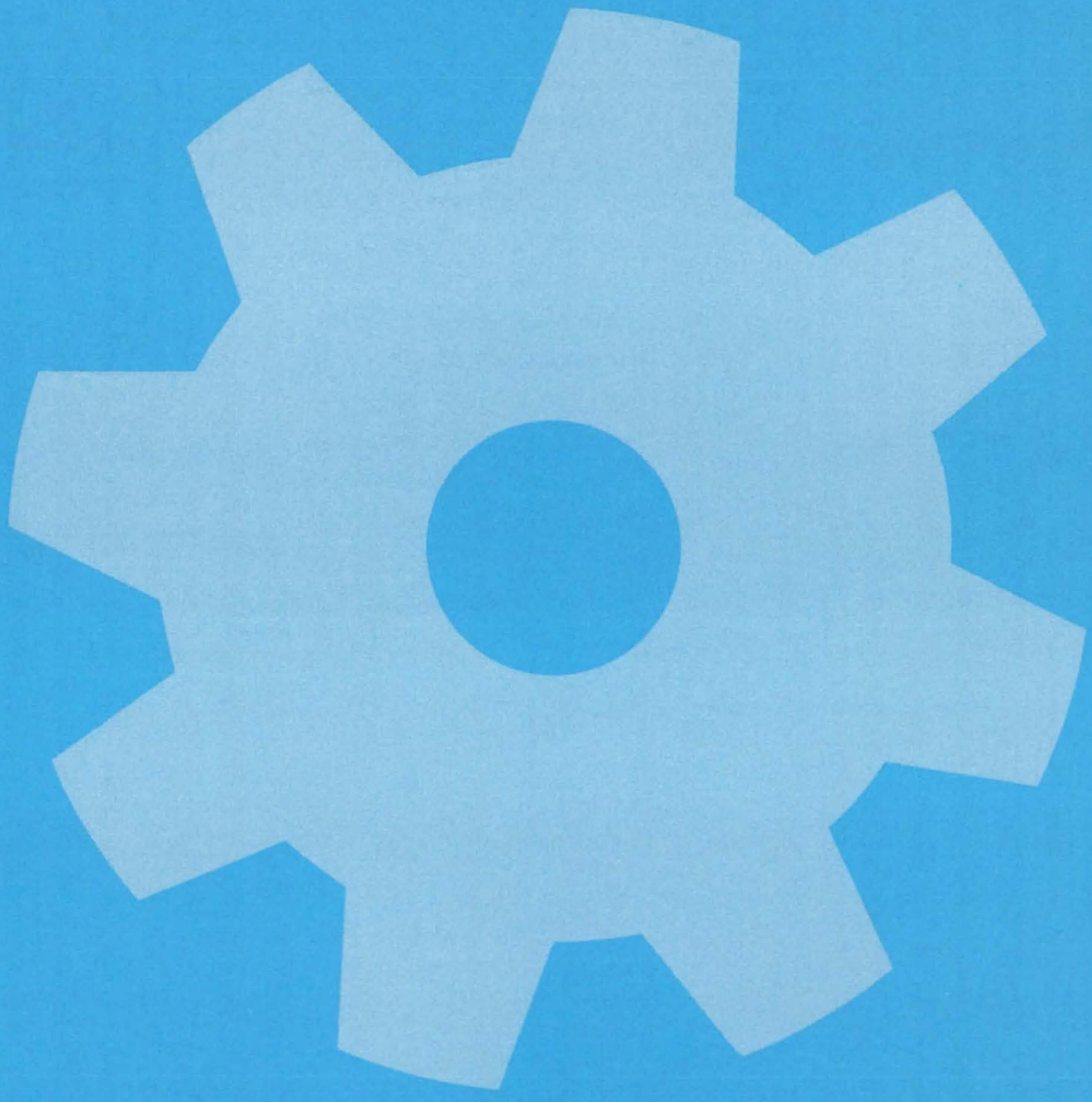

Hardware, Techniques, and Processes

Computer Programs

Coaxial Redundant Drives

Harmonic drives allow redundancy and high output torque in a small package.

Marshall Space Flight Center, Alabama

Originally developed for positioning an 800-lb (363-kg) X-ray telescope, an electromechanical drive provides high torque and redundancy in a compact package. If the main drive should fail, a standby drive takes over and produces torque along the same axis as that of the main drive. Potential uses include power units in robots for internal pipeline inspection, manipulators in deep submersible probes, or other applications in which redundancy could protect against costly failures.

The drive consists of two transmissions and brushless dc motors arranged in tandem in a single assembly (see figure). When the main drive is operating, the standby drive simply rotates with the main drive. If a failure occurs in the main drive, it is held stationary. The standby drive is then energized and rotates independently, delivering power to the output shaft.

Harmonic drives are employed in both the main and standby transmissions. A harmonic drive consists of an elliptical wave generator that drives a conforming flexible spline against a rigid circular spline. The flexible spline rotates the output shaft of the drive. Essentially, the circular spline is a fine-tooth internal gear, and the flexible spline is a fine-tooth external gear. As the wave generator is rotated by the motor, it continuously engages teeth on the flexible spline with teeth on the circular spline. Teeth on opposite ends of the major elliptical axis of the flexible spline mesh with the circular spline while teeth on the minor axis do not mesh.

The harmonic transmission provides a large speed reduction in a single stage — 200:1 for the X-ray telescope application. With an 8,500-r/min motor and a 170:1 planetary-gear reduction in the motor housing, the net speed reduction is 34,000:1. The output shaft thus turns at 0.25 r/min.

The harmonic transmission offers additional advantages. Tooth friction losses are low because motion is almost purely radial at the points of tooth contact. Many spline teeth are in simultaneous engagement to carry high-torque loads. Teeth adjacent to load-bearing teeth are in near engagement and provide reserve capacity to accommodate shocks and overloads. Since the regions of tooth engagement are diametrically opposed, forces on the gears are symmetrical and balanced.

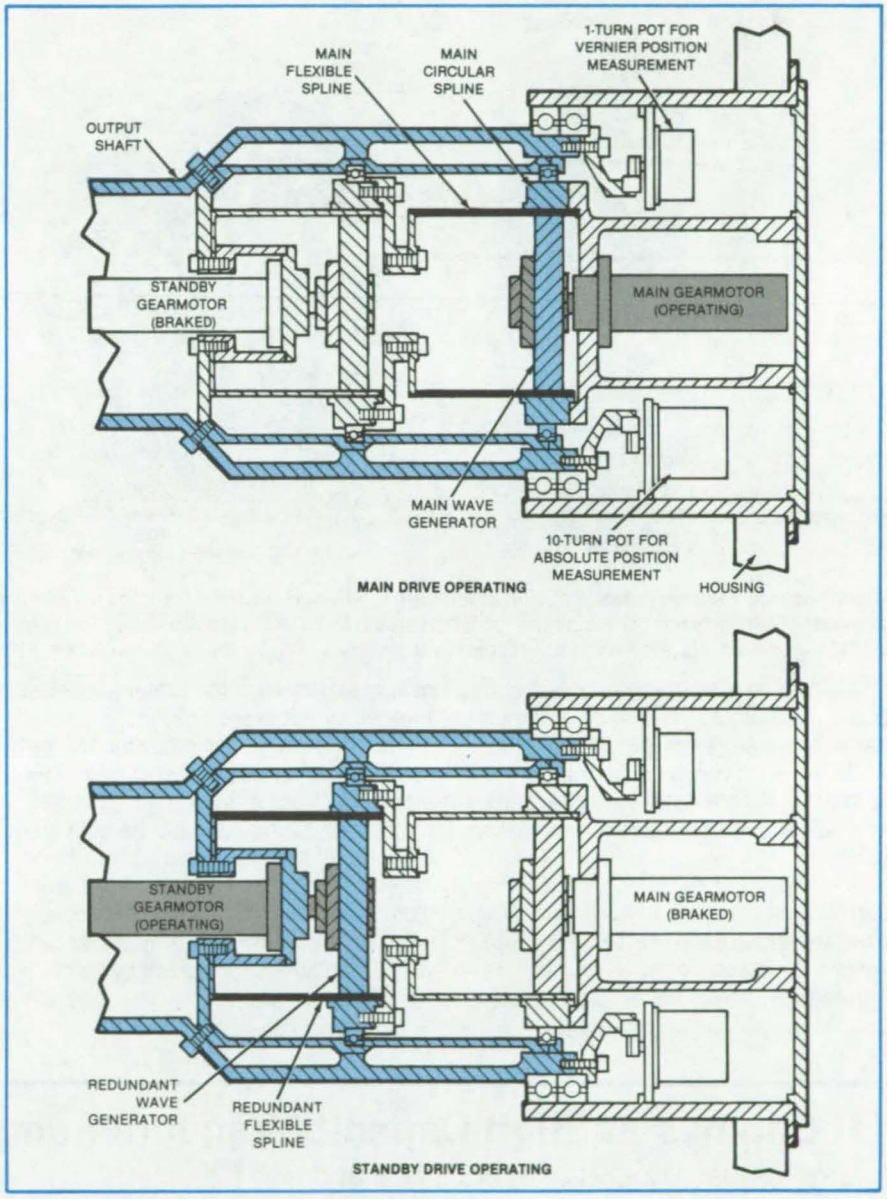

Main and Standby Drives complement each other. With the main drive operating, the standby drive turns along with the output shaft (top). With the main drive not operating, the standby drive rotates on its own (bottom).

[See the related article "Redundant Gear Train" (NPO-15317) on page 73 of *NASA Tech Briefs*, Vol. 7, No. 1.]

This work was done by R. Brissette of American Science & Engineering, Inc., for **Marshall Space Flight Center.** *For further information, Circle 51 on the TSP Request Card.*
MFS-25171

Cryogenic Vacuum Pump

System provides high pumping capacity, even for noble gases.

NASA's Jet Propulsion Laboratory, Pasadena, California

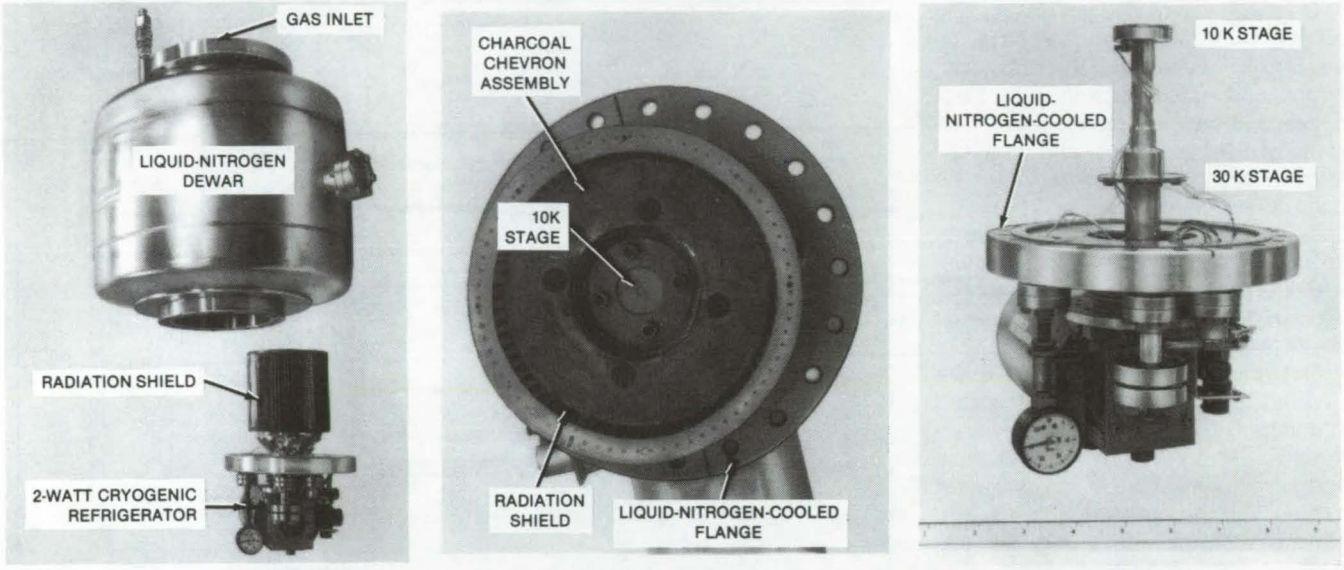

The **Cryogenic Vacuum Pump** is shown at left with the flange unbolted from the liquid-nitrogen Dewar. At the middle is a top view of the charcoal chevron assembly inside the radiation shield (with the radiation-shield top cover removed for visibility). Shown at the right are the 30 K and 10 K stages (which are hidden in the other views by the radiation shield and charcoal chevron assembly).

A three-stage cryogenic vacuum pump (see figure) has high pumping capacity for all gases, including helium, while requiring only a 2-watt refrigerator to cool its two coldest stages. The pump is small enough for general laboratory use.

The first stage, which is cooled by liquid nitrogen, removes water and CO_2 from the input gas. The second stage, which is cooled to 38 K by the refrigerator, removes noble gases except helium and some of the lighter gases not trapped by the first stage.

The third stage, cooled by the refrigerator, traps all remaining gases. This stage realizes a very high pumping capacity by using a large-area cold surface: A compact cylindrical chevron assembly holds 200 g of charcoal granules. The charcoal granules are loosely held in the chevrons by a nylon screen, which is in turn held in place by loops of nylon thread encircling the chevron assembly. The total surface area of the charcoal granules is 360,000 m^2.

A radiation shield around the charcoal assembly is held at 30 K. All three stages are mounted inside the liquid-nitrogen Dewar that cools the first stage.

This work was done by Charles A. Zachman of Caltech for **NASA's Jet Propulsion laboratory.** *For further information, Circle 52 on the TSP Request Card.*
NPO-15517

Jet Engines as High-Capacity Vacuum Pumps

A large diffuser operational envelope and and long run times are possible.

Marshall Space Flight Center, Alabama

Two gas-turbine jet engines would provide the primary ejection stream in a high-capacity eductor vacuum pump. Originally proposed to create a low-pressure environment for testing rocket engines, the system could find applications in such industrial processes as handling corrosive fumes, the evaporation of milk and fruit juices, petroleum distillation, and the dehydration of blood plasma and penicillin.

In contrast to an equivalent steam-driven system, the jet-engine-driven system for testing rocket engines would cost half as much to build and one-fourth as much to operate, would require less space, and would operate for longer times. Shown in the figure, the proposed system can be used for testing rocket engines at pressures as low as 40 psia (276×10^3 N/m^2) and run times of 30 min or longer. An equivalent steam-ejector system would require a three-stage ejector and a building 100 by 300 ft (30.5 by 91.4 m) three stories high.

The use of the jet-engine-driven ejector would result in a large range of

operating pressures. Other advantages include nearly instantaneous startup and greater energy efficiency and more reliable operation than with steam.

This work was done by C.J. Wojciechowski of Lockheed Missiles & Space Co., Inc., for **Marshall Space Flight Center.** *For further information, Circle 53 on the TSP Request Card.*

This is the invention of a NASA employee, and a patent application has been filed. Inquiries concerning license for its commercial development may be addressed to the inventor, Mr. C. J. Wojciechowski, Lockheed, P.O. Box 1103, Huntsville, AL 35807.
MFS-25791

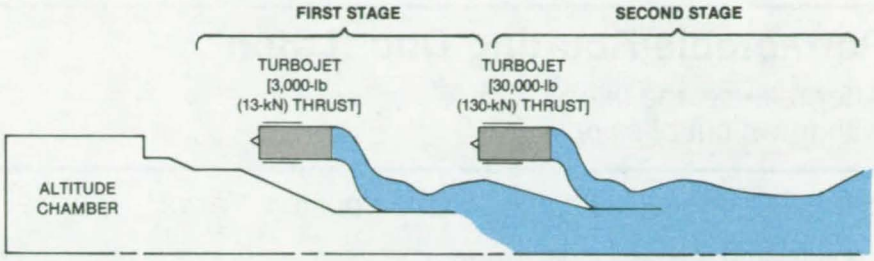

The **Jet-Engine-Driven Ejector/Diffuser System** combines two turbojet engines and a variable-area-ratio ejector in two stages. The first stage uses a small turbojet engine that is about one-tenth the size of the second-stage engine. The two-stage variable-mach-number ejector can evacuate the diffuser down to 0.06 psia (400 N/m^2) prior to startup of a rocket-engine test. After startup, the pressure rises to 40 psia with the rocket engine running at 10 percent of full power.

Spool-Valve Pressure-Difference Regulator

Valves maintain a preset pressure difference between gas flows.

Lyndon B. Johnson Space Center, Houston, Texas

A pair of valves maintains a constant pressure difference between two gas streams. Consisting of two connected spools that slide in multiport cylinders, the valves were originally developed to regulate the relative pressures of hydrogen and oxygen gases flowing to a fuel cell. The valves allow the gases to be supplied in the quantities required by the electric load while maintaining the proper proportions of the reactants. The simple spool valves replace custom-made regulator valves.

Pressure-sensitive diaphragms center the connected-spool assembly when the gas pressures are in the proper relationship. A spring on the hydrogen diaphragm provides a bias force so that the oxygen pressure is maintained about 2 lb/in.^{2} (13.8 kPa) above the hydrogen pressure. The gases flow unimpeded through their respective entrance ducts, around their spools, and through their exit ducts to the fuel cell.

When the gas-pressure differential changes, the net effect of the opposing pressures on the two diaphragms is to push the spools away from the side on which the pressure is rising. If the displacement is sufficiently large, a spool-valve edge will restrict the supply duct on the higher pressure side, thereby reducing the pressure on that side and allowing the spool assembly to recenter. If there is a great increase in pressure in a chamber, its supply duct will be completely shut off and a vent duct opened.

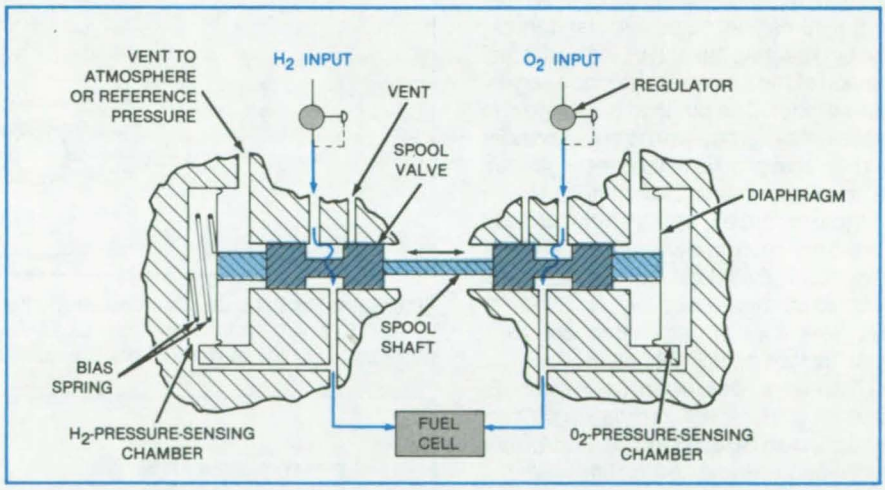

Two Spool Valves Connected by a Shaft move back and forth in response to changes in pressure in the oxygen and hydrogen chambers. The spool-valve assembly acts to restore the pressures to their preset difference. By eliminating the diaphragms, the pressure could be exerted directly on the external end of the spool valve; however, the forces and therefore the sensitivity of the assembly would be reduced.

The relative-pressure regulator can be used for gases other than hydrogen and oxygen. The pressure differential can be adjusted by selecting a bias spring of the proper stiffness. If equal pressures are required in the two gases, the spring would be eliminated.

This work was done by Albert P. Grasso of United Technologies Corp. for **Johnson Space Center.** *No further documentation is available.*

This invention is owned by NASA, and a patent application has been filed. Inquiries concerning nonexclusive or exclusive license for its commercial development should be addressed to the Patent Counsel, Johnson Space Center [see page A5]. Refer to MSC-20127.

Retractable Rotating Door Latch

After release, the latch withdraws out of sight.

Lyndon B. Johnson Space Center, Houston, Texas

A new mechanism turns a door latch, latching or unlatching the door, and then retracts until the latch is flush with the surface of the door frame. Figure 1 shows the latch and the door.

Concentric cylinders have cam grooves machined in their surfaces (Figure 2). When rotated relative to each other, the cylinders impart rotation and translation to the shaft of the door latch. The motions may proceed separately or simultaneously.

The outer concentric cylinder is motor driven, and the inner cylinder is stationary. When the motor rotates the outer cylinder, it also rotates a pin that extends through the inner and outer cylinders and is attached to the latch shaft. The outer cylinder thus rotates the latch so that it releases the doors. As the motor turns the outer cylinder farther, the pin reaches the end of the horizontal portion of the groove in the stationary inner cylinder. The pin then begins to rise in the helical groove in the outer cylinder and vertical groove in the inner cylinder. In so doing, it retracts the latch.

More complex motions can be obtained by separately rotating the inner and outer cylinders with suitably-programed motors. These might include, for example, several translations and rotations as well as spiral hook motions.

This work was done by Renton B. Carsley of Rockwell International Corp. for **Johnson Space Center.** *For further information, Circle 54 on the TSP Request Card.*

This invention is owned by NASA, and a patent application has been filed. Inquiries concerning nonexclusive or exclusive license for its commercial development should be addressed to the Patent Counsel, Johnson Space Center [see page A5]. Refer to MSC-20304.

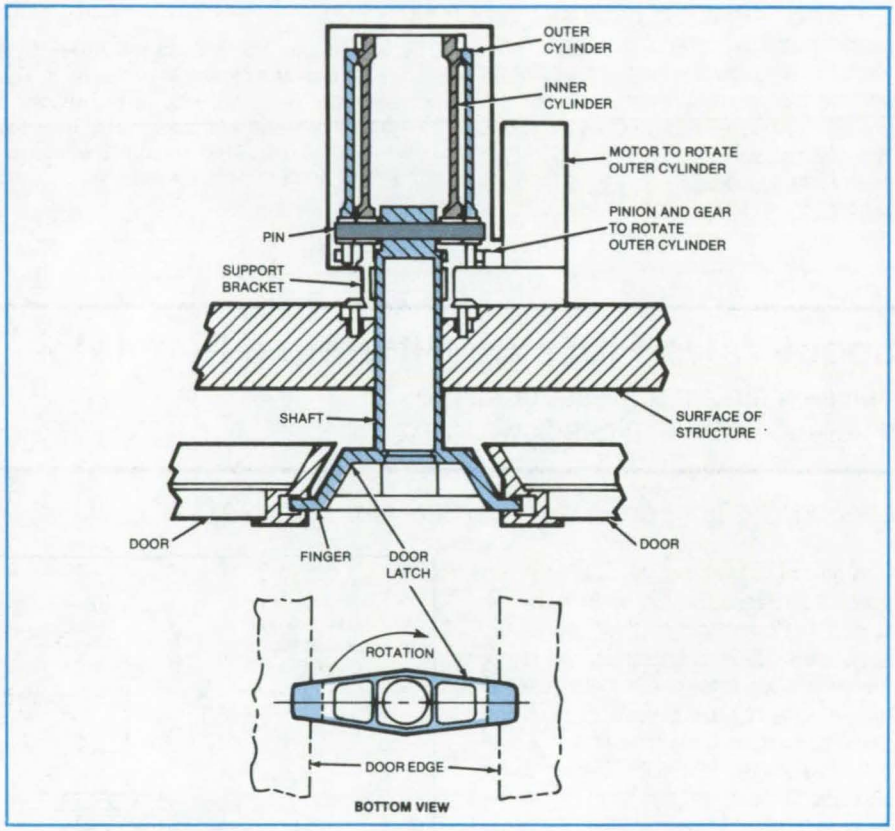

Figure 1. **In the Extended Position** shown here, the fingers of a door latch engage grooves in the doors. After it is rotated, the latch releases the doors. It is then retracted to a position flush with the surface of the frame.

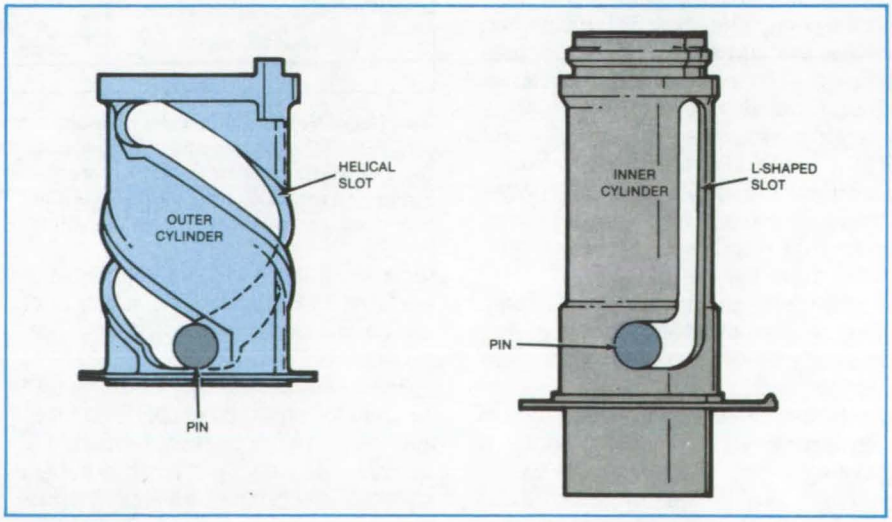

Figure 2. **Slots in Concentric Cylinders** control motions of a pin and of a shaft and door latch attached to the pin. The motor-driven outer cylinder has a helical slot, and the stationary inner cylinder has an L-shaped slot. The pin (which is attached to the shaft) is constrained to lie at the intersection of the cam slots.

Locking Bolt

A locking ball in the bolt head holds the wrench in place.

Lyndon B. Johnson Space Center, Houston, Texas

The head of a proposed bolt would contain a locking ball and a release pin to grasp a box wrench or other tool. The locking bolt could be installed in cramped spaces that would prevent an operator from using both hands or where the operator's maneuverability is restricted by bulky clothing or obstacles.

The bolt was originally proposed for an extravehicular space environment where the use of handtools is restricted by space suits and by the effects of zero gravity. Under these conditions, the force is applied in only one direction; that is, a crewmember is not expected to hold a wrench on a bolt and rotate the bolt simultaneously.

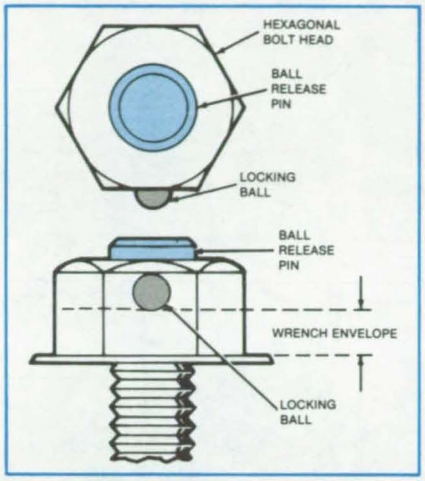

This **Locking Bolt** incorporates an extra-long head and a choice of ball locks. It can be used in any application where access to the bolt is limited.

The new bolt, shown in the figure, could be made in two variations: either with a spring-loaded locking ball to restrain the wrench if the operator momentarily releases it or with a locking ball and release pin to lock the wrench on the bolthead. A similar design can be applied to other handtools.

This work was done by Barry E. Boswell of McDonnell Douglas Corp. for **Johnson Space Center.** *No further documentation is available.*
MSC-20439

Expander for Thin-Wall Tubing

A tool locally expands small-diameter tubes.

Marshall Space Flight Center, Alabama

Originally developed to expand a liquid-oxygen tube fitting, an easily constructed tool uses an elastomer to expand a section of thin-wall, small-diameter tubing. The tool is readily adaptable to other situations in which a tube must have a small bulge for mechanical support or flow control.

As shown in the figure, a metal sleeve with a diameter slightly smaller than that of the tube slides on a metal rod. One end of the rod widens to a flange of the same diameter as that of the metal sleeve. An elastomeric sleeve is placed on the rod between the metal sleeve and the metal flange.

When the metal sleeve is pushed axially toward the flange, the elastomeric sleeve is squeezed and acts somewhat like a hydraulic fluid. The resulting pressure forces the tube wall outward.

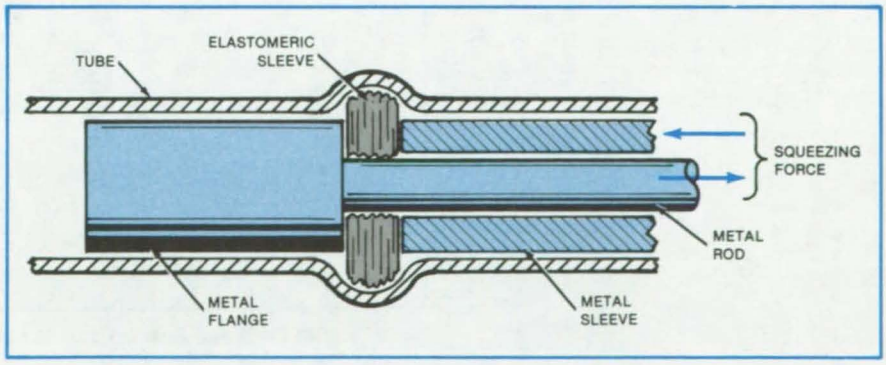

The **Tube Expander** locally expands and deforms the tube: A compressive lateral stress is induced in the elastomeric sleeve by squeezing it axially between the two metal tool parts.

This work was done by R. Pessin of Rockwell International Corp. for **Marshall Space Flight Center.** *No further documentation is available.*

Inquiries concerning rights for the commercial use of this invention should be addressed to the Patent Counsel, Marshall Space Flight Center [see page A5]. Refer to MFS-19739.

Transporter for Treated Sheet Materials

Plastic spacers keep parts separated during transport or storage.

Lyndon B. Johnson Space Center, Houston, Texas

A cart with rods and spacers holds sheets with delicate finishes for storage or transport. The sheets can be supported vertically by the rods, as shown at the top of the figure, or horizontally, as shown at the bottom. The spacers keep the sheets separated.

The sheets may have holes drilled at their edges so that they can slide onto the rods. They can also be held by a rod "fence" around the perimeter of the stack, as shown at the bottom of the figure.

The cart was originally designed to eliminate the time and expense of taping, wrapping, and sometimes refinishing aluminum sheets with delicate anodized finishes. It could have similar benefits in the optical and plating industries.

This work was done by Martin H. Pollack of Fairchild Republic Co. for **Johnson Space Center.** *No further documentation is available.*
MSC-20332

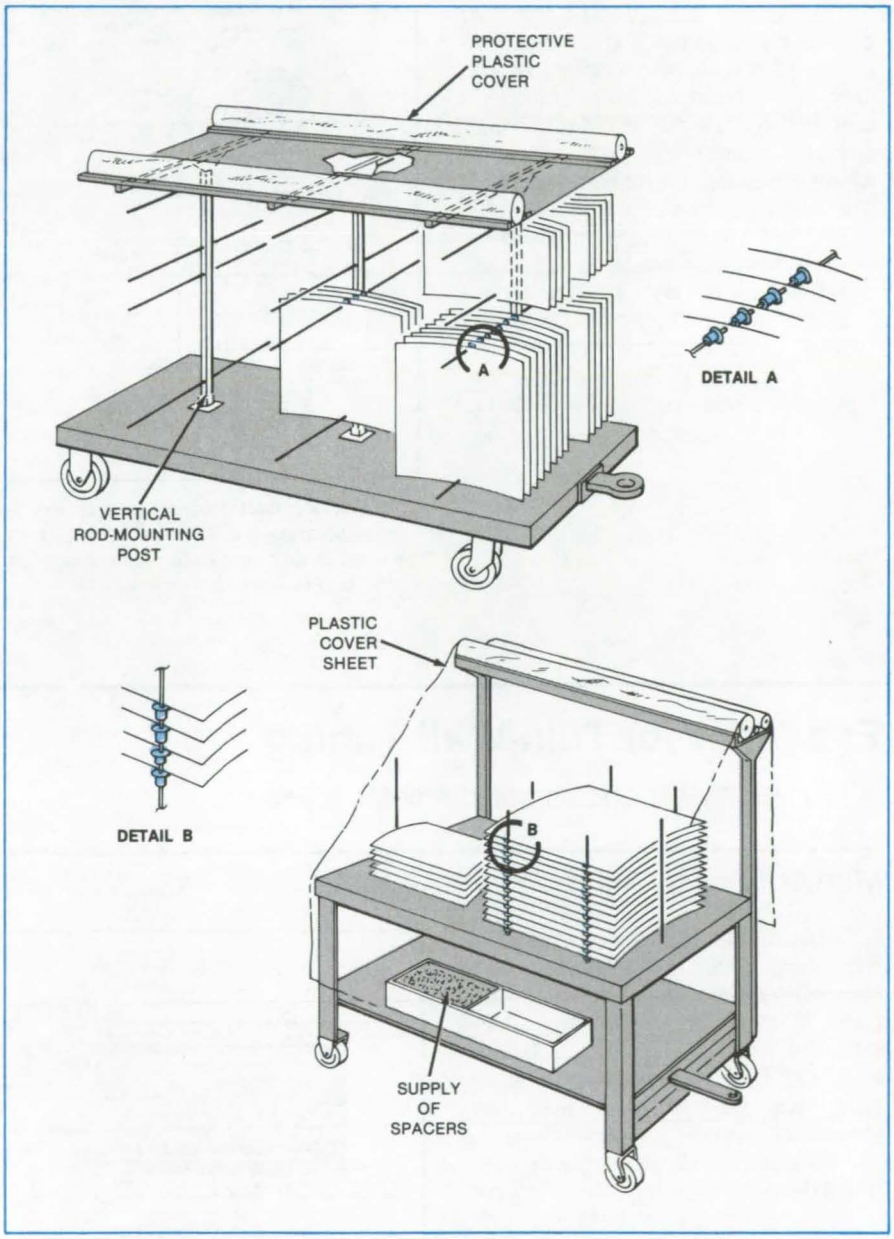

A **Dolly With Rods and Spacers** can be used to stack treated sheets horizontally or vertically. The sheets can be held by spacers on stacking rods or by rods that surround the parts. A standard four-wheel dolly can be the basis for designing the cart. The spacers are conventional plugs or "protective closures" used in many industrial applications.

Tool for Guiding an Auger

A threaded ram with the same pitch as the auger reduces potential damage to fragile workpieces.

Lyndon B. Johnson Space Center, Houston, Texas

Fragile materials, such as the surface-insulation tiles on the Space Shuttle orbiter, are easily damaged when drilled or bored. However, the tool shown in the figure, designed to guide an auger, significantly reduces the possibility of such damage. A threaded ram that has the same pitch as the auger guides it at the rate at which it "naturally" tries to move through the material. Since it does not overdrive the auger, the tool reduces the chances of breaking the workpiece.

As shown, the tool includes a handle, a frame, and a collar that holds and guides the ram to which the auger is attached. A screw with a flattened end slightly narrower than the groove in the ram threads passes through the collar and into the groove to control the ascent and descent of the ram and, in turn, the auger. The auger is prevented from rotating on the ram by a slot machined into its stem and by a mating lug on the ram. Depending on the hardness of the material being tapped, the workpiece can be held on, or clamped to, the base of the tool frame.

The dimensions of the tool depend on that of the auger. In one particular application, the blade pitch of a metallic auger was 0.5 in. (1.3 cm). The auger diameter was 2 in. (5.1 cm), and its length was 1.5 in. (3.8 cm). The corresponding ram shaft was about 1.25 in. (3.2 cm) in diameter. The shaft contains a helical groove, about 0.125 in. (0.3 cm) deep and 0.125 in. wide, machined on it. The pitch of the groove was 0.5 in., corresponding to that of the auger blade.

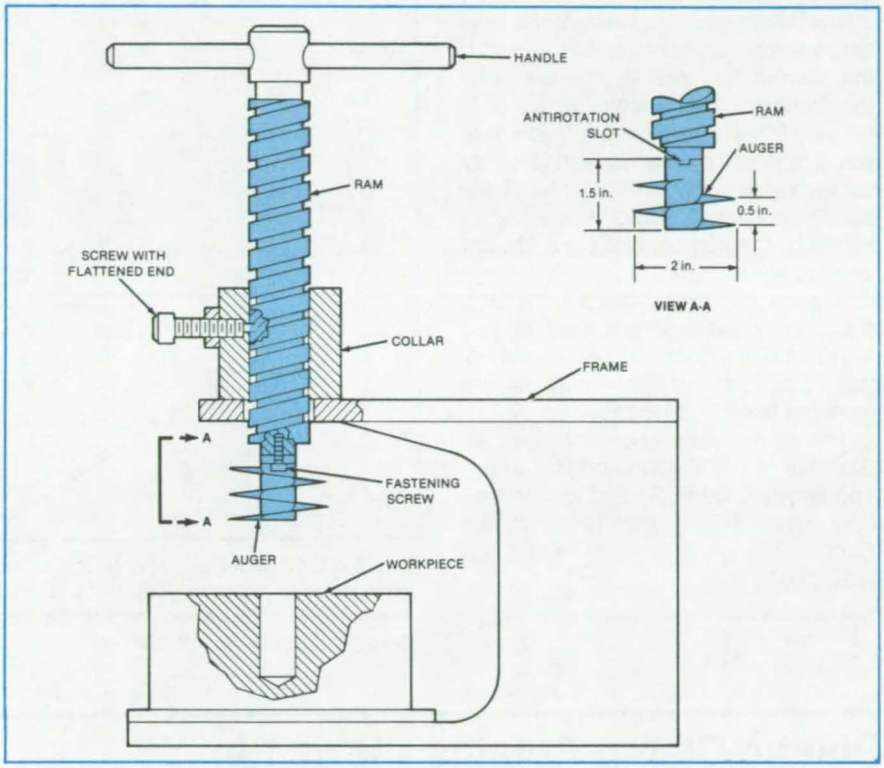

The **Auger and Ram** both have the same pitch, which minimizes damage to the workpiece and the load carried by the auger. The auger is firmly fastened onto the ram shaft by a screw and is kept from rotating on the shaft by a slot machined into the end of its stem and by a male driving lug that engages the slot.

The tool has been used to tap the surface-insulating tiles on the Space Shuttle. Previously, a drill press fed the auger, but it tended to break off large chunks from the tiles because of an excess pressure on the tile. The principle of the tool could be applied to installing threaded studs in plastic or rubber, where it is impractical to mold them in.

This work was done by Clarence J. Wesselski of **Johnson Space Center.** *No further documentation is available.*
MSC-20194

Bender/Coiler for Tubing

An easy-to-use tool makes coils of tubing.

Lyndon B. Johnson Space Center, Houston, Texas

A new tool bends tubing through any required angle, even through 360° for coil-winding. Conventional tube benders, in contrast, are limited to bends of 180° or less, and most tube coilers require considerable skill to set up.

In the new tool, the operator turns the handle shown in the figure, causing a die to wrap the tubing around a mandrel. The mandrel diameter is equal to the required diameter of the tubing bend.

A groove in the mandrel is slightly wider than the outside diameter of the tubing being bent, and the depth of the groove is slightly less than the radius of

(continued on next page)

the tubing. The groove may be oriented in a right-handed or left-handed spiral.

The radius of the groove in the die is the same as that of the mandrel groove. The die must be smooth, hard, and well lubricated to prevent galling, scratching, or other damage to the tubing. The die is positioned on the handle so that it fits snugly — but not tightly — on the tubing.

The handle post and the center hole in the mandrel may be threaded to match the pitch of the mandrel groove so that the handle moves vertically as it is turned. This provision helps guide thin-wall tubing as it is bent: It is unnecessary for thick-wall tubing. The lengths of the handle post and mandrel are determined by the number and pitch of coils on the mandrel.

When a bend is completed, the stop post is removed to release the tubing. If the bend was around an angle of greater than 180°, the coiled tubing is unscrewed from the mandrel.

This work was done by Joel M. Stoltzfus of Lockheed Corp. for **Johnson Space Center.** *For further information, Circle 55 on the TSP Request Card.*
MSC-20410

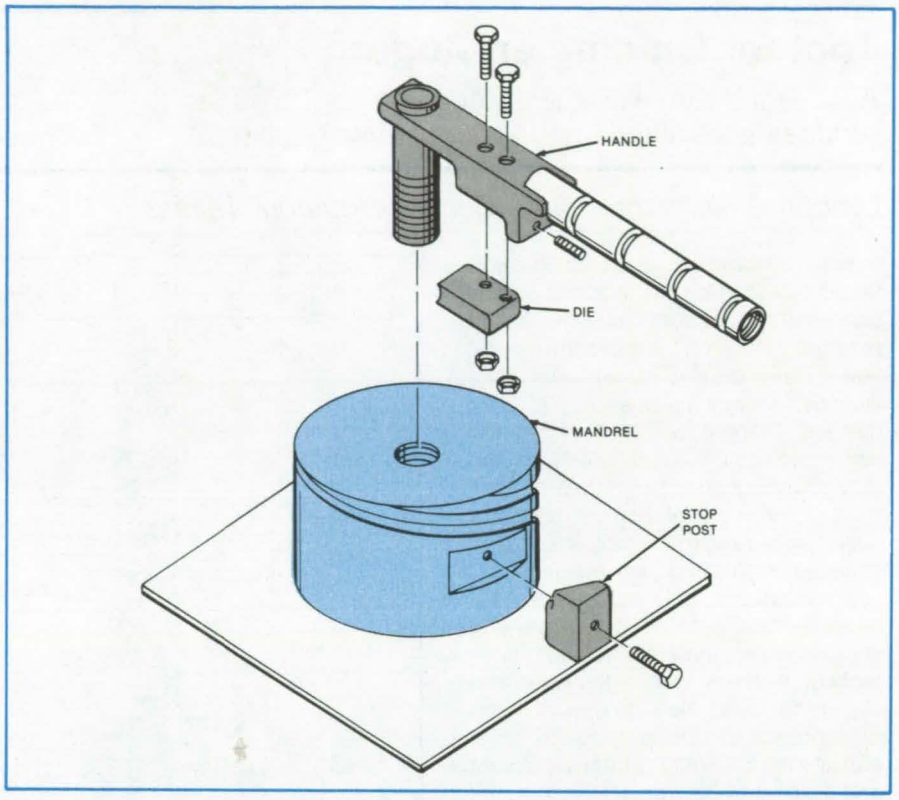

This **Tubing Bender** is simple to construct and easy to use. The tubing to be bent is first clamped with the stop post. The die is positioned snugly against the tubing. Then the operator turns the handle to slide the die along the tubing, thus pushing the tubing into the spiral groove on the mandrel.

Plastic Clamp Retains Clevis Pin

A plastic clamp requires no special installation or removal tools.

Marshall Space Flight Center, Alabama

The triangular plastic clamp shown in the figure replaces a metal retaining ring for clevis-type pivots. The groove that receives the new clamp does not have to be as precisely machined as that for the metal ring, so assembly and fabrication costs are reduced.

The new clamp slips easily over the end of the pin. Once engaged in the groove, it holds the pin securely. Moreover, it can be installed and removed easily without special tools — a screwdriver or putty knife is adequate for prying it out of the groove.

The clamp can be used to retain bearings, rollers, pulleys, and other parts that rotate. Potential applications might include slowly and intermittently rotating parts in appliances.

This work was done by Reuben G. Cortes of Rockwell International Corp. for **Marshall Space Flight Center.** *No further documentation is available.*

Inquiries concerning rights for the commercial use of this invention should be addressed to the Patent Counsel, Marshall Space Flight Center [see page A5]. Refer to MFS-19747.

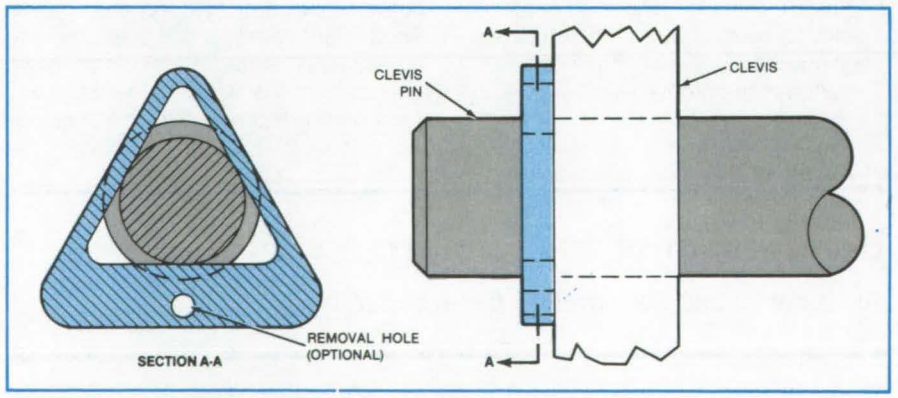

A **Triangular Nylon Clamp** snaps into the groove on a clevis pin. In this application, the pin is 5/16 inch (7.9 mm) in diameter, the groove is 1/4 inch (6.4 mm) in diameter, and the clamp is 1/16 inch (1.6 mm) thick.

Portable Roller Staking Tool

Staking tool is compact and portable.

Lyndon B. Johnson Space Center, Houston, Texas

A new tool combines clamping and staking operations in a single unit. The tool clamps the workpiece (a bearing or bushing), alines it, and stakes one of the flat faces.

Figure 1 gives an overall view of the tool, and Figure 2 illustrates its operation. The tool applies an axial force to the workpiece by clamping it. The axial force is transmitted along the bolt, through the motor housing, and through the needle thrust bearing that supports the roller housing. The rollers impart the staking/clamping force to one face of the workpiece while the anvil applies an opposing force to the other face. The bearing or bushing alinement is maintained by a dowel pin.

The roller housing is turned by a pneumatic motor equipped with a 90° drive adapter. As the rollers turn under load, they deform the outer portion of the workpiece face, so that it locks the workpiece into the frame. The bolt is gradually tightened during the turning operation to take up the slack and maintain the staking/clamping force. After staking the edge around one face, the tool is removed and reattached to operate on the opposite face.

The unit is compact and light in weight. It can accommodate numerous bearing or bushing sizes through changes in dowel pins and staking-roller heads. It can be used for most roller staking operations for which there is access to both faces of the workpiece.

This work was done by Richard G. Bird and Leo A. Berson of Rockwell International Corp. for **Johnson Space Center.** *For further information, Circle 56 on the TSP Request Card.*
MSC-20281

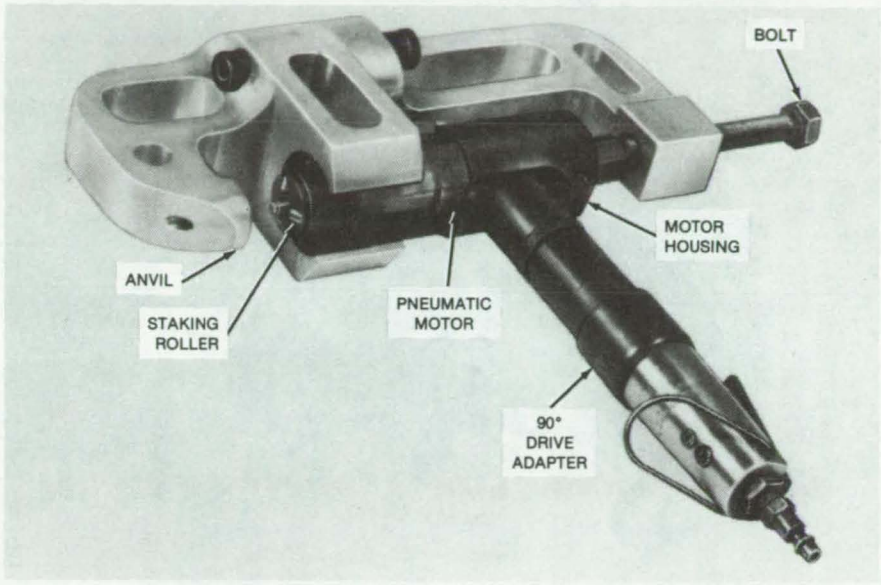

Figure 1. The **Roller Staking Tool** is constructed like a C-clamp to grip the workpiece and apply the axial staking/clamping compression.

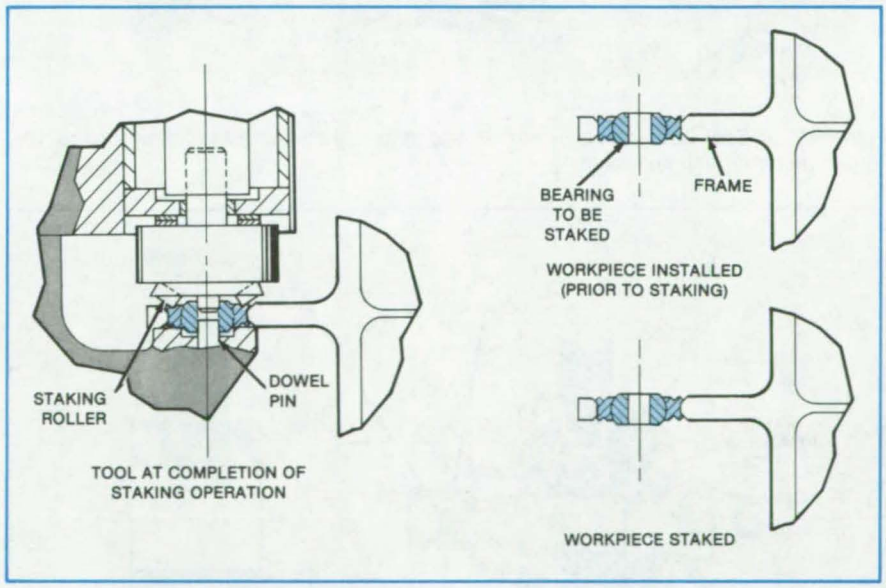

Figure 2. The **Rollers Deform the Material** at the edge of the workpiece so that the workpiece grips the frame. After staking the upper face as shown, the tool is flipped over to stake the lower face.

Tool for Replacing Bushings

The centerlines of the original bushings are maintained.

Lyndon B. Johnson Space Center, Houston, Texas

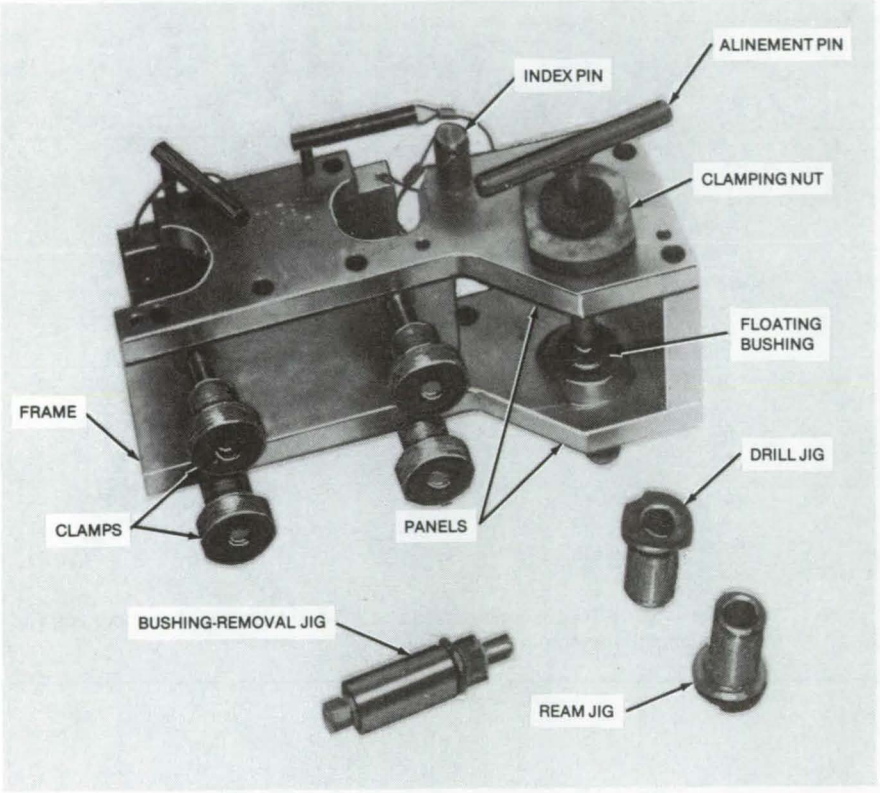

Figure 1. The **Tool Set** includes a boxlike frame fixture and accessories to maintain a centerline for drilling and reaming.

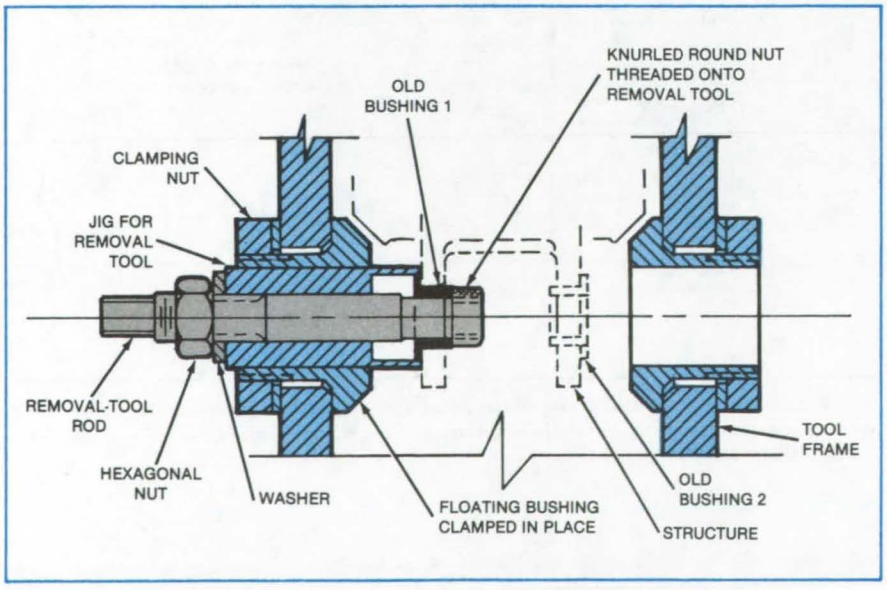

Figure 2. The **Bushing-Removal Tool,** shown in position for the removal of one of a pair of bushings, grips a bushing and pulls it free from the structure.

A tool originally developed to replace two adjacent wing bushings on the Space Shuttle could be redimensioned for bushing replacement in other applications as well. The tool set, shown in Figure 1, performs the following tasks:

- picking up the centerline of the old bushings so that the new bushings can be installed on the same axis,
- forcing out the old bushings,
- redrilling and reaming the hole left by the old bushings, and
- forcing new bushings into place.

As shown in Figure 2 the tool frame extends around the structure that holds the bushings to be removed. The floating bushings of the tool are positioned with a jig pin that slides snugly in both the old bushing and the floating tool bushings. The floating bushings are then clamped to the tool frame.

With the floating tool bushings thus fixed on the old bushing centerline, the jig pin is removed, and a bushing-removal tool is inserted in its place. The hexagonal nut is then tightened so that the knurled round nut pulls out the old bushing. The removal tool is then inserted from the opposite side to remove the other bushing.

The bushing-removal tool is replaced by a drill jig, which picks up the centerline for drilling to enlarge the hole so that it accommodates the new, larger bushings. After the hole has been drilled, and reamed, the new bushing is press-fitted in the hole. The procedure is repeated for the second bushing.

This work was done by Richard G. Bird of Rockwell International Corp. for **Johnson Space Center.** *For further information, including detailed drawings of the tool and step-by-step instructions for using the tool, Circle 57 on the TSP Request Card.*
MSC-20282

Testing Bearings in Tight Spaces

Tool turns a force around 90° to test bearings in cramped places.

Lyndon B. Johnson Space Center, Houston, Texas

A portable tool checks bushings and bearings in hard-to-reach places to ensure that they are properly staked. The tool applies a force around a right-angle bend — a capability that can make it unnecessary to disassemble equipment to gain access to the parts.

The tool is used with a hydraulic cylinder and a load-cell. Previously, the cylinder could exert only an in-line force on a bushing or a bearing. Now, however, the force can be applied at right angles to the cylinder axis.

The tool contains internal shafts, pull rods, and a load-transfer surface at 45°, all running on nearly-friction-free ball bushings (see figure). The toolhead is inserted around a bushing or a bearing so that it grips the part. The location of a pressure disk determines the direction of force on the part — inboard for a pull, outboard for a push. The force is measured by the load cell.

The tool could be used to install or remove bearings, to press-fit parts, to remove nails, and to force sheet metal into position. In the original application — checking bearings on the Space Shuttle orbiter — the tool internal shaft was designed for travel of 0.350 in. (0.889 cm). For other tasks, a hydraulic cylinder with greater travel could be used, and the other tool components could be appropriately redimensioned.

This work was done by Richard G. Bird and Leo A. Berson of Rockwell International Corp. for **Johnson Space Center.** *For further information, Circle 58 on the TSP Request Card.*

Inquiries concerning rights for the commercial use of this invention should be addressed to the Patent Counsel, Johnson Space Center [see page A5]. Refer to MSC-20250.

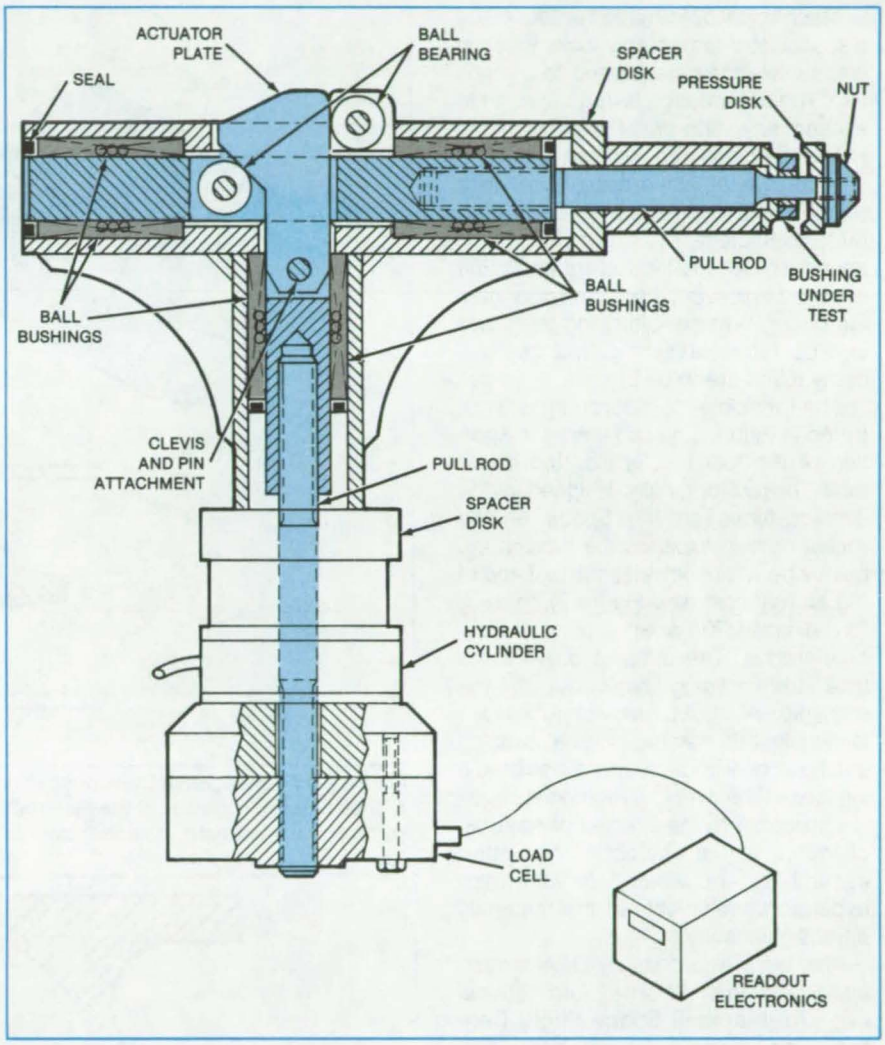

An **Actuator Plate With Surfaces at 45°** to the hydraulic-cylinder shaft turns the push or pull so that it is perpendicular to its original direction.

Holding Tubes in Place for Brazing

Simple method prevents loosening due to thermal mismatch.

Marshall Space Flight Center, Alabama

Mechanical deformation produced by a special tool temporarily locks tubes in place while they are brazed to a manifold. The deformation is large enough to exceed any differential expansion between the tubes and the manifold.

When metal tubes are brazed to a metal manifold having a different thermal coefficient of expansion, it is necessary to secure the tubes to the manifold to prevent them from disengaging during brazing. Clamping the tubes can be time consuming and costly if many tubes are to be brazed.

The principle of operation is illustrated in Figure 1, which shows the portion of the tool that is inserted in the tube. The tool, originally designed for the coolant tubes on the Space Shuttle rocket nozzle, expands the tube at the point where it penetrates the exit end of the aft manifold (see Figure 2), forming four dimples 90° apart around the circumference. The dimples prevent the tube from sliding back out of the manifold. All 1,080 coolant tubes are locked in this manner so that brazing can be done without fear of tubes breaking loose. The dimpling method is equally applicable to the brazing of heat exchangers, thrust chambers, and other assemblies in which the thermal-expansion coefficients of the materials differ significantly.

This work was done by D. Ambrisco and P. Arbino of Rockwell International Corp. for **Marshall Space Flight Center.** *For further information, Circle 59 on the TSP Request Card.*
MFS-19658

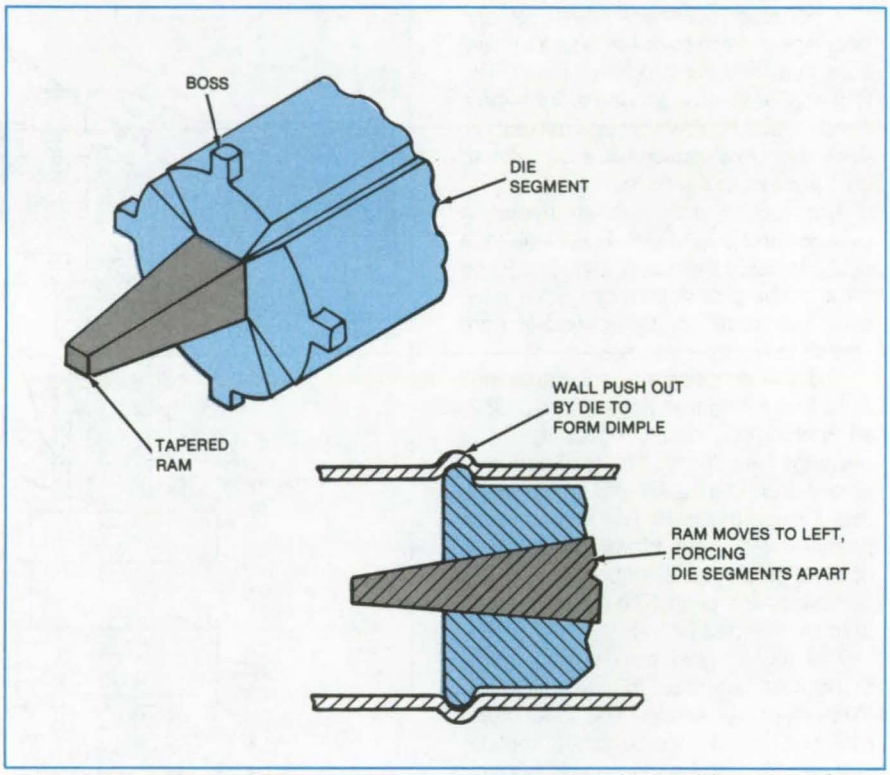

Figure 1. A **Four-Segment Die** is pushed outward against the tubing wall by a tapered ram. A boss on each segment of the die produces a dimple in the wall. The ram is driven by a commercial pneumatic cylinder powered by air at 250 psi (1.7 mN/m^2).

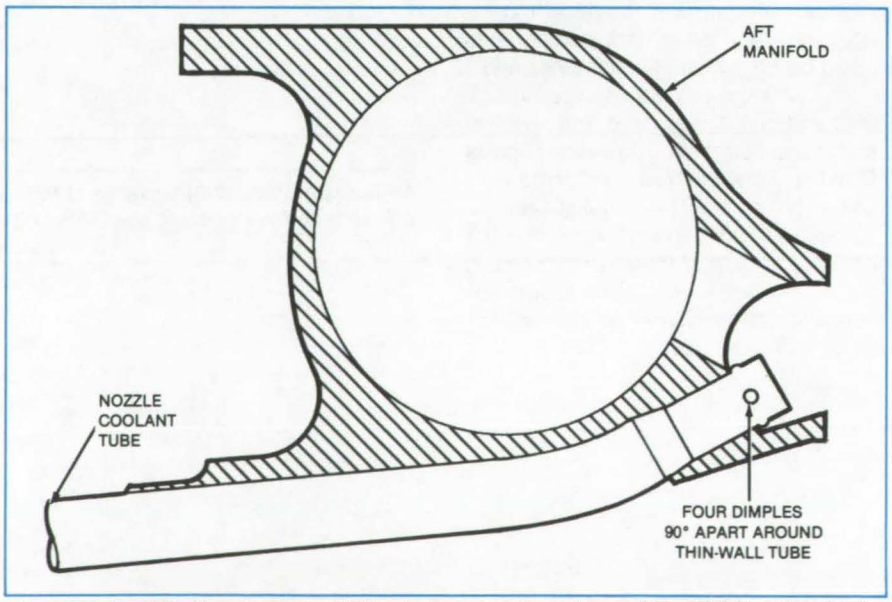

Figure 2. An **A286 Nozzle Coolant Tube Is Secured to an Inconel Manifold** by dimples in the thin wall of the tube. (A286 and Inconel are Cr/Fe/Ni alloys with different coefficients of thermal expansion.) The outside diameter of the tube is 0.224 inch (5.7 mm); thickness of the tube metal is 0.015 inch (0.38 mm).

Holder for Fragile Parts

A fixture with many springfingers holds irregularly-shaped parts.

Marshall Space Flight Center, Alabama

Designed to hold glass ampoules in a furnace, a gripping fixture has hundreds of springfingers each of which applies a minute force. The total force approximates hydrostatic pressure, resulting in a well-distributed load that maintains a firm grip without high stress concentrations.

Because the loading forces are distributed over the surface of the object and the spring contacts are flexible, the fixture is a good holder for irregularly-shaped fragile objects. Applied to industrial robot manipulators, the fixture could enhance the ability to grasp delicate parts.

The gripper consists of a set of spring rings (see figure) set in a metallic sleeve. Each of the spring rings has a number of fingers that contact the object. The rings may be punched from thin sheet stock and bent to shape. The rings may be set in grooves in the sleeve, spot-welded, or soldered in place. For high thermal conductivity, the spring rings may be made of beryllium copper or bronze. To withstand high temperatures, the springs might be made of a nickel alloys.

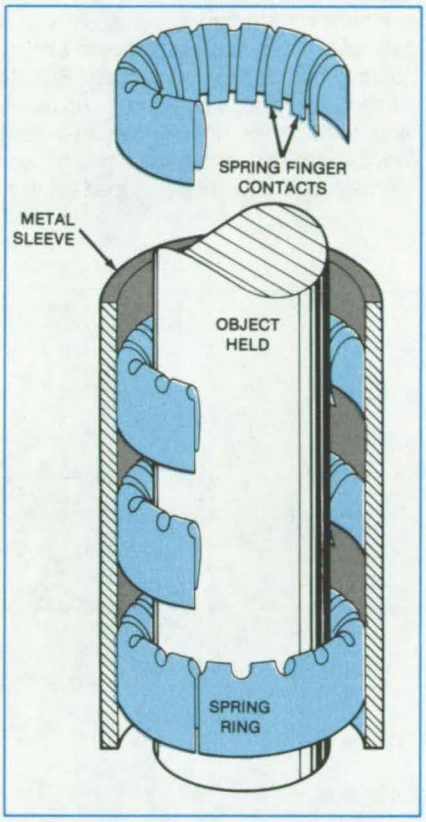

A **Spring-Ring Holder** grips irregularly shaped objects with distributed loading. Each springfinger exerts only a fraction of the total holding force, so that a fragile object will not be damaged.

The glass tube, rod, or other object to be supported is pushed into the center of the gripper where it is held axially by friction. This friction force is the sum of the friction forces of all fingers and can be increased or decreased by using a greater or lesser number of fingers.

In one experimental arrangement, a glass rod was held by 10 rings, each of which had 15 fingers. The glass rod was 12 mm in diameter and was surrounded by a metal sleeve with an inner diameter of 17 mm.

This work was done by Lawrence R. Holland of Athens State College for **Marshall Space Flight Center.** *No further documentation is available.*

Inquiries concerning rights for the commercial use of this invention should be addressed to the Patent Counsel, Marshall Space Flight Center [see page A5]. *Refer to MFS-25772.*

Computer Programs

These programs may be obtained at very reasonable cost from COSMIC, a facility sponsored by NASA to make new programs available to the public. For information on program price, size, and availability, circle the reference letter on the COSMIC Request Card in this issue.

Thermal Elastohydrodynamic Lubrication of Spur Gears

Program and analysis predict lubricant film thickness and the variations of dynamic load and temperature.

An analysis and a computer program (TELSGE) predict the variations of dynamic load and surface temperature and the lubricant film thickness along the contacting path of a pair of involute spur gears. The dynamic load is assumed to be not influenced by the lubricant film thickness or by the surface temperature and therefore is analyzed independently. The analysis of dynamic load includes the effect of gear inertia, the effect of load sharing of adjacent teeth, and the effect of variable tooth stiffnesses, which are obtained by a finite-element method.

The surface temperature at a point along the tooth profile is assumed to be

(continued on next page)

an equilibrium value when the tooth is not in contact with the mating gear. The temperature is assumed to rise suddenly to a flash temperature during the sliding contact. The distribution of the equilibrium temperature is solved by a three-dimensional finite-element heat conduction analysis, and the flash temperature is solved by a simplified energy equation using a limiting shear concept for the heat dissipation. The lubricant film thickness is based on a transient EHD analysis, which includes the squeeze-film effect. These mutually dependent quantities are solved simultaneously with an iterative process.

A series of solutions can be obtained to simulate gears of different gear ratio, diametral pitch, and subjected to wide ranges of operating conditions. The effects on the lubrication performance of lubricant viscosity, heat-transfer coefficient, speed, and load are included.

Results obtained from TELSGE for the dynamic load distributions along the contacting path for various speeds of a pair of test gears show patterns similar to that observed experimentally. Effects of damping ratio, contact ratio, rip relief, and tooth error on the dynamic load were examined. In addition, two dimensionless charts were developed for predicting the maximum equilibrium surface temperature, which can be used to estimate directly the lubricant film thickness based on well-established EHD analysis. TELSGE is written in FORTRAN IV for use on a UNIVAC computer.

This program was written by K. L. Wang and H. S. Cheng of Northwestern University for **Lewis Research Center.** *For further information, Circle P on the COSMIC Request Card.*
LEW-13528

Fabrication Technology

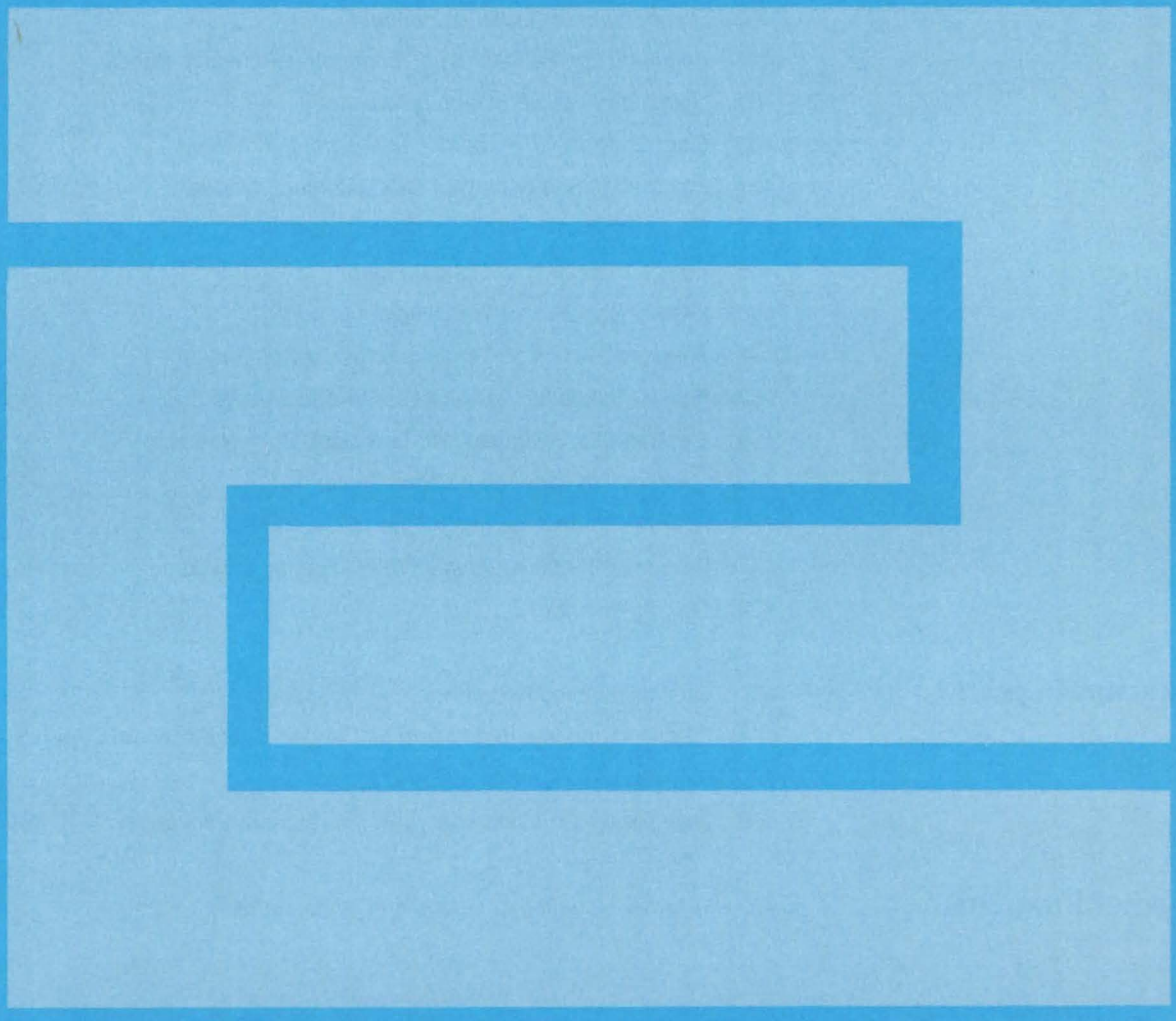

Hardware, Techniques, and Processes

Books and Reports

Computer Programs

Fabricating Slotted-Waveguide Arrays From Sheet Metal

Low-cost lightweight waveguides are formed from rolls of aluminum.

NASA's Jet Propulsion Laboratory, Pasadena, California

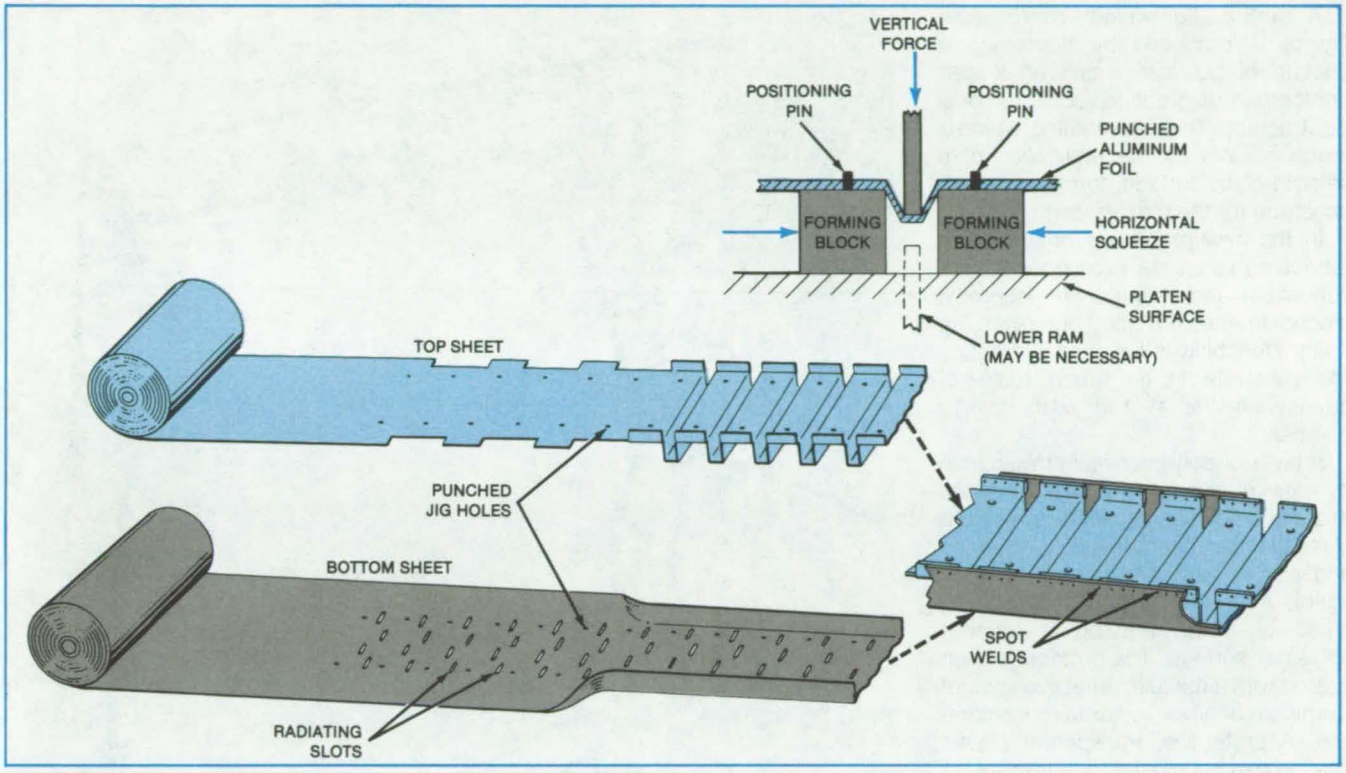

The **Slotted-Waveguide Array** is formed from sheared, punched, and bent aluminum sheets. The sheets are alined with the punched jig holes and joined by laser-beam or resistance spot welding.

In an experimental fabrication process, a microwave transmitting antenna consisting of slotted waveguides was made from aluminum sheet. When automated, the process is expected to require minimum labor and tooling. The process permits the use of thin metal to reduce raw material costs and mass. It also holds closer tolerances than are usually attained in sheet-metal work.

In the fully developed process as proposed, the slotted waveguide would be fabricated from two separate aluminum sheets or foils (see figure). These form, respectively, the corrugated top sheet and the slotted bottom sheet of the waveguide. The top sheet forms three sides of the rectangular waveguide, while the bottom sheet serves as the fourth side. Microwave energy radiates through the slots in the bottom sheet.

As the aluminum sheets are drawn from the roll, the upper sheet is sheared to form the edge serrations. The slots are pierced in the lower sheet and jig holes are punched in both sheets. Before the upper sheet is bent to form the corrugations, the sheet is first positioned on the forming blocks by engaging a set of jig holes with a set of positioning pins on the blocks (see inset). Then the vertical force is applied by a ram, and the forming blocks slide part way inward. The bending operation is completed by squeezing the forming blocks inward. If necessary, the bottom corners of the bent sheet are squared by pushing up with a ram from the underside, so as to squeeze the sheet between the upper and lower rams.

The formed upper and lower sheets are merged and alined by the jig holes. The folded edges of both sheets are spot-welded together, as shown at the right of the figure. The assembled sheets are then sheared into modular arrays of the desired length.

The prototype waveguide array was made with aluminum sheet 0.020 inch (0.5 mm) in thickness. To reduce weight and cost, sheets of 0.005-inch (0.13-mm) thickness would more likely be used, and fabrication may even be possible with thinner sheets or foils. With the lesser thickness, the broad faces of the waveguide members, both top and bottom, may need some stiffening to prevent bending. The thin, flat channels that are proposed to house the phase and amplitude references and auxiliary power lines perform this function on the slotted surface. The unslotted surfaces could be embossed to stiffen them.

The individual slotted waveguides in an array are fed from a transverse feed waveguide. The radiation energy is transferred through diagonal slots between the feed waveguide and radiating waveguides. The feed waveguide is attached to the array with pop rivets.

This work was done by William C. Brown of Raytheon Co. for **NASA's Jet Propulsion Laboratory.** *For further information, Circle 42 on the TSP Request Card.*
NPO-15664

Forming Mirrors on Composite Materials

Smooth coatings are deposited on hard-to-polish substrates.

NASA's Jet Propulsion Laboratory, Pasadena, California

A strong, lightweight mirror (see figure) is produced by depositing a coating of polyester resin on a carbon/carbon or graphite/epoxy composite structure. (The resin coating, which is made smooth by the replication of a smooth glass surface, forms a smooth substrate for the metalization.)

In the new procedure, a previously fabricated substrate is roughened with sandpaper and cleaned with isopropyl alcohol to ensure a good bond with the resin. Wettability is obtained by treating the substrate in an argon radio-frequency plasma at 100 watts for 10 minutes.

A layer of polyester resin mixed with its catalyst is applied to the substrate and covered with a piece of smooth glass that has been previously cleaned and coated with a silicone-oil release agent. After the resin has cured, the glass is lifted, leaving a smooth polyester surface. The surface is then coated with a metallic reflective layer of aluminum or silver by vacuum evaporation. A protective, transparent plastic coating can be applied for durability.

This work was done by Robert E. Gauldin and Kumar Ramohalli of Caltech for **NASA's Jet Propulsion Laboratory.** *For further information, Circle 60 on the TSP Request Card.*
NPO-15912

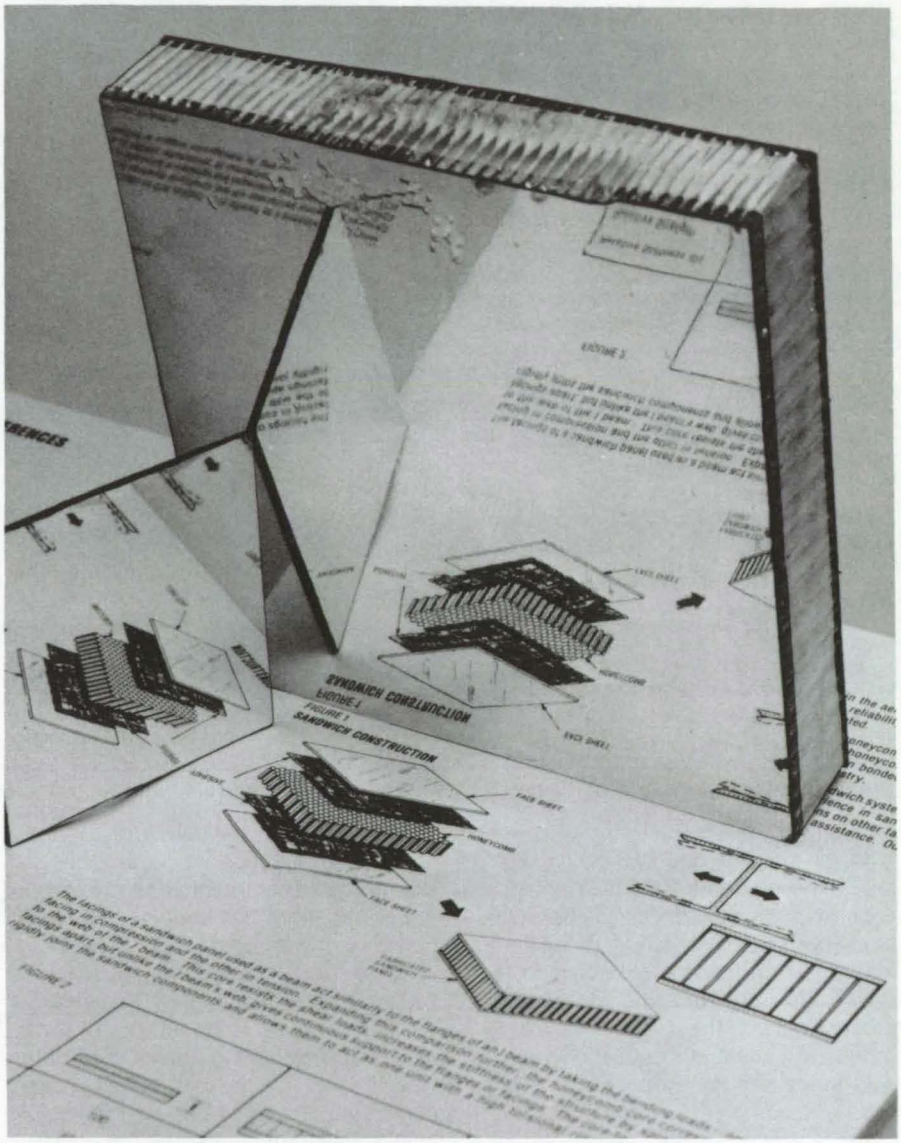

The **Lightweight Mirror,** shown leaning against a conventional glass mirror, consists of a metallic reflective layer on a substrate coated with polyester resin. The smooth surface of the polyester resin is made by covering the freshly applied resin with a piece of smooth glass that is coated with a release agent.

Better Seals for Vacuum Bags

A roller tool spreads an even layer of adhesive.

Marshall Space Flight Center, Alabama

The simple expedient of smoothing out the adhesive along the periphery of a vacuum bag improves the chances for a successfully-cured composite layup. A tool that resembles a paint roller compresses the adhesive to an even layer prior to the application of a vacuum, reducing the chance of a leak developing after the bag is evacuated. Such a tool could be purchased or put together easily out of scrap parts.

In a typical vacuum cure, the preimpregnated composite material ("prepreg") is laid up on a metal plate. A heat-resistant plastic film is placed over the layup and sealed to the plate by a layer of adhesive along the edge of the film. The bag is then evacuated, and the entire assembly is heated.

With the help of the tool shown in the figure, the adhesive is compressed to an even layer between the metal plate and the plastic film. The tool is rolled around the periphery, as shown, until the entire bead is compressed.

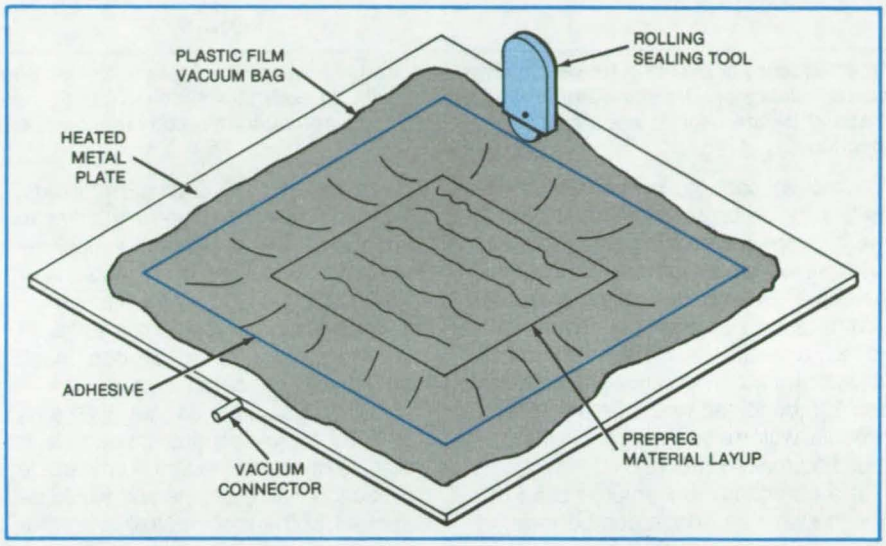

The **Tool Is Rolled and Pressed** against the plastic film to assure an even layer of adhesive around the periphery.

The tool is easily constructed from metal, plastic, or wood. A sewing-thread spool could serve as the roller, a nail as the axle, and a jigsawed block of wood as the handle.

This work was done by Benjamin Penn and Johnny M. Clemons of **Marshall Space Flight Center.** *No further documentation is available.*
MFS-25875

Absorbable-Susceptor Welding of Ceramics

The susceptor would become part of the joint.

NASA's Jet Propulsion Laboratory, Pasadena, California

A proposed technique for welding ceramic parts is based on the radio-frequency (RF) induction heating of a metal strip or other electrically conductive material (the susceptor) placed at the joint between the ceramic pieces. The susceptor, heated to a high temperature by the RF energy, melts the adjacent ceramic material. The susceptor then dissolves in the molten ceramic. When cooled, the ceramic parts form a monolithic assembly.

The absorbable-susceptor technique should be suitable for joining complex subassemblies in heat exchangers or other ceramic process equipment for high temperatures. The joints would be strong, pressure-tight, and resistant to a variety of corrosive atmospheres. They are expected to outperform pressed mechanical joints, adhesive- or cement-bonded joints, and even brazed joints (which are limited by the properties of the brazing material). Absorbable-susceptor welding would be more reliable and sometimes less expensive than diffusion welding. In comparison with fusion welding (for example, by laser, electron beam, or gas torch), absorbable-susceptor welding would be deeper and less prone to thermal-stress cracking.

The susceptor (for example, a thin film of refractory metal) is placed between the ceramic surfaces to be joined (see figure). This sandwich is inserted into an RF induction coil in a chamber in which the atmosphere can be changed readily. Initially, the atmosphere is either vacuum or an inert gas.

When the RF power is turned on, the susceptor, having a greater electrical conductivity than the ceramic, is heated preferentially until it begins to melt the adjacent ceramic surfaces. In some cases, the molten ceramic will act as a susceptor — even after the metal susceptor has completely dissolved. When

(continued on next page)

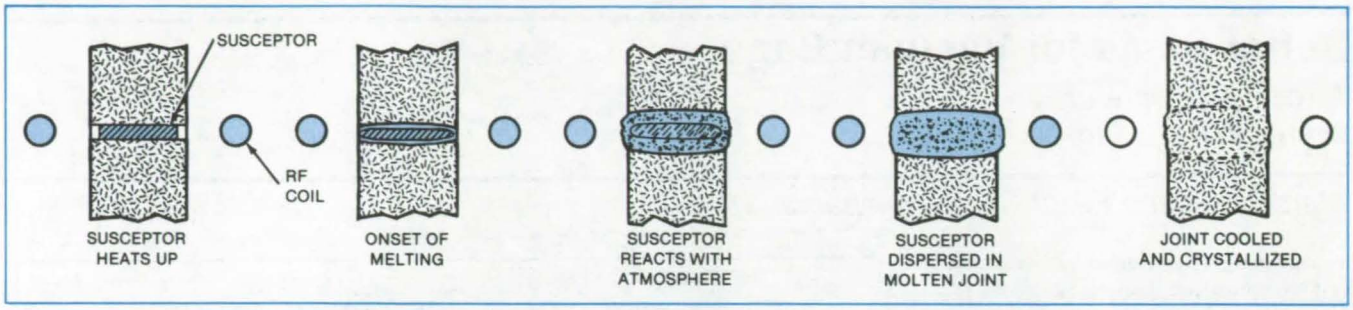

This **Sequence of Events** in RF welding with an absorbable susceptor fuses a joint between ceramic parts. The ceramic is melted by the heated susceptor. The susceptor is then reacted with an externally supplied gas to form a ceramic that dissolves in the molten joint material before cooling and solidification. Some susceptor/ceramic combinations permit direct absorption without the additional reaction.

the molten ceramic layers are sufficiently thick to ensure subsequent joining, the atmosphere is changed to one that oxidizes or otherwise reacts with the susceptor to form a ceramic material that dissolves in the molten ceramic zone. For example, a zirconium metal-foil susceptor between two pieces of zirconia to be joined would be oxidized to zirconia, which would dissolve in the surrounding molten zirconia.

If a chromium susceptor is used between alumina parts, it can be reacted with oxygen to form chromium trioxide, a compound that dissolves in alumina to form a range of stable solid solutions, all of which have melting points equal to or higher than that of pure alumina. Thus, the maximum service temperature of the assembly would not be decreased below that of the ceramic parts.

Similarly, tantalum can be used as a susceptor for joining niobium carbide. It would be converted to tantalum carbide by reaction with methane and would be dissolved in the molten NbC to form a solid solution with an even higher melting point than the NbC itself. (Most solid solutions, however, have melting points well below the melting point of the pure ceramic and would therefore entail some loss of service temperature.)

This work was done by James E. Schroeder and Paul J. Shlichta of Caltech for **NASA's Jet Propulsion Laboratory.** *For further information, Circle 61 on the TSP Request Card.*
NPO-15640

Preparing Solar Cells for Soldering

Solder paste and contact ribbon are dispensed in synchronism.

NASA's Jet Propulsion Laboratory, Pasadena, California

The robotic machine shown in Figure 1 applies dots of solder paste to solar cells and positions the contact ribbons on them. The machine operates on one cell at a time, preparing each cell for the soldering steps that follow.

The solder-paste dispenser includes two manifolds. Each consists of a hollow aluminum box in which the solder paste is injected from a single supply cylinder to six nozzles. The two sets of nozzles are seen in the underside view shown in Figure 2.

The solder dispensing and ribbon-feeding operations are overlapped. To accommodate the overlap, the front end of the manifold tapers to a sharp leading edge, forming a ramp where the manifold meets the ribbon at the edge of the vacuum chuck that holds the cell. When the dispenser is in position over a cell, the ribbon is fed up the ramp and over the top of the dispenser.

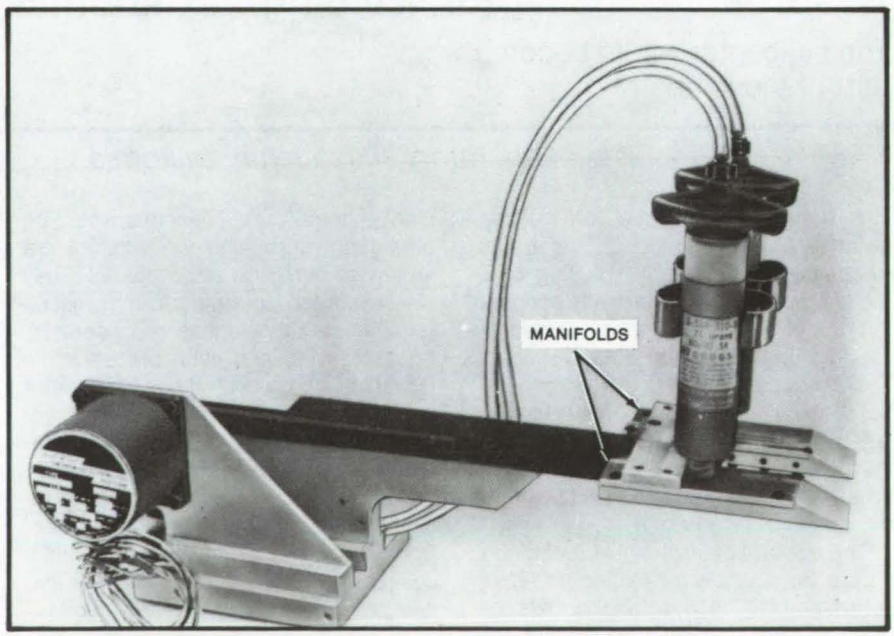

Figure 1. The **Solder-Paste Dispenser** operates on one cell at a time. Ribbon is fed up the ramps and into position while solder paste is being applied. When the ramps are moved out of the way, the ribbon lies down onto the cell.

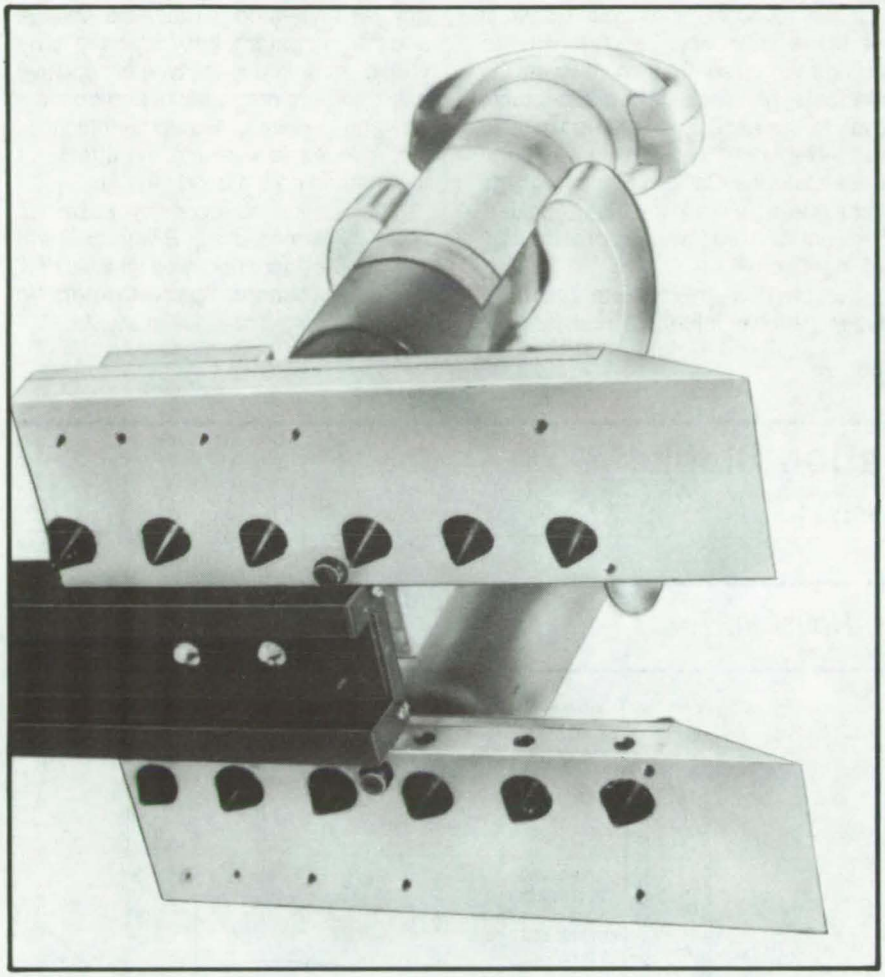

Figure 2. This **Underside View** of paste-dispensing manifolds shows 12 nozzles that apply solder to a solar cell. Contact ribbons are guided into place by the wedge-shaped ends of the manifolds.

A groove in the ramp and top of the dispenser guides the ribbon. When the dispenser retracts, the ribbon simply lies down onto the cell.

[For a related article on preparing solar cells for soldering, see "System To Prepare Solar Cells for Assembly" (NPO-15489), *NASA Tech Briefs*, Vol. 6, No. 4 (Spring/Summer 1982), page 459.]

This work was done by John J. Hagerty of MB Associates for **NASA's Jet Propulsion Laboratory.** *For further information, Circle 62 on the TSP Request Card.*
NPO-15626

Reducing the Resistance of Conductive-Adhesive Bonds

Current pulses lower the resistance of silver-filled epoxies.

Lyndon B. Johnson Space Center, Houston, Texas

Capacitive discharge reduces the interfacial resistance between aluminum surfaces joined with silver-filled epoxy. The technique offers a noninvasive solution to the problem of attaching grounding brackets to aluminum honeycomb structures.

Metal parts that are to be joined both mechanically and electrically are sometimes bonded together with silver-filled epoxy. However, when very good electrical contact is necessary (resistances less than about 10 mΩ), available epoxies may not have sufficiently low con-

(continued on next page)

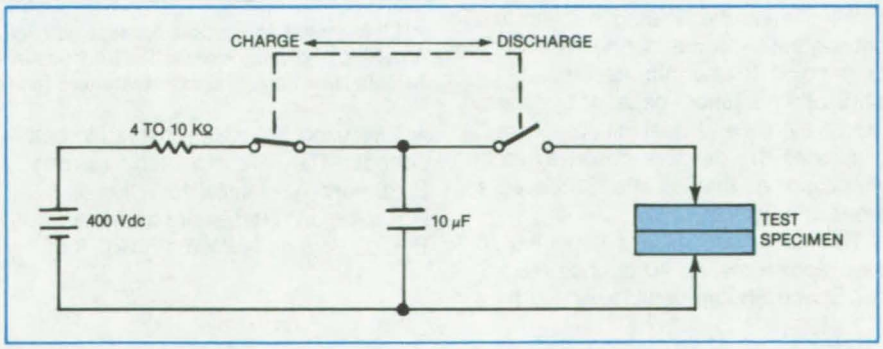

This **Capacitive-Discharge Circuit** was used to apply high current pulses to epoxy bonds of area approximately 0.5 in.^{2} (3 cm^2). The test specimen was similar to the aluminum grounding strap that was used on the Space Shuttle to ground fluorescent light brackets to the air-lock interior.

ductivity. Moreover, in some applications, substitute methods, such as welding or riveting, may be ruled out by constraints on weight, strength, or surface finish.

The new technique has been tested for possible use on the Space Shuttle orbiter for grounding fluorescent light brackets to the air-lock interior. The maximum tolerable resistance for this application is 10 mΩ, but "as-applied" epoxy had measured resistances greater than this limit.

It was found that the circuit shown in the figure could apply a current pulse through the epoxy that would lower the interfacial resistance to an acceptable level. In this application the epoxy used was Ablebond 463-1 (Ablestik Laboratories, Gardena, California), although the technique may work for other epoxies. The bond area was approximately 0.5 in.^{2} (3 cm^2).

The physical mechanism that produces the lower interfacial resistance is not yet understood. Thus, the voltage and current parameters may have to be varied according to the type of adhesive used, surface preparation, and conductor configuration. Experimentation is also needed to evaluate the effects of the method on the bond strength.

This work was done by Lester J. Guertin, Kennard L. Billington, and Vernie R. Ward of Rockwell International Corp. for **Johnson Space Center.** *No further documentation is available.*
MSC-20427

Light, Serviceable Insulation Blanket

New features are a lighter facing and easy-to-use fastening system.

Lyndon B. Johnson Space Center, Houston, Texas

An improved thermal-insulation blanket is lighter in weight, easier to remove and install, and less susceptible to crushing than was a previous design. The blanket should prove useful in vehicle construction and other applications in which low weight, easy removability for repairs, and long service life are important.

The new blanket facing (see figure) is made from an aluminized polyester (Kapton* or equivalent) that has an organic antioxidant coating and is reinforced by nylon (Nomex* or equivalent). Unlike the facing used in the earlier version [textured stainless-steel foil 0.002 in. (0.05 mm) thick], the new facing springs back after crushing. This increased resistance to crushing assures longer service life.

Whereas a capstan-and-lockwire system was previously used to hold the blanket in place, the improved blanket is held by grommets and hook-and-loop fasteners. This reduces servicing time by eliminating the time spent tying and untying the lockwires during installation or removal. It also increases safety by eliminating injuries caused by sharp lockwire ends and steel-foil corners and eliminates the dangers posed by lockwire clippings that fall into inaccessible areas in a vehicle.

The new blankets are expected to save approximately 40 pounds (18 kg) per Space Shuttle vehicle, where they will be used to insulate hydraulic components. They are expected to save up to 30 percent of installation time.

[* Kapton and Nomex are trademarks of E. I. du Pont de Nemours & Co., Inc.]

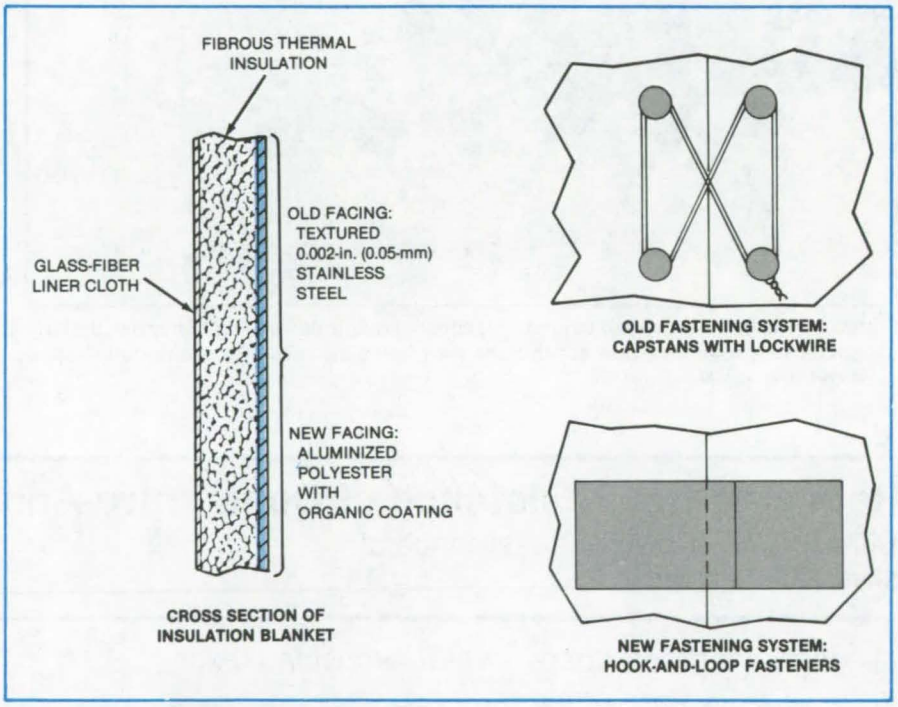

A **Lightweight Insulation Blanket** with aluminized, reinforced polyester facing resists crushing and weighs less than previous insulation blankets with textured stainless-steel facing. New hook-and-loop fasteners facilitate installation and removal.

This work was done by Alan J. Swirsley of Rockwell International Corp. for **Johnson Space Center.** *No further documentation is available.*
MSC-20452

Electrodeposition Repair of Damaged Metal Parts

Damaged material is replaced by electrodeposited copper.

Lyndon B. Johnson Space Center, Houston, Texas

Damaged combustion-chamber coolant channels are repaired by a process that includes the electrodepositon of new metal in areas that are cracked or gouged. A similar technique could be used to repair other metal parts, provided that the metal to be electrodeposited has physical properties nearly identical to those of the original material.

The restoration process requires several machining and plating operations (see figure). First, the damaged material is removed by machining, sanding, or grinding. Then a molten wax is poured to fill all exposed channels and to act as a plating surface. Silver powder is burnished into the wax for electrical conductivity.

A dam or a small plating tank is constructed around the area to be plated. The electrolyte is added and copper is deposited from an anode at about 0.001 inch (0.025 mm) per hour, with the part to be plated serving as the cathode.

Part of the deposited copper is machined away, but only just deep enough to expose the underlying channels. Copper deposited in the channels is then machined away, so that the channels are reformed, with reconstructed lands between the channels consisting of deposited copper.

The channels are again filled with wax, up to a surface flush with the tops of the reconstructed lands. Copper is deposited on this surface in the same manner as before, thus reforming the outer wall that enclosed the channels. In a final machining operation, the deposited outer-wall material is machined to the original surface contour.

This work was done by Mark Kaufman and Jacob Rietdyk of Rockwell International Corp. for **Johnson Space Center.** *No further documentation is available.*

Inquiries concerning rights for the commercial use of this invention should be addressed to the Patent Counsel, Johnson Space Center [see page A5]. *Refer to MFS-19783.*

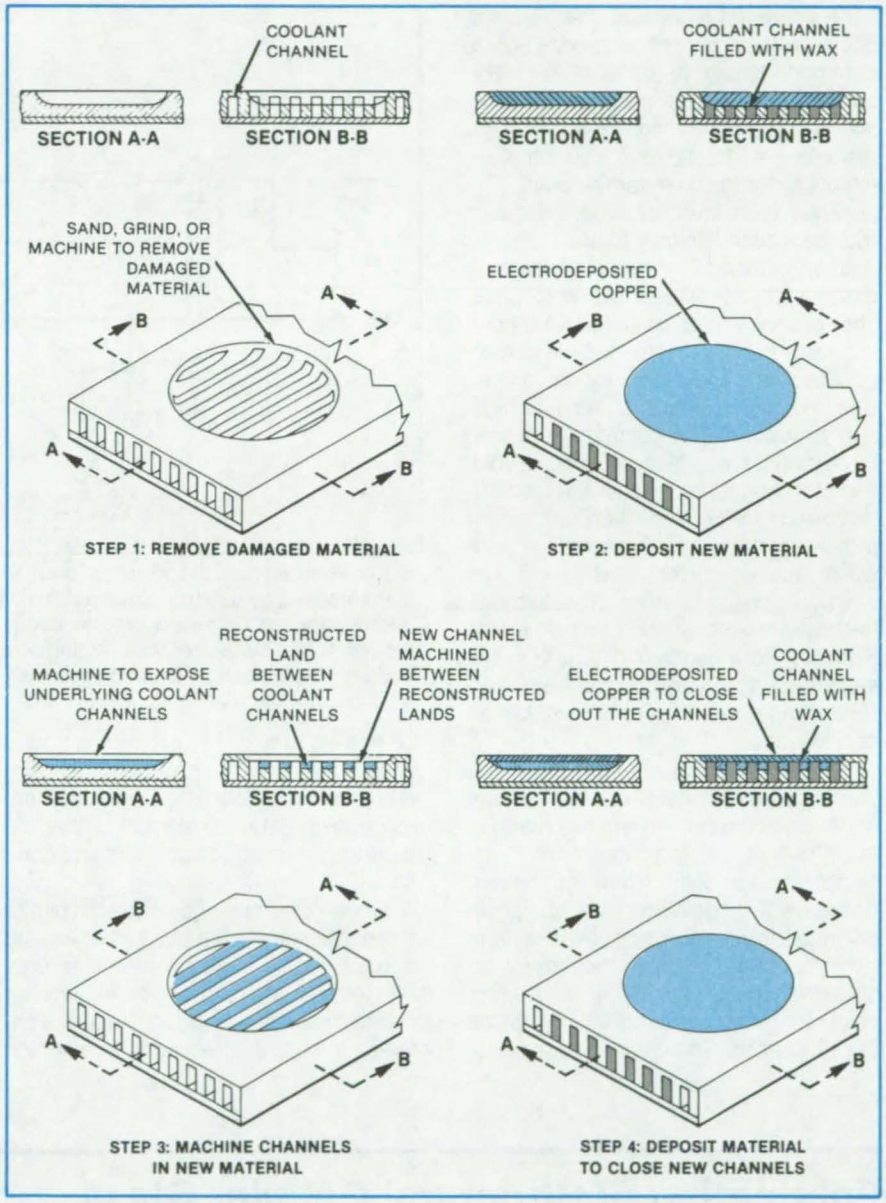

Channel Restoration consists of alternately machining damaged material and reconstructing the material by electrodeposition. Solid wax is processed into the coolant channels to provide plating surfaces that match the original channel surfaces.

Electrolytic Sharpening of Diode-Contact Whiskers

Phosphor bronze wire is pointed without highly-toxic chemical reagents.

NASA's Jet Propulsion Laboratory, Pasadena, California

An improved technique sharpens the point on tiny phosphor bronze wires commonly used to contact Schottky-barrier diodes. The process not only allows control of the cone angle and the diameter of the tip but also employs relatively-nontoxic sulfamic acid. The previous technique involved chromium trioxide, which is highly toxic.

In preparation for the sharpening process, a stress-relieved grade C phosphor bronze wire is mounted on a holding post, thoroughly cleaned with an organic solvent, and blown dry with a dust-free and oil-free gas, such as ultra-high-purity nitrogen. The point is sharpened by dipping the end of the wire into a solution of 4 weight percent sulfamic acid in deionized water and then anodically dissolving the wire by passing a half-wave rectified current (see figure). The whisker wire is immersed by a micrometer with a nonrotating spindle (typically, to a depth of 125 μm) in the sulfamic acid and, the cell current/voltage trace is observed on an oscilloscope.

For a 12-μm-diameter whisker, the starting current should be in the range of 5 mA. Once the cell current has reached the 1-mA range, the whisker/post assembly is removed from the holder, rinsed well in deionized water, blown dry, and the whisker point observed with a microscope. The lower the magnitude of the minimum current just before process termination, the more blunt will be the whisker tip. The desired tip may not be formed at first: The process is begun once again; and the processing parameters (current, dissolution time, and immersion depth) are systematically varied to attain the desired tip radius and cone angle.

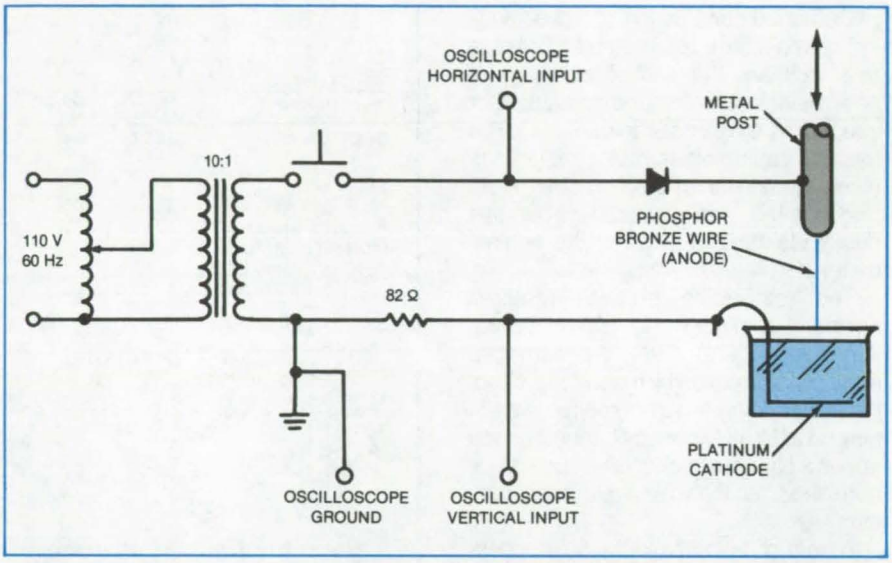

In this **Pointing Cell,** the phosphor bronze wire to be pointed is affixed to a metal post that is in turn held by a fixture, such as a pin vise. This fixture is moved axially by means of a micrometer that allows a precise control of the position of the end of the wire with respect to the surface of the pointing solution. The solution consists of 4 weight percent sulfamic acid crystals in deionized water. The dissolution current is adjusted via the autotransformer setting.

Since the specific current/voltage trace that signals the point at which the current should be terminated is a function of the sharpness of the whisker point, there is strong correlation between the trace observed at termination and the bluntness of the resulting whisker point. The resulting shape of the whisker tip is also dependent on the relative humidity of the pointing-cell ambience. Quite consistent results have been achieved by controlling this relative humidity.

This work was done by Gordon Green and Robert J. Mattauch of the University of Virginia for **NASA's Jet Propulsion Laboratory.** *For further information, Circle 63 on the TSP Request Card.*
NPO-15789

Fabrication of Structural Cellular Glass

A surface layer is quickly heated and compressed.

NASA's Jet Propulsion Laboratory, Pasadena, California

In a manufacturing process for cellular (foamed) glass, a densified skin is formed by heating, then compressing a surface layer. The skin imparts additional strength against bending. The new glass is intended for use in the manufacture of large, low-cost, parabolic-dish solar collectors.

A postcellulation approach (see figure) is employed to obtain the dense surface skin while retaining a low-density glass core. After the cellulation stage, the material is cooled to 1,150° F (621° C). The surface is then rapidly heated with gas burners to reduce the viscosity of the outer layer to a value significantly lower than that of the core. The material is then passed through a

pair of pinch rollers: The lower-viscosity surface layer is compressed more than the rest of the material, so that the material emerges from the rollers with a densified skin.

Panels were made of 0.040-in. (1-mm) and 0.060-in. (1.5-mm) mirror glass bonded to cellular glass with densified skin. These were tested for strength and stiffness and found to meet the design requirements for a 50-lb (22.7-kg) paraboloid. A contoured small-scale monolithic gore having a low-density core and a dense skin was thermally sag-formed.

The gas burners are spaced 3 in. (76 mm) apart, with the nearest burner being 6 in. (152 mm) from the center of the pinch rollers. The rollers are positioned at a 2-in. (51-mm) separation for processing a panel nominally 3 in. (76 mm) thick. The resulting panel thickness is approximately 2¼ in. (57 mm), there being some rebound after pinching. Although a displacement-controlled pinching technique was used, a force-controlled system might be capable of more-consistent skin formation.

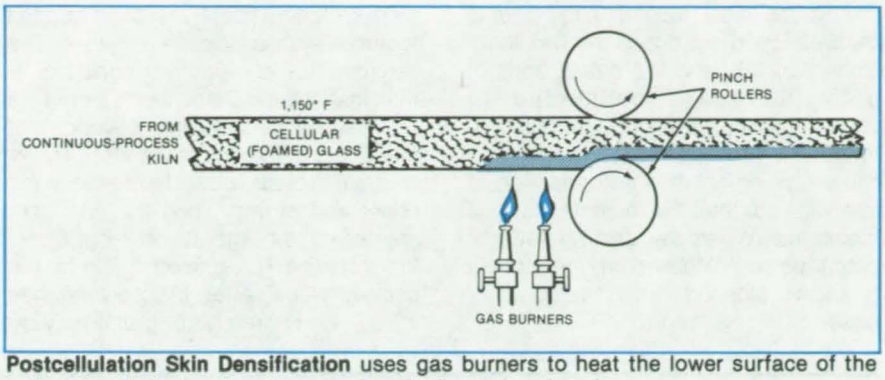

Postcellulation Skin Densification uses gas burners to heat the lower surface of the material and pinch rollers to compress the heated-surface layer.

This work was done by William D. Mitchell and Donald J. Maxwell of Solaramics, Inc., for **NASA's Jet Propulsion Laboratory.** *For further information, Circle 64 on the TSP Request Card.*
NPO-15731

Polymer Bonding of Optical Fibers

Optical waveguides are coupled through their sides.

NASA's Jet Propulsion Laboratory, Pasadena, California

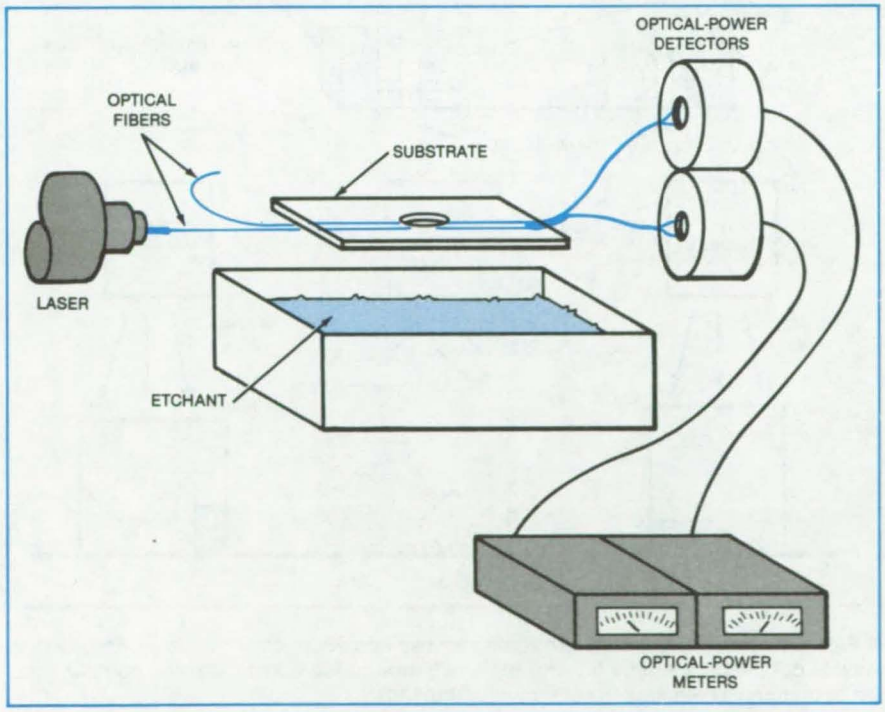

In **the Fiber Etching Process,** the bonded length for coupling is determined by observing optical output powers in the two fibers. Surface tension of the etchant remaining between the two fibers holds them in contact when they are raised from the solution for power measurements. When the fibers are reimmersed, they separate, thus allowing free access by the etchant.

In a new optical-waveguide coupling technique, two glass fibers are bonded along their sides with a polymer, rather than coupled at their ends. The method employs no critical optical alinement procedures and eliminates the need for precisely cutting fibers or controlling the high fusion temperature required to weld the fibers together.

In the new technique, individual waveguides are bonded together after much of the core cladding is removed along a selected length of both fibers. Coupling occurs where the fibers make contact in the selected region. By varying the length of the coupled region, the amount of coupling is controlled.

The fibers are mounted side by side on a substrate that is resistant to a dilute hydrofluoric- acid etching solution. Both wax-coated glass and bare polymethylmethacrylate can be used as the substrate. The initial rapid etching process is monitored by observing the Fraunhofer diffraction pattern generated by a test fiber placed in a laser beam. When the fiber diameter reaches about 15 μm, the etching process is stopped.

(continued on next page)

After the initial rapid etch, the laser is then launched into one of the two fibers to be coupled, and the output ends of both fibers are connected to photodetectors (see figure). In this configuration, the fibers are dipped in a dilute etching solution and removed at intervals so that the outputs can be monitored. When the desired ratio of output powers is observed, the etching process is stopped with a distilled-water rinse.

The etched fibers are then bonded together with a silicone polymer. The polymer has a refractive index higher than that of the etchant, thus it increases the degree of coupling beyond that measured at the end of the etch. Therefore, a thin blade is inserted between the fibers and moved along the fiber pair shortening the interaction length until the coupling is reduced back to the desired value. After the polymer has cured, the entire coupling unit may be encapsulated to protect it against vibration.

This work was done by Willis Goss and Mark D. Nelson of Caltech for **NASA's Jet Propulsion Laboratory.** *For further information, Circle 65 on the TSP Request Card.*

Inquiries concerning rights for the commercial use of this invention should be addressed to the Patent Counsel, NASA Resident Office-JPL [see page A5]. Refer to NPO-15464.

X-Ray Inspection of Transistors

A component holder speeds examination of matched pairs.

NASA's Jet Propulsion Laboratory, Pasadena, California

A simple but effective technique speeds and helps to assure the regularity of X-ray inspection of matched pairs of potted transistors. The only extra equipment required is small blocks of plastic and a roll of adhesive tape.

Multiple-channel imaging systems require large numbers of electronic components in pairs having matched characteristics. For reliability, the connections within each component must be inspected by X-ray photography.

Each component must be photographed in two perpendicular planes. When unmounted components are photographed, it is difficult to provide a precise 90° turn for the second view. When several pairs are placed on the same film, unmatched components often become paired by mistake. Since the components are delivered in lots of about 500 pairs and must be ready for assembly on circuit boards the next day, radiographic inspection can be a bottleneck.

The new procedure is faster, assures proper orientation, and reduces confusion. The components within each pair are affixed to opposite sides of a small polymethylmethacrylate block (see figure) by fastening their leads to a common face with thin plastic adhesive tape. The components are placed near a corner in contact with the film. A single flip of the block around the corner adjacent to the components positions the components for the second view.

Since a pair is attached to the same block, its members travel together; it is impossible for them to get mixed up with members of other pairs. The procedure allows inspection of up to 50 pairs — two views of each pair — on a single X-ray film, in the same time previously required for 1 unmounted pair. One thousand pairs can be inspected readily within 24 hours.

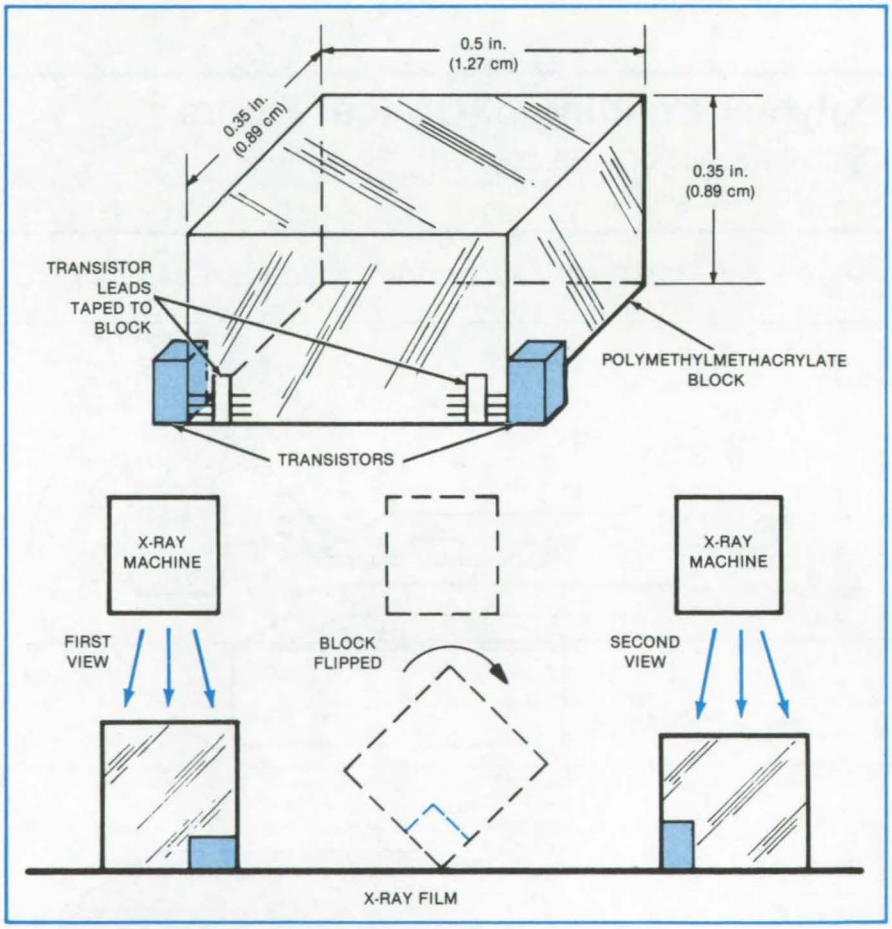

A Pair of Matched Transistors is oriented for two perpendicular X-ray views. The second view is obtained by simply flipping the block around the corner near the components, while that corner remains in contact with the film.

This work was done by William P. Hubbard of Caltech for **NASA's Jet Propulsion Laboratory.** *For further information, Circle 66 on the TSP Request Card.*

NPO-15675

Pressure-Reduction Technique for Crystal Growth

Large crystals could be grown by varying the pressure rather than the temperature.

NASA's Jet Propulsion Laboratory, Pasadena, California

A new method for growing crystals from hydrothermal solutions may permit the rapid growth of large, regular crystals with little or no undesirable convection. In contrast with earlier techniques, the new method would promote crystal growth from a solution by varying the pressure rather than the temperature.

The proposed method is based on the fact that, in the near-critical and supercritical regions of most solutions, the solubility of the solute increases significantly with pressure (see figure). Therefore, the supersaturation of a solution can be increased by lowering the pressure, thus promoting crystal growth at constant temperature.

Unlike conventional hydrothermal crystal growth, which requires rapid circulation of the solution, the pressure-reduction method permits crystals to be grown with as much or as little convection as is desired. This degree of freedom may facilitate the minimization of such crystal defects as fluid inclusions.

It is also easier to program pressure rather than temperature. Whereas temperature changes take hours to equilibrate throughout a large volume of solution, pressure changes propagate at sonic speeds, thus permitting many control feedback loops per second. Therefore, pressure-down programing of a constant-temperature of adiabatic pressure vessel can be done with greater precision and homogeneity than temperature programing.

In addition to being a potentially practical method of growing large crystals, the new technique can also be used to study crystal growth kinetics by a "pressure wave" analog of conventional "thermal wave" experiments. Here also, the new technique would have the advantages of faster response and freedom from convective interference.

This work was done by Paul J. Shlichta of Caltech for **NASA's Jet Propulsion Laboratory.** *For further information, Circle 67 on the TSP Request Card.*

NPO-15772

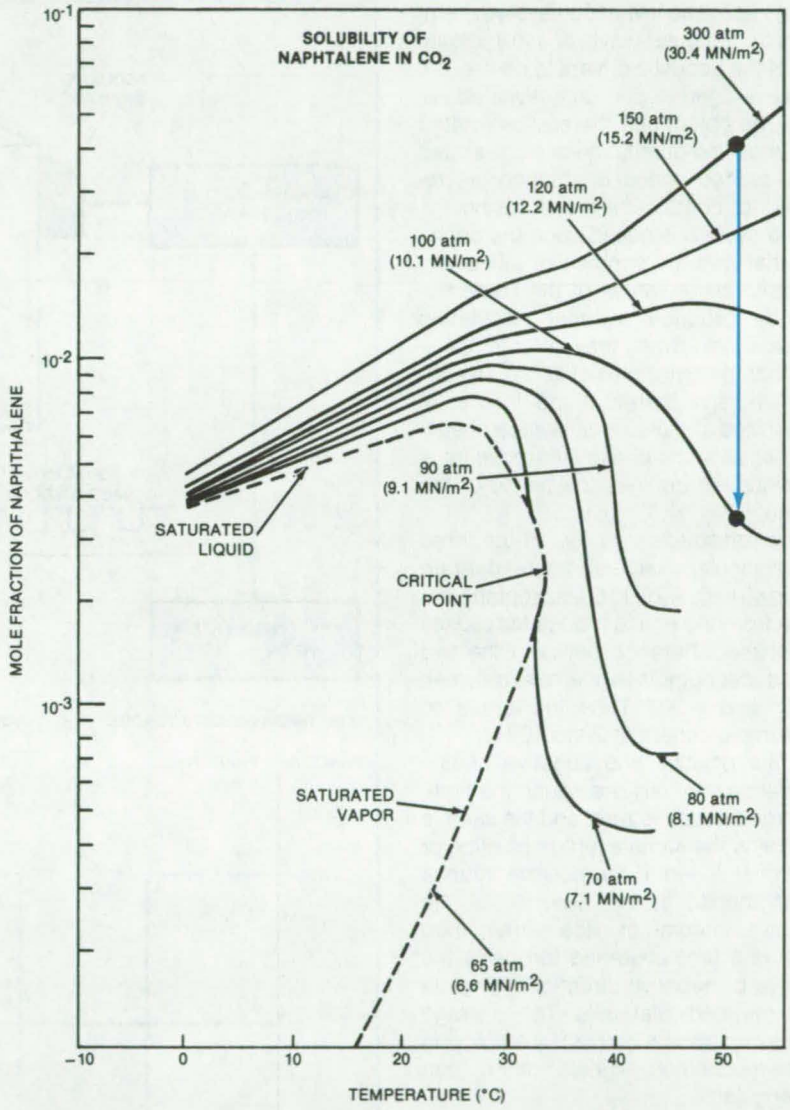

The Supersaturation of a Solution can be increased by lowering either pressure or temperature. Whereas a temperature change takes a considerable time to diffuse through solution, a pressure change propagates at the speed of sound. In the constant-temperature pressure-reduction process illustrated by the vertical arrow, crystal growth would be promoted as the solubility decreases by a factor of more than 10.

Phase Modulation Varies Average Acoustic Torque

Rotation of acoustically levitated objects can be controlled.

NASA's Jet Propulsion Laboratory, Pasadena, California

An acoustic-levitation system employs rectangular-wave phase modulation of the acoustic drivers to control the time-averaged torque on a levitated object. The object can thereby be rotated to a specified orientation or accelerated to a desired speed of rotation, as required for containerless processing.

The system is based upon the principle that two perpendicular sinusoidal acoustic plane waves of the same frequency produce a local circulating acoustic field (when they differ in phase by other than multiples of 180°). The circulation, and therefore the torque, is maximized at a phase difference of 90°. The sense of the phase difference (plus or minus) determines the sense of the torque.

The transducers for two of the three perpendicular axes (see figure) operate at 1 to 40 kHz. A 20- to 50-Hz rectangular wave from the phase modulator causes the phase difference between the two transducer outputs to alternate between +90° and −90°: Thus, the torque on the sample dithers at 20 to 50 Hz.

If the positive and negative phase-difference intervals are equal, the time-averaged torque is zero, and the sample maintains the same average position or rotational speed. If the positive interval is lengthened at the expense of the negative interval or vice versa, then there is a time-averaged torque in the positive or negative direction along the third perpendicular axis. The average torque can also be derived by employing phase-modulation signals other than rectangular.

This work was done by Daniel D. Elleman, Arvid P. Croonquist, and Taylor G. Wang of Caltech for **NASA's Jet Propulsion Laboratory.** *For further information, Circle 68 on the TSP Request Card.*

NPO-15689

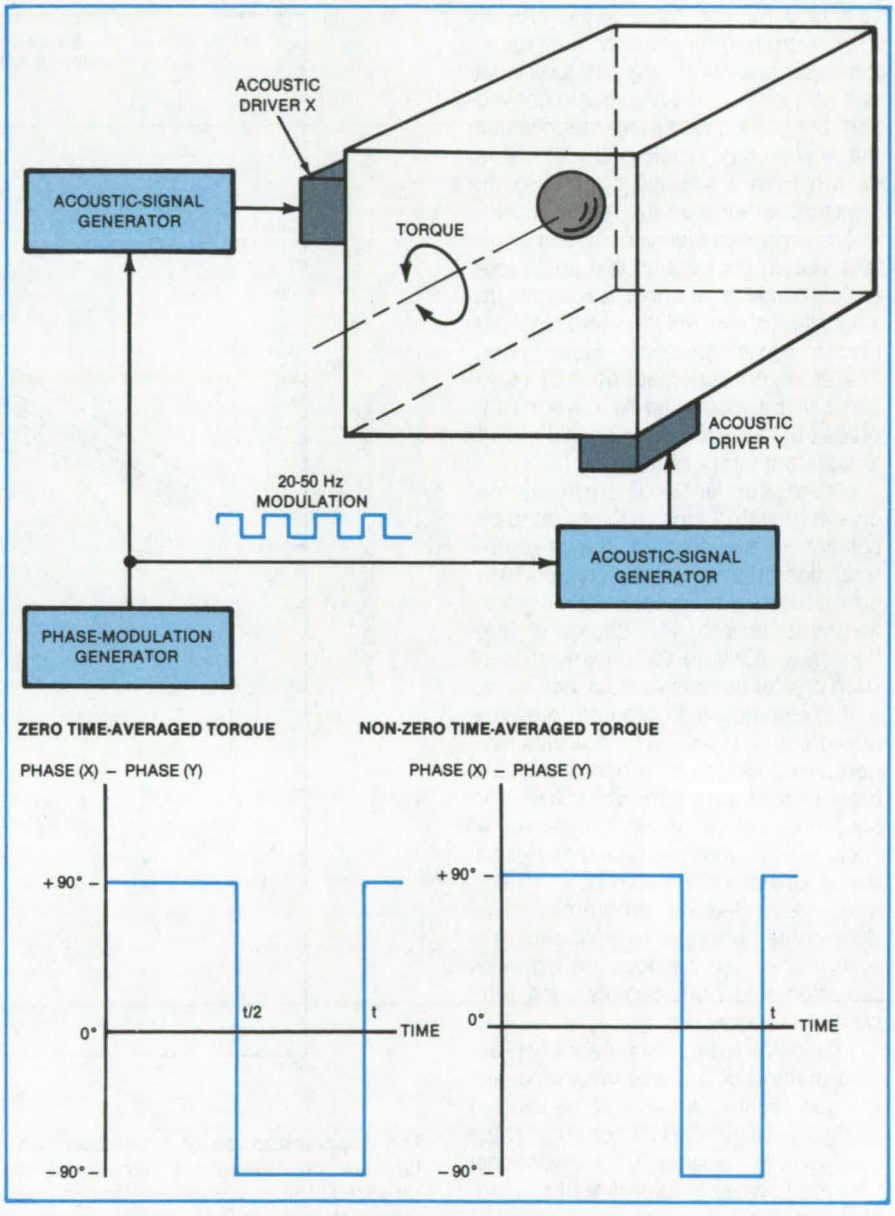

The **Phase Difference Between Two Perpendicular Acoustic Drivers** is modulated to dither the acoustic torque on an acoustically levitated object: The phase difference is alternated between +90° and −90°. If the system is at the positive phase difference during a greater portion of the modulation cycle than it is at the negative phase difference (or vice versa), then there is a nonzero time-averaged acoustic torque.

Electrostatic Levitator With Feedback Control

Sample position is automatically maintained.

NASA's Jet Propulsion Laboratory, Pasadena, California

An electrostatic levitation system includes a closed feedback loop to hold the levitated object at the desired position. The vertical position of the object is sensed and compared with the preset value. When a position error is detected, the amplitude of the levitating field is increased or decreased to restore a zero error.

The levitating electrostatic field is produced by applying high voltages (0 to 20 kV) to the electrodes. The curved electrode shape (see Figure 1) causes the electrostatic force field at every position in the levitation volume to point slightly toward the vertical symmetry axis. As a result, the levitation force everywhere has a horizontal component that pushes the object toward the axis, and no active horizontal position stabilization is needed.

The position of the object is monitored by a camera with a charge-coupled device (CCD) in the image plane (see Figure 2). The CCD output is a raster scan that is fed to a computer through an interface. Within each frame, the computer determines the vertical position by counting the number of scanning lines from the top of the frame to the line containing the brightness modulation of the top edge of the object. A similar count is taken for the bottom edge.

When the brightness-modulation edges lie at unequal numbers of scanning lines above or below the set position, the computer puts out a digital signal that represents the position error modified to include the velocity-damping correction necessary for stability. The modified error signal is fed to a digital-to-analog converter. The converter output is fed to the input terminal of the high-voltage controller, thus causing the voltage across the electrodes to change in response to the position error.

The system offers a number of options that lend themselves well to containerless processing. Many positioning and manipulating algorithms can be performed by the computer, both for dynamic movement and for static positioning: By varying the "set-to" position in the computer, the high-voltage source can be made to vary its output accordingly. Noncircular electrodes can be used to provide stable levitation at different work stations, with sample transportation between stations effected by traveling electrostatic waves or other force fields.

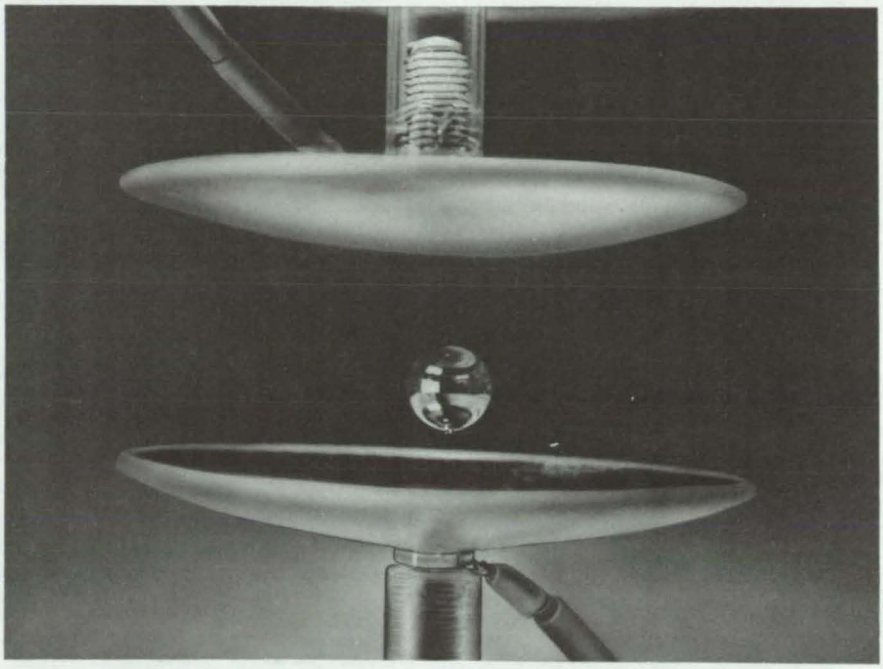

Figure 1. An **Object is Levitated** by the electrostatic field between two electrodes. Because of the particular curved electrode shape, the levitation field has a stable horizontal position on the vertical axis of symmetry.

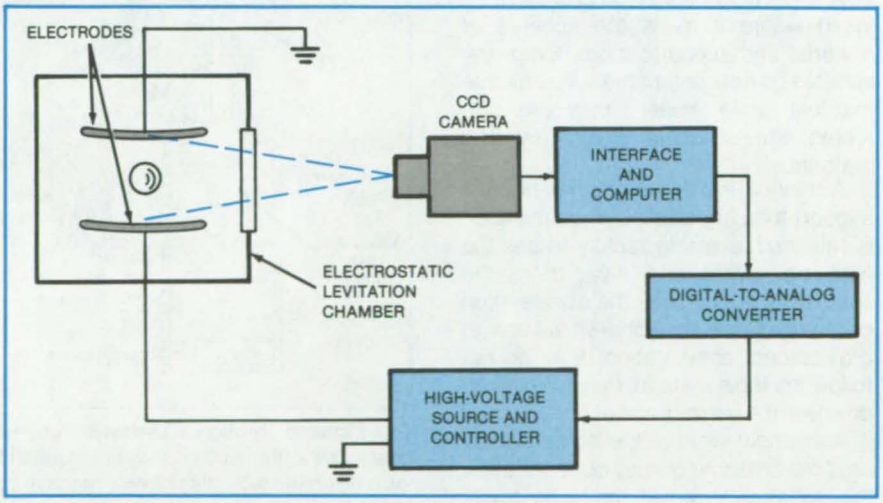

Figure 2. The **Feedback-Control System** maintains the vertical position of the levitated object. The CCD camera senses the position, and the computer generates a position-error signal that controls the high-voltage source. The high voltage between the electrodes is varied to restore the object to the desired position.

This work was done by Won Kyu Rhim, Melvin M. Saffren, and Daniel D. Elleman of Caltech for **NASA's Jet Propulsion Laboratory.** *For further information, Circle 69 on the TSP Request Card.*

NPO-15553

Gas-Bearing Crucible for Shot Tower

Device protects molten drops from contamination and distortion.

NASA's Jet Propulsion Laboratory, Pasadena, California

A perforated crucible supports molten drops on a cushion of air, allowing them to assume nearly spherical shape. The crucible introduces the drops into an evacuated tower where they harden as they fall. Since the drops fall through vacuum, they are not distorted by air resistance and therefore they retain their shape as they harden. The crucible/tower combination can be used to fabricate targets for thermonuclear power experiments and spherical cavities for lasers.

The crucible chamber consists of a cylindrical quartz heater with an inlet port and an endoscope viewing port (see figure). The cylinder is enclosed in an insulating blanket. The bottom of the chamber connects to a vacuum pump that maintains the chamber at near vacuum. The crucible at the end of the levitator lies at the center of the chamber. The material to be processed is dropped onto the crucible through the feed port.

Gas flowing through the levitator tube is heated by a filament. The hot gas emerges from holes in the crucible (see inset) where it melts the spheres of material and supports them. Since the spheres do not contact the solid crucible material while molten, they are protected against contamination by that material.

A solenoid latch holds the gas-bearing support tube in position. When the latch is released, a spring rapidly forces the tube downward and away from the spheres at about twice the acceleration of gravity. Since the spheres fall only at gravitational acceleration, they do not follow the tube: Instead, they fall directly downward toward the shot tower.

A solenoid valve at the bottom of the crucible chamber quickly opens to allow the spheres to enter the drop tower below, then closes. The spheres continue down the shot tower into a foam bath that is created by blowing gas bubbles through an oil. By the time the spheres reach the foam, they have been cooled sufficiently by radiation to retain their shape. The bath cushions their landing.

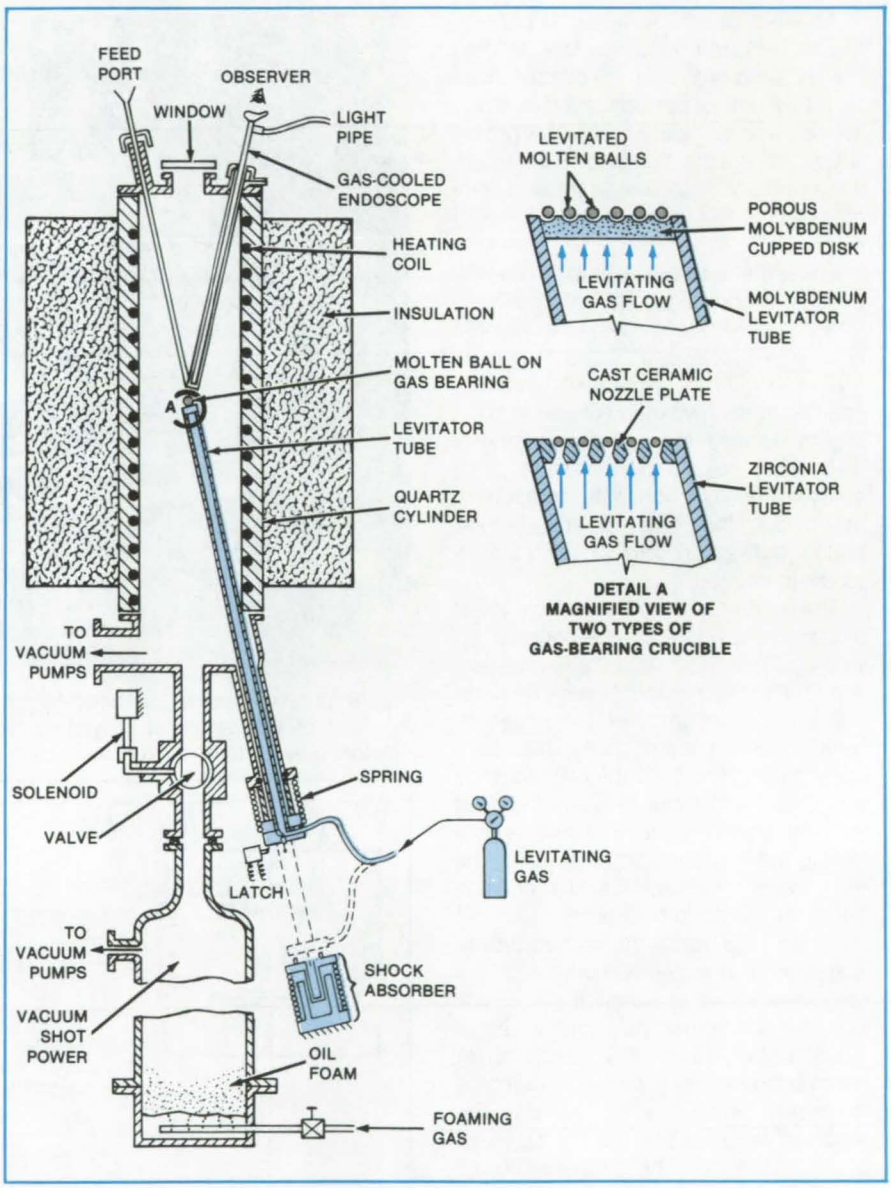

Gas Flowing Through a Levitator Tube levitates small balls while they melt. The gas is heated by a filament extending through the center of the tube. The gas-bearing crucible (nozzle) on the tube may have a concave configuration to hold a single relatively large ball or, as shown in the inset, may have many recesses to hold many small balls.

This work was done by Charles L. Youngberg, Charles G. Miller, James B. Stephens, and Anthony A. Finnerty of Caltech for **NASA's Jet Propulsion Laboratory.** *For further information, Circle 70 on the TSP Request Card.*
NPO-15070

Hollow-Sphere Production Line

After initial formation, spheroids are processed without the contaminating touch of solid objects.

NASA's Jet Propulsion Laboratory, Pasadena, California

A proposed scheme for contactless handling and fabrication would allow fusion-target pellets to be manufactured automatically at a fusion powerplant. The scheme also has potential for the manufacture of precise microcapsules for catalysts and medications. The reproducible wall thickness, size, and sphericity of the contactless-handling technique would yield uniform dissolution rates.

In the fusion-reactor application, the scheme would be used to prepare a continuous supply of hollow glass or metal spheres with cores of deuterium and tritium for direct insertion in the reactor. A spheroid in process is supported by acoustic levitation at each work station and is transported between stations by a combination of acoustic levitation and acoustic propulsion. The preparation sequence consists of the following steps (also see the figure):

1. A frit of water-soluble glass or of glass, metal, or metallic glass containing a chemical bubble-generating agent is used as the raw material. The frit is melted by laser irradiation until a bubble forms from evaporation of the solvent.
2. The amplitude of the acoustic field is modulated so that the thin molten shell of the bubble oscillates. This action centers the bubble core.
3. The bubble is cooled rapidly by acoustic streaming so that it forms a hollow spheroid of nearly uniform wall thickness and outer-surface sphericity.
4. The hollow sphere is held for several days in a pressure chamber containing deuterium and tritium as well as a diagnostic gas. Under 200 atm (20 MN/m^2) pressure and elevated temperature, the gases diffuse to the interior of the sphere. The diagnostic gas may be argon, the spectral lines of which show high pressure broadening and thus allow the pressure inside the sphere to be measured.
5. A liquid coating material is sprayed or deposited from vapor on the sphere and is oscillated acoustically for uniform distribution. The coating improves the electromagnetic impedance match with the imploding energy.
6. Alternatively, the coating is applied as a layer of fine particles. The coating is then melted so that capillary attraction distributes it over the sphere, is oscillated, and allowed to solidify.
7. The concentricity of the layers is checked by X-ray inspection; and the outer-surface sphericity, at an interferometry station.
8. Finally, the finished sphere is moved into the inertial confinement chamber of the powerplant and is consumed in the nuclear-fusion reaction.

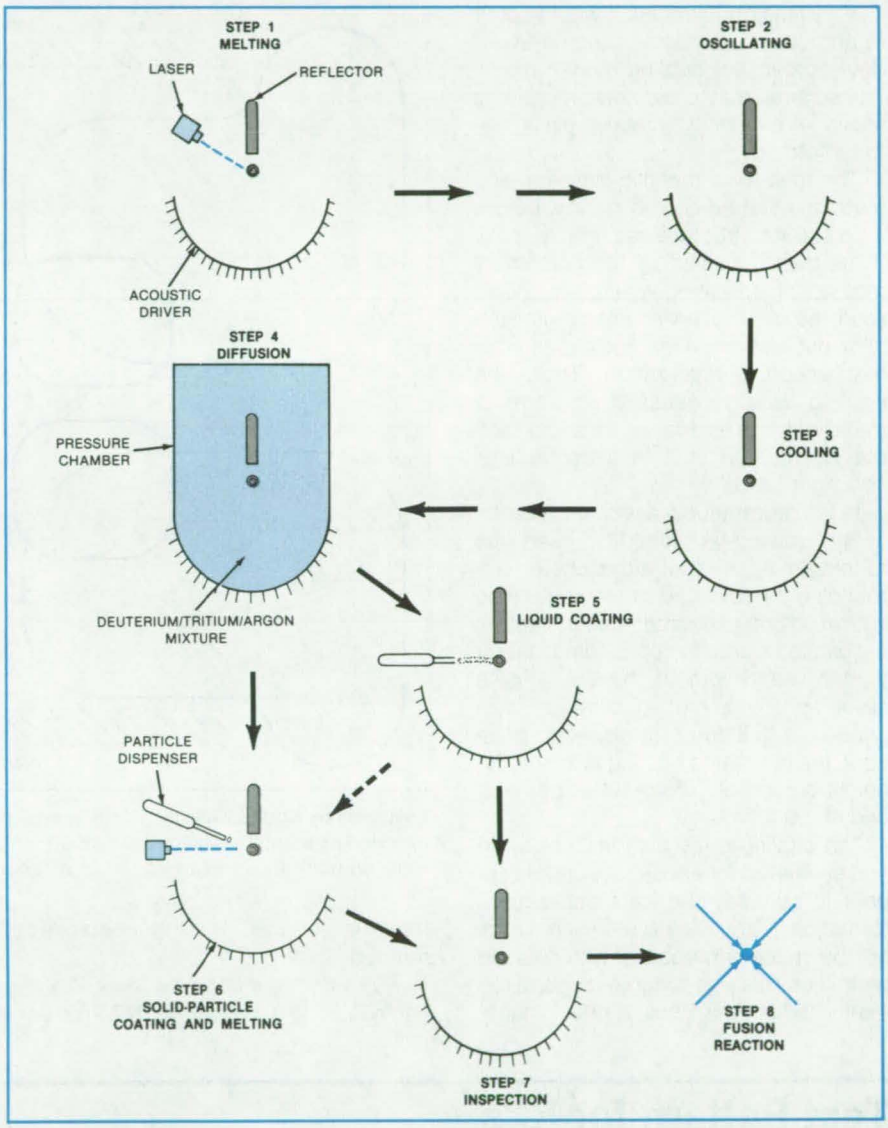

This **Automatic Sequence** of target-pellet fabrication allows no contact of solid objects with spheroids in process.

This work was done by Mark C. Lee of Caltech for **NASA's Jet Propulsion Laboratory.** *For further information, Circle 71 on the TSP Request Card.*

This invention is owned by NASA, and a patent application has been filed. Inquiries concerning nonexclusive or exclusive license for its commercial development should be addressed to the Patent Counsel, NASA Resident Office-JPL [see page A5]. Refer to NPO-15592.

Producing Metallic Glasses With Acoustic Levitation

Acoustic fields support and cool liquid particles.

NASA's Jet Propulsion Laboratory, Pasadena, California

Very little contamination would occur in an acoustic-levitation scheme under development for cooling molten metal. The scheme may allow new amorphous alloys — including "metallic glass" — to be formed.

The melt for a metallic-glass-forming material must be cooled rapidly, before a crystalline structure has time to form. If the melt is cooled by the customary method of splashing against a chilled solid, the solid not only contaminates the alloy but also provides nucleation sites that speed crystallization. Thus, the cooling rate necessary to form a metallic glass is higher in a contact-cooling method than in a contactless cooling method.

In the new method, a focused bidirectional acoustic levitating field gives rise to streaming in the atmosphere surrounding the levitated molten drop (see figure). In one experiment, such streaming caused a drop to cool 20 times faster than it would without the field. For a silver sphere 1 mm in diameter suspended in helium at atmospheric pressure, the estimated cooling rate is in the neighborhood of 10^4 to 10^6 K per second at 1,000° C.

The cooling rates thus far measured and estimated for acoustic levitators appear to be adequate for metallic-glass formation. Many alloy systems that cannot be made amorphous with existing techniques may be suitable for glass formation when the cooling-rate requirement is reduced by the contactless method.

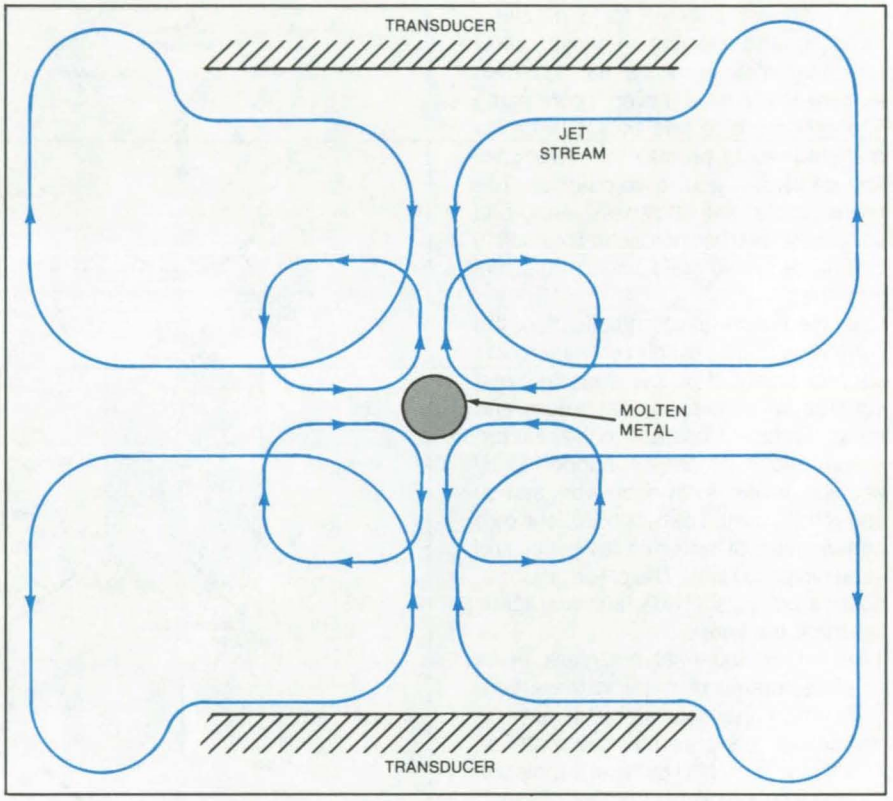

Levitated by Sound Energy, a liquid-metal drop in an acoustic standing-wave field is surrounded by acoustically-induced jet streams. The streaming gas cools the drop below its freezing point in a small fraction of a second.

This work was done by Mark C. Lee and I-an Feng of Caltech for **NASA's Jet Propulsion Laboratory.** *For further information, Circle 72 on the TSP Request Card.*
NPO-15658

Test Pattern for IC's

Random-fault densities are measured in an array of standard structures.

NASA's Jet Propulsion Laboratory, Pasadena, California

Random-fault densities in negatively-doped-channel metal-oxide-semiconductor (NMOS) integrated circuits are measured with the aid of an integrated test pattern consisting of 10 separate areas, each sensitive to different defects. A test pattern is an array of standard circuit elements built into a circuit chip along with, or in lieu of, the integrated circuit that is the objective of the process. Measurements on the array are made and interpreted so that the fabrication process can be corrected as necessary.

The 10 test areas are labeled as areas A through H. There are three "E" areas. Areas A through F provide statistically significant data on random-fault occurrences. The other two areas (G and H) are for obtaining information on process parameters, evaluating design rules,

and assessing experimental structures.

- *Area A* is an array of polycrystalline silicon islands over a gate oxide on a diffused region. It is used to detect excess leakage from metal to the bulk material (caused by photolithography-induced defects or dielectric breakdown of the gate oxide) as well as continuity of the metal-to-polysilicon contacts. Two contacts are made to each island, and the islands are connected by metal straps for a total of 15,120 contacts. The array is connected in electrically parallel groups of 216, 216, 648, 1,080, 2,160, 3,240, and 7,560 contacts.
- *Area B* is an array of polysilicon islands over a field oxide interconnected by metal straps. It is used to detect the lack of continuity between the metal and polysilicon. As in area A, 2 contacts are made to each island for a total of 15,120 contacts, and the array is connected in electrically parallel groups of 216, 216, 648, 1,080, 2,160, 3,240, and 7,560 contacts. With the polysilicon and metal cross-bridge resistors of area H, this area is used to obtain an estimate of the polysilicon-to-metal contact resistance.
- *Area C* is an array of diffused tubs. It is used to detect the lack of continuity of metal-to-diffused-region contacts. The array consists of 7,560 diffused tubs with 2 contacts each, giving a total of 15,120 metal-to-diffusion contacts. Again, the array is connected in electrically parallel groups of 216, 216, 648, 1,080, 2,160, 3,240, and 7,560 contacts. With the metal and diffused cross-bridge structures in area H, this area is used to obtain an estimate of the metal-to-diffused-region contact resistance.
- *Area D* is a matrix of polysilicon strips over gate oxides intersected by diffused strips. This arrangement produces a total of 23,550 polysilicon-gate capacitors in electrically parallel groups of 300, 750, 1,500, 3,000, 6,000, and 12,000. A metal cap is deposited over each of the paralleled groups. Metal-to-polysilicon, polysilicon-to-diffused-region, and polysilicon-to-substrate leakage as a function of array size can be measured.
- *Area E_1* is a 10-by-10 array of n-channel minimum-geometry metal-oxide-semiconductor field-effect transistors. The devices are interconnected so that the drains and gates are common. Each device is electrically isolated from its neighbor and can be individually tested by addressing the appropriate pads. Area E_1 is intended to test the feasibility of using an individually-addressed transistor array to determine the random-fault density of an NMOS logic array.
- *Area E_2* is similar to E_1 except that the transistors are depletion-mode instead of enhancement-mode devices.
- *Area E_3* is similar to E_1 and E_2 except that the transistor configuration is that of standard NMOS pullup transistors (depletion-mode) with a width-to-length ratio of 1 to 4.
- *Area F* contains serpentine aluminum metal over polysilicon and field oxide, with a total of 52,640 metal/polysilicon steps. The array is connected in electrically parallel groups of 1,504, 1,504, 4,512, 7,520, 15,040, and 22,560 steps. Its purpose is to aid in determining the fault density of metal-over-polysilicon steps.
- *Area G* is two large (625- by 625-μm) capacitors over a gate oxide. One capacitor is placed over an implanted region and the other over bulk material. Its purpose is to provide basic device information, such as gate-oxide thickness, substrate doping concentration, and mobile charge densities.
- *Area H* contains many different structures, including several types of sheet resistors, field-effect transistors with straight and serpentine gates, two types of 27-stage ring oscillator, inverters with various combinations of pulldown transistors, line-definition patterns, and thick-oxide transistors. The structures allow a wide range of experiments and assessments.

This work was done by Thomas W. Griswold and Eugene T. Bates, Jr., of Caltech for **NASA's Jet Propulsion Laboratory.** *For further information, Circle 73 on the TSP Request Card.*
NPO-15645

Manometer Measures Gas Flow

A simple apparatus uses a manometer to monitor the gas generated in a lead/acid battery. It measures the time required for the gas to displace a known volume of water. In determining the charging efficiency of a lead/acid battery, the gas generated during charging must be measured accurately since the energy required to generate the gas reduces the amount of energy left for charging.
(See page 428.)

Testing Bearings in Tight Spaces

A portable tool checks bushings and bearings in hard-to-reach places to ensure that they are properly staked. The tool applies a force around a right-angle bend — a capability that can make it unnecessary to disassemble equipment to gain access to the parts. The tool could be used to install or remove bearings, to press-fit parts, to remove nails, and to force sheet metal into position.
(See page 451.)

Eddy-Current Damage Test for Carbon Composites

An eddy-current technique detects cracks in reinforced carbon/carbon composites of low electrical conductivity. The method can be used in many other applications where materials of low conductivity are to be evaluated for damage. The test setup includes an eddy-current unit with a frequency of 2 to 20 MHz and a storage oscilloscope.
(See page 427.)

Circuitry for Angle Measurement

An electronics package for a shaft-angle measurement system features a resolver, a high-speed data-acquisition system, and a microprocessor. It is suited for such applications as rate tables, robots, antenna direction controllers, and machine tools. The resolver is pulsed and read under microprocessor control.
(See page 383.)

Fracture Strength of Silicon Solar Cells

A four-point twisting test has been developed as a standard test for determining the strength of silicon solar cells. It is used to study cell cracking and changes in fracture strength at various process steps as a blank silicon wafer is converted to a finished photovoltaic cell.
(See page 431.)

Jet Engines as High-Capacity Vacuum Pumps

Two gas-turbine jet engines would provide the primary ejection stream in a high-capacity eductor vacuum pump. The system could be used in such industrial processes as the handling of corrosive fumes, petroleum distillation, and blood-plasma dehydration.
(See page 442.)

Books and Reports

These reports, studies, and handbooks are available from NASA as Technical Support Packages (TSP's) when a Request Card number is cited; otherwise they are available from the National Technical Information Service.

Quality-Planning-Requirements Document

Report describes orderly methods for planning quality-assurance inspection procedures.

A new report outlines planning procedures that were used in establishing the inspection and quality-assurance activities required of contractors constructing and testing the Space Shuttle and its ground-support equipment. Since many of the planning procedures are described generically, the report should also be useful to contractors, subcontractors, and customers for establishing mutually-agreeable inspection points, whether in aerospace production or in commercial manufacturing operations.

The report contains definitions of terms, lists of decisionmaking ground rules, and sample documents. It also contains the full table of contents of the Quality-Planning-Requirements Document (QPRD) developed for the Space Shuttle. The QPRD is an official compilation of current versions of the various planning documents. These documents are kept in a large indexed looseleaf binder. Two actual QPRD Change Notices are included in the report to show how revisions to the QPRD were handled: Each Change Notice indicates what pages in the QPRD are to be replaced.

A list of 14 inspection ground rules gives criteria that should be considered when deciding on quality-assurance inspection points. For example, the list advises that the inspection of a part should be considered: "Where a part cannot be inspected when installed in the next higher assembly or when once installed, requires significant schedule time to gain access or to replace." A similar list presents criteria for establishing manufacturing-verification points.

An alphabetized list codifies the types of inspections and manufacturing verifications required (and who is responsible for doing them) for various types of steps that occur repeatedly in manufacturing operations. The list includes such general terms as: clean, crimp, mark, paint, rivet, solder, and weld.

Many of the quality-planning decisions are made by a committee known as the Manufacturing Verify group or by subgroups established by that committee. The customer can independently establish mandatory inspection points.

This work was done by Peter A. Leonard and Amado Flores of Rockwell International Corp. for **Johnson Space Center.** *To obtain a copy of the report, Circle 74 on the TSP Request Card.*
MSC-20280

Studies of the Inverted-Meniscus Deposition of Silicon on Ceramic

Controlled temperature profiles are essential to the production of solar cells.

Studies of the inverted meniscus process for depositing silicon coatings on ceramic substrates are described in a new report. When fully developed, the process will be used to manufacture low-cost solar photovoltaic cells.

In the SCIM (silicon-coating-by-inverted-meniscus) process, a substrate of mullite (an orthorhombic aluminum silicate) is pulled through the meniscus at the top of a crucible of molten silica. Silicon adheres to the bottom of the substrate. The pull rate is important: At too low a speed (typically below 6 cm/min), the coated substrate buckles or breaks in response to thermal stresses. At too high a speed (typically above 30 cm/min), the thermal inertia of the substrate helps to reduce the thermal stresses, but the deposit is too thin (less than 50 μm) for solar cells. Therefore, the process design must simultaneously meet the competing needs to pull slowly enough to deposit an adequate thickness of silicon, to pull rapidly enough to achieve a sufficient production rate, and to maintain a temperature profile that keeps thermal stresses below the buckling and breaking levels.

A thermal-profile-management strategy developed in the investigation is based on the division of the process into three portions, or temperature-profile zones: heating, coating, and cooling. In the heating and cooling zones, the variation of temperature with position along the substrate is kept as linear as possible (because the thermal stress is proportional to the second derivative of temperature with position).

In the coating zone, the thermal conditions are similar to those in the dip coating of substrates. Although the temperature variation is highly nonlinear in the coating zone, the temperature is high enough ($\geq$1,000° C) to permit stress relief by plastic deformation with relaxation times of a few seconds, so that no buckling or breakage occurs. In the low-temperature zones ($\leq$500° C) near the ends, temperature nonlinearities can be tolerated as long as the resulting thermal stresses do not exceed the elastic limit of the silicon on ceramic.

The experimental apparatus includes an active preheater and a passive postheater to generate the desired temperature profile. The apparatus is tilted because a wedge-shaped liquid/solid interface helps to increase the coating thickness at high speeds. Substrates of 10-cm width have been coated at 10° and 20° coating angles.

This work was done by J. D. Zook, B. L. Grung, S. B. Schuldt, F. M. Schmit, and J. D. Heaps of Honeywell Inc. for **NASA's Jet Propulsion Laboratory.** *For further information, Circle 75 on the TSP Request Card.*
NPO-15602

Polymeric Applications in Electronics

A training manual shows how to use polymeric materials in fabricating electronic components.

A 148-page report discusses polymeric applications in the fabrication of electronic components and equipment. It is intended as a training manual for a 6-day quality-assurance and technician certification course in the use of polymeric materials.

Various polymers are employed in electronic packaging as embedding resins, organic protective and insulating coatings, and adhesives. The training manual establishes a uniform method for the use of these materials. The manual stresses the importance of cleanliness, the effects of static discharges, and the proper methods for handling toxic chemicals.

Material selection is given in a table, listing the usage and type of material suggested. The processes that are involved in the application of polymeric materials are illustrated and covered in the following order:

- The Cleaning of Electronic Components (Methods and Solvents),
- Mixing Polymeric Materials,
- Plated-Through-Hole Filling in Printed-Circuit (PC) Boards,
- PC-Board Bonding,
- Connector Sealing,
- The Encasement of Transformers and Electronic Modules,
- Wire-Bundle Bonding,
- Fastener Bonding,
- Component Bonding,
- Protective Conformal Coating of Components, and
- Conformal Encapsulation.

A video tape of approximately 1 hour, showing the application of some materials and the suggested processes, is also part of the training program.

This work was done by William S. Read of Caltech for **NASA's Jet Propulsion Laboratory.** *Further information may be found in "Quality Assurance Training and Certification Program, Polymeric Applications" [$25]. A paper copy may be purchased [prepayment required] from the NASA Industrial Applications Center, University of Southern California, Research Annex, 3716 South Hope Street, Los Angeles, California 90007. The report is also available on microfiche at no charge. To obtain a microfiche copy, Circle 76 on the TSP Request Card.*
NPO-16081

Low-Cost Alternatives in Hybrid Microcircuit Packaging

Adhesive sealing, nickel plating, and multiwire boards are evaluated.

Ways of reducing the cost of packaging hybrid microcircuits are evaluated in a report. Based on a study involving fully developed hardware, the report considers adhesive packaging instead of seam welding, nickel-plated Kovar (a commercial Fe/Ni/Co alloy) packages instead of gold-plated ones, and multiwire circuit boards instead of multilayer boards as alternatives for reducing the cost of hardware without reducing reliability. The major conclusions of the study are that nickel plating and multiwire boards are recommended. Adhesive sealing is not recommended.

The evaluation was made by manufacturing specific hybrid circuits and board assemblies for the Space Shuttle flight-accelerometer safety cutoff system using the alternative low-cost packaging methods. The circuits and boards were subjected to standard screening and functional tests. Their costs were compared with those of the same hardware fabricated by conventional methods.

The study included developing the techniques for sealing the packages with adhesive and for removing the lids after sealing; fabricating, assembling, and testing the hybrid circuits; designing a multiwire board functionally equivalent to the original multilayer board; and assembling and testing multiwire board assemblies. Additional work included identifying the important cost factors and determining the cost differences resulting from the changes, exposing adhesive-sealed hybrids to a 10-day moisture-resistance test and 1,000-hour life tests, and functionally testing the hybrid circuits and analyzing their internal atmospheres after these tests.

The adhesive-sealed packages could not withstand the stresses imposed during the fine-leak test, even for a gage pressure of only 15 lb/in.^{2} (103 kPa). This is probably a result of the large size of the hybrid-circuit package [1 by 2 in. (2.54 by 5.08 cm)]. Moreover, it was found that there is no cost advantage to adhesive sealing, since the procedure for large packages is more labor-intensive than seam welding.

This work was done by S. V. Caruso, V. L. Champion, R. N. Bassett, and J. N. Gayer of Rockwell International Corp. for **Marshall Space Flight Center.** *To obtain a copy of the report, "Development of Low Cost Custom Hybrid Microcircuit Technology," Circle 77 on the TSP Request Card.*

Inquiries concerning rights for the commercial use of the technology described in the report should be addressed to the Patent Counsel, Marshall Space Flight Center [see page A5]. Refer to MFS-25809.

Computer Programs

These programs may be obtained at very reasonable cost from COSMIC, a facility sponsored by NASA to make new programs available to the public. For information on program price, size, and availability, circle the reference letter on the COSMIC Request Card in this issue.

Thermal Modeling of Bridgman Crystal Growth

Heat flow is modeled for a moving or stationary rod-shaped sample inside a directional-solidification furnace.

In the design of vertical Bridgman directional-solidification experiments, it is important to be able to predict the thermal profiles in the specimen. A computer program for the one-dimensional thermal modeling of Bridgman crystal growth provides an approximate analytical solution. The solution may be used as a guide for numerical modeling in

(continued on next page)

more-comprehensive thermal-analysis programs and for designing experimental procedures. Although the model contains several significant assumptions that limit its ability to match actual thermal profiles exactly, it is useful for predicting thermal gradients, estimating solidification interface position, and analyzing the effects of sample translation and sample insertion length.

The program effectively models the one-dimensional heat flow in a translating or motionless rod-shaped sample inside of a directional-solidification furnace in which an adiabatic zone separates the hot zone and the cold zone. Allowance is made for an optional booster heater in the hot zone just in front of the adiabatic zone.

The program is applicable to systems for which the Biot numbers in the hot and cold zones are less than unity. The Biot number for the adiabatic zone is assumed equal to zero. The user may specify different thermophysical properties for the sample in the solid and liquid states. The user may also specify that the space between the sample and the furnace wall is either a vacuum or filled with a stagnant or flowing fluid. Samples enclosed in ampoules are also accommodated by the program.

This program is written in BASIC and has been implemented on an HP9835 computer with a central-memory requirement of approximately 18K of 8-bit bytes. It was developed in 1982.

This program was written by Ernestine Cothran of **Marshall Space Flight Center.** *For further information, Circle Q on the COSMIC Request Card.*

MFS-27003

Mathematics and Information Sciences

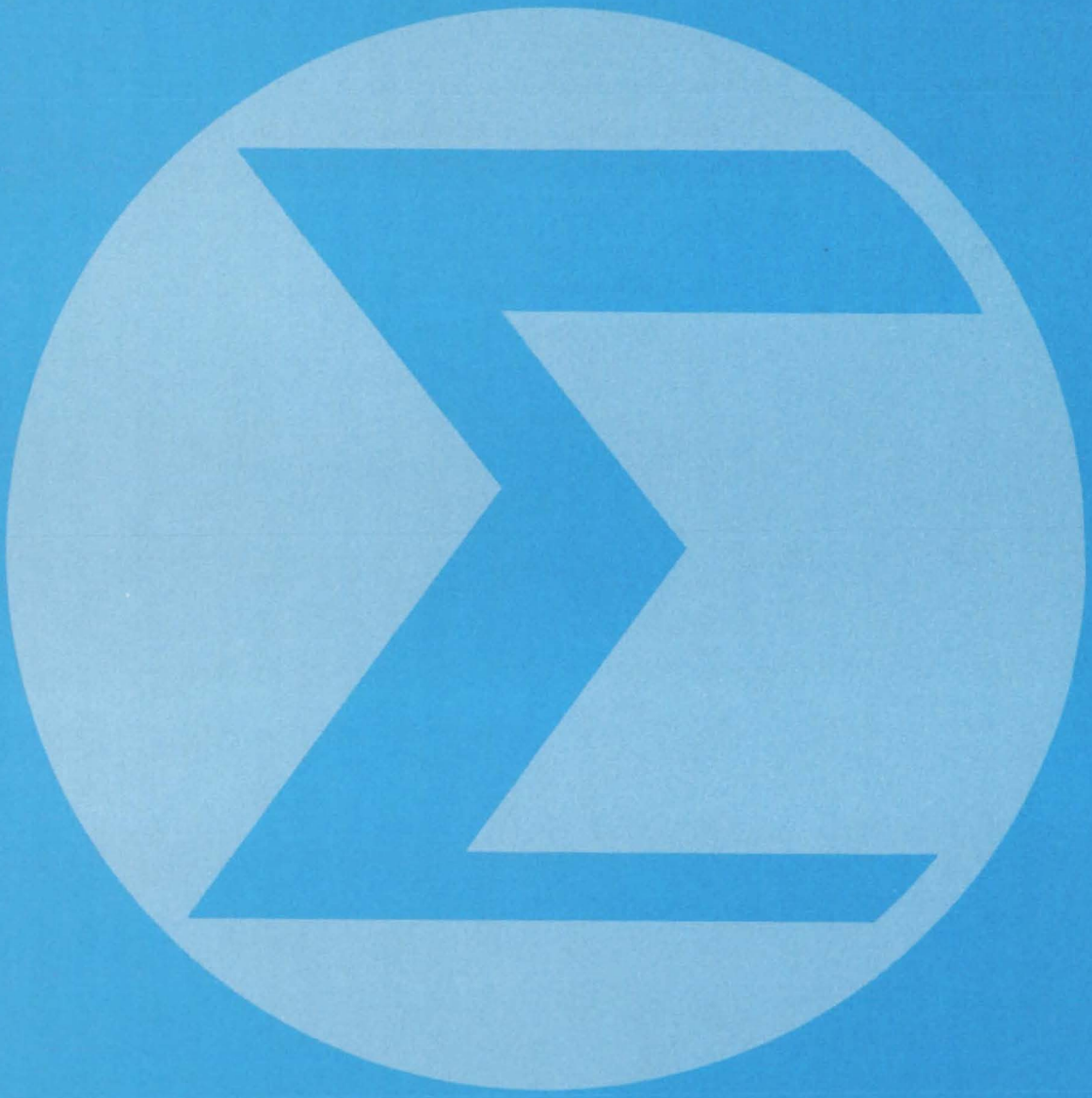

Determining Normal-Distribution Tolerance Bounds Graphically

Graphical method requires minimal calculations and table lookup.

Lyndon B. Johnson Space Center, Houston, Texas

The tolerance boundaries for a normal statistical distribution may be established from only three points: the mean upper and lower confidence bounds and the lower confidence bound of standard deviation. The method requires only a few calculations with simple equations; extensive table lookup is unnecessary. It is accurate enough for graphical analysis at any confidence level and any range of distribution percentile.

The new method allows conservative predictions of reliability, life expectancy, performance, and other characteristics of components. Such data are typically tabulated only for 95- and 99-percent confidence levels and for limited percentile values, usually above 75 percent.

The method is carried out in seven steps:

1. Plot two points on a sheet of normal-probability graph paper (see figure): $\overline{X}$ at the 50th percentile, representing the mean of the data, and $\overline{X} - s$ at the 16th percentile, representing the mean less the standard deviation. Draw a "best-fit" line through the two points.
2. At the 50th-percentile line, plot μ_{uc} and μ_{lc}, respectively the upper and lower confidence bounds for the mean at a confidence level of C. The values of the bounds are calculated from the equations shown in the figure. The value of t in the equation comes from a table of Student's t distribution with n − 1 degrees of freedom and 1 − C confidence level.
3. Draw a dotted vertical line down from μ_{lc}. Plot a point μ_{lc}^* on the vertical line a distance below the best-fit line equal to the distance from μ_{lc} to the best-fit line.
4. Calculate σ_{lc}, the lowest confidence bound for the standard deviation from the equation in the figure. The value of χ^2 in the equation comes from tabulated values of the chi-square distribution for n − 1 degrees of freedom and (1 − C)/2 significance level. Draw a dotted line from the mean value $\overline{X}$ through $\overline{X} - \sigma_{lc}$ at the 16th-percentile level. Label as X_M the point where this dotted line intersects the 0.1-percentile value.
5. Use a French curve to draw a line through μ_{uc}, μ_{lc}^*, and X_M. This line is the lower-half 1 − C confidence bound.
6. Draw the upper half of the upper confidence bound symmetrical about point X with the curve drawn in step 5.

(continued on next page)

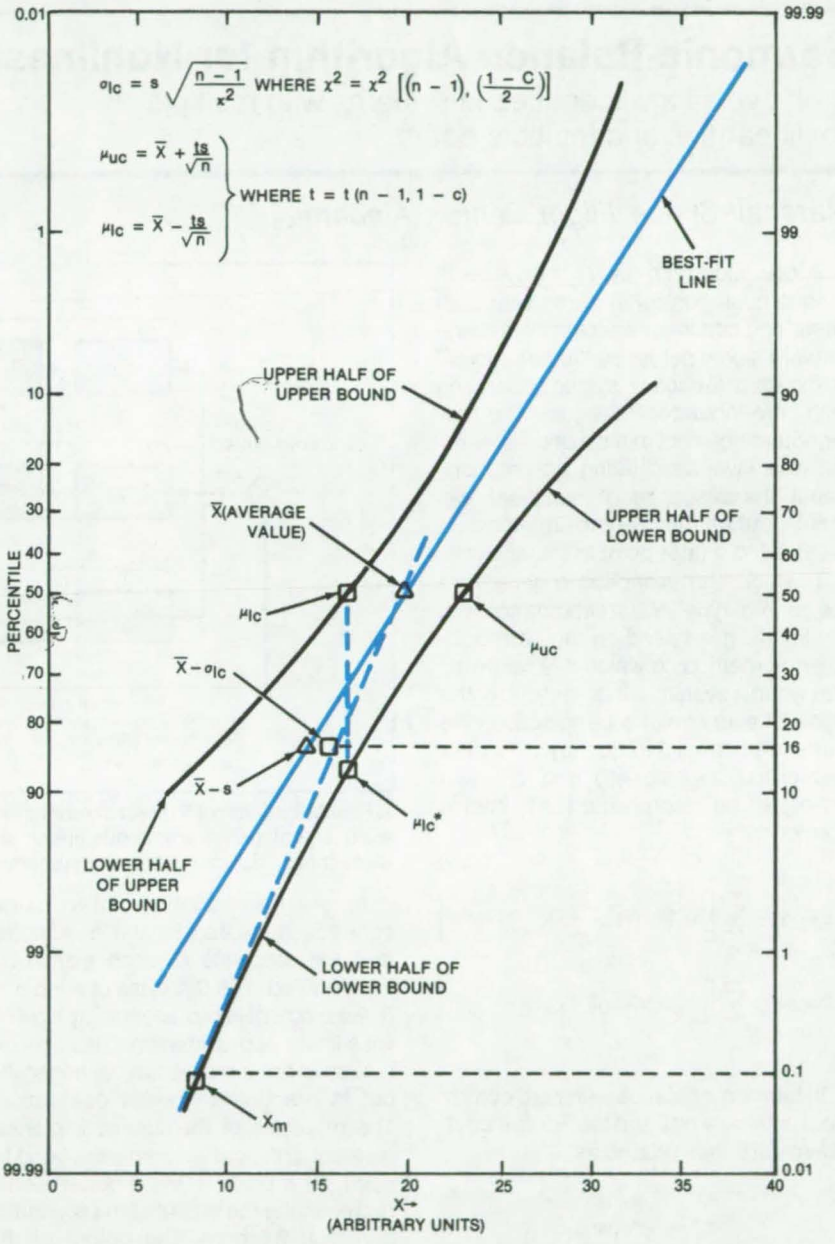

A Graphical Procedure establishes the best-fit line for measured data and the bounds for a selected confidence level and any distribution percentile.

7. Draw the remaining halves of the confidence bounds by plotting the locus of points equidistant from the best-fit line with the points of equal X value on the previously drawn lines.

The construction procedure requires only those parameter values that can be found in almost any elementary textbook on statistics. For sample sizes from 10 to 100, maximum errors of 1 to 3 percent were observed at the 90th and 10th distribution percentiles — well within the accuracy that can be expected from a graphical procedure.

This work was done by Michael A. Mezzacappa of Rockwell International Corp. for **Johnson Space Center.** *For further information; Circle 78 on the TSP Request Card.*
MSC-20115

Harmonic-Balance Algorithm for Nonlinear Systems

Limit cycles are identified in systems with multiple nonlinearities and multiple paths.

Marshall Space Flight Center, Alabama

A new algorithm finds limit cycles in autonomous control systems with both linear and nonlinear elements in several forward signal paths. By "autonomous" is meant a feedback system operating with zero input control signal. The new algorithm does not make a priori linearizing and low-pass-filtering assumptions about the response of nonlinear elements; rather, these approximations are deferred to a later point in the analysis.

The algorithm is applied to systems of the general type shown schematically in the figure. It is based on the harmonic-balance method, in which it is assumed that when a system is in a limit cycle, the signal at every point is periodic with the same fundamental frequency. The input and output signals e(t) and c(t) can therefore be represented as infinite Fourier series:

$$e(t) = a_0 + \sum_{k=1}^{\infty}\left[a_k \cos(k\omega_0 t) + b_k \sin(k\omega_0 t)\right]$$

$$c(t) = A_0 + \sum_{k=1}^{\infty}\left[A_k \cos(k\omega_0 t) + B_k \sin(k\omega_0 t)\right]$$

In harmonic balance with zero control input, $e(t) = -c(t)$, and the Fourier coefficients are thus related as

$$a_0 = -A_0,$$
$$a_k = -A_k, \text{ and}$$
$$b_k = -B_k.$$

To obtain exact values for the set of Fourier coefficients that satisfies this condition, one would have to solve an infinite number of nonlinear equations in an infinite number of unknowns. Since that is impossible, the problem must be reduced to a finite set of equations from which an approximate solution is obtained.

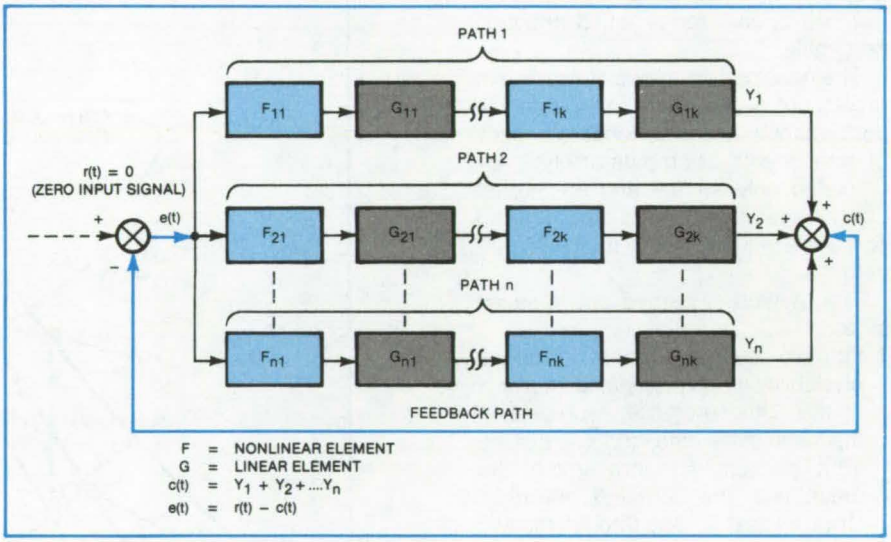

A Feedback Control System or other physical system with feedback may have several forward signal paths with both linear and nonlinear elements in each path. The new algorithm finds limit cycles for systems of this configuration.

In the new algorithm, the Fourier series is truncated by the assumption that the response of each element is band-limited. The response of each nonlinear element is represented by a piecewise-linear approximation. (This approximation is not a mathematical necessity, but in practice it speeds calculation.) The response of the succeeding linear element in the path is then calculated for each harmonic in the Fourier series representing the output of the preceding nonlinear element. The output of this linear element becomes the input to the next nonlinear element in the path, and so forth. The outputs of the separate paths are added to obtain c(t).

The calculation begins with the assumption of an input signal e(t). The system response c(t) to that particular e(t) is calculated. The input is then refined to produce an output that more nearly matches the input. This is a zero-finding problem in which the variables are the fundamental frequency and the Fourier coefficients.

Instead of attempting to solve the complex set of nonlinear equations analytically, the algorithm proceeds by a multidimensional Newton-Raphson gradient method that has been modified to improve convergence. The method automatically increments the input to the set of Fourier coefficients for the next iteration. The system response to the new input is calculated and the cycle repeated until the input and output Fourier coefficients converge to within the specified tolerance.

This work was done by Jerrel R. Mitchell and Ottis L. Barron of Mississippi State University for **Marshall Space Flight Center.** *For further information, Circle 79 on the TSP Request Card.*
MFS-25821

Digital Filters for Two-Dimensional Data

Computationally efficient filters speed the processing of two-dimensional experimental data.

Marshall Space Flight Center, Alabama

A set of digital data filters known as two-dimensional convolute integers is especially suited for efficient computer analysis of two-dimensional experimental data or of images. Each use of such a filter requires only integer multiplications, a summation, and a single normalizing division. Regression calculations were required to generate the filters but are not required to use them. The use of such a filter gives a result equivalent to that of fitting a power-series expansion to the data in the vicinity of each data point to determine a smoothed value either for the data point or for one of its partial derivatives, depending on the filter used.

The numerical filtering methods used in digital optical image processing are also useful in analyzing other two-dimensional experimental data; for example, time-resolved spectroscopic data in which intensity is a function of wavelength and time. The data from such a measurement can be represented as a rectangular array of numbers, which necessarily includes some random noise. If noise were not present, one would locate peaks in the data by finding the zeros in the image-density gradients; but differentiation accentuates high-frequency noise in the data, complicating the analysis. Such analyses can be facilitated by subjecting the data to a low-pass digital filter to suppress the noise, either before or simultaneously with differentiation.

Two sets of digital filter arrays have been prepared. One set combines the low-pass-filtering or noise-smoothing step with the computation of the desired first-, second-, or third-order partial derivative. The other set performs noise smoothing only.

5-BY-5 SMOOTHING FILTER					
	−13	2	7	2	−13
	2	17	22	17	2
	7	22	27	22	7
	2	17	22	17	2
	−13	2	7	2	−13

NORMALIZING DIVISOR: 175

A Two-Dimensional Smoothing Filter can be used to attenuate high-frequency noise in two-dimensional numerical data arrays. When used as described in the text, this filter provides smoothed data values equal to the values that would be obtained by fitting a surface with second- and third-order terms to a 5 by 5 subset of data points centered on each of the points and replacing the datum at each point by the value of the surface fitted at that point.

Each filter consists of a square array of numbers and an accompanying normalizing divisor. One such smoothing filter is shown in the figure. To use the filter to obtain the smoothed value s_{ij} corresponding to the data value z_{ij} (in the ith row and the jth column of the data array), a square array of data points of the same size as the filter being used and centered on z_{ij} is multiplied element by element by the number in the corresponding position in the filter. All of these products are then summed and finally divided by the normalization divisor to obtain the smoothed value, s_{ij}.

Each of the filters has symmetry properties that should be exploited to maximize the speed of computation. Numbers at symmetrically located points in different quadrants of the filter array differ by no more than a sign. To reduce the number of multiplications required, data values corresponding to such locations should be added or subtracted (depending on the signs in the filter) before multiplying by the value in the filter.

The numbers in the filters and the normalizing divisors are universal sets of numbers, independent of the data, dependent only on the powers included in the fitted surface and on the size of the filter array chosen. The numbers in the filters are integers because only integers are used in their calculation; that is, the number of positions a data point lies away from the center of the filter. The minimum permissible size of the filter is determined by the highest order terms required in the fitted surface. For example, a 5 by 5 smoothing filter is the smallest that permits second- and third-order terms.

This work was done by Thomas R. Edwards of **Marshall Space Flight Center.** *For further information, Circle 80 on the TSP Request Card.*
MFS-25790

Books and Reports

These reports, studies, and handbooks are available from NASA as Technical Support Packages (TSP's) when a Request Card number is cited; otherwise they are available from the National Technical Information Service.

KSC Construction Cost Index

The Kennedy Space Center Cost Index aids in conceptual-design cost estimates.

A 28-page report discusses the development of the Kennedy Space Center (KSC) Cost Index since January 1974. The index provides management, design engineers, and estimators an up-to-date reference for local labor and material prices. It also provides the

(continued on next page)

amount and rate of change in these costs, which are used to predict future construction costs. The cost index is provided to the many engineering firms doing business with NASA/KSC so as to arrive at realistic and consistent cost estimates.

One part of the cost index includes a graph of the KSC labor and material indices, which is used as an aid to evaluate past and present costs and for predicting the cost escalation on facility design and construction. This index incorporates price adjustments related to the KSC location and specialized construction requirements.

As part of the index, over 230 rule-of-thumb unit costs are used in the conceptual formulation of budget costs for new and modified facilities. These rule-of-thumb costs have been developed using historical data based on past bid abstracts and the system summary of the Government estimate. Some of these rule-of-thumb unit-cost items are for paving, earthwork, piling, reinforced concrete, structural steel, access platforms, special pneumatic sealed doors, bridge cranes, stainless-steel piping systems, and control panels. Also included are Halon fire-protection systems, mechanical, electrical, and metal building systems, and exterior utilities.

This work was done by Joseph A. Brown of **Kennedy Space Center.** *To obtain a copy of the report, Circle 81 on the TSP Request Card.*
KSC-11252

Conceptual Cost Estimating

Kennedy Space Center cost data aid in efficient construction-cost management.

A 14-page report discusses the development and use of NASA TR-1508, a Kennedy Space Center Aerospace Construction price book for preparing conceptual, budget, funding, cost-estimating, and preliminary cost-engineering reports. The 300-page book, updated annually from 1974 through 1983, is based on actual bid prices and Government estimates. It details labor and material quantities and unit prices with general and subcontractor markups for commonly-used aerospace-facility and ground-support equipment elements and systems.

A conceptual cost estimate is used to assure cost control throughout a project. One of the methods for making order-of-magnitude conceptual estimates is to find similar items, buildings, systems, and elements already designed, built, and costed and to adjust those costs for time, location, and current design requirements. With the aid of unit bid prices thus derived, the conceptual budget estimates are more accurate and timely. The set of prices also serves as a rule of thumb and as cross-check feedback for evaluating cost estimates of project details.

This work was done by Joseph A. Brown of **Kennedy Space Center.** *To obtain a copy of the report, Circle 82 on the TSP Request Card.*
KSC-11253

Frost Forecasting for Fruitgrowers

Progress in forecasting from satellite data is reviewed.

Data from satellites can be displayed in color and used to predict frost, a university study has found, and thus can be a valuable aid to agriculture. Although satellite frost prediction has had modest success in limited, intrastate regions, much remains to be done before an effective prediction system is available nationwide.

The results of the study are documented in a report containing contributions from the University of Florida, Michigan State University, and The Pennsylvania State University. The study evaluated a scheme to use Earth-temperature data from the Geostationary Operational Environmental Satellite in a computer model that determines when and where freezing temperatures could endanger developing fruit crops, such as apples, peaches and cherries in the spring and citrus crops in the winter. The scheme would not only predict frost but also would distribute the predictions to growers.

The report covers work on developing and evaluating computer models and discusses field experience with predictions in Michigan and Pennsylvania. The report also presents an extensive set of recommendations for implementing a Satellite Frost Forecast System (SFFS):

- **Orientation of Satellite Data** — Growers must be able to relate thermal maps to their orchards. Thus the system must insert precise and reliable geographic reference marks into the data so that users can quickly and easily identify their orchards on the temperature maps.
- **Dissemination of Forecasts** — Private and public communication networks should be utilized to distribute information, and home computer links are a likely medium for the future.
- **Satellite Data Acquisition** — A direct downlink from satellite to a local SFFS antenna and computer will speed up processing and forecast distribution.
- **Alternative Forecasting Models** — Simpler models that can be processed on simple, low-cost computers will make forecasts available to counties and local grower organizations. The models would be tailored to the characteristics of the locality.

This work was done by J. David Martsolf and Ellen Chen of the University of Florida for **Kennedy Space Center.** *Further information may be found in NASA CR-166827 [N82-20607/NSP], "Application of Satellite Frost Forecast Technology to Other Parts of the United States, Phase II" [$22]. A copy may be purchased [prepayment required] from the National Technical Information Service, Springfield, Virginia 22161.*
KSC-11241

Computer Programs

These programs may be obtained at very reasonable cost from COSMIC, a facility sponsored by NASA to make new programs available to the public. For information on program price, size, and availability, circle the reference letter on the COSMIC Request Card in this issue.

Software Specification Language

SSL translator aids in developing and checking software systems.

The Software Specification Language, SSL, aids in the process of decomposing software functions into subfunctions or, equivalently, systems into subsystems. The principal goal of SSL is to provide a form of verification and consistency checking early in the design phase. Secondarily, it may serve as a formal document with which to communicate the software architecture to the detailed designers.

Since SSL is a nonprocedural language for which a formal syntax and semantics exist, it was possible to develop an automatic translator. Systems described in SSL are partitioned into one or more subsystems where each subsystem corresponds to a level of abstraction. Within each subsystem, one or more modules are described nonprocedurally. Module description statements permit module connections and data flow to be depicted in a variety of ways, subject to the restraints imposed by the underlying flow model.

SSL minimizes barriers to creativity on the part of the designer while encouraging "good" programing practices, such as modularity, levels of abstraction, and high-level data types by providing constructs to represent them conveniently. SSL has proved successful in checking module and data interconnections for consistency with an assumed system flow.

SSL does not impose artificial restrictions on data flow or architecture but does insist that both conform to a separately-developed system flow model. This affords the opportunity to perform extensive nontrivial consistency verification and develop a document that aids the communication of design intentions and testing criteria to subsequent development phases.

The SSL translator is written in FORTRAN IV Level H and OS Assembler for batch execution and has been implemented on an IBM 360-series computer with a central-memory requirement of approximately 250K of 8-bit bytes. The SSL translator was developed in 1978.

This program was written by B. P. Buckles, J. P. Ryan, and S. L. Austin of Science Applications, Inc., for **Marshall Space Flight Center.** *For further information, Circle R on the COSMIC Request Card.*
MFS-23737

Forest Resource Information System

Twenty-three processing functions aid in utilizing LANDSAT data for forest resource management.

LARSFRIS is a multi-image analysis system developed as part of the Forest Resource Information System (FRIS) project to demonstrate the benefits of multispectral-data image processing in forest resource management. LARSFRIS represents a modified version of the LARSYS software developed at the Laboratory for Applied Remote Sensing (LARS) at Purdue University.

LARSFRIS consists of 23 integrated processing functions that provide techniques for handling and processing remotely-sensed multispectral and multitemporal data. It is designed to work primarily with digital data obtained from measurements recorded by multispectral remote sensors mounted on aerospace platforms, such as the NASA Landsat satellites. Communication between processing functions, the simplicity of control, and the commonality of data files in LARSFRIS enhance the usefulness of the system as a tool for the research and development of remote sensing systems.

Six LARSFRIS "utility" functions enable a user to extract or manipulate data from the Multispectral Image Storage Tapes:

1. BIPLOT allows the user to plot the data in two-dimensional space.
2. CHANNELTRANSFORM copies a run from one tape to another and makes algebraic transformation to a subset of channels to provide a user with private access to a particular run.
3. IDPRINT provides lists of the ID record information to aid users in identifying available data runs.
4. MERGESTATISTICS allows the user to merge multiple statistics decks into one deck and pool or delete classes.
5. RATIOMEANS allows the user to ratio means from user-specified channels.
6. TRANSFERDATA extracts data values from a run and prints them in a listing, punches them into a card deck, or writes them on a formatted tape.

Four LARSFRIS functions assist the user in evaluating Multispectral Image Storage Tape data:

1. LINGRAPH prints a graph showing the relative magnitude of data points from lines stored in a given run.
2. COLUMNGRAPH prints a similar graph of columns of data.
3. HISTOGRAM calculates a histogram of data values for each requested channel for a specified area.
4. GRAPHHISTOGRAM prints graphs of the resulting histogram.

A LARSFRIS function is provided to assist in the selection of areas used to design and evaluate a classifier. PICTUREPRINT prints data in image orientation to enable a user to select manually subsets of data that will be useful as "training fields" for classifier design and as "test fields" for classification evaluation. The results can then be used to specify the location of these areas to LARSFRIS in other processing functions. PICTUREPRINT also has the capabilities to generate a histogram of an area, to graph histograms, and to print the locations of previously-defined training and test fields.

Three LARSFRIS functions perform preliminary operations to assist the user in defining a classification run:

1. CLUSTER is an unsupervised classifier that groups data vectors into the number of classes specified by the user.
2. STATISTICS calculates mean vectors and covariance matrices for each class specified by the user and produces these data as outputs in the form of a statistics file and several printed formats.

(continued on next page)

3. SEPARABILITY uses data from a statistics file to measure the separability between classes of interest as a function of combinations of spectral bands.

There are three supervised classification functions in LARSFRIS:

1. SAMPLECLASSIFY classifies groups of points by considering group statistical characteristics.
2. CLASSIFYPOINTS performs the maximum-likelihood classification on a point-by-point basis over an area specified by the user. It produces a classification results file for use by other processing functions.
3. SECHO classifies through supervised extraction and classification of homogeneous objects.

Six LARSFRIS functions enable the user to analyze or handle data from a classification results file:

1. COMPARERESULTS allows the user to detect differences from two classification results files.
2. COPYRESULTS duplicates a classification results file on magnetic tape.
3. LISTRESULTS produces a formatted listing of identification information pertaining to a classification results file.
4. PRINTRESULTS produces a number of printed outputs, including performances tables for training classes and training fields and for text classes and text fields. Also, the results of classification can be printed in their image orientation.
5. PUNCHSTATISTICS punches on cards the statistics file that was used in the classification.
6. SMOOTHRESULTS allows the user to enhance a classification results file by specifying parameters.

The processing and initialization functions are controlled by the user primarily through entries on the control deck that comprise an input file. This deck specifies to LARSFRIS which functions are to be performed and which procesing options are to be exercised. The file also may include data that are required as inputs by some of the processing functions. Since the principal interface between LARSFRIS and the user is the input control file, considerable attention has been given to the simplicity of its specification. The generally-free-form format, the extensive use of English-like words for keywords and parameters, and the few simple syntax and punctuation rules greatly simplify the user's preparation and use of input commands. In addition, extensive error checking is provided.

The LARSFRIS system also includes a set of LARSFRIS preprocessors. These preprocessors provide the user with two additional image-processing functions. The first preprocessor reformats Landsat or other digital image data in EROS Data Center format into a format compatible with the LARSFRIS processors. The second preprocessor provides for the systematic geometric enhancement of image data from the first processor.

The LARSFRIS software is written in FORTRAN IV and Assembler for operation in interactive, batch, and disconnect modes. LARSFRIS has been implemented on an IBM 3031 running under VM/370 CP release 6, with the CMS Version 370 operating system. The largest functional load module has a main storage requirement of approximately 960K of 8-bit bytes. LARSFRIS was developed in 1980.

This work was done by Richard P. Mrocznyski of Purdue University for **Johnson Space Center.** *For further information, Circle S on the TSP Request Card.*
MSC-20270

Security Package for the VAX

Four programs deal with intruders and resource management.

A package available from COSMIC provides the DEC VAX-11/780 with certain "deterrent" security features. Although the package is not a comprehensive security system, it should be of interest for any VAX installation where security is a concern.

The VAX security package has four parts: Two deal with resource management, and two deal directly with intruders. AUTOBAUD deals with the allocation of remote terminal lines. It adjusts the baud rates, preparing for a remote user log-in. If a remote terminal is not logged in, AUTOBAUD performs a periodic handup to prevent accidents involving lengthy long-distance connections.

MONITOR examines all the terminals every 15 minutes for users who fail to perform any CPU activity and, after a specified period of time, performs a logoff and hangup. Since terminals and remote lines are usually scarce, MONITOR aims to allocate these resources to users who need them the most. MONITOR also keeps an inactivity log that should be useful in setting allocation policies.

GUARDIAN records data concerning every unsuccessful log-in in a protected file. It also performs hangups and logouts on multiple attempts to enter the same account from the same terminal within a 10-minute period, with an intruder alert sounding on the system console. INSPECT allows a system manager to examine suspicious processes and take certain actions against would-be intruders.

The programs in this computer security package are written in FORTRAN IV and MACRO Assembler for real-time and interactive execution. They have been implemented on a DEC VAX-11/780 operating under VMS2.4 with a total memory requirement of approximately 180 blocks. The programs were developed in 1982.

This program was written by Victor J. Marks and Clayton E. Benigus of MATSCO for **Johnson Space Center.** *For further information, Circle T on the COSMIC Request Card.*
MSC-20423

SUBJECT INDEX

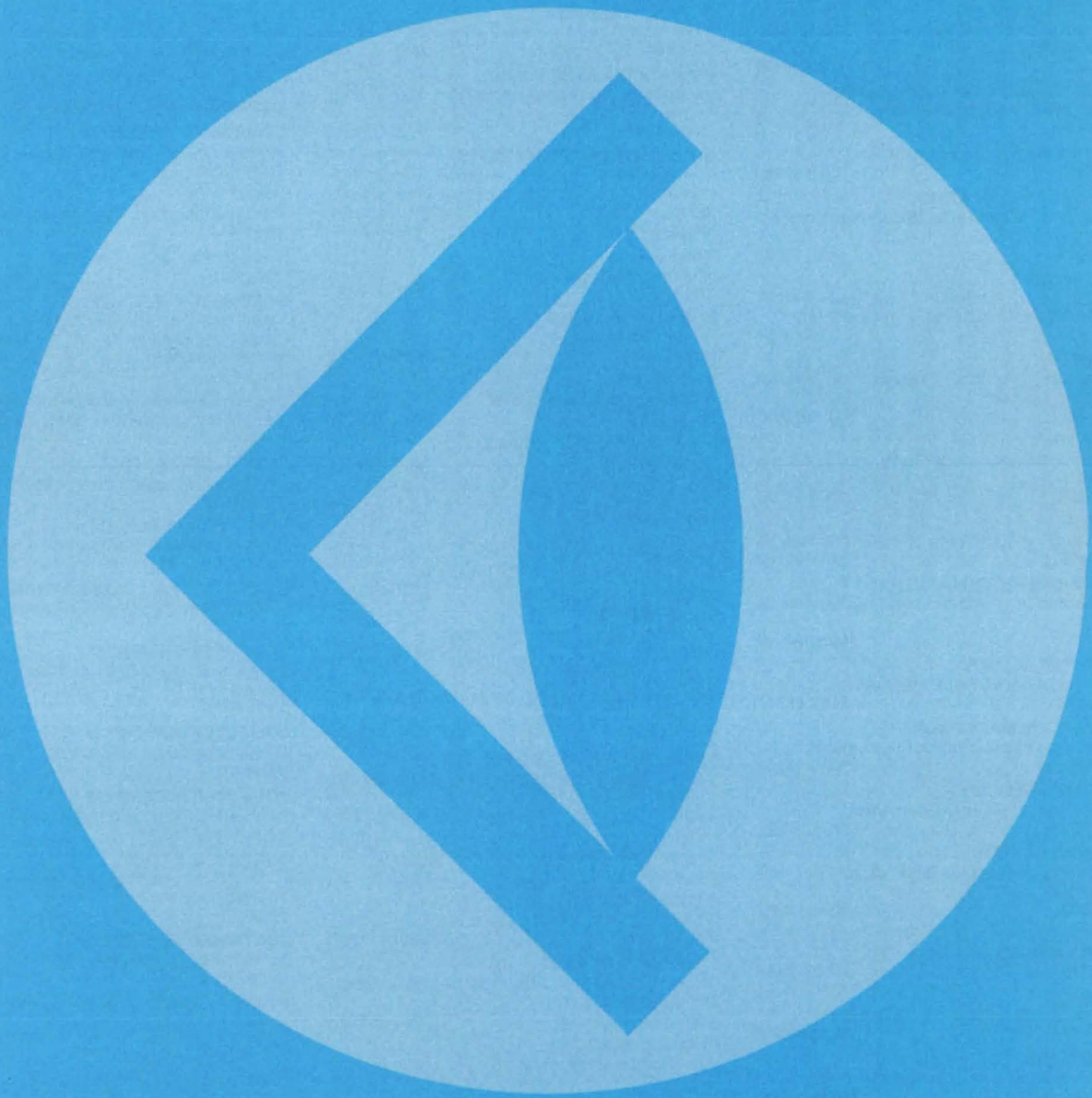

National Aeronautics and
Space Administration

Washington, D.C.
20546

THIRD-CLASS BULK

25th Anniversary
1958-1983

NASA

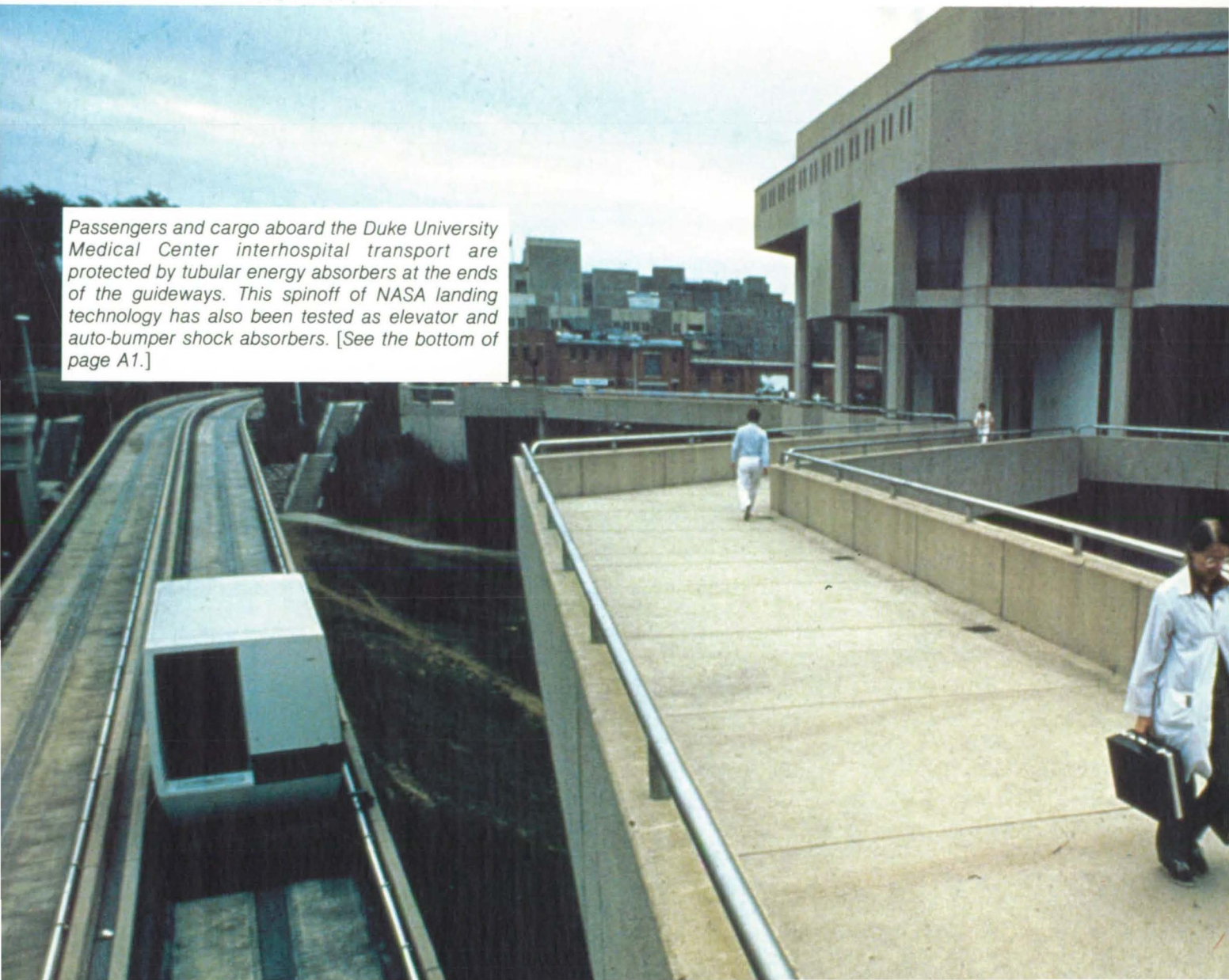

Passengers and cargo aboard the Duke University Medical Center interhospital transport are protected by tubular energy absorbers at the ends of the guideways. This spinoff of NASA landing technology has also been tested as elevator and auto-bumper shock absorbers. *[See the bottom of page A1.]*